

Session 4

WASTE PROCESSING

TUESDAY: August 3, 1982
Co-CHAIRMEN: M.J. Kabat, Ontario Hydro
C.H. Cheh, Ontario Hydro

OFF-Gas CHARACTERISTICS OF LIQUID-FED JOULE-HEATED CERAMIC MELTERS

R.W. Goles, G.J. Sevigny

IMMOBILIZATION OF KRYPTON-85 IN ZEOLITE 5A⁺

A.B. Christensen, J.A. DelDebbio, D.A. Knecht, J.E. Tanner, S.C. Cossel

THE LONG-TERM STORAGE OF RADIOACTIVE KRYPTON BY FIXATION IN ZEOLITE 5A⁺

R.D. Penzhorn, H. Leitzig, K. Gunther, P. Schuster, H.E. Noppel

VOLATILIZATION AND TRAPPING OF RUTHENIUM IN HIGH TEMPERATURE PROCESSES

M. Klein, C. Weyers, W.R.A. Goossens

RADIOCARBON TREATMENT SYSTEMS

PLANT FOR RETENTION OF ¹⁴C IN REPROCESSING PLANTS FOR LWR FUEL ELEMENTS

H. Braun, H. Gutowski, H. Bonka, D. Gundler

MECHANISM OF THE CO₂-Ca(OH)₂ REACTION

V.S. Chew, C.H. Cheh, R.W. Glass

¹⁴C RELEASE AT LIGHT WATER REACTORS

C. Kunz

CARBON-14 IMMOBILIZATION VIA THE Ba(OH)₂·8H₂O PROCESS

G.L. Haag, J.W. Nehls, Jr., G.C. Young

17th DOE NUCLEAR AIR CLEANING CONFERENCE

OPENING REMARKS OF SESSION CHAIRMAN:

Welcome to Session 4 of the 17th DOE Nuclear Air Cleaning Conference. Eight papers will be presented on radioactive waste processing and radiocarbon treatment systems. We are aware of the possibility that long-lived, volatile fission and activation products could cause in the future an increase in ambient radiation levels on a global scale, if they are allowed to accumulate in the biosphere. Their global impact has not been clearly established; however, to comply with the ALARA policy, their release from fuel cycle operations should be maintained at minimal achievable levels. Requirements for their removal should be based on realistic cost-benefit analysis.

Four radionuclides represent this class: Carbon-14, Krypton-85, Tritium and Iodine-129. There is no significant hazard from ^{129}I liberated from fuel cycle operations because its efficient effluent control has been well established. The removal of ^{14}C complies with cost-benefit criteria because it is based on relatively simple and inexpensive processes. The high proportion of presentations on ^{14}C at this session indicates that this task has been given proper attention. However, systems for the immobilization of ^{85}Kr and its long term storage are also being developed and the volatilization and trapping of other radiobiologically significant radionuclides is also being investigated.

Let us hear from experts about recent developments in this area.

17th DOE NUCLEAR AIR CLEANING CONFERENCE

OFF-GAS CHARACTERISTICS OF LIQUID-FED JOULE-HEATED CERAMIC MELTERS*

R. W. Goles and G. J. Sevigny
Pacific Northwest Laboratory
Richland, Washington 99352

Abstract

The off-gas characteristics of liquid-fed, joule-heated ceramic melters have been investigated as a function of melter operational conditions and simulated waste feed composition. The results of these studies have established the identity and behavioral patterns of gaseous emissions, the characteristics of melter-generated aerosols, the nature and magnitude of melter effluent losses and the factors affecting melter operational performance.

I. Introduction

Liquid-fed, joule-heated ceramic melters are to form the basis of the planned Defense-Waste Processing Facility (DWPF) to be constructed at the Savannah River Plant (SRP). The purpose of this facility (DWPF) is to isolate and immobilize defense-related nuclear waste as a borosilicate glass. The Pacific Northwest Laboratory (PNL) is assisting the Savannah River Laboratory (SRL) in establishing the design criteria for the DWPF by providing a technology transfer and all necessary liquid-fed ceramic melter research and development.

Off-gas characterization studies have been established as part of the SRL-DWPF melter development program being conducted at PNL. The objective of these studies is to establish the off-gas properties of liquid-fed, joule-heated melters as a function of melter operational parameters and feed composition.

The scope of these studies is quite broad and covers all aspects of off-gas concern including: 1) effluent characterization, 2) emission abatement, 3) flow rate behavior, and 4) corrosion effects. This paper will discuss the results obtained from each of these areas after a brief description of the liquid-fed melter process.

II. Liquid-Fed Melter Processing System

The following is a brief description of the liquid-fed melter processing system which was developed at PNL in support of the SRP-DWPF. A much more detailed account of the liquid-fed melting process can be obtained from Reference 1.

Melter

Several processes for solidifying and immobilizing high-level (radioactive) liquid waste as a stable borosilicate glass have been and are currently being evaluated at PNL.⁽²⁾ The process being

* Work performed for the Office of Nuclear Waste Management under U.S. Department of Energy contract TDO-954 (AR-05-15-10).

evaluated in this study utilizes a joule-heated ceramic-lined melter which is directly fed a uniform slurry composed of glass formers and simulated liquid radioactive waste. Upon entry into the melter, the waste components of the slurry are oxidized and melted with the glass formers present in the feed to form a molten borosilicate glass. The power required to maintain this continuous glass production process is supplied by resistive ac heating of the melter glass pool. In addition to the primary source of power, auxiliary radiant heaters located in the melter plenum above the glass melt surface have also been employed to increase or "boost" feeding and glass production rates. Limited use has also been made of plasma and propane combustion torches to supply supplemental heating to the melter plenum. Figure 1 schematically illustrates the liquid-fed melting process.

Two different joule-heated ceramic melters were used in these developmental studies and are referred to as the Liquid-Fed Ceramic Melter (LFCM), which has a melting surface area of 1.05 m², and the Pilot-Scale Ceramic Melter (PSCM), which possesses a 0.73 m² surface area. The maximum glass production rates associated with

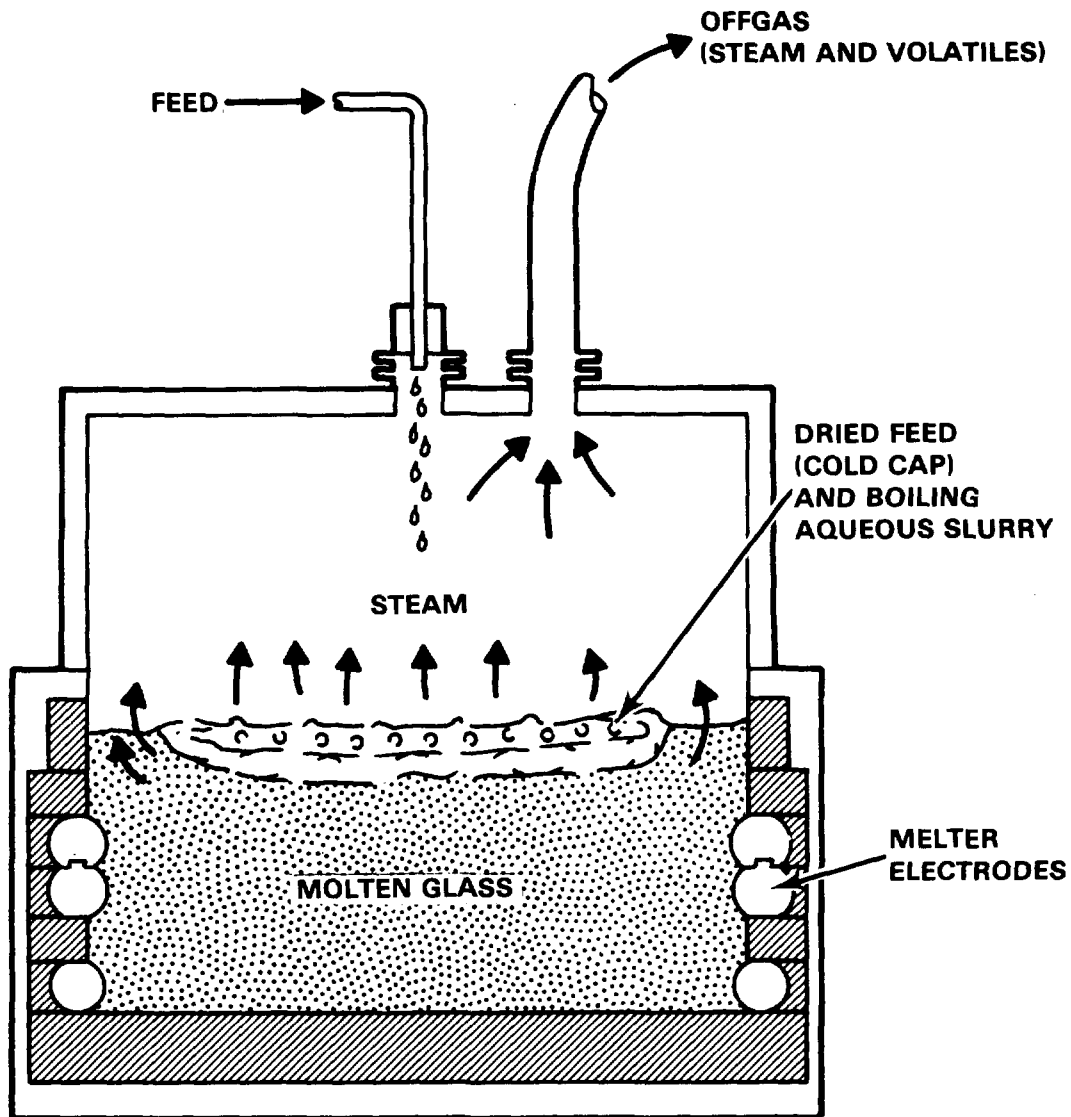


Figure 1. Liquid-fed, joule-heated ceramic melter system.

17th DOE NUCLEAR AIR CLEANING CONFERENCE

these melters are nominally 40 kg/h-m² for unboosted operation, and 60 kg/h-m² when auxiliary plenum heaters are employed. Table I summarizes all important operational parameters associated with liquid-fed melter tests involving the LFCM and PSCM melters. These melter tests, which are arranged chronologically in Table I, form the bases of the experimental off-gas studies which are discussed below.

Melter Off-Gas System

Both melters being studied in this report share a common 0.1-m (4-in.) stainless steel off-gas system consisting of an ejector venturi, a downdraft condenser, a packed scrubbing tower and a final absolute filter, physically arranged in the order listed. In addition to these common off-gas elements, both melters are equipped with a close-coupled HEPA filter receptacle and a total (condensable and noncondensable) off-gas flowmeter. Since the purpose of the DWPF off-gas support studies was to establish melter off-gas characteristics, the performance of the generic off-gas processing equipment present in the common melter off-gas system was of little programmatic interest and consequently will not be discussed here.

Feed Composition

The liquid slurry feed used in the SRL-DWPF melter development program is a uniform mixture of simulated defense waste sludge and glass formers (frit). The composition of this slurry as equivalent oxides is detailed in Table II. The actual waste loading of the slurry is 29 wt% of the total oxides present. In addition to the major elemental constituents listed in Table II, SRL simulated waste also contains stable elemental substitutes for all volatile and semi-volatile isotopes which are present in typical defense waste and which are of radiological concern. The trace elemental composition of the SRL feed slurry is presented in Table III.

Although the waste composition of the liquid feed remained essentially constant throughout the period of testing covered in this report (see Table II), the rheology of the feed was dramatically affected with the addition of formic acid to the DWPF waste stream flowsheet. Initial experiments were conducted with an alkaline (pH 11 to 12) slurry having the physical characteristics of a Bingham plastic fluid. Acidification (pH 5 to 6) of the liquid waste stream with formic acid resulted in slurries which behaved more like an ideal Newtonian fluid. The presence of formic acid in melter feed slurries not only changed the fluidic properties of the feed, it also dramatically influenced the off-gas emission properties of the liquid-fed melter.

III. Melter Effluent Characterization

One of the major tasks involved in the DWPF off-gas studies was that of determining melter emission characteristics. The nature and extent of melter-generated effluents had to be established before off-gas system criteria could be finalized for the DWPF melters. Consequently, an off-gas sampling system was developed to provide this basic off-gas design data.

Table I. Liquid-fed melter operational parameters.

Operational Parameters	Experiment									
	PSCM-1	LFCM-4	PSCM-2	LFCM-6	PSCM-3	LFCM-7	PSCM-4	PSCM-5	PSCM-6	PSCM-7
Feed Type	Basic	Basic	Basic	Basic	Acidic	Acidic	Acidic	Acidic	Acidic	Acidic
Feed Rate, L/h-m ²	45	90	110	100	62	121	83	100	122	68
Glass prod. Rate, kg/h-m ²	22	41	50	45	28	57	39	50	60	43
Plenum Temp., °C	400	600	400-800	600	300	500	400	520	850	300
Boosting Type	None	Elec. Lid Heat	Propane Combustion	Elec. Lid & Plasma Torch	None	Elec. Lid Heat	None	Elec. Lid Heat	Elec. Lid Heat	None
Boosting Power, kW	--	30	35	40	--	15	--	36	55	--
Off-Gas Temp., °C	375	375	375	400	250	300	275	375	400	270
Off-Gas Cooling, L/h	0	8	23	24	0	Variable	0	23	23	0
Experiment Duration, h	120	120	120	120	125	111	107	99	138	115

Table II. Simulated waste slurry and glass compositions.

Waste Slurry Composition				Typical Slurry and Glass Oxide Composition*					
Alkaline Waste		Acid Waste		Equivalent Oxide Concentration, g/L					
Compound	Conc., g/L	Compound	Conc., g/L	Oxide	Waste Sludge	Frit-131 [†]	Zeolite ^{††}	Total	Final Glass Composition, Wt. %
Frit-131	338.0	Frit-131	341.3						
Zeolite	14.7	Zeolite	9.9						
Anth. Coal	3.30	HCHO ₂	>18.0	Fe ₂ O ₃	60.7			60.7	12.7
Fe(OH) ₃	90.9	Fe(OH) ₃	81.2	Al ₂ O ₃	22.3		1.9	24.2	5.1
Al(OH) ₃	21.0	Al(OH) ₃	34.2	MnO	13.8			13.8	2.9
MnO ₂	19.5	Mn(CHO ₂) ₂	28.2	NiO	4.1			4.1	0.8
Ni(OH) ₂	10.4	Ni(CHO ₂) ₂	8.3	CaO	7.2		1.1	8.3	1.7
CaCO ₃	8.90	Ca(CHO ₂) ₂	16.7	SiO ₂	15.6	197.6	4.7	219.9	45.6
SiO ₂	5.84	SiO ₂	15.6	Na ₂ O	4.6	60.4	0.2	65.2	13.6
NaOH	4.93	NaCHO ₂	8.42	Na ₂ SO ₄	0.7			0.7	0.1
NaNO ₃	2.01	NaNO ₃	2.01	B ₂ O ₃		50.2		50.2	10.5
Na ₂ SO ₄	0.73	Na ₂ SO ₄	0.72	Li ₂ O		19.4		19.4	4.1
				MgO		6.8		6.8	1.4
				TiO ₂		3.4		3.4	0.7
				La ₂ O ₃		1.7		1.7	0.4
				ZrO ₂		1.7		1.7	0.4
				TOTAL	129.0	341.2	7.9	480.1	100.0

* Feed slurry glass content = 0.48 kg/L.

(†) Frit-131 Composition (-200 mesh).

Oxide	Wt%
SiO ₂	57.9
B ₂ O ₃	14.7
Na ₂ O	17.7
Li ₂ O	5.7
MgO	2.0
TiO ₂	1.0
La ₂ O ₃	0.5
ZrO ₂	0.5
TOTAL	100.0

(††) Zeolite Composition (Linde Ionsiv IE-95)

Component	Wt%
CaAl ₂ Si ₄ O ₁₂ ·6H ₂ O	80
Na ₄ Ca _{1.5} Al ₃ Si ₈ O ₂₄ ·8H ₂ O	20
TOTAL	100
Assumed Oxide Forms	Wt%
CaO	10.6
Al ₂ O ₃	19.2
SiO ₂	47.7
Na ₂ O	2.5
H ₂ O	20.0
TOTAL	100.0

17th DOE NUCLEAR AIR CLEANING CONFERENCE

Table III. Concentration of trace melter feed additives.

Trace Additives	Concentration, g/L	
	Oxides	Elemental
Cs ₂ O	0.25	0.24
SrO	0.098	0.083
Sb ₂ O ₃	0.16	0.060
SeO ₂	0.04	0.029
CdO	0.38	0.033
TeO ₂	0.05	0.036
RuO ₂	0.085	0.064

Melter Off-Gas Sampling Network

The sampling network, which was developed in support of melter emission characterization studies, is schematically illustrated in Figure 2. The components making up this network were designed to determine the composition of melter exhaust with regard to the effluents listed below.

- Gases: H₂
- N₂
- O₂
- CO
- CO₂
- SO₂
- Semivolatiles: Cs
- Sb
- Se
- Te
- Mn (Tc)
- Ru
- Cd (Cm)
- Sr
- Halogens
- Others
- Particulates

The gaseous composition of melter off-gas emissions was established using a gas chromatograph (GC) and real-time gas analyzers. The gas sample stream used for this purpose is extracted prior to any off-gas processing. This hot, water-laden gas stream is first passed through a tube and shell condenser, which reduces the water loading of the gas while minimizing the gaseous interactions with condensed-phase water. The quenched gas stream is subsequently passed through a filter and a permeation dryer and is finally distributed to the individual gas analyzers using a stainless steel bellows pump.

The GC used in these studies is programmed to sample and analyze the composition of the continuously-flowing gas stream every 30 min. The gaseous components, which are routinely quantified by this instrument, include O₂, N₂, CO and CO₂. In addition, the GC pro-

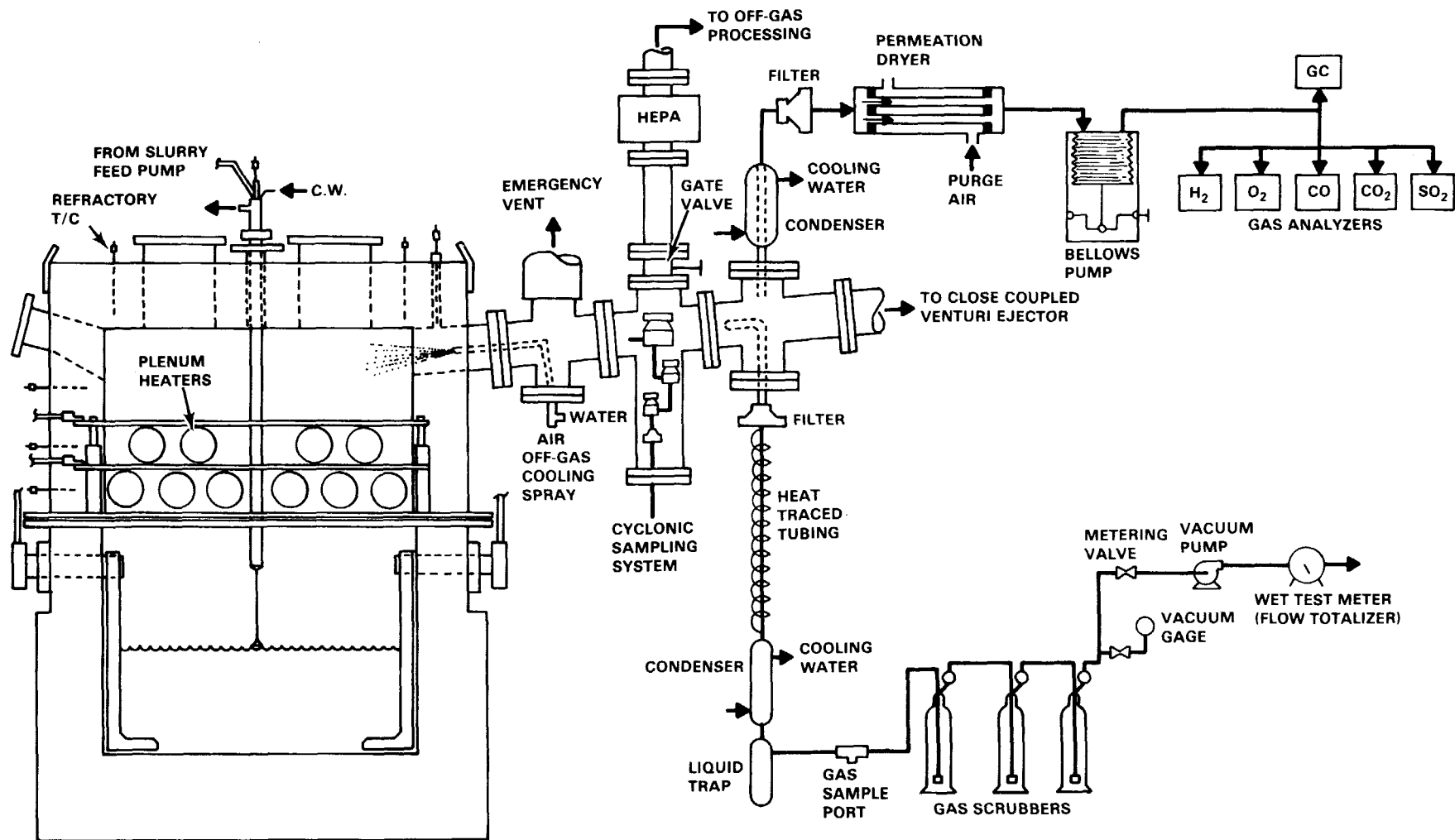


Figure 2. Melter off-gas sampling network.

17th DOE NUCLEAR AIR CLEANING CONFERENCE

vides semi-quantitative information with regard to gaseous concentrations of H_2 , SO_2 and NO_x .

Real-time measurements of melter off-gas concentrations were initiated during the latter part of this study with the installation of five continuous gas monitors. These instruments have provided continuous compositional off-gas data with regard to H_2 , O_2 , CO , CO_2 and SO_2 for all melter tests following the PSCM-4 experiment.

Characterization of the pathways and magnitudes of melter-generated semivolatile emissions were assessed using a differential sampling system composed of a filter, a heat-traced sampling line, a condenser and a series arrangement of three gas scrubbing units (Figure 2). The distribution of semivolatiles across the five discrete sample fractions generated by the system were analytically determined using emission spectrometry (ICP), atomic absorption (AA), ion chromatography (IC) and x-ray fluorescence techniques. All semivolatile studies conducted have been exclusively concerned with characterizing the unquenched melter exhaust composition.

Melter-generated aerosols were characterized with regard to concentration, size and composition. Total off-gas particulate loading was most directly established, gravimetrically, by HEPA filtration of the entire melter off-gas stream (Figure 2). Particle size information is obtained from a cyclonic sampling system consisting of a series arrangement of three cyclones and a final absolute filter. The cut points of the cyclones employed are 16 μm , 6 μm and 1 μm at 18 actual L/m. The final absolute filter is designed to collect submicron fines which are able to pass through all three preceding cyclones. The elemental composition of the particulate matter collected by these sampling devices is established using ICP, AA and IC analytical techniques.

Melter Exhaust Composition

The noncondensable ($20^\circ C$) gases generated by liquid-fed melters are functionally dependent upon the slurry feed composition as well as melter operating conditions. The alkaline waste feed used during the initial stages of this study possessed very low concentrations of organic matter. Consequently, the gross melter off-gas composition was essentially CO_2 -enriched inleakage. The emission rates of the combustible gas CO during all of the alkaline feed tests were always less than 1/10 the rate associated with CO_2 . Table IV summarized the average gross compositional data associated with alkaline-feed melter exhausts. The dramatic difference existing between the PSCM-2 data and that of all other experiments listed in Table IV is due to the method of boosting used in that test. During PSCM-2, a propane torch was used to supply supplemental heat to the melter plenum in order to facilitate increased feeding rates. Consequently, the major source of off-gas combustion products was the boosting torch and not the melter. Figure 3 illustrates the time-correlated behavior of the gross composition of the melter exhaust during the PSCM-2 test. The relationships illustrated are consistent with the propane combustion process.

The composition of melter-generated, noncondensable gases was dramatically affected when formic acid was added to the simulated

Table IV. Melter noncondensable off-gas composition (basic waste).

Experiment	Melter Inleakage, scfm	Molar %											
		CO ₂			CO			O ₂			N ₂		
		Hi	Avg	Lo	Hi	Avg	Lo	Hi	Avg	Lo	Hi	Avg	Lo
PSCM-1	5-10	6.4	3.4	1.8	<0.01	--	--	20	14.0	7.1	89	81	73
LFCM-4	32	1.1	0.58	0.40	0.03	0.02	0.001	21	20.5	20.0	78	78	78
PSCM-2	45	8.6	4.6	0.20	3.0	0.50	0.001	21	14.0	8.0	82	80	79
LFCM-6	29	0.87	0.54	0.13	0.07	0.02	<0.001	20	20.0	18.0	80	79	78

Table V. Melter generated off-gas components (acid waste).

Experiment	Melter Inleakage, scfm	Molar %								
		CO ₂			CO			H ₂		
		Hi	Avg	Lo	Hi	Avg	Lo	Hi	Avg	Lo
PSCM-3*	20	2.9	1.3	0.26	1.3	0.40	0.04	1.11	NA	0.17
LFCM-7	90	2.2	0.74	0.03	0.44	0.13	0.002	0.63	0.54	0.40
PSCM-4	20	4.4	2.9	1.5	0.75	0.44	0.20	1.3	1.1	0.94
PSCM-5	30	6.5	2.8	2.0	0.90	0.35	0.10	1.8	0.80	<0.10
PSCM-6	30	6.5	4.1	2.0	0.60	0.09	<0.005	1.2	NA	<0.05
PSCM-7	12**	8.0	5.0	1.5	1.2	0.75	0.10	3.5	1.9	0.30

* Sample stream diluted ~2.5 times.

** Off-gas dilution was used.

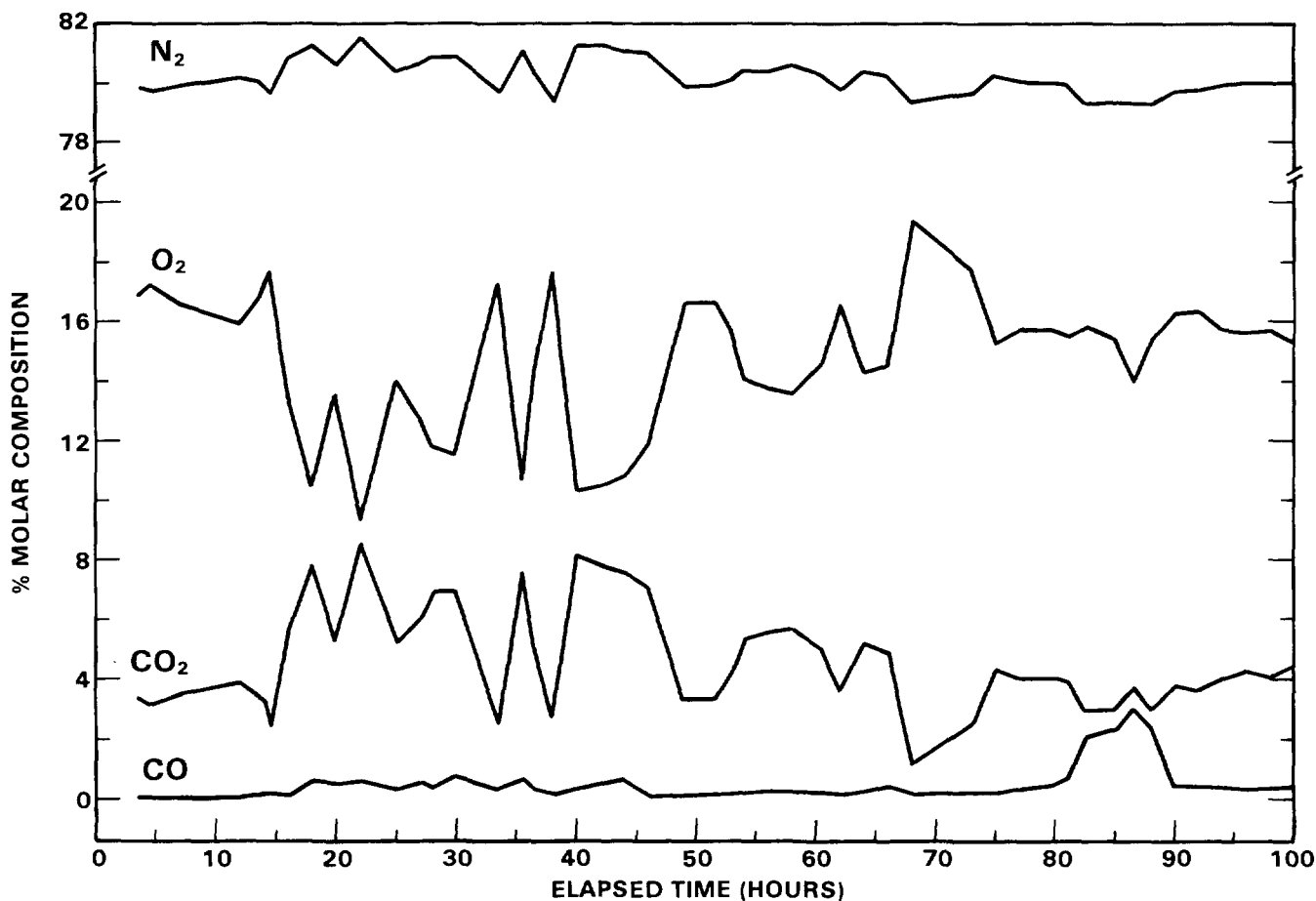


Figure 3. Combustion boosted melter exhaust composition.

melter feed. This compositional alteration increased the organic loading in the melter feed by approximately an order of magnitude. Consequently, melter exhaust gases were of particular interest during these acidified feed tests due to the possibility of generating H₂ and CO (water gas) in sufficient quantities to present a flammability hazard after off-gas quenching. Figure 4 illustrates the time-related behavior of gross melter exhaust gases during a 120-h melter test which employed 100 h of radiant lid heat boosting followed by 20 h of unboosted operation. The presence of plenum heaters during liquid feeding clearly reduces melter emissions of the combustible gases H₂ and CO. With the termination of lid heating, the melter plenum cooled, reducing the oxidation rates of these gases sufficiently to allow significant quantities of each gas to escape the plenum through the off-gas system. This result is quite reproducible; however, virtual elimination of combustible gas emissions during boosting, as is illustrated in Figure 4, may not always be achievable. Similarly, the concentration of combustibles leaving an unboosted melter may be significantly higher than is indicated in Figure 4 since they are slurry composition-, temperature-, feed and inleakage rate-dependent variables. Indeed, dilution air was required during the unboosted PSCM-7 test to reduce H₂ in the quenched off-gas stream to below 70% of its lower inflammability limit (~4%). A summary of the gaseous concentrations of organic

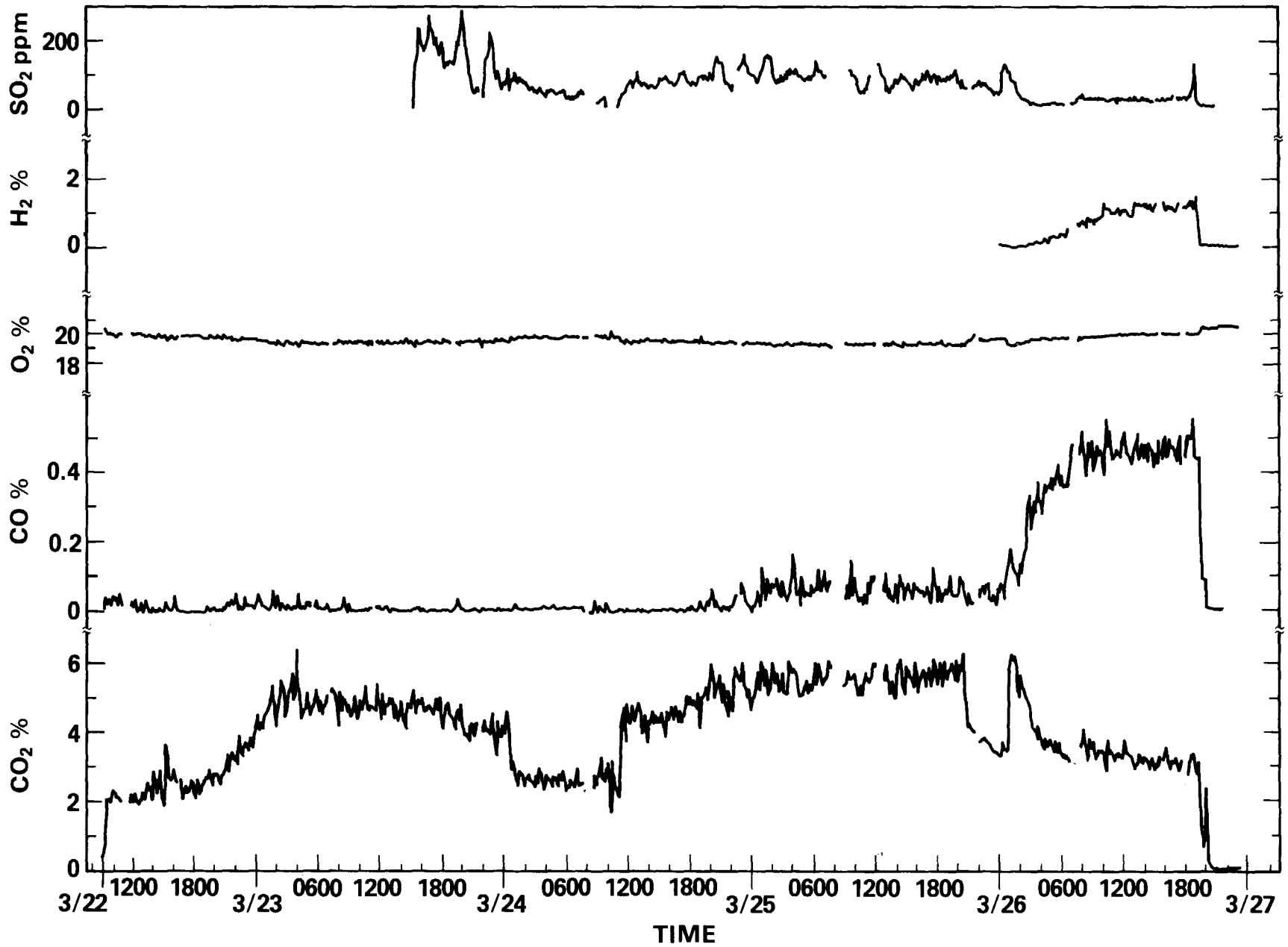


Figure 4. Melter exhaust gas composition of a 100-h boosted, 20-h unboosted test.

17th DOE NUCLEAR AIR CLEANING CONFERENCE

decomposition and reaction products generated during all formate feed melter testing is presented in Table V, along with average melter inleakage rates.

The off-gas data presented in Figure 4 clearly illustrates that melter generated emissions are not smooth and continuous functions even under the most controlled operational conditions. This behavior is due to the erratic, nonuniform way in which melter feed is dried, oxidized and melted during the liquid feeding process. Large excursions in melter gas generation rates usually occur when dammed up liquid feed lying atop an insulating layer of dry feed (the cold cap) abruptly flows out upon a hot glass surface. The liquid quickly flashes off this hot surface, producing a flow pulse composed of steam and volatile organic reaction products. Figure 5 illustrates the behavior of some of the more important melter-generated gases accompanying flow surging events. The frequency and magnitude of these surging events are positive indicators of melter system instabilities which are most often associated with erratic or overfeeding conditions.

The ability of melter-generated gases to accompany steam flow surges suggests that the evolution of combustible gases from the melter cold cap is quite prompt. Figure 6 portrays the time-dependent compositional behavior of the melter exhaust stream upon feed interruption or termination. With the exception of SO_2 , none of the melter-generated gases increase in concentration when feeding was terminated. This fact implies that volatile decomposition and reaction products generated from the melter feed are formed soon after introduction of the feed into the melter environment. Consequently, significant accumulations of chemically-reactive organic feed components within the melter cold cap apparently do not occur under stable steady-state feeding conditions.

On the other hand, the increase in terminal SO_2 exhaust concentration (illustrated in Figure 6) suggests sulfur, as Na_2SO_4 , may be accumulating within the melter as a molten salt. This was indeed found to be the case, as post-run inspection of the idling melter glass surface later proved. This observation stimulated speculation that accumulations of Na_2SO_4 could be responsible for changes in the melting capacity of liquid-fed melters that occur during the initial ~24 hours of liquid feeding (the startup phase). Melter emission characteristics of SO_2 further support this notion, as is shown in Figure 7. During the initial startup phase, when the melter's ability to handle feed is limited, feed-rate normalized SO_2 emission rates are uncharacteristically low, indicating that accumulation of Na_2SO_4 is probably occurring. As processing continues at a fixed feeding rate, SO_2 emission rates gradually increase along with the melting capacity of the liquid-fed melter. It is known⁽³⁾ that the presence of a molten Na_2SO_4 phase within a ceramic melter will increase the heat transfer rate between the molten glass and the feed, thereby boosting melting capacity. All of the above-mentioned liquid-fed melter characteristics are consistent with this fact.

Although Figure 7 suggests that SO_2 evolution is an important mechanism responsible for sulfur melter feed losses, this is true only for boosted experiments where plenum temperatures are greater

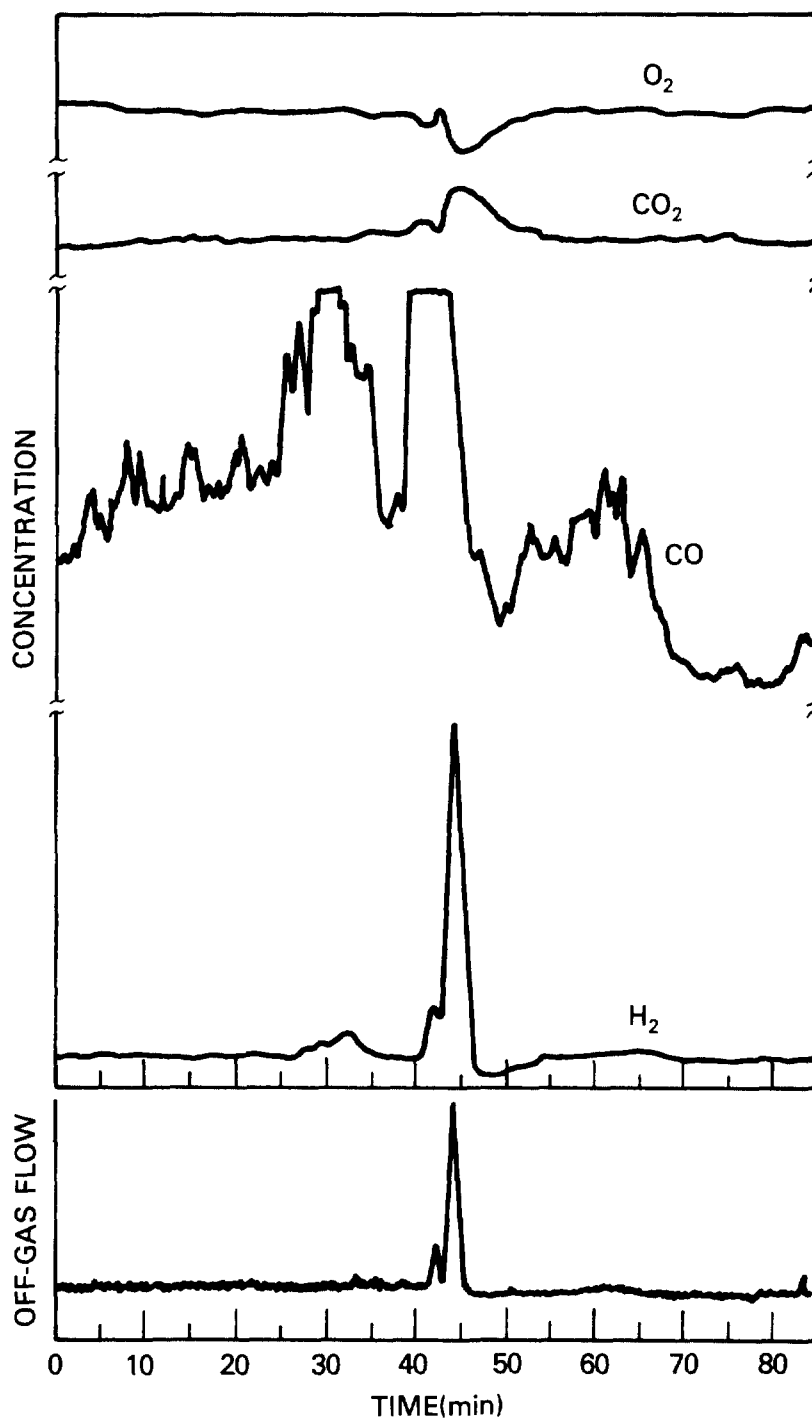


Figure 5. Compositional behavior of noncondensable melter exhaust gases accompanying a flow surge. (Maximum extent of the surge event: flow-3X; $H_2 < 3.5\%$; $CO \gg 0.5\%$; $CO_2-15\%$; $O_2-17\%$.)

than $700^\circ C$. Emission rates of SO_2 during unboosted runs are at least an order of magnitude lower than when boosting techniques are employed. However, total melter losses of sulfur are found to be more or less independent of boosting, indicating the presence of other volatile chemical channels of escape (SO_3). Filtered gas-scrubbing techniques have further verified that significant

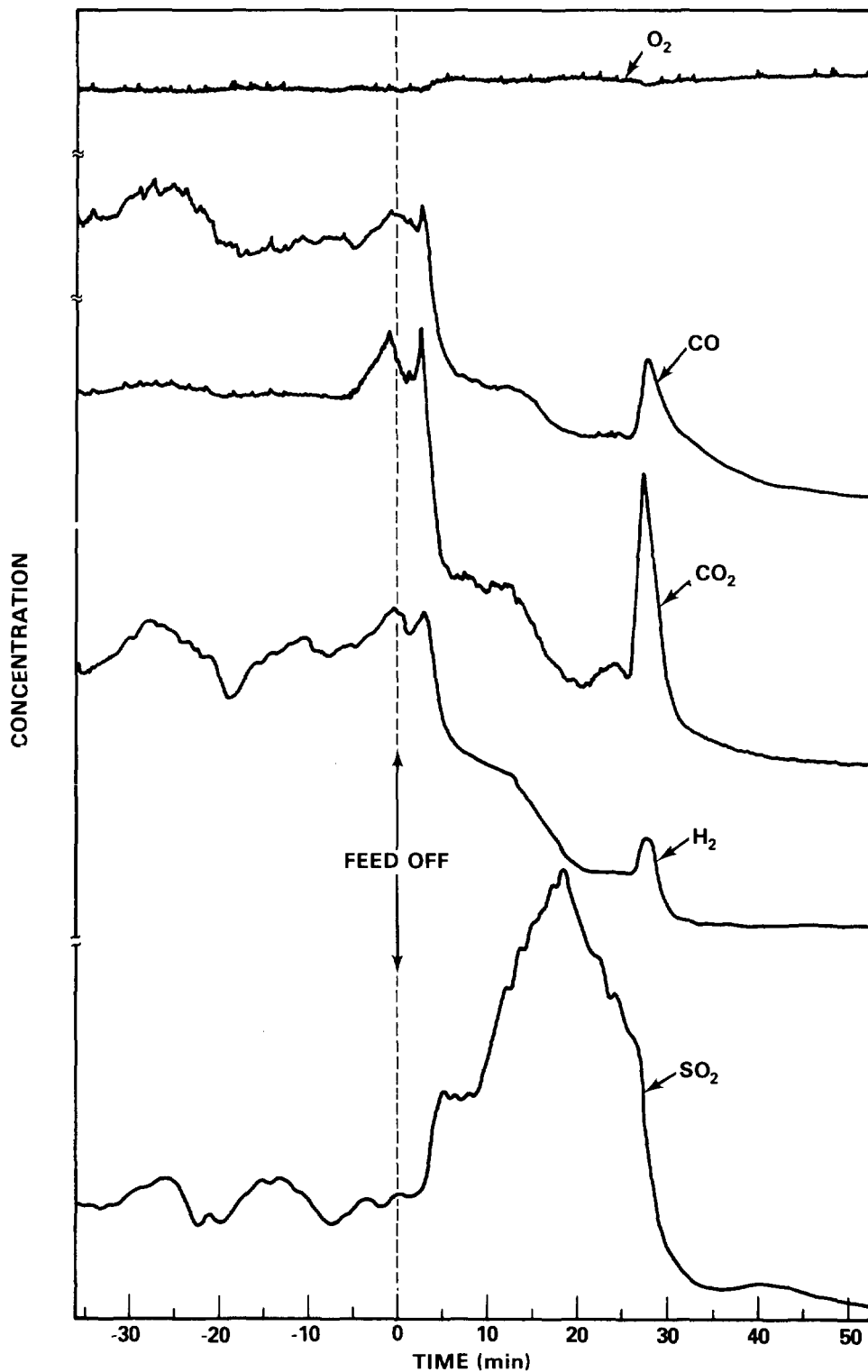


Figure 6. Melter off-gas compositional behavior associated with feed termination. (The $t = 30$ min compositional spike is due to the injection of a small quantity of liquid feed.)

concentrations of acidic volatile gases of sulfur as well as the halogens always exist in unquenched melter exhaust streams independent of any and all melter operating conditions. This subject will be further developed in discussions that follow.

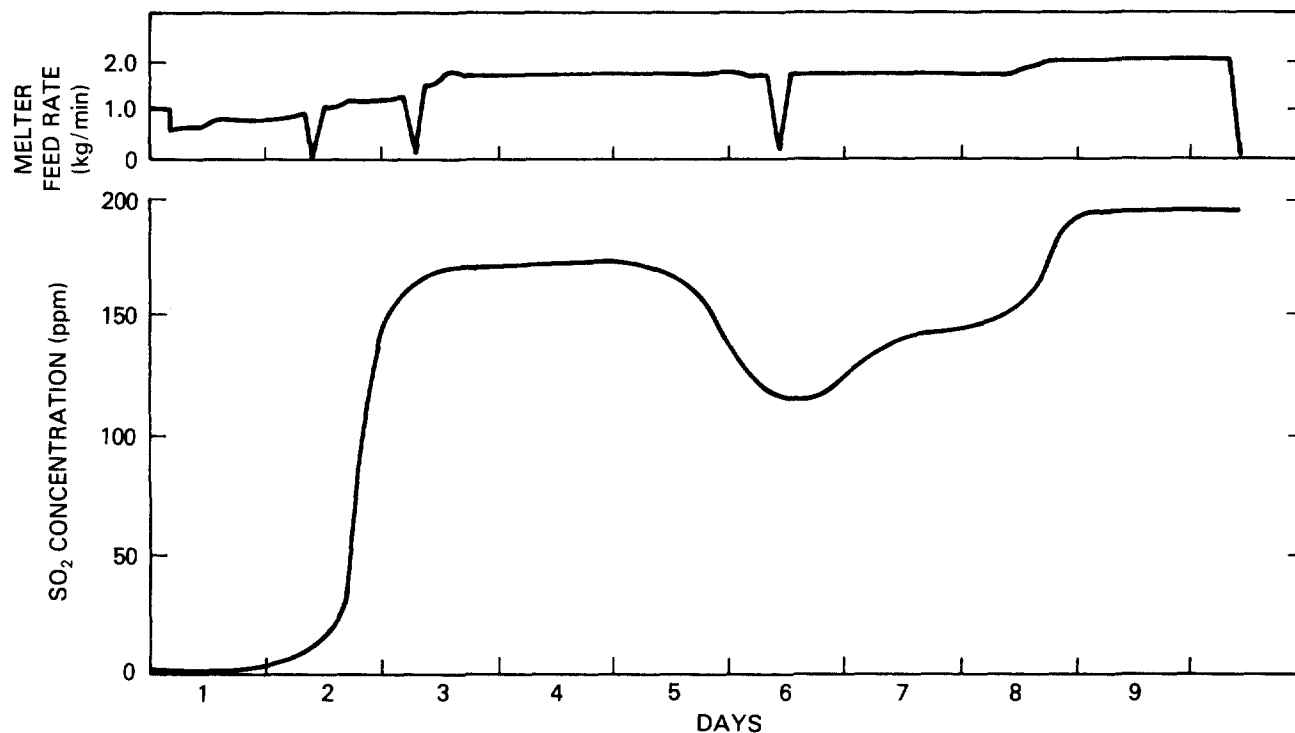


Figure 7. Melter SO₂ emission characteristics accompanying a ~240-h test.

Nature of Melter Feed Component Losses

In order to characterize the pathways and magnitudes of melter feed component losses, a differential sampling system composed of an aerosol filter, condenser and a series arrangement of three gas-scrubbing units was employed. The manner in which any given element is distributed across the five discrete sampling fractions of this device is indicative of the physical state or states assumed by the effluent. Typical data generated with this differential sampling system during a formate-feed melter test is summarized in Table VI. The DF values listed in this table are melter decontamination factors, which are ratios of the rate at which feed components enter the melter to the rate at which they are evolved. Particulate DFs are partial DFs relating to only a single loss mechanism: aerosol emission. The data presented in this abridged table clearly shows that melter gas-phase losses to the off-gas system are only significant for Cl, S and B, which readily form volatile acid gases previously referred to. This is not to say that melter-induced volatilization has no influence upon melter losses of other feed component elements. On the contrary; the low DFs associated with the semivolatile elements Cd, Cs and Te, as well as Se and Sb, clearly underscore the importance of this volatilization process. What is being said is that apart from the mechanisms responsible for producing airborne effluents, particulate transport through the off-gas system is the predominant loss mechanism associated with liquid-fed melter operation.

17th DOE NUCLEAR AIR CLEANING CONFERENCE

Table VI. PSCM-6 particulate and total feed component DFs.

<u>Element</u>	<u>Average DF</u>	
	<u>Particulate</u>	<u>Total</u>
Al	27,000	22,000
B	6,800	100
Cd	9.9	9.9
Cl	21	2.9
Cs	14	14
Fe	1,900	1,800
La	2,100	2,100
Mn	1,800	1,800
Na	300	300
S	11	5.5
Sr	1,800	1,800
Te	3.0	3.0
Zr	22,000	22,000

Characteristics of Melter Aerosols

Since most melter off-gas system losses are associated with aerosol emission, establishing the characteristics of these aerosols was of particular engineering interest. The size distribution of melter-generated aerosols was established using a cyclonic particle-size analysis system, which was described earlier. Table VII details the manner in which melter particulate matter was distributed across the cyclonic sample fractions as a function of melter experiment. All melter tests, with the exception of PSCM-4, exhibited aerosol-size distributions which were definitely bimodal in nature. This suggests that the overall aerosol distribution may be comprised of two independent components, each having its own characteristic size distribution. Gross compositional dissimilarities between the discrete cyclonic size fractions illustrated in Table VIII strongly reinforce this argument. Moreover, since the submicron size fraction detailed in this table (LFCM-7) contains only 12% of the total sample mass, but possesses essentially all the semivolatile matter of the sample, the mechanism responsible for the small diameter component of the overall distribution is probably a volatilization/condensation process that occurs within the melter plenum. The composition of the large cyclonic size fractions are very similar to that of the slurry feed as shown in Table IX. Consequently, the large component of the bimodal distribution must almost certainly be associated with a gross entrainment mechanism.

Since the major melter loss mechanism associated with the radiologically important semivolatiles is associated with submicron aerosol emission, the elemental makeup of this size fraction is of particular interest. Table X presents representative submicron compositional data collected during the PSCM-4 experiment. If one attempts to conduct a material balance for this submicron matter by assuming an oxide form for all elements except for a stoichiometric quantity of Na, which is associated with the Cl in the sample, one can account for 99% of the matter present. It should be noted that while the submicron sample fraction is quite rich in semivolatiles, it is essentially salt (83 wt% NaCl).

17th DOE NUCLEAR AIR CLEANING CONFERENCE

Table VII. Size distribution of melter aerosols.

Experiment	Average wt% Versus Cut Point			
	16 μm	6 μm	1 μm	<1 μm
LFCM-7	76.7	2.8	8.5	11.9
PSCM-4	--	0.9	3.6	95.6
PSCM-5	13.5	3.9	20.2	62.2
PSCM-6	46.1	0.5	12.7	40.7
PSCM-7	7.5	3.2	9.4	79.9

Table VIII. Elemental distribution across cyclonic sampling system.

Element	Elemental Distribution, %			
	16 μm	6 μm	1 μm	<1 μm
Al	96.2	0.9	2.5	0.4
B	87.8	1.8	7.8	2.6
Ba	83.7	5.8	10.5	0
Ca	77.7	2.7	15.2	4.4
Cd	10.7	0.8	7.3	81.2
Ce	92.1	0	7.9	0
Cr	46.4	21.7	23.3	8.6
Cs	7.5	0	5.4	87.1
Cu	82.6	4.9	4.2	8.3
Fe	77.3	2.6	17.0	3.1
La	91.9	1.5	6.1	0.5
Li	83.2	1.5	5.3	10.0
Mg	91.5	1.6	5.8	1.1
Mn	89.4	6.4	3.6	0.6
Mo	77.5	5.6	9.8	7.1
Na	68.8	1.7	5.6	23.9
Nd	93.4	0	6.6	0
Sb	100.0	0	0	0
Se	56.9	1.9	11.4	29.8
Si	92.0	1.8	5.6	0.6
Sr	77.6	2.8	19.6	0
Te	5.5	0.4	3.2	90.9
Ti	91.2	1.8	6.0	1.0
Zr	91.6	1.6	5.6	1.2

Melter Emission Performance

Melter performance with regard to effluent emission is commonly expressed in terms of a unitless decontamination factor or DF. By definition, a melter feed component DF is the ratio of the rate at which that particular feed component enters the melter to the rate at which it is evolved from it. Consequently, melter DFs are related to the liquid-fed melter process efficiencies for converting feed components into a borosilicate glass. Table XI presents experimental feed component DFs for all pertinent DWPF melter tests conducted at PNL. The entries in this table are grouped according to feed type and each group is ordered with respect to the experimental melter employed. This ordering has significance with regard to the interpretation of the data. The initial melter tests conducted with

17th DOE NUCLEAR AIR CLEANING CONFERENCE

Table IX. Composition of 16 μm cyclonic sample fraction.

Compound	Wt%	
	16 μm	Feed
Al_2O_3	3.4	5.1
B_2O_3	9.0	10.5
CaO	1.6	1.7
Fe_2O_3	14.4	12.7
La_2O_3	0.3	0.4
LiO_2	3.5	4.1
MgO	1.1	1.4
MnO	3.2	2.9
Na_2O	13.0	13.6
SiO_2	38.0	45.6
TiO_2	0.7	0.7
ZrO_2	0.3	0.4

alkaline feed were, with one exception, all boosted experiments (see Table I). Consequently, a major goal of all of these tests was to establish maximum melter feeding rates under a variety of plenum heating conditions. To complicate matters, an evolving slurry feed system being developed during this same period was often responsible for inconsistent feed delivery to the melter. As a result, stable steady-state operating conditions during these early melter scoping tests were rarely, if ever, achieved. The spread in melter emission performance data during this initial testing phase is in large part a reflection of the unequilibrated conditions that existed when this data was collected. The average DFs listed for the alkaline feed components should, however, provide a fairly representative description of the ceramic melter effluent emission behavior that occurred during this initial development period.

With the exception of the LFCM-7 test (melter capacity scoping study), all acid feed melter experiments sought to establish operational stability under a variety of running conditions. Table XII presents partial melter DFs associated with off-gas aerosol emission for the PSCM-5 and PSCM-6 experiments. The data associated with each of these tests were collected over several days of stable, steady-state melter operation using three independent sampling devices. The internal agreement between results obtained in each test is, without question, indicative of the stability associated with each of these experiments. Consequently, effluent results of individual acid feed experiments should be more representative of average melter behavior than were those associated with the alkaline feed.

A comparison of melter DFs achieved with alkaline and acidic waste slurries reveals that, with only a single exception, higher effective emission rates (lower DFs) were observed for the

17th DOE NUCLEAR AIR CLEANING CONFERENCE

Table X. Submicron particulate composition.

<u>Element</u>	<u>Elemental Wt%</u>	<u>Assumed Form</u>	<u>Compound Wt%</u>	<u>Feed Composition, %</u>
Al	0.04	Al ₂ O ₃	0.08	4.95
B	0.07	B ₂ O ₃	0.24	9.86
Ca	0.14	CaO	0.20	1.66
Cd	0.55	CdO	0.63	0.006
Cs	2.1	Cs ₂ O	2.2	0.044
Cu	0.06	CuO	0.09	--
Fe	0.29	Fe ₂ O ₃	0.41	13.69
K	0.36	K ₂ O	0.43	--
Li	1.1	Li ₂ O	2.4	3.98
Mg	0.02	MgO	0.03	1.29
Mn	0.08	MnO ₂	0.13	3.25
Na	33.7	} NaCl Na ₂ O	83.0	--
			6.7	13.88
Ni	0.03	NiO	0.04	0.76
Pb	0.04	PbO	0.05	--
Si	0.66	SiO ₂	1.4	44.47
Te	0.56	TeO ₂	0.71	0.006
Zn	0.02	ZnO	0.02	--
Cl	55.0	--	--	0.4
TOTAL			98.8	

radiologically important semivolatiles when acidified melter waste was employed. The reducing power of the formic acid feed component apparently promotes volatilization in the plenum and thereby produces greater effective off-gas losses of these elements.

Ruthenium is an exception to the above statement. Ever since melter experiments with a formate feed formulation began, no significant airborne ruthenium has been detected in melter exhaust streams, except for the very atypical LFCM-7 test. Feed and glass sample analyses, on the other hand, indicate significant ruthenium melter losses (DF = 2), and yet no specific sink has been conclusively identified to account for these losses. In all probability, ruthenium is being reduced by the formic acid to its elemental state, whereupon it is lost to the melter floor as slag. A surface plate-out mechanism is a possible, but less likely, explanation for these losses; however, no evidence of off-gas line plating has ever been found. A thorough examination of the melter and its plenum is planned to establish the nature of the observed ruthenium losses.

The effect of feed-boosting techniques upon overall melter emission performance has been studied under controlled conditions. If

Table XI. Melter effluent emission performance.

Element	Alkaline Feed Melter DFs					Acid Feed Melter DFs					
	PSCM-1	LFCM-4	PSCM-2	LFCM-6	Average	LFCM-7	PSCM-3	PSCM-4	PSCM-5	PSCM-6*	Average**
Al	11000	530	990	330	3200	190	6000	23000	14000	22000	16000
B	210	130	160	90	150	75	200	230	140	100	170
Ca	1840	260	610	180	720	62	1100	1900	1100	1200	1300
Cd	190	70	47	80	100	8.0	--	9.2	5.7	9.9	8.3
Cl	3.1	2.2	3	2.7	2.8	--	4	5	1.5	2.9	3.4
Cs	51	57	3	10	30	12	3.8	16	9.4	14	11
Fe	3800	260	680	230	1200	69	1600	2000	1100	1800	1600
La	--	--	--	--	--	--	--	--	10000	2100	6100
Li	1900	310	340	160	680	89	2600	3200	730	1300	2000
Mg	9000	350	920	260	2600	120	8200	--	3500	7800	6500
Mn	5700	420	630	330	1800	76	3300	2100	7100	1800	3600
Na	830	340	130	90	350	60	900	180	160	300	390
Nd	--	--	--	--	--	--	--	--	--	2500	--
Ni	1500	260	--	930	900	--	9400	1400	580	1100	3100
Ru	32	26	48	13	30	16	--	--	--	--	--
S	1	1	19	11	8	--	8	16	4.5	5.5	8.5
Sb	--	1800	100	--	950	67	--	--	440	--	--
Se	--	--	--	--	--	1	--	--	130	--	--
Si	15000	420	1600	280	4300	120	3000	9200	5300	13000	7600
Sr	7400	204	640	290	2100	55	640	250	--	1800	900
Te	170	62	58	210	130	5.6	32	3.1	3.1	3.0	10
Ti	--	--	1400	170	790	120	4100	8700	7200	5900	6500
Zr	--	--	--	--	--	--	--	5000	13000	22000	13000
Total ±σ	1100	290	430	180±10	500	120±50	980	490±30	480±90	800±80	690

* Slightly different frit used in this test.

** LFCM-7 not used in averaging.

Table XII. Steady state aerosol emission performance

PSCM-5 Boosted Test				PSCM-6 Boosted/Unboosted Test			
Sample Type*	Feed Rate, L/h	Particulate		Sample Type*	Feed Rate, L/h	Particulate	
		Loading, mg/L	DF			Loading, mg/L	DF
C	51	0.55	470	S	68	0.29	820
S	72	0.49	460	HEPA	68	--	810
S	79	0.44	510	C	67	0.37	840
C	81	0.61	440	S	74	0.25	910
HEPA	81	--	370	C	90	0.41	700
S	86	0.48	492	S	91	0.28	840
C	93	0.78	440	HEPA	90	--	720
HEPA	93	--	670	S	58**	0.32	870
ALL			480	C	58**	0.54	660
				ALL			800

* C = cyclone; S = differential samples; HEPA = absolute filtration.

** Unboosted operation.

the previous melter stability comments are neglected, Table XI strongly suggests that melter DFs are dramatically reduced when boosting is employed. However, tests designed to illustrate this effect have failed to show any significant relationships between feeding rates and melter emission performance. Table XII presents gross aerosol DF values associated with the boosted PSCM-5 and PSCM-6 tests. Clearly, this data shows no correlation between feeding rates and DF. Moreover, the boosted PSCM-6 experiment did not utilize electric radiant lid heaters for the entire melter test, yet no significant differences in melter emission performance were observed throughout the experiment. Consequently, this data suggests that electric radiant plenum heaters can be employed to boost liquid feeding rates of ceramic melters without significantly deteriorating melter emission performance.

The implementation of feed-boosting techniques, however, are not without operational difficulties. The high exhaust stream temperatures ($>600^{\circ}\text{C}$) resulting from the auxiliary plenum heaters present various off-gas problems associated with the formation of fused off-gas-line deposits and accelerated material corrosion rates. A cooling spray (see Figure 1) has been successfully used to control exiting melter exhaust gas temperatures to 400°C or less. However, the spray nozzle itself acts to collect entrained feed. These feed deposits ultimately grow to form a local obstruction to melter off-gas flow. Although these deposits are soft and easily removed, the current cooling spray configuration clearly compromises melter off-gas system design.

IV. Melter Idling Test

Because of the high ($\sim 1000^{\circ}\text{C}$) plenum temperatures associated with idling (unfed) joule-heated ceramic melters, volatilization losses of radiologically important glass components sustained during these periods could overwhelmingly influence the overall melter source term. The composition of typical melter idling emission deposits, which appears in Table XIII, verifies the importance of this loss mechanism for the semivolatiles. In order to determine the overall importance of this melter loss mechanism, emission rates of semivolatile elements were investigated as a function of plenum temperature and, consequently, melter surface glass viscosity. Temperature control was maintained through use of plenum water sprays, which cooled but did not disturb the surface of the melter glass pool.

This study was immediately initiated upon completion of a 120-h liquid-fed melter test (PSCM-5). With a 42 L/h water spraying rate and the melter under automatic resistance control, the melter glass surface was cooled to the point that it formed a continuous nonconvective layer above the bulk melter glass pool (plenum 280°C). At a 27 L/h spray rate, the surface viscosity decreased significantly. Convective mixing opened vents in the glass surface that migrated at random across the melter glass pool. However, plenum temperatures were not high enough to melt feed deposits formed upon the melter walls and lid during the preceding PSCM-5 experiment. Finally, the cooling spray was terminated and the melter was allowed to idle at a fixed current rate, which slowly brought the melter plenum up to 850°C . Samples were collected from the plenum during all phases of this study.

17th DOE NUCLEAR AIR CLEANING CONFERENCE

Table XIII. Melter idling deposit

Elements As Oxides	Weight Percent		
	Gray Deposits	White Deposits	Glass
Al ₂ O ₃	1.2	0.11	3.7
B ₂ O ₃	14.2	1.6	10.0
CaO	0.22	0.46	1.2
CdO	0.02	0.02	0.009
Cr ₂ O ₃	0.57	0.58	0.02
Cs ₂ O	3.7	8.3	0.05
Fe ₂ O ₃	0.10	0.17	14.8
K ₂ O	0.79	0.85	*
Li ₂ O	1.92	2.6	4.4
MgO	<0.05	<0.05	1.4
MnO ₂	0.05	0.05	3.9
Na ₂ O	31.0	31.0	15.7
NiO	0.25	<0.02	1.2
RuO ₂	0.82	2.1	0.01
Sb ₂ O ₃	<0.01	<0.01	0.02
SiO ₂	<0.02	0.47	45.1
SrO	<0.005	<0.005	0.02
TeO ₂	0.70	0.70	0.002
TiO	<0.01	<0.01	0.8
ZnO	0.02	0.02	0.008

* Used in sample preparation.

The results obtained from these plenum samples are graphically summarized in Figure 8, which characterizes the emission rates of the semivolatile elements under various idling conditions (temperature) employed during this test. These data indicate that emission rates of all semivolatile elements decreased as a function of time after the completion of PSCM-5 under the influence of a 42 L/h water-spraying rate. Reducing the cooling spray rate to 27 L/h caused measurable increases in both plenum temperature and semivolatile emission rates; however, an equilibrated plenum temperature was not achieved during the brief period (24 h) of reduced spraying.

Termination of the water-cooling spray caused the plenum temperature to increase steadily to the point where plenum surface deposits formed during PSCM-5 began to melt and "burn" away. This period was responsible for the dramatic peaking of emission rates of the semivolatile elements. The fact that all semivolatiles do not form maxima at the same point in time is most probably due to temperature,

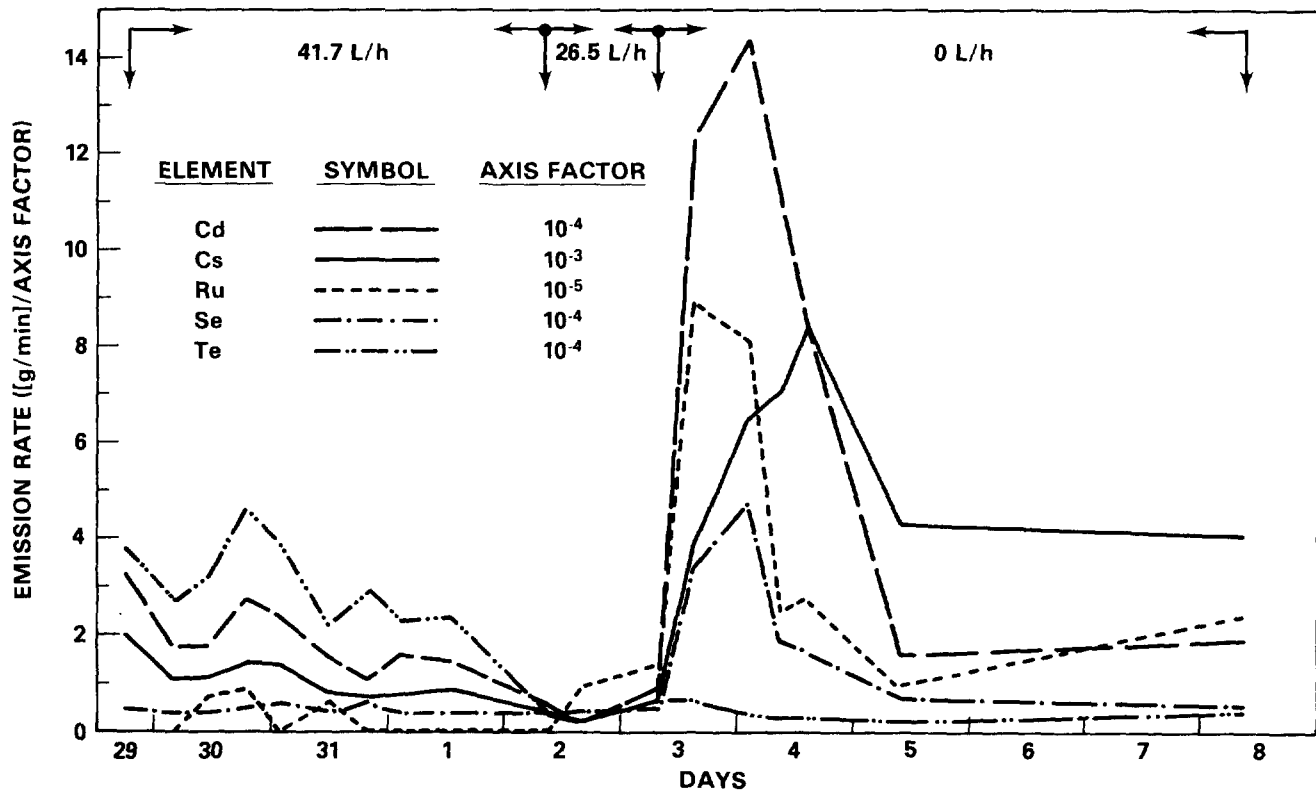


Figure 8. Melter idling emission rates of semivolative elements.

which was steadily increasing throughout the interval over which these maxima occurred.

The plenum temperature during the last two sampling periods was $\sim 850^{\circ}\text{C}$, and all plenum surfaces appeared clean. The emission rates occurring during these periods are, with the exception of Se and Te, significantly greater than the minimum emission rates exhibited by these elements during full 42 L/h spray cooling. However, these elevated idling emission rates are still significantly below those rates observed during moderate liquid feeding conditions. Specifically, the Cs emission rate expected from the PSCM for a liquid feeding rate of 50 L/h (1.1 kg/min) would be of the order of 10 mg/min. This is more than twice the value observed during the hot melter idling conditions. Consequently, it appears that the plenum cooling approach, although capable of reducing emission rates of most semivolatiles (by a factor of ~ 10 for Cs), is of little practical value in reducing the overall melter off-gas radiological burden.

It should be noted that the effect of directly feeding water onto the surface of an idling melter has also been investigated as an alternative method for reducing idling emissions. On a qualitative as well as a quantitative basis, this approach was a less satisfactory means of cooling the plenum and melter glass surface than was the plenum spray approach. The water feeding technique produced a high degree of entrainment and aerosol carryover into the off-gas system. Moreover, at the water feeding rates used (45 L/h), convective mixing was actually exacerbated, although total melter surface

17th DOE NUCLEAR AIR CLEANING CONFERENCE

flooding was never attempted. On the other hand, the water plenum spray initiated no observed entrainment and minimized or eliminated convective surface mixing.

V. Melter Flow Rates

The off-gas flow rate behavior of the two liquid-fed melters has been examined over the past year as part of the SRL-DWPF melter development program. During this period of study, two separate feed formulations have been used and a variety of melter operational running conditions have been employed. The results of these studies have shown that both feed composition and melter feeding rates have a preponderant influence upon the stability of melter off-gas flow rate.

The effect of feed composition upon melter flow rate behavior is related to the physical ability of the feed components to form a structurally sound insulating layer (cold cap) between the incoming liquid feed and the hot glass surface. As portions of the insulating cold cap become calcined, structural collapse occurs, bringing dammed up liquid feed into contact with the extremely hot glass surface. This results in the flashing off of the water component (and volatile reaction products) of the feed, producing a flow pulse or an off-gas surge. The magnitude and extent of these surges are naturally dependent upon the amount of liquid feed present on the cold cap that is delivered to the hot glass surface. Consequently, an erratic melter exhaust flow rate is often indicative of an unstable, overfed operational condition. Exhaust flow rate patterns associated with stable and unstable melter operating conditions are illustrated in Figure 9.

The two melter feed formulations used in these studies exhibited significantly different melter off-gas properties. The alkaline waste formulation produced a noisy, erratic melter flow rate with surges as high as seven times that of the average flow. The acid feed, on the other hand, possessed a very compliant, nonbridging cold cap, which reduced the frequency and magnitude of off-gas surging events. Average melter flow characteristics associated with each of these feed formulations are summarized in Table XIV. These data clearly show the stabilizing influence of the formic acid feed component upon melter flow rate behavior.

Due to the conservative, stable manner in which most PSCM runs were conducted, PSCM flow rate data associated with acidified feed are probably more representative of average melter behavior than are the values associated with the LFCM. The LFCM data, on the other hand, can be used in assessing the effects of heavy melter feeding conditions.

VI. Corrosion

Extensive metal corrosion has been observed in liquid-fed melter plenums and in associated melter off-gas lines and processing equipment. The nature of the corrosion observed suggests acidic chemical attack by volatile halogens and sulfur compounds. In order to identify suitably corrosive-resistant melter off-gas materials, corrosion coupons representing different groups of alloys were exposed to the plenum environment of liquid-fed melters during processing (300°C to

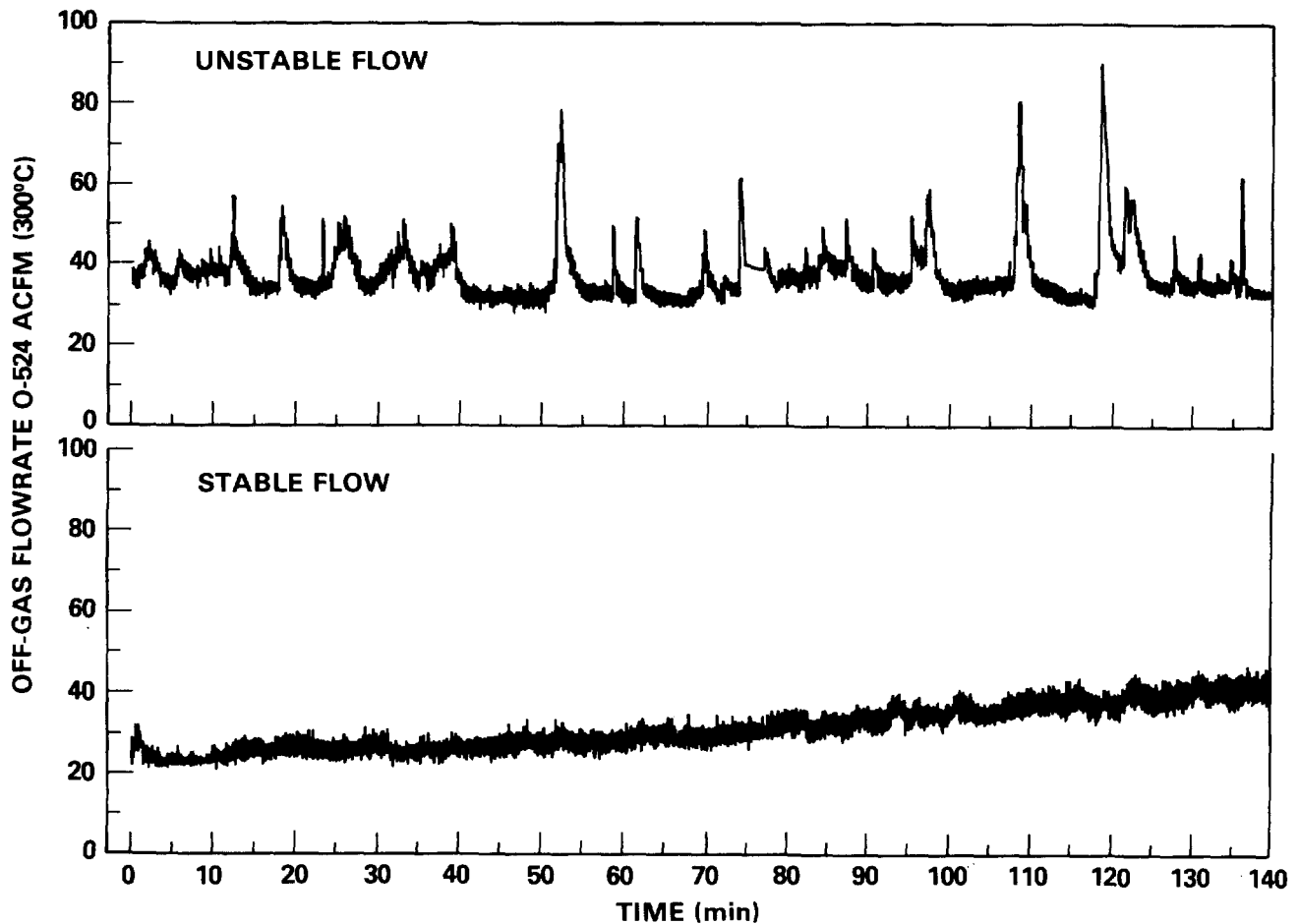


Figure 9. Typical off-gas flow rate behavioral patterns associated with liquid-fed melters.

Table XIV. Liquid-fed melter flow rate behavior.

<u>Experiment</u>	<u>Feed</u>	<u>Average, Flow, scfm</u>	<u>Maximum Surge, scfm</u>	<u>Average Surge Duration, min</u>
LFCM-4	Alkaline	90	620	3
LFCM-6	Alkaline	90	470	3
PSCM-3	Acid	70	220	3
LFCM-7	Acid	240	710	3
PSCM-4	Acid	70	300	4
PSCM-5	Acid	80	230	3
PSCM-6	Acid	80	190	3

500°C) and idling (850°C) conditions. The extent of corrosion as a function of operating conditions was established gravimetrically through coupon weight loss. The results of these studies, which are summarized in Table XV, indicate that the corrosion rates occurring during actual liquid feeding are much greater than those occurring during hot idling, although temperature cycling between feeding and idling conditions has been found to accelerate overall corrosion rates. In addition, titanium, tantalum and all alloys having high iron concentrations were found to be quite unsuitable for liquid-fed

Table XV. Corrosion sample results.

Material	Exposure, h		Weight Change g/cm ²	Cor. Rate, cm/y	Observations			Approximate Composition, Wt%					
	Idling	Operating			Spalling	Deposits*	Color**	Cr	Co	Fe	Ni	Mo	W
Inconel [®] -690	1134	214	-0.025	0.020	Light	Light	Blk-Silver	30	--	9.5	60	--	--
	198	214	-0.014	0.074	Light	None	Black						
	1256	214	-0.036	0.023	Light	Light	Multi						
	320	330	-0.011	0.015	Light	Light	Black						
Inconel [®] -625	1134	214	+0.015		None	Heavy	Brown	21.5	--	2.5	61	9	--
	198	214	+0.007		None	Heavy	Brn-Silver						
	1256	330	+0.013		None	Heavy	Brn-Black						
	320	330	+0.012		None	Heavy	Brn-Silver						
Inconel [®] -617	122	116	-0.004	0.008	Med-Pits	Medium	Gr-Silver	22	12.5	1.5	52	9	--
	122	116	-0.013	0.024	Med-Pits	Medium	Gr-Silver						
Inconel [®] -600	122	116	-0.008	.015	Medium	Light	Multi	15.5	--	8	76	--	--
	122	116	-0.002	0.004	Medium	Light	Multi						
Haynes [®] -188	1134	214	+0.059			Very Light	Bl-Black	22	40	<3	10	--	15
	198	214	+0.004		Light	Light	Bl-Black						
Haynes [®] -25	1134	214	+0.005		Light	Light	Bl-Black	21	54	<3	10	--	15
	198	214	+0.003	0.008	Light	Light	Bl-Black						
	60	110	+0.001		None	None	Black						
RA [®] -330	1134	214	-0.025	0.020	Medium	None	Multi	18	--	47	35	--	--
	198	214	-0.036	0.185	Medium	None	Gr Spots						
RA [®] -446	1134	214	-0.18	0.145	Heavy	None	Multi	25	--	75	--	--	--
	198	214	-0.17	0.472	Heavy	None	Multi						
Titanium	122	116	-0.063	0.210	Heavy	None	Silver-Brn	--	--	--	--	--	--
Tantalum	122	116	-3.3	>3	Disappeared								

* Feed material sintered on coupon surface.

** Bl - Blue
Blk - Black
Brn - Brown
Gr - Green

®Inconel is a registered trademark of Huntington Alloys, Huntington, West Virginia

®Haynes is a registered trademark of the Cabot Corporation, Kokomo, Indiana.

®RA is a registered trademark of Rolled Alloys, Detroit, Michigan.

17th DOE NUCLEAR AIR CLEANING CONFERENCE

melter service. The most promising alloys are those possessing low iron, high nickel or cobalt and a chromium content greater than 20%. Inconel®-625 and the Haynes® alloys were the most corrosive-resistant materials employed during this study.

VII. Conclusions

The off-gas studies discussed in this report have sought to establish the effluent characteristics of liquid-fed joule-heated ceramic melters. The results of these studies have shown particulate emission to be responsible for most melter effluent losses. Moreover, a large fraction of the total particulate mass evolved from an operating melter is conveyed to the off-gas system by submicron aerosols which are almost exclusively responsible for semivolatile transport. Melter operational conditions have had little effect upon these results as long as quasi steady-state conditions are maintained. Even hot melter idling conditions do not significantly affect the overall melter source term.

Melter-generated gases have been found to be potentially flammable as well as corrosive. Hydrogen generation presents the greatest flammability hazard of the combustibles generated by liquid-fed melters. Off-gas dilution was required during a melter test to maintain the H₂ concentration below 70% of its lower flammability limit in the quench melter exhaust. The combustible gas CO has never achieved a quenched off-gas concentration greater than 1/10 of its flammability limit. Auxiliary plenum heating has been found to significantly reduce melter emission rates of both these combustible gases.

Significant concentrations of acidic volatile compounds of sulfur and the halogens exist in unquenched melter off-gas streams independent of melter operational conditions. These gases have been responsible for extensive corrosion observed in melter plenums and in associated off-gas lines and processing equipment. Alloys possessing low iron, high nickel or cobalt and high chromium content have been found to be most suitable for liquid-fed melter service.

VIII. References

- (1) Buelte, J. L. and C. C. Chapman. Liquid-Fed Ceramic Melter, A General Description Report. PNL-2735, Pacific Northwest Laboratory, Richland, Washington (1978).
- (2) Bonner, W. F. The High-Level Waste Immobilization Program: An Overview. PNL-3094, Pacific Northwest Laboratory, Richland, Washington (1979).
- (3) Conroy, A. R., W. H. Manning and W. C. Bauer. "The Role of Sulfate in the Melting and Fining of Glass Batch." Glass Ind. 47(2):pp 84-89, February-March (1966).

IMMOBILIZATION OF KRYPTON-85 IN ZEOLITE 5A*

A. B. Christensen, J. A. Del Debbio, D. A. Knecht,
J. E. Tanner and S. C. Cossel

Exxon Nuclear Idaho Company
P. O. Box 2800
Idaho Falls, ID 83401

Abstract

This paper describes the technical feasibility and presents a summary of a preconceptual design and cost estimate for a process to immobilize krypton-85 by sintering in zeolite 5A at 700°C and 100 MPa (1000 atm) for 2-4 h. Krypton loading of 30-60 m³ at STP per m³ solid can be achieved. The initial water concentration in zeolite 5A has a catalytic effect on the sintering rate and must be kept at approximately 1 wt% by heating prior to the encapsulation run. High initial water loadings and/or encapsulation times longer than 4 h must be avoided because the sintered zeolite 5A recrystallizes to an anorthite-type feldspar and releases the trapped krypton. Data are presented to show how the process conditions affect krypton encapsulation in zeolite 5A and how to assure the quality of the product. Krypton leakage experiments are used to predict leakage rates of less than 0.03% and 0.3% for 10-year storage at 300° and 400°C, respectively. By adding a powdered glass frit to the commercial zeolite 5A 2 mm beads, a solid mass is formed during encapsulation, which can be further compacted using standard hot isotatic pressing techniques at 33 MPa and 600°C to form a fused glassy matrix enclosing the amorphous zeolite.

A process for encapsulating the annual krypton-85 production at a commercial 2000 metric ton of heavy metal (MTHM) spent fuel reprocessing plant is developed. A hot isostatic press (HIP) with an isolated work zone of 8 or 16 L capacity is required to operate for 600 or 300 cycles per year, respectively. Existing HIP technology uses work zones from 1 to 3500 L capacity at similar production rates. A combined encapsulation/compaction cycle is proposed as an option to most effectively immobilize the krypton and the zeolite. A preconceptual design and cost estimate is given for a commercial-scale Kr encapsulation facility. The facility is designed to withstand a worst case rupture of the HIP. The maximum krypton-85 release is estimated to result in an off-site dose well below accident protective action guidance levels. Major licensing concerns appear to be in compliance with applicable codes for HIP fabrication and with developments associated in scaling up demonstration encapsulation plants.

*Work performed under DOE Contract DE-AC07-79ID01675

I. Introduction

U.S. regulation 40 CFR 190 limits krypton-85 releases to 50,000 Ci per gigawatt-year of commercial electric power production for fuel placed into a reactor after January 1, 1983.¹ For light water nuclear reactors, the release limits would correspond to about 15% of the krypton-85 inventory in the spent fuel. If krypton-85 is recovered, storage methods would be required to meet the overall release limits in the regulation.² While storage in pressurized cylinders is technically feasible, there may be large costs associated with long-term storage.³ By trapping krypton in a solid on an atomic or microbubble scale, a less expensive disposal facility, such as shallow dry wells,⁴ could be used, with potentially low release rates. Ion implantation sputtering^{5,6} and zeolite/glass encapsulation⁷⁻¹¹ are two candidate immobilization processes currently under development. Both have krypton storage volumes comparable to that in pressurized cylinders, low krypton release rates at 300 to 400°C, and mechanically strong structures.

The high temperature/high pressure encapsulation process uses existing technology found in the hot isostatic pressing (HIP) industry, where molds containing metal or ceramic powders are compacted and sintered under high pressure of argon to fabricate items such as tungsten carbide bits, superalloy aircraft components, ferrite ceramics for computer memory and turbine components.^{12,13} Typical commercial-scale HIP work-zone volumes range from 1 to 3500 L.

This paper summarizes recent technical and economic developments in the process to encapsulate krypton in zeolite 5A. The technical feasibility for the encapsulation process and of further immobilizing the granular zeolite 5A material in a compacted glass matrix is demonstrated.

The design and cost estimate of a facility to encapsulate the krypton-85 produced at a 2000 metric ton of heavy metal (MTHM) commercial fuel reprocessing plant is presented, including considerations necessary for obtaining a license to operate the facility. The full-scale process design is based on existing commercial hot isostatic pressing technology, using HIP work zone volumes of 8-16 L.

II. Technical Feasibility

Krypton trapping by sintering at 550°C in zeolite 5A was reported by Penzhorn⁷, and the results were confirmed at the INEL at 700°C.^{8,9} Typical gas loading of 46 cc at STP per gram of solid were obtained in zeolite A samples at various pressures, temperatures, and time ranging from 550-700°C, 1000-2000 atm, and 1-6 hours. A schematic for the process to encapsulate krypton by sintering in zeolite 5A is shown in Figure 1.

Figure 2 shows a structural representation¹⁴ of zeolite A and the relative size of a krypton atom. The room temperature gas kinetic diameter of a krypton atom is 0.35 nm; the zeolite A cage opening and internal diameter is 0.5 nm and 1.1 nm, respectively, for calcium-exchanged zeolite A (zeolite 5A).¹⁴

Krypton trapping will occur by sintering in zeolite 5A. The mechanism in zeolite 5A may involve hydrothermal decomposition to form an amorphous structure, which is catalyzed by residual water.^{14,15,16} Recrystallization from the amorphous phase to an anorthite type feldspar occurs at high temperatures. The rate of recrystallization is directly dependent on initial water loadings. Hoss and Roy found that calcium-exchanged zeolite A transforms to a silicate whose X-ray pattern resembled that of anorthite after being exposed to 1000 atm H₂O vapor at 270°C for 10 days.¹⁶

Experimental

Zeolite 5A was obtained from W.R. Grace Co. in 2 mm spheres and is produced by a 67% exchange of calcium for sodium in zeolite 4A. Zeolite 5A spheres are activated for a minimum of 24 hours in the atmosphere at 460°C (1k Pa water vapor pressure) to remove the adsorbed water so that the equilibrium water loading of 0.8 wt% is achieved. Following drying, the sample is quickly transferred into a glovebox with water vapor partial pressure of 10 Pa, where it is weighed, loaded into sample holders, and sealed inside the autoclave.

The experimental system for krypton encapsulation has been described elsewhere¹⁷. The pressure vessel used for encapsulation studies is a 25 mL Leco pressure capsule, surrounded by a cooling jacket and two independently controlled heaters. Heating and cooling times were 2 and 1 hour, respectively. The encapsulation temperatures were calibrated at the sodium iodide melting point of 651°C.¹¹

Experiments were also carried out using a hot isostatic press (HIP) with a 1.0-litre work-zone volume. Argon was used in place of krypton to minimize costs and because Ar behaves similarly to Kr. The system is shown in Figure 3. The cooled pressure bearing walls of the HIP contain a furnace in the high pressure zone and a heat shield to keep wall temperatures below 200°C. Figure 4 shows the furnace, thermocouples, work package, and heat shield. Heating and cooling times were thirty minutes for the HIP.

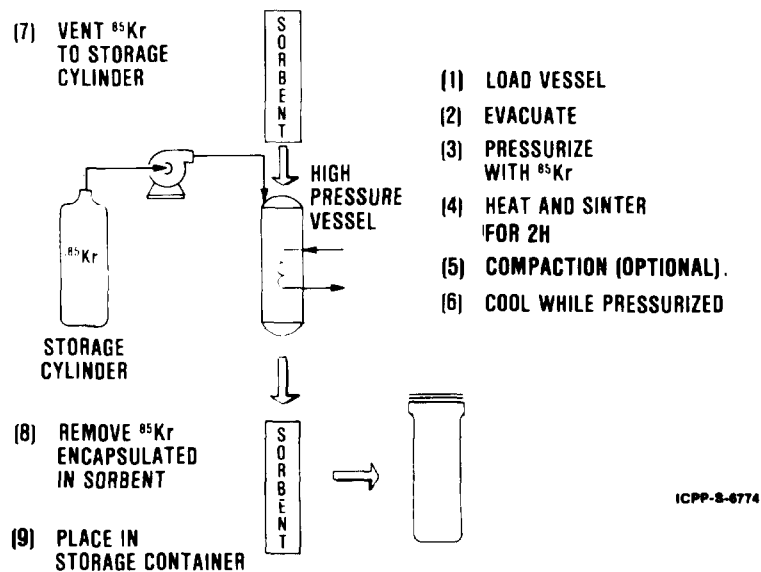


Figure 1. Schematic of the Process Used to Encapsulate Krypton by Sintering in Zeolite 5A.

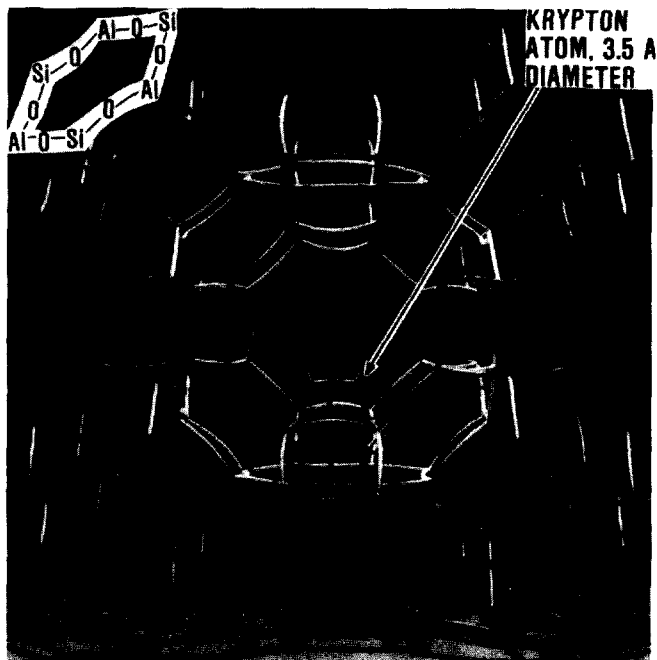
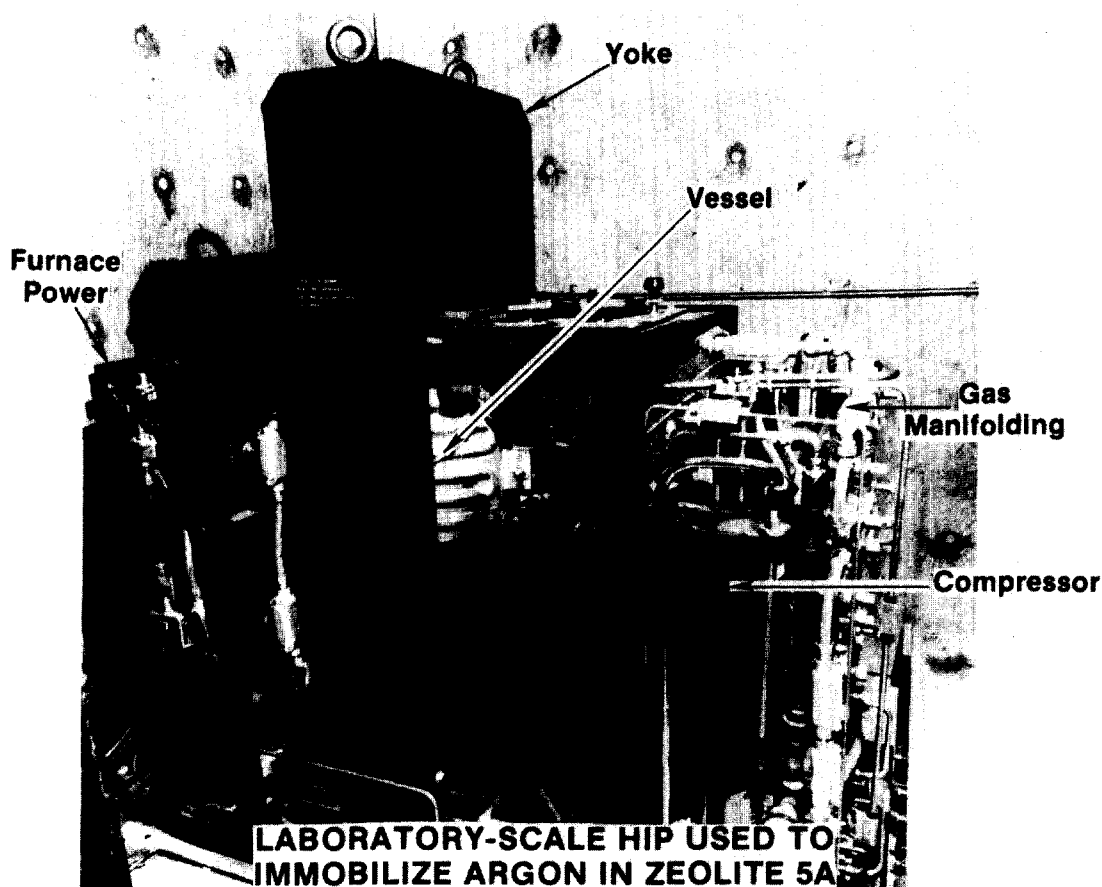


Figure 2. Structural Model of Zeolite 5A Containing a Krypton Atom Encapsulated in the Middle Alpha Cage (0.5 nm Opening).



Routine analysis of sintered zeolite 5A samples after encapsulation use mass spectrometry to determine gas loading, x-ray powder diffraction to determine zeolite 5A structure, and thermogravimetric analysis (TGA) to determine gross gas leakage. Krypton and argon leakage rates were measured by gas chromatography and mass spectrometry at 150 to 800°C.^{11,17}

Results of Encapsulation Tests

Approximately 46 and 70 cm³/g STP of krypton or argon are encapsulated in zeolite 5A at 1000 and 2000 atm, respectively, at the sintering conditions of 650-700°C, 1-6 h, and 0.7 wt% residual water content in zeolite 5A. The effect of initial water loading on product form is shown in Figure 5. Amorphous product containing large amounts of encapsulated krypton was typically formed at 700°C, 102 MPa (1020 atm), and 2-4 h with Grace-Davison zeolite 5A containing 0.8 wt% water in this work, while a similar product was formed by Penzhorn at 520°C 100 MPa, and 2 to 4 h with Bayer zeolite 5A containing 3 wt% water.^{7,11}

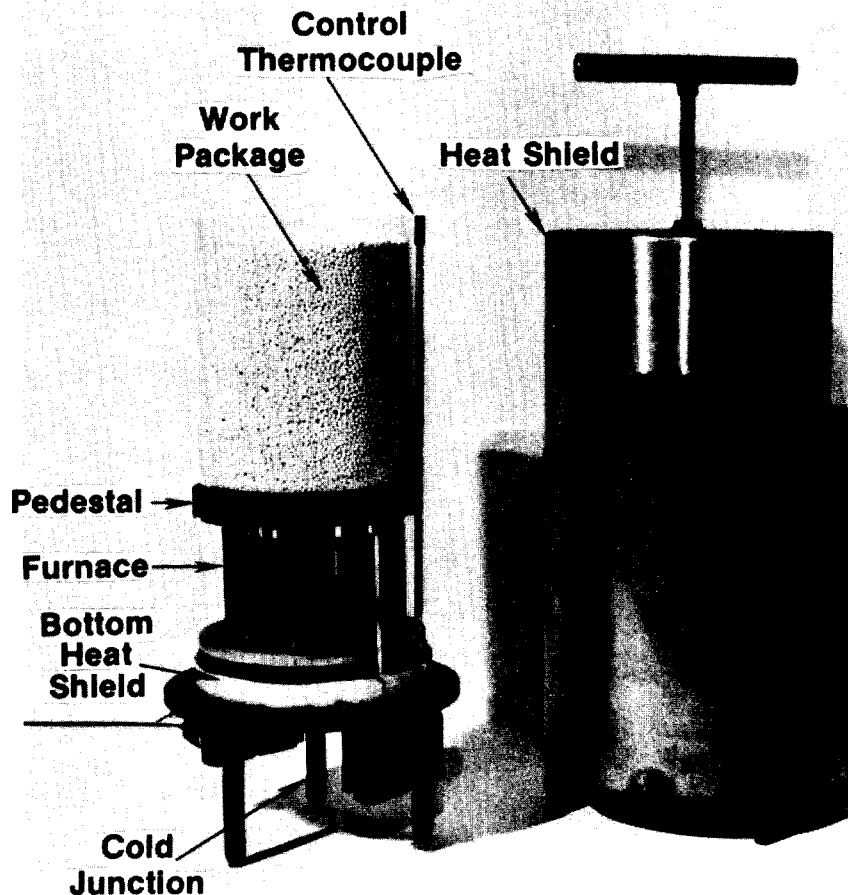


Figure 4. Interior Components of the Laboratory-Scale HIP.

Thermogravimetric analysis (TGA) measures weight changes to within 1% of the total sample weight. Kr loaded in crystalline zeolite 5A quickly leaks out upon heating. As the zeolite becomes amorphous to x-rays, the rate of leakage decreases until no leakage is seen for samples heated to 750°C.

Figure 6 shows x-ray powder diffraction scans for zeolite 5A, amorphous product, recrystallized product, and an anorthite reference material. Based on the encapsulation experiments, the crystalline zeolite 5A appears to pass through the amorphous state, which traps krypton, before it recrystallizes to an anorthite material, which does not trap krypton.

Infrared scans of unsintered and sintered zeolite 5A show a large broadening of the asymmetric stretching and bending vibrations as a result of sintering.¹¹ This broadening and the almost complete loss of the vibrations assigned to double ring structures indicate that the zeolite structure has been eliminated.

Differential thermal analysis (DTA) of untreated zeolite 5A show that the crystalline to amorphous (exothermic) transition occurs at a higher temperature (825°C) than during encapsulation (650-700°C), probably due to lower water concentration in the

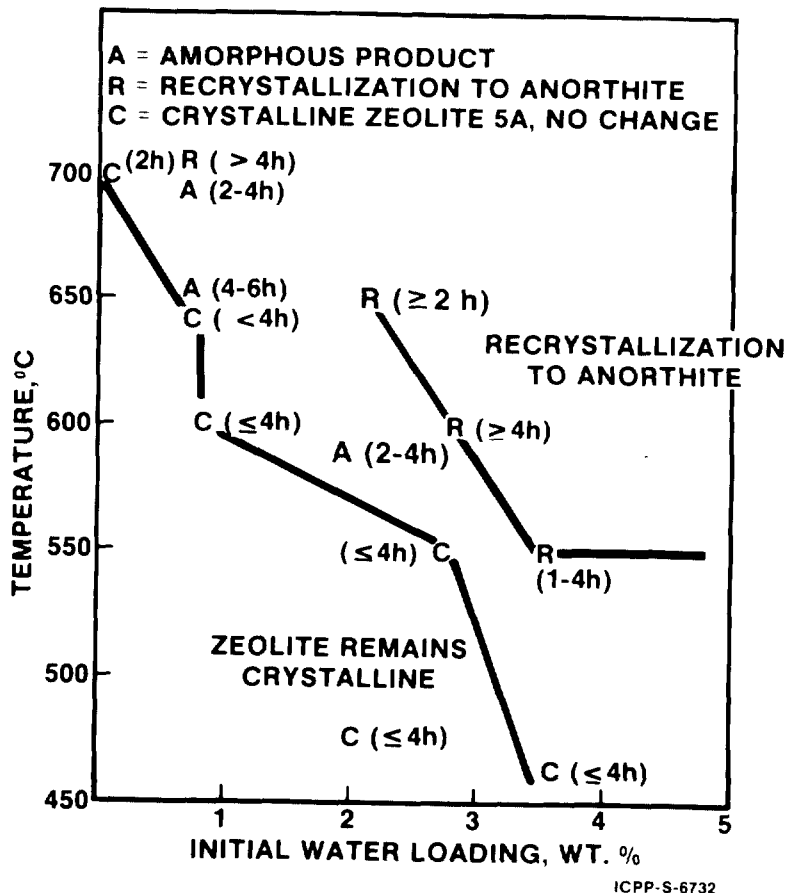


Figure 5. Effect of Encapsulation Temperature, Time, and Initial Water Loading on the Product Formed from Grace-Davison Zeolite 5A.

DTA analysis. The amorphous transition is not observed in sintered zeolite 5A, indicating that the sintered material is already amorphous. A small endotherm is observed due to the krypton release in the sintered sample. Both untreated and sintered zeolites show an exothermic transition due to recrystallization at 800°C for untreated and 1000°C for sintered samples.

Gas pressure does not seem to affect the sintering rate of zeolite 5A; however, it strongly affects gas loading. The Kr loading increases nonlinearly with gas pressure, but almost linearly with gas density, indicating that the sorbed gas is at the same density in the zeolite structure as in the gas surrounding it.

The effect of gas composition on Kr loading in zeolite 5A was studied using gas mixtures composed of N₂, O₂, Ar, Kr, and Xe, with Kr content of 54 or 68%. The encapsulation runs were made using zeolite 5A containing 0.8 wt% H₂O and sintered at 700°C and 100 MPa (1000 atm). Compared to the partial pressures during encapsulation, the component gases are loaded at slightly larger

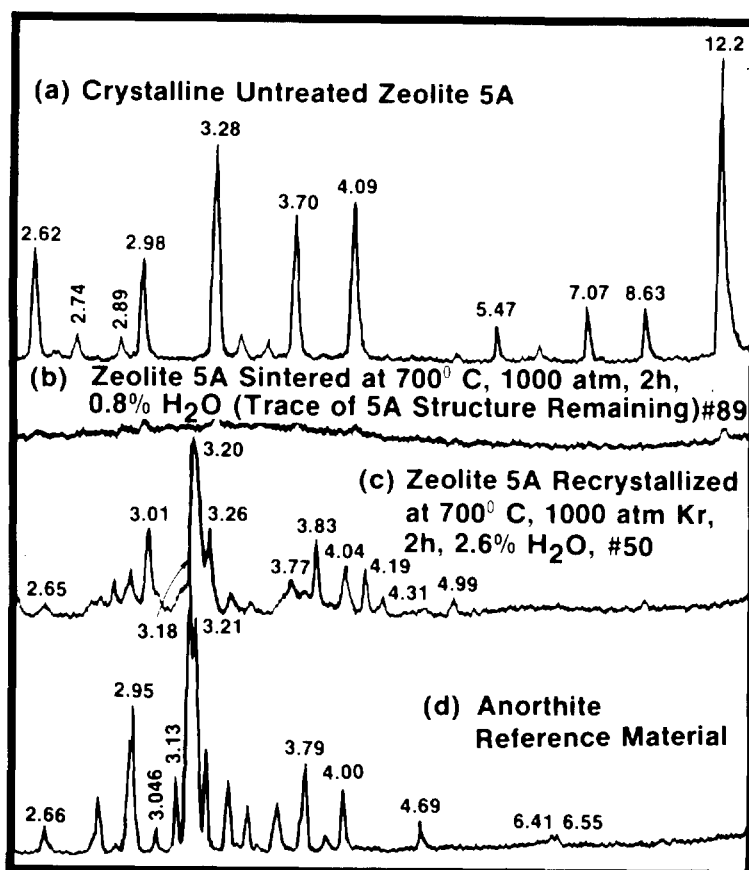


Figure 6. X-Ray Analysis of (a) Crystalline Zeolite 5A, (b) Sintered Product, (c) Recrystallized Product, and (d) an Anorthite Standard.

amounts for larger atoms (Kr and Xe) and at slightly smaller amounts for smaller atoms (Ar, O₂, and N₂). The Kr loading per atmosphere of Kr gas partial pressure (0.05 cm³STP/g/atm) in the gas mixture is the same as for pure Kr gas, and total leakage using TGA analysis is as low as from runs using pure Kr as the encapsulated gas.

The structural transformations occurring in zeolite 5A during the encapsulation process are depicted in the electron micrographs and electron diffraction patterns shown in Figure 7. Based on lower resolution micrographs not shown, atoms are not pulled apart sufficiently during sintering to cause a complete breakdown of the larger structure of the crystal. The high resolution transmission electron microscope (TEM) image shown in Figure 7a is a two-dimensional structural image of zeolite 5A for the (001) orientation which is parallel to the sides of the unit cell. The white dots represent channels 1.1 nm in diameter formed by the alpha cages (see the zeolite 5A model in Figure 2). This picture is similar to one obtained by L. A. Bursill of zeolite 3A.¹⁸ Amorphous areas where the crystal lattice has collapsed due to the energy of the electron beam (200 kV) can be seen as dark patches. Figure 7b and c shows the difference between partial and complete sintering. A sharp interface between the amorphous (glassy) and crystalline areas can be seen in 7b, whereas complete loss of crystallinity is evident

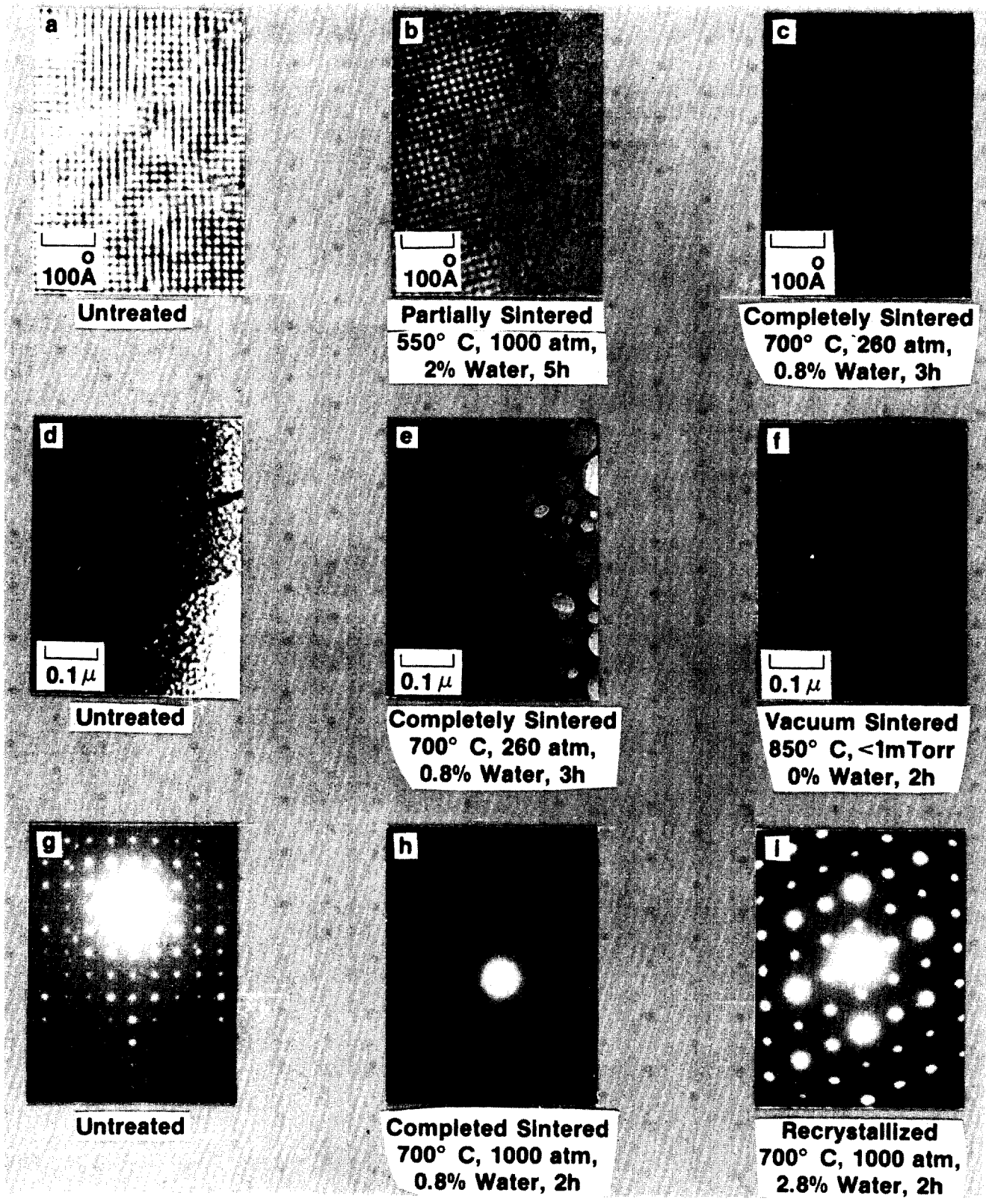


Figure 7. Electron Micrographs and Electron Diffraction Patterns of Zeolite 5A.

in 7c. Krypton leakage on the TGA for the partially sintered zeolite was 21% Kr lost below 825°C, as compared with less than 1% for the completely sintered material. Lower magnification images of untreated and sintered zeolite are shown in Figure 7d through f. Numerous irregularly shaped bright areas can be seen in 7d. These represent amorphous material caused by electron beam damage. The zeolite sintered at 700°C under krypton pressure shown in 7e contains bubbles from 5 to 100 nm in diameter while the vacuum sintered sample (7f) has none. These bubbles probably contain krypton gas under the run pressure of 26 MPa (260 atm). Electron micrographs of zeolite sintered at low pressure (20 atm) and 3.5 wt% water also showed bubbles, indicating that pressure has no effect on the structure of the sintered zeolite.

The appearance of the recrystallization product anorthite type feldspar, which results from too much water (2.8 wt%) being present at 700°C, is seen in other micrographs not shown here.¹¹ The large grains are observed with no bubbles and no uniform contrast, suggesting a sponge-like porous structure, which accounts for krypton leakage. The halo electron diffraction pattern in Figure 7h indicates an amorphous structure, while the pattern in Figure 7g and i indicates crystallinity.

Preliminary compaction tests of zeolite 5A have been carried out, before and after encapsulation with argon or krypton. Figure 8 shows samples of zeolite 5A compacted after encapsulation. In pellets which were formed before encapsulation, the krypton loadings varied, presumably depending on the initial water content; further work is required to determine conditions for obtaining the proper initial water loading. In compaction tests after encapsulation, activated Grace-Davison zeolite 5A beads were mixed with a borosilicate glass frit powder of composition in wt%: SiO₂-57.7, B₂O₃-19.4; Na₂O-16.1; CuO-1.7; Li₂O-5.1 and encapsulated at 700°C and 100 MPa (1000 atm) for 2-4 hours. During the encapsulation the powdered glass frit fused. The mass was further compacted isostatically at 700°C, 1000 atm, and 2 h. Figure 8 shows the reactants before and products after encapsulation and compaction.

Samples of sintered zeolite 5A having krypton loadings of 30-50 STP cm³/g were stored at 460 and 600°C in ovens open to the atmosphere for eight months. X-ray analysis after storage revealed no structural changes. Amorphous samples showed no evidence of recrystallization and samples which initially had traces or significant amounts of anorthite (a recrystallization product) showed no further recrystallization. Apparently the amorphous product recrystallization rate is reduced significantly below 700°C.

Results of Leakage Measurements

Argon and krypton leakage results are reported for zeolite samples which appear by X-ray diffraction to be totally amorphous. Samples which have an amount of crystallinity detectable by X-ray diffraction show much higher initial gas leakage rates during TGA and are not suitable products. Long term immobilization of krypton-85 would require a fully amorphous product.

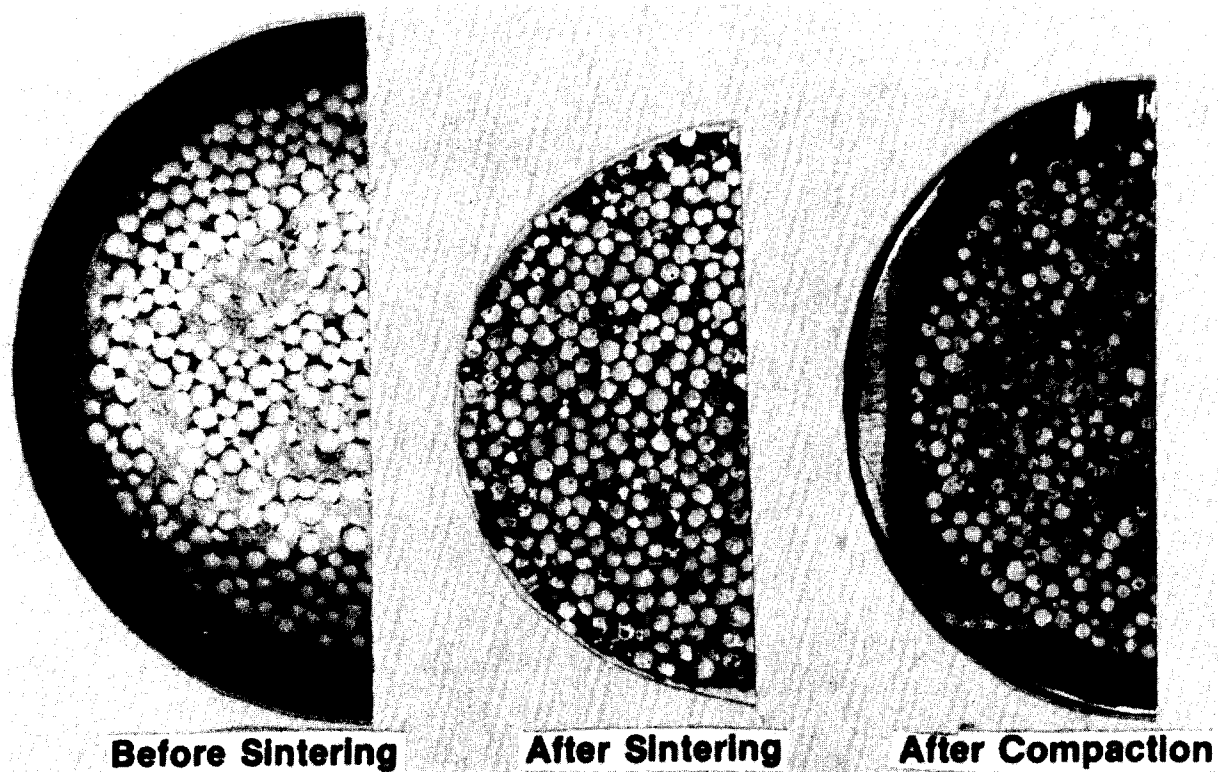


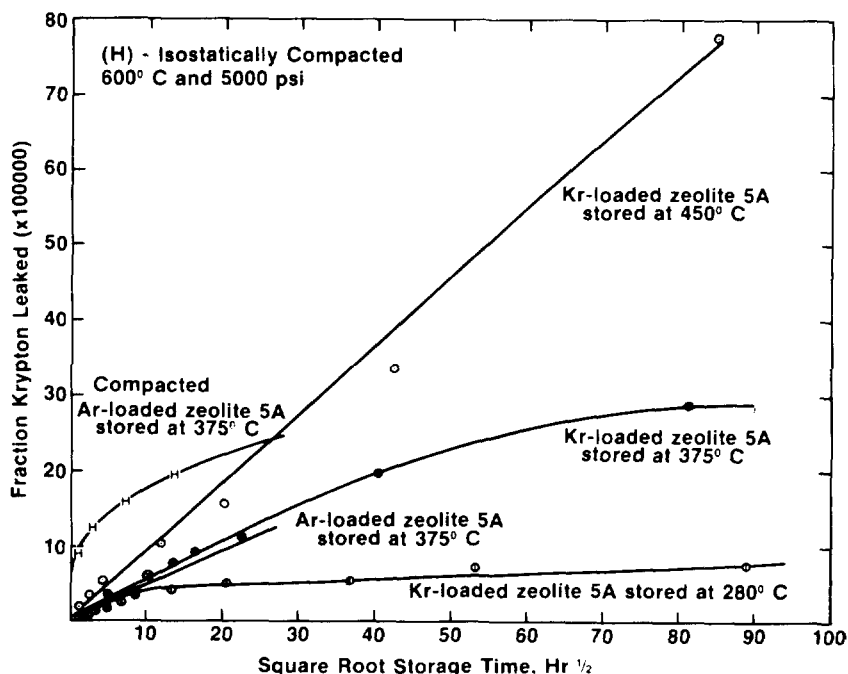
Figure 8. Zeolite 5A Samples Compacted After Encapsulation.

Initial diffusion from a homogeneous body is proportional to the square root of time, according to

$$Q_t/Q_\infty = (\alpha Dt)^{\frac{1}{2}}$$

The fractional leakage of krypton encapsulated in zeolite 5A is shown as a function of the square root of time in Figure 9 at 280, 375, and 450°C for samples which were heated to 600-700°C under vacuum for 1-4 h. The heat treatment apparently removes loosely held krypton from the solid surface, cracks or unsintered portions, resulting in initial constant slopes in Figure 9 when cumulative release is plotted as a function of square root of time. In samples which are not heat treated, the constant slopes are also apparent after a small initially rapid release of krypton. The loosely held krypton does not exceed a few tenths of a percent of the immobilized gas in a sintered sample and can be removed following encapsulation by heating the sample under vacuum for a short time. For samples which are encapsulated at 700°C and then compacted at 600°C and 33 MPa (5000 psi), the leakage rate is the same, after a slightly larger initial release of loosely held gas. The initial leakage data

in Figure 9 can be extrapolated to give leakage rates of less than 0.03% in 10 years' storage at 300°C; based on the observed curvature at later times, these predicted values are clearly overpredictions.



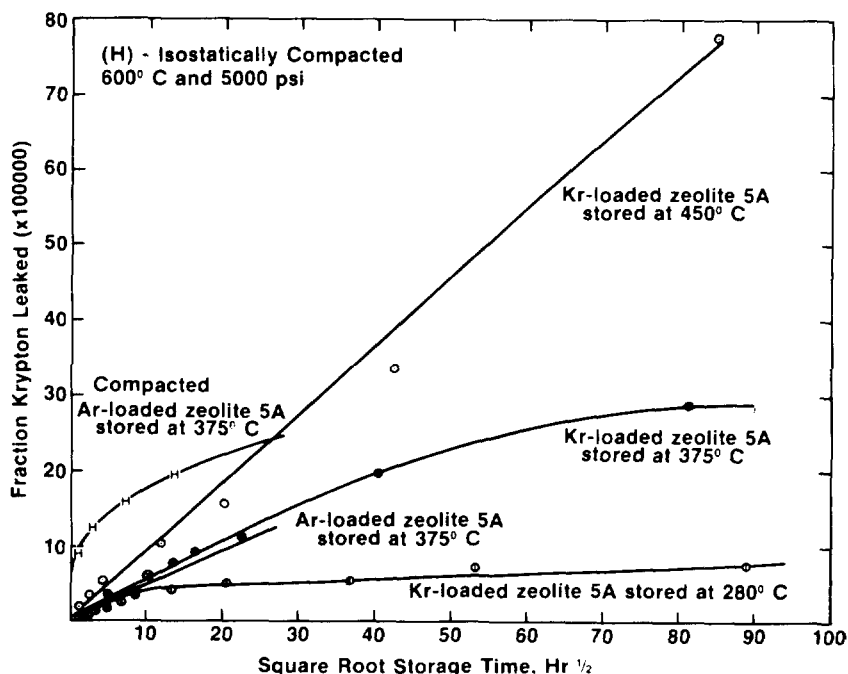
ICPP-S-8859

Figure 9. Fractional Leakage of Tightly Held Krypton from Sintered Zeolite 5A Samples (Heated to 700°C for 2-4 h).

Figure 10 shows the temperature behavior of the diffusivity. The activation energy of 197 kJ/mole was calculated from the leakage rate data, which is similar to a value of 209 kJ/mole obtained by Penzhorn.⁷ Similar results are observed in Figure 10 using sintered porous Vycor containing krypton.

Long-term leakage studies were made using sintered zeolite 5A samples immobilized with Kr, Xe, Ar, N₂ and O₂. Gas loadings were proportional to the partial pressure of the component in the gas phase. The relative leakage rates of these gases from sample stored at 370°C show that, except for an initial release of loosely held gas, the release rate of each component is linear with the square root of the storage time. A similar result was obtained at 700°C. Generally, the gases leak with rates inversely proportional to their smallest molecular dimension. The presence of other gases does not influence the leakage of Kr. The diffusivities calculated for gas mixture components are included in Figure 10.

in Figure 9 can be extrapolated to give leakage rates of less than 0.03% in 10 years' storage at 300°C; based on the observed curvature at later times, these predicted values are clearly overpredictions.

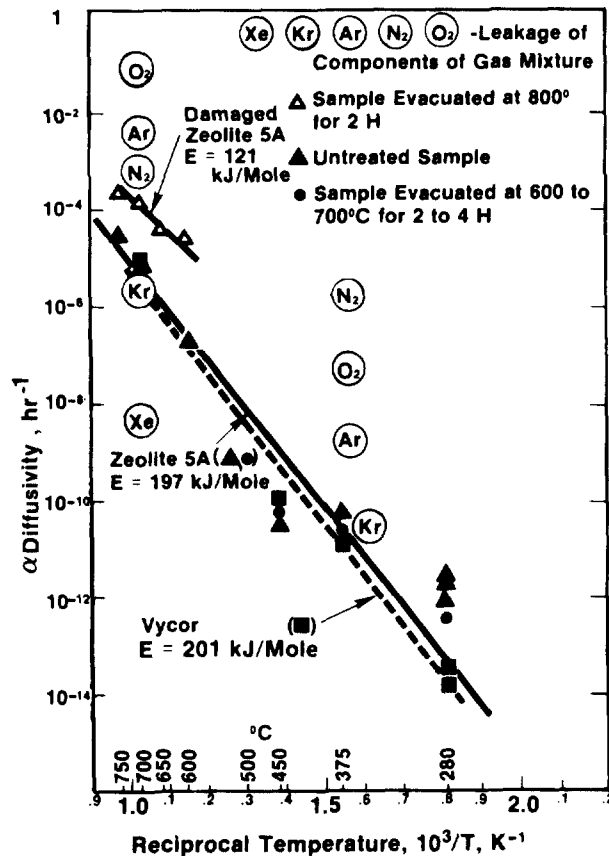


ICPP-S-8859

Figure 9. Fractional Leakage of Tightly Held Krypton from Sintered Zeolite 5A Samples (Heated to 700°C for 2-4 h).

Figure 10 shows the temperature behavior of the diffusivity. The activation energy of 197 kJ/mole was calculated from the leakage rate data, which is similar to a value of 209 kJ/mole obtained by Penzhorn.⁷ Similar results are observed in Figure 10 using sintered porous Vycor containing krypton.

Long-term leakage studies were made using sintered zeolite 5A samples immobilized with Kr, Xe, Ar, N₂ and O₂. Gas loadings were proportional to the partial pressure of the component in the gas phase. The relative leakage rates of these gases from sample stored at 370°C show that, except for an initial release of loosely held gas, the release rate of each component is linear with the square root of the storage time. A similar result was obtained at 700°C. Generally, the gases leak with rates inversely proportional to their smallest molecular dimension. The presence of other gases does not influence the leakage of Kr. The diffusivities calculated for gas mixture components are included in Figure 10.



ICPP-5-6759

Figure 10. Temperature Dependence of Diffusivity of Krypton from Sintered Zeolite 5A.

III. Preconceptual Design And Cost Estimates For A Krypton Encapsulation Facility

A preconceptual design and cost estimate of a facility to encapsulate the krypton-85 produced at a 2000 MTHM per year spent fuel processing plant was prepared under contract by the R. M. Parsons Co. The basis for a commercial-scale encapsulation facility is shown in Table I. The facility is assumed to be located with the reference commercial spent fuel reprocessing plant and noble gas cryogenic separation facility described in the DOE draft environmental impact statement on waste management.³

The flow scheme for ⁸⁵Kr encapsulation is shown in Figure 11. Zeolite is loaded into a capsule, activated and the capsule loaded into the HIP. Krypton is pumped from two storage cylinders into the HIP isolation work-zone, simultaneously with a balancing pressure of He or Ar around the work-zone. After the soak time, Kr and balancing pressure gas are vented to storage. The capsule containing the sintered zeolite is removed and placed into a storage container, which is then welded shut. After inspection the storage container is placed into storage. Transportation casks are used to transport the containers to long-term storage. One year's production is estimated at 5 m³ of sintered zeolite.

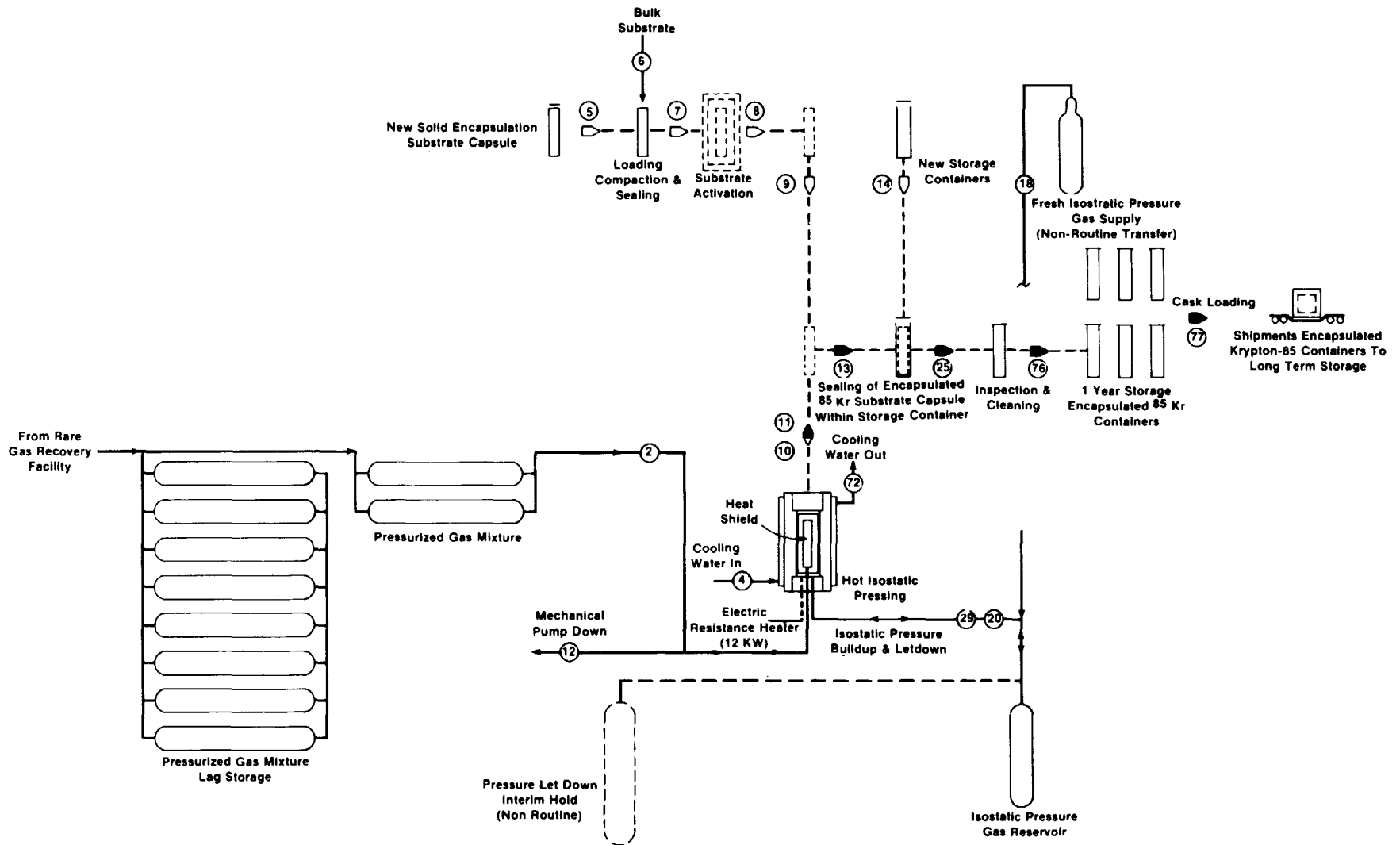


Figure 11. Krypton Encapsulation Process flow Diagram

17th DOE NUCLEAR AIR CLEANING CONFERENCE

A HIP containing an isolated work zone, similar to one in operation at General Electric Aerospace Company in Valley Forge, PA, is used to confine krypton-85 and the zeolite 5A. A schematic of an isolation work zone HIP is shown in Figure 12. The isolation work zone contains the work-load of zeolite 5A and krypton-85 gas during encapsulation and is surrounded by a balancing pressure of inert gas, such as helium or argon. As a result the krypton-85 inventory is reduced, and the corrosion of the pressure-bearing vessel walls by the decay product rubidium is eliminated.

The work-load may be preheated before placement to speed the heating time, and the heat-shield, work-load, and furnace may be placed into the HIP in one package, if desired. A crane is normally used to load and unload a HIP. HIPs are placed in concrete pits to facilitate work-package handling and minimize hazards from accidental failure at high pressures.

TABLE I
DESIGN BASIS FOR A COMMERCIAL-SCALE KRYPTON-85
ENCAPSULATION FACILITY

Process Throughput:	110% of 17 MCi/yr of ⁸⁵ Kr, Based on Reprocessing 2000 MTHM/Year of LWR Fuel
Total Volume of Feed Gas: (at 110% Capacity)	230 m ³ at STP
Feed Gas Composition: (by Volume)	2% Xenon 8% Argon 90% Krypton, with ⁸⁵ Kr Making up 6% of the Total Kr
Operation:	Batch Operation Using HIP
Lifetime:	24 Hours/Day, 300 Days/Yr, for 30 Yr
HIP Operating Parameters:	100 MPa and 700°C
Zeolite 5A Material Characteristics:	Bulk Density of 1.0 g/cm ³ Void Fraction of 40%
Gas Lag Storage:	60 Days' Production from Rare Gas Plant or 3.6 MCi
Product Storage:	1 Yr Production or 5 m ³ Sintered Zeolite

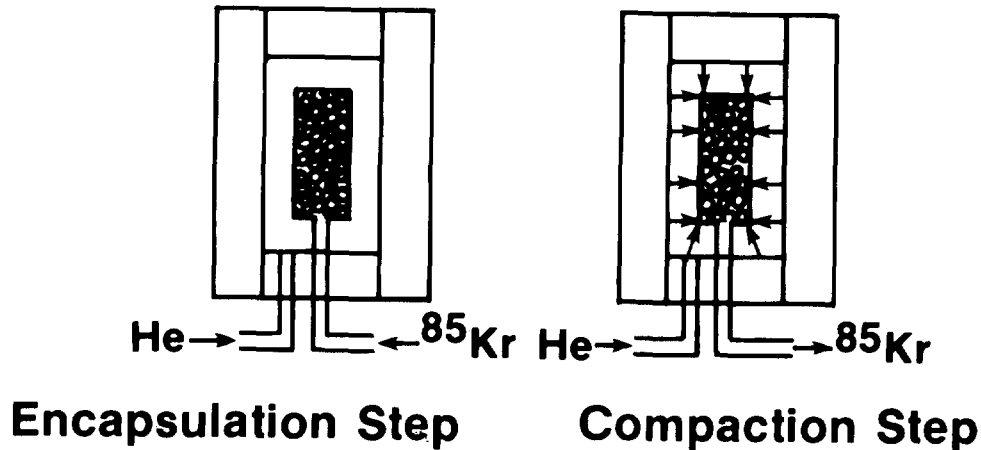


Figure 12. Schematic of ^{85}Kr (A) Encapsulation and (B) Compaction in the Isolation Work Zone of a Hot Isostatic Press. In (A), Pressures Are Balanced; in (B) ^{85}Kr is Withdrawn, Causing Isostatic Compaction of the Work Volume

The laboratory-scale HIP shown in Figures 3 and 4 has recently been modified to accept an isolation work zone for radioactive krypton-85 experiments. A photograph of the modified bottom cover and isolation work zone canister is shown in Figure 13. The two sets of inlets allow simultaneous pressurization of the isolation work zone canister with krypton-85 and of the surrounding volume with helium.

Mock-up vessels which simulate the laboratory-scale HIP vessel, isolation work zone canister, and heat shield were tested for remote operation. An additional alignment fixture, removable bayonet fixture, and manipulator extension fingers (Figure 14) were designed and fabricated. The remote tests demonstrated that the isolation work zone canister containing krypton-85 sintered in zeolite 5A can be remotely loaded and unloaded in the lab-scale, HIP. Radioactive krypton-85 tests are currently under way using this equipment. Modifications for full scale remote operation appears to be feasible, based on the lab scale tests and available HIP technology.

Figure 15, shows the conditions as a function of time during a commercial scale encapsulation process, including temperature, krypton pressure in the isolation work zone, and argon or helium pressure in the volume surrounding the isolated work-zone. The isolation work package is filled with zeolite beads, zeolite bead-glass frit powder mixture or compacted zeolite and heated at conditions necessary to give a residual water loading of approximately 1%. In order to avoid loss of solid material, a porous metal filter is enclosed in the tubing connected to the isolated work package.

Isolation Canister For Krypton Encapsulation System

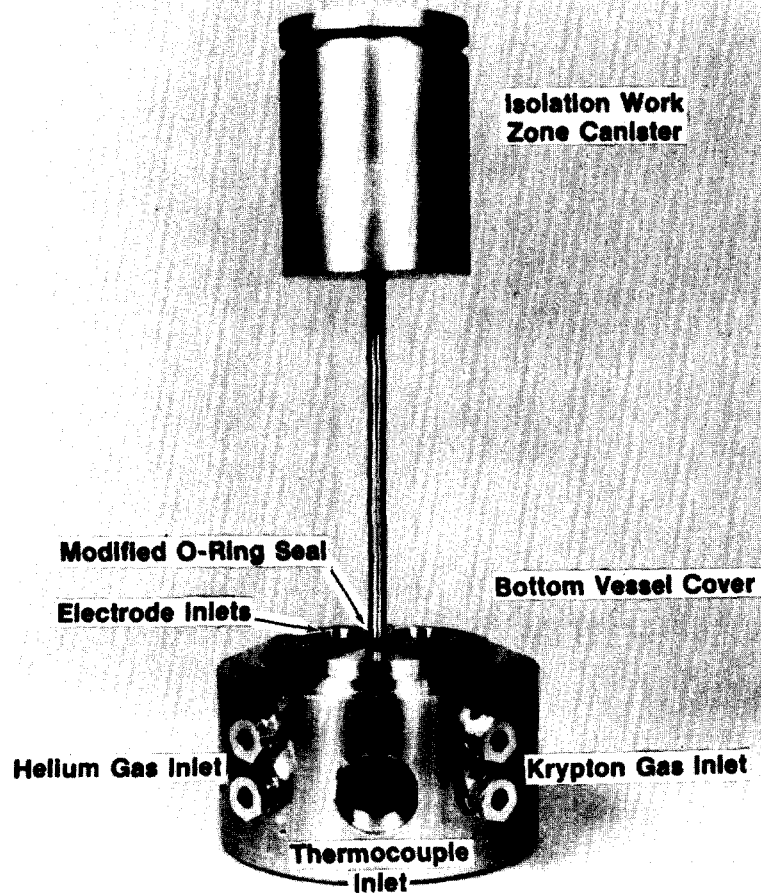


Figure 13. Photograph of Modified Bottom Cover to Lab-Scale HIP with Isolation Work Zone Canister Inserted

During the encapsulation soak time, the krypton pressure inside the work package and the argon or helium pressure outside the work package remain balanced. After the encapsulation soak time, the inner krypton gas can be vented back to storage, resulting in a compaction of the solid in the canister to form a monolithic block. If no compaction is desired, both gases can be vented and the work package cooled. The compaction step is included in the processing conditions shown in Figure 15 and is illustrated schematically in Figure 12. The compacted work package can then be removed remotely and sealed into a second container for long term storage. The total time required for the encapsulation and compaction cycle is about ten hours, including loading and unloading the isolated work package.

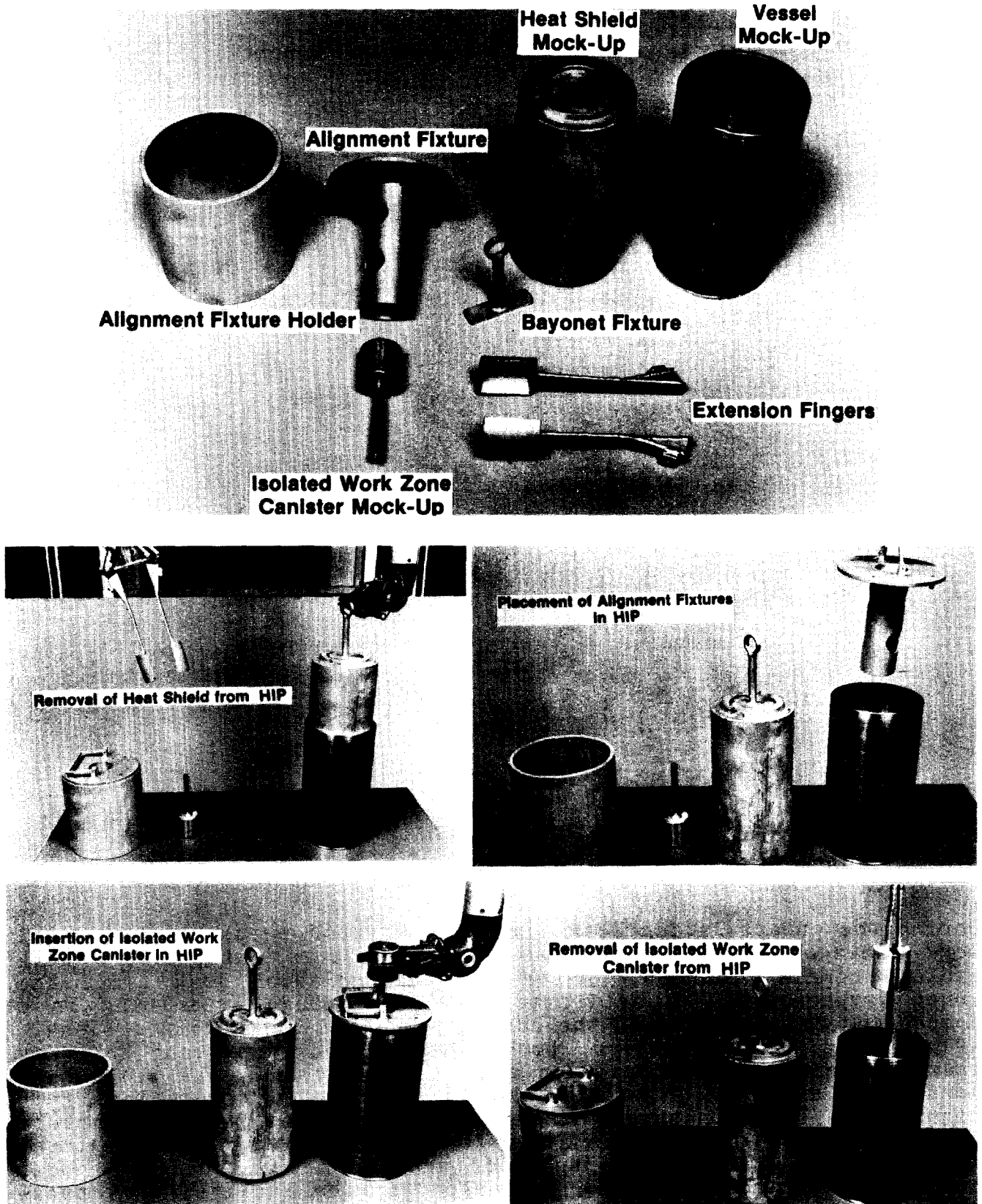
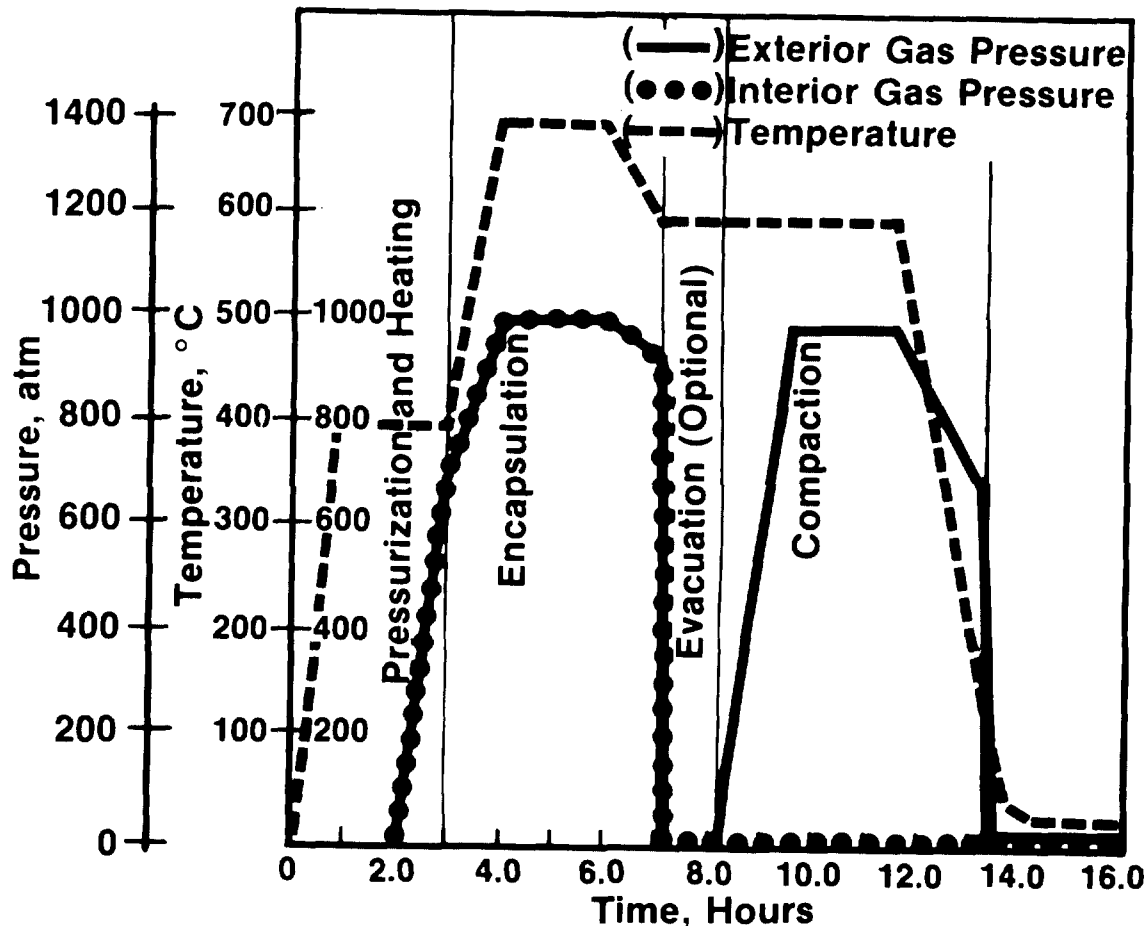


Figure 14. Mock-up of Lab-Scale HIP Components and Tools Required for Remote Operations



ICPP-S-6757

Figure 15. Temperature and Pressure Inside and Outside the Isolated Work Zone as a Function of Time for a Commercial-Scale Krypton-85 Encapsulation Process

The facility floor plan is shown in Figure 16. The facility is rectangular with dimensions 84 feet long by 52 feet wide and a total floor area of 4,368 square feet. All radiation areas are constructed with reinforced concrete. The facility consists of cells to contain the HIP processing, krypton-85 gas storage, immobilized product storage, and other support activities. The structure was designed to withstand and contain the dynamic and static overpressure and fragments resulting from a worst case rupture of the HIP.^{11,20}

A krypton-85 release of $\sim 128,000$ Ci is estimated to result in an off-site dose at 3 km of ~ 17 mrem for an ORNL Hydrofracture facility.²¹ A maximum krypton-85 accidental release from an encapsulation facility is expected to be similar, resulting in a similar off-site dose.¹¹ Thus the maximum emergency off-site dose is well below the emergency protective action guide level of 5 rem thyroid and 1 rem whole body.²²

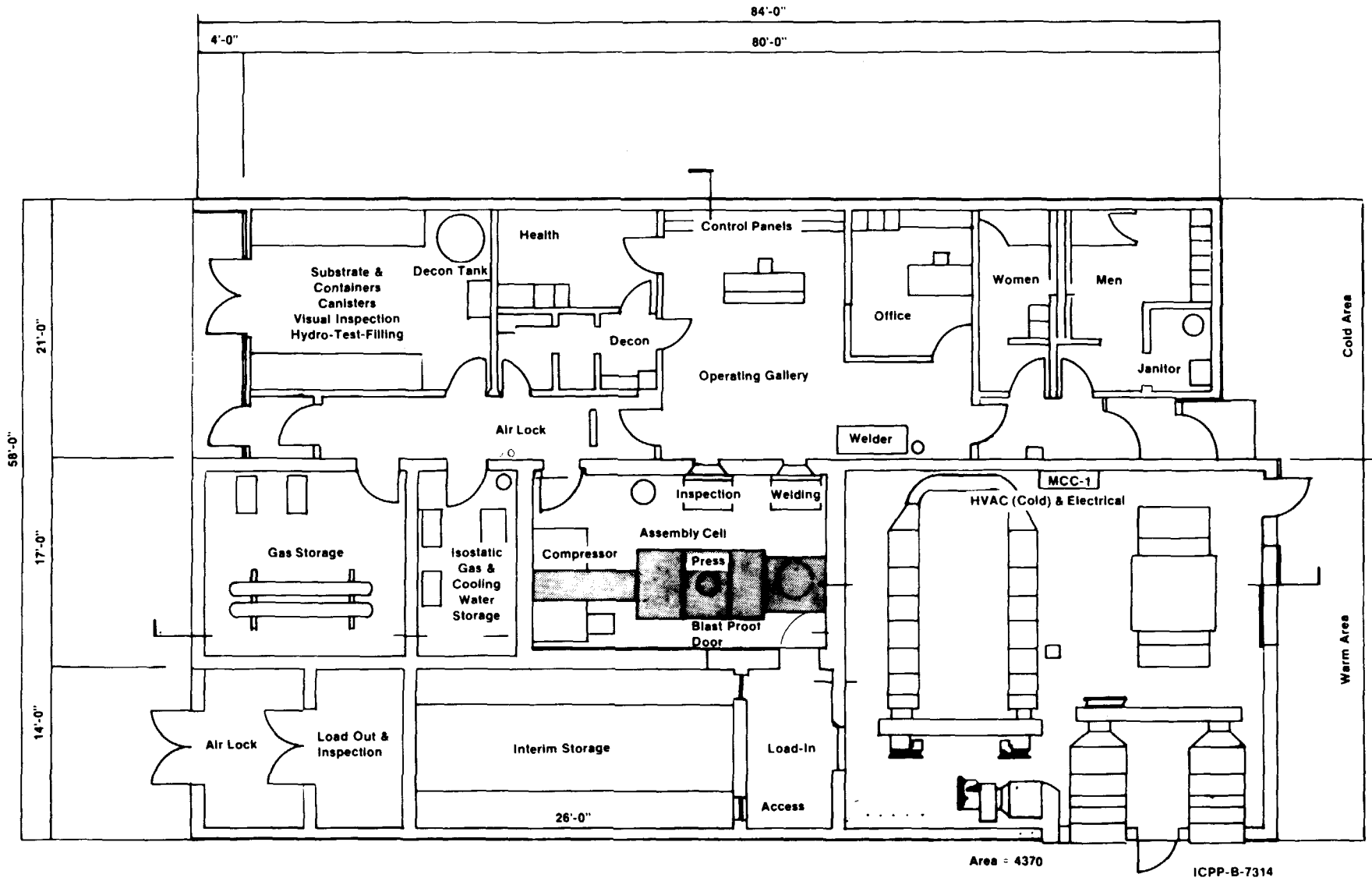


Figure 16. Krypton Encapsulation Facility Floor Plan

17th DOE NUCLEAR AIR CLEANING CONFERENCE

Based on a review of nuclear licensing procedures and requirements, it was concluded that major concerns appear to be in compliance with applicable codes for HIP fabrication and with developments associated in scaling up demonstration plants.¹¹ The licensing of a krypton-85 encapsulation facility should not be excessively expensive or lengthy.¹¹

Total facility and operating costs were evaluated on a life-cycle cost basis, following procedures of the Life-Cycle Manual for the Federal Energy Management Program.²³ The manual specifies that the total present value of the facility is calculated, using a 7 percent per year discount rate for annual costs. The facility was assumed to operate for 30 years, with no salvage value remaining thereafter.

The costs of a Kr encapsulation facility described above are provided in Table II for two sets of design conditions, operating at 300 and 600 cycles per year. Details are provided elsewhere.¹¹

TABLE II
KR ENCAPSULATION PROCESS LIFE-CYCLE COSTS

	<u>300 cycles/yr^a</u>	<u>600 cycles/yr^b</u>
1. Present Value Initial Capital Investments (90% of total)	9.1	9.5
2. Present Value of Life Cycle	0.5	0.6
3. Present Value of Life Manpower	5.1	6.8
4. Present Value of Life Cycle Materials	4.1	4.1
5. Present Value of Life Cycle Replacement/Maintenance	0.9	0.9
6. Present Value of Life Cycle Replacement/Insurance	0.1	0.1
Total Present Value of All Life Cycle Costs	19.8	22.0

^a Calculated using the base case from Parsons¹¹.

^b Base case from Parsons¹¹.

IV. Conclusions

The process to encapsulate krypton-85 in zeolite 5A is technically and economically feasible and can be used to produce a product with a compact solid mass at 700 °C and 100 MPa. A 2000 MTHM per year reprocessing plant would result in up to 5 m³ of zeolite containing krypton-85. At long term storage conditions of 300 or 400°C, less than 0.03% or 0.3% of the krypton inventory, respectively, will leak from sintered zeolite 5A.

The encapsulation process requires a hot isostatic press (HIP) with an 8 or 16 L isolated work zone to operate for 600 or 300 cycles per year, respectively. Since existing HIP technology uses work zones ranging from 1 to 3500 L in capacity at similar production rates, a great deal of flexibility is available, such as operating with a larger volume work zone, fewer cycles per year, or lower encapsulation pressures.

Based on a preconceptual design and cost estimate of a krypton encapsulation facility, the process is economically feasible. No major technology development is required for the process. Maximum krypton-85 release from a worst-case incredible accident would result in maximum doses at the site boundary which are well below the Protective Action Guides for accidental releases. The licensing of a krypton encapsulation facility should not be inordinately lengthy or excessively expensive.

Acknowledgment

The assistance of the following is gratefully acknowledged: H. S. Cole, J. R. Delmastro, E. S. Dickerson, L. L. Dickerson, N. S. Graham, S. H. Hinckley, J. C. Mittl, R. A. Rankin, and E. S. Wade of Exxon Nuclear Idaho Co.; Dr. R. D. Penzhorn of Karlsruhe KfK, Germany; Dr. S. Iijima of Arizona State University; Dr. A. Ruoff of Cornell University; and Dr. G. L. Messing of Pennsylvania State University.

V. References

1. Code of Federal Regulations, 40 CFR 190 (1977).
2. National Council on Radiation Protection and Measurements, Krypton-85 in the Atmosphere. Accumulation, Biological Significance, and Control Technology, NCRP Report No. 44 (July 1, 1975).
3. Management of Commercially Generated Radioactive Waste, Draft Environmental Impact Statement, DOE/EIS-0046-D (April 1979).
4. R. D. Klett, ed., Krypton-85 Disposal Program Conceptual Design Phase: Final Report, SAND-81-1957 (December 1981).

17th DOE NUCLEAR AIR CLEANING CONFERENCE

5. D. S. Whitmell, R. S. Nelson, and M. J. S. Smith, "Containment of krypton in a metallic matrix by combined ion implantation and sputtering," Management of Gaseous Wastes from Nuclear Facilities, IAEA-SM-245/7, 263-278 (December 1980).
6. G. L. Tingey et al., Entrapment of Krypton in Sputter Deposited Metals - A Storage Medium for Radioactive Gases, PNL-2879 (April 1979).
7. R. D. Penzhorn, "Long-term storage of ^{85}Kr in zeolite 5A," Proceedings of the 16th DOE Air-Cleaning Conference, CONF-801038, 2, 1047-1058 (October 1980).
8. A. B. Christensen, J. A. Del Debbio, J. E. Tanner and D. A. Knecht, "Loading and leakage of krypton immobilized in zeolites and glass," Sci. Basis Nucl. Waste Mgmt., 3, 251-8 (1981).
9. A. B. Christensen, J. A. Del Debbio, D. A. Knecht, and J. E. Tanner, "Immobilization and leakage of krypton encapsulated in zeolite or porous glass", ibid, 4 (to be published 1982).
10. G. L. Tingey et al., Solid State Storage of Radioactive Krypton in a Silica Matrix, PNL-3612 (December 1980).
11. A. B. Christensen, J. A. Del Debbio, D. A. Knecht, J. E. Tanner, and S. C. Cossel, The Immobilization of Krypton-85 in Zeolite 5A and Porous Glass, ENICO - 1102 (December 1981).
12. H. D. Hanes et al., "Hot isostatic processing", High-Pressure Science and Technology, 2 (1979).
13. H. T. Larker, "Hot isostatic pressing for the consolidation and containment of radioactive waste", Sci. Basis Nucl. Waste Mgmt., 1, 207-10 (1979).
14. D. W. Breck, Zeolite Molecular Sieves, John Wiley and Sons, New York (1974).
15. G. Denny, J. Wyart, and G. Sabatier, "Structural mechanism of thermal and compositional transformations in silicates", Z. Kristallographie, 112, 161-168 (1959).
16. H. Hoss and R. Roy, "Zeolite studies III: On natural phillipsite gismondite, harmatome, chabazite, and gmelinite", Beitr. Minem U. Petrogr., 7, 389 (1969).
17. R. W. Benedict, A. B. Christensen, J. A. Del Debbio, J. H. Keller, and D. A. Knecht, Technical and Economic Feasibility of Zeolite Encapsulation for Krypton-85 Storage, ENICO-1011 (September 1979).
18. L. A. Bursill, E. A. Lodge, and J. M. Thomas, "Zeolite structures as revealed by high-resolution electron-microscopy", Nature, 286, 111 (July 1980).

17th DOE NUCLEAR AIR CLEANING CONFERENCE

19. J. Crank, The Mathematics of Diffusion, Clarendon Press, Oxford (1956).
20. A. B. Christensen, J. E. Tanner, and D. A. Knecht, Preliminary Safety Evaluation of a Commercial-Scale Krypton-85 Encapsulation Facility, ENICO-1055 (September 1980).
21. F. J. Peretz et al., ⁸⁵Kr Hydrofracture Engineering Feasibility and Safety Evaluation, ORNL/ENG/TM-22 (July 1981).
22. US Environmental Protection Agency, Manual of Protective Action Guides and Protective Actions for Nuclear Incidents, EPA-520/1-75-001 (June 1980).
23. Life-Cycle Cost Manual for Federal Energy Management Program, NBS Handbook 135.

DISCUSSION

SIEGLER: What is the feed stream and where do you get the concentrated feed streams?

KNECHT: The compositions are given in the paper. We have encapsulated mixtures of N₂, O₂, Ar, Kr, and Xe with a Kr content of 54 or 68%. The Kr loading and leakage were not affected by the added components if based on the partial Kr pressure. There does not seem to be a limitation on the source of a concentrated feed stream. It could come from a Kr recovery facility using cryogenic distillation or fluorocarbon absorption.

MONSON: Why did you choose zeolite 5A over all other materials and what is the krypton loading capacity for zeolite 5A encapsulation?

KNECHT: We initially used sodalite, which trapped krypton physically and did not change its structure. Dr. Penzhorn at KFK discovered that zeolite 5A could be sintered in the presence of krypton, trapping the gas atoms by changing the alumino-silicate structure. We find that the sintered zeolite 5A exhibits much lower leakage rates than sodalite and is available commercially at low cost. The krypton loading capacity is quite high, 30 to 60 m³ of gas at STP per m³ of zeolite solid. This density is equivalent to krypton storage in pressurized cylinders at 1,000 psi.

MOELLER: Would it be practical to use this system for the immobilization of ⁸⁵Kr from commercial nuclear power plants?

KNECHT: Yes. This system is being designed for a 2,000 MTHM per year commercial-scale reprocessing plant which would reprocess the fuel from 67 commercial nuclear power plants.

KABAT: Have you considered that there is any need for krypton-85 removal from the nuclear power plant?

KNECHT: No. The U.S. regulation, which applies to nuclear fuel in the reactor and goes into effect on January 1, 1983, limits the amount of krypton-85 that you can release to 50,000 curies per gigawatt year of electrical generation. About 86% of the krypton that is in the fuel cannot be released. The regulation does not say exactly when the release can take place, so presumably you could recover more of it and then release it later, or use some other arrangement. The regulation is there even though most people recognize that the fuel cladding will retain most of the krypton within the reactor core.

BONKA: I want to comment on the last question. The retention of ⁸⁵Kr at nuclear power plants is not important. The emission rate is only approximately 20 Ci/GW(e). Without ⁸⁵Kr retention, the emission rate at a reprocessing plant with 1,400 T/y is nearly 10⁷ Ci/y

THE LONG-TERM STORAGE OF RADIOACTIVE KRYPTON BY FIXATION
IN ZEOLITE 5A⁺.

R.-D. Penzhorn, H. Leitzig, K. Günther, P. Schuster and H.E. Noppel

Kernforschungszentrum Karlsruhe, IRCh/PWA , 7500
Karlsruhe, Postfach 3640, Federal Republic of Ger-
many.

ABSTRACT

A process developed in Karlsruhe for the long-term storage of radioactive krypton is based on the observation that, in the temperature range 340 - 650 °C and at pressures above 100 bar, krypton can be trapped efficiently in zeolite 5A. The fixation involves a transformation of the original crystal framework into an amorphous state of the solid substrate. After conditioning the gas is neither liberated by elevated temperatures, liq. Rb at 150 °C nor gamma radiation.

In this report data are presented on the presumable temperature profiles in a final storage vessel, expressed as a function of the immobilized Kr-85 inventory. The obtained results correlate well with data estimated from measured thermal conductivities of zeolite 5A.

To verify the process hot experiments were carried out that so far have led to samples with up to 0.03 [Ci/g]. Qualitatively, these samples were shown to be stable. A quantitative evaluation, also with samples having much higher specific activity, is in progress.

A demonstration facility is now under construction. The immobilization of Kr will be carried out at $t < 520$ °C and $p < 300$ bar in a thick-walled one-way autoclave, having a capacity of 5 litres. Gas pressurization will take place by one of two alternatives: a] sorption/desorption of Kr in zeolite 5A at above atmospheric pressure and room temperature or b] sorption/desorption of Kr in zeolite 5A at low temperature and atmospheric pressure. The one-way autoclave concept leads to a very simple process and provides a highly safe second containment during final long-term storage.

+ Supported in part by the Commission of the European Communities under its program on radioactive waste and storage.

INTRODUCTION

Zeolite 5A was recently proposed as a matrix for the long-term storage of ^{85}Kr , after it was discovered that noble gases can be immobilized in this molecular sieve by hydrothermal chemifixation and it was shown that the conditioned gas is very stable towards elevated temperatures, radioactive radiation and certain chemicals [1,2,3]. Work carried out in Idaho has confirmed and extended these first observations [4].

The present paper contains results on the chemifixation of Kr in compacted zeolite 5A. Data are also given on the thermal conductivity of zeolite 5A, the transport of heat in the final storage vessel and the fixation of radioactive krypton in zeolite 5A. In addition, the demonstration facility presently under construction is discussed.

RESULTS AND DISCUSSION

Krypton fixation in compacted zeolite 5A

The bulk density of 2 mm 5A zeolite pellets and the density of activated pellets, measured pycnometrically in toluene, were found to be 0.83 and 1.58 [g/cm³] respectively. The resulting external void fraction is 0.47. If this void fraction is reduced by compaction a decrease in free ^{85}Kr inventory during chemifixation is achieved. Also, heat transport during final storage is improved and less waste is obtained. Therefore, it appeared interesting to examine compaction techniques like mechanical compression and dessication of a slurry. By mechanical compression of 2 mm zeolite pellets, with pressures up to 178 [kN/cm²], tablets having diameters between 12 and 50 mm and heights up to 30 mm were prepared. Application of progressively increasing hydraulic pressures yielded tablets showing a regular increase in bulk density [see table 1]. As apparent from the data, the specific BET surface area experiences a significant decrease only, when the employed hydraulic pressure exceeds 100 [kN/cm²]. In consequence, since the BET determination is carried out at atmospheric pressure, it is anticipated that at several hundred bar pressure,

Table I . Manufacture of tablets from 2 mm 5A zeolite pellets

Hydraulic pressure [kN/cm ²]	Density [g/cm ³]	Specific surface area [m ² /g] ⁺
25	1.31	479.0 ± 10.9
50	1.40	-
75	1.46	458.4 ± 8.4
100	1.52	445.8 ± 12.0
125	1.56	367.1 ± 10.6
175	1.60	-

+ the specific surface area of 2 mm 5A zeolite pellets, determined with N₂ at -196 °C, is 459.9 ± 10.2 [m²/g].

i.e. during chemifixation, compaction will have little influence on the rate of gas diffusion into the zeolite crystals. That this is indeed the case is apparent from the results compiled in table II. They demonstrate that under identical fixation conditions the volu-

Table II . Krypton fixation in various Ca exchanged type 5A zeolites [p = 1000 bar]

Zeolite [MO/Al ₂ O ₃ , M = Ca]	Loading [cm ³ STP Kr/cm ³ zeolite]	
	2 mm pellets	tablets ⁺
0.102	1.4	1.12
0.298	8.4	52.4
0.466	26.6	43.4
0.550	35.7	69.7
0.600	35.7	71.2
0.910	22.4	67.1

+ tablets with ρ = 1.4 [g/cm³], prepared with a hydraulic pressure of 50 [kN/cm²]

metric loading of tablets is at least twice as high as that of 2 mm pellets.

In one run Kr was trapped in a desiccated 5A zeolite slurry. Employing a fixation pressure of 1000 bar at a temperature of 520 °C, a loading of 57.3 [cm³ STP Kr/g] was obtained, which is higher by a factor 1.8 than that achieved under identical fixation conditions in 2 mm pellets.

The effect of compaction on the volumetric loading of an autoclave is illustrated in table III.

Table III Degree of filling of an autoclav

Aggregation form of matrix	Density of matrix [kg/l]	Filling [kg/l autoclav]	Loading ⁺ [l STP Kr/l autoclav]
2 mm pellets	1.4	0.7	14
slurry	1.0	1.0	20
tablets ⁺⁺	1.4	1.1	22
tablets + pellets	1.4	1.2	24

+ based on a loading of 20 [cm³ STP Kr/g zeolite]

++ \varnothing tablet/ \varnothing autoclav = 0.33

The highest loading is achieved when the autoclav is filled with a combination of pellets and tablets. Filling can also be improved when pellets of two different diameters are employed [5] .

Thermal conductivity of zeolite 5A

Because most of the β -radiation [average energy = 0.246 MeV] emitted by ⁸⁵Kr is absorbed by the solid matrix a temperature rise in the fixation media is expected. For a reliability assesment, but also to maximize loading without sacrificing safety gained by immobilization, it is necessary to know the temperature profile that developes. The maximum temperature will depend upon the specific ⁸⁵Kr activity, the thermal conductivity of the fluid media surrounding the solid, the void fraction of the solid and the thermal conductivity of the solid. At atmospheric pressure the heat conductivity of most gases is low. Therefore, heat transport will take place essentially near the contact points of the granular material.

To measure the thermal conductivity of zeolites a comparison method was chosen, which involves a measurement of the temperature difference between two points in a material when, under steady state conditions, heat flows linearly from one point in the direction of the other. The temperature difference is related to the heat flow by Fourier's equation. Several types of samples were examined, employing Pyrex 7740 as the reference material: fluid medium/fiber glass, 2 mm 5A pellets in several fluid media and zeolite 5A tablet. No attempt was made to determine accurate thermal conductivity values of the gases. A few measurements with argon, krypton and air were only carried out to calibrate the system. For this purpose, a fiber glass filling material, having a bulk density of $0.1 \text{ [g/cm}^3\text{]}$ and a thermal conductivity about 25 times lower than that of Pyrex 7740, was placed between the reference cylinders.

One aspect that needs to be considered when determining the thermal conductivity of zeolites is the high affinity of these molecular sieves for water. For instance, a activated sample, left under ambient conditions for several hours, will sorb up to 21 weight % of water. It is thus clear that, in a study on the temperature dependence of the thermal conductivity, the initial water content of a non activated zeolite will not remain constant. Since the water content in the crystalline framework has an influence on the thermal conductivity it is difficult to obtain meaningful results. These considerations may explain the observation that, whereas at low temperature, i.e. 300 K, the thermal conductivity of non activated 5 A tablets [$\emptyset = 50 \text{ mm}$, height = 15.8 mm and $\rho = 1.5 \text{ [g/cm}^3\text{]}]$ is higher by approx. 0.03 [w/m · deg] than that of a pretreated tablet [0.19 [w / m · deg], at temperatures above 550 K both samples have about equal thermal conductivity [at 550 K 0.25 [w/m · deg]].

Zeolite 5A containing trapped gas will no longer sorb water [2]. Its internal void fraction is nearly zero as indicated by the specific surface area, which decreases from an initial 450 [m^2/g] of the pretreated, unloaded 5A zeolite to about 2 - 3 [m^2/g] after noble gas fixation. Thus the thermal conductivity in air of zeolite 5A containing 43 [$\text{cm}^3\text{STP/g}$] noble gas was measured both in form of 2 mm pellets and as a tablet [dimensions as above]. It was found that the thermal conductivity of the pellets increases linearly with temperature from 0.11 up to 0.16 [w/m · deg] in the range 20 - 280 °C. In the same temperature

range the thermal conductivity of the tablet was about twice as high.

The thermal conductivity of zeolite pellets increases in the order 1 : 1.3 : 1.5 when the measurement is carried out in the presence of Kr, Ar or air. Analogous measurements with a monolithic zeolite block indicate that after compaction the influence of the surrounding fluid medium becomes negligible

A very crude estimation of the absolute thermal conductivity of zeolite type A gives a value of about 1 [W/m · deg] at 300 °C, similar to that glass or quartz

Heat transport measurements

Christensen [6] calculated the heat transport through cylinders containing piled zeolites cooled by natural heat convection. He examined the interaction of cylinder radius, ^{85}Kr loading, and centerline temperature for sodalite pellets. An experimental verification of the calculation was however not carried out.

To simulate a final storage vessel two stainless steel cylinders of equal length [1000 mm] but different diameters, i.e. 89 and 134 mm, were employed. The respective wall thicknesses were 3 and 4.5 mm. Each cylinder was provided with 12 axially and radially distributed Fe/constantan thermocouples as well as four heating coils [see fig. 1 , which shows zeolite pellets in a pyrex glass tube]. All measurements were carried out with activated, unloaded 2 mm 5A zeolite pellets. Cooling occurred by natural convection. Fig. 2 shows a tridimensional plot giving the axial cylinder temperatures vs the radioactive gas loading and the cylinder radius of the larger vessel. Fig. 3 shows similar data together with temperature profiles [dotted lines] estimated with thermal conductivity values obtained in this work. The agreement between the experimental temperature profiles and those calculated employing appropriate heat conduction equations, is satisfactory. It is seen that natural convection will remove the heat generated by radioactive ^{85}Kr decay and will maintain the maximum centerline temperature in a 134 mm \varnothing storage vessel at temperatures below 80 °C, provided the specific loading is lower than 30 [cm³ STP/g]. These temperatures are to be considered upper limits, because activated zeolites conduct heat less

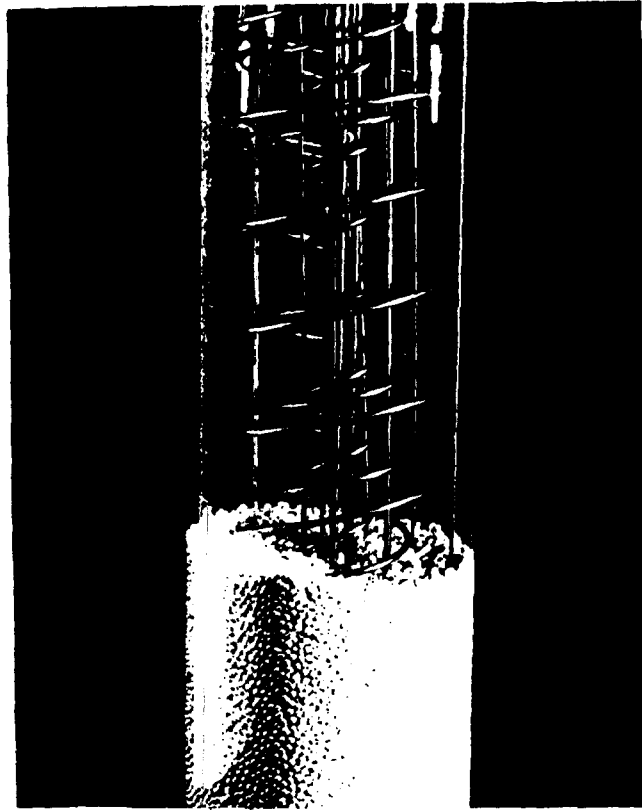


Fig. 1 Experimental set-up showing heating coils, and thermocouples.

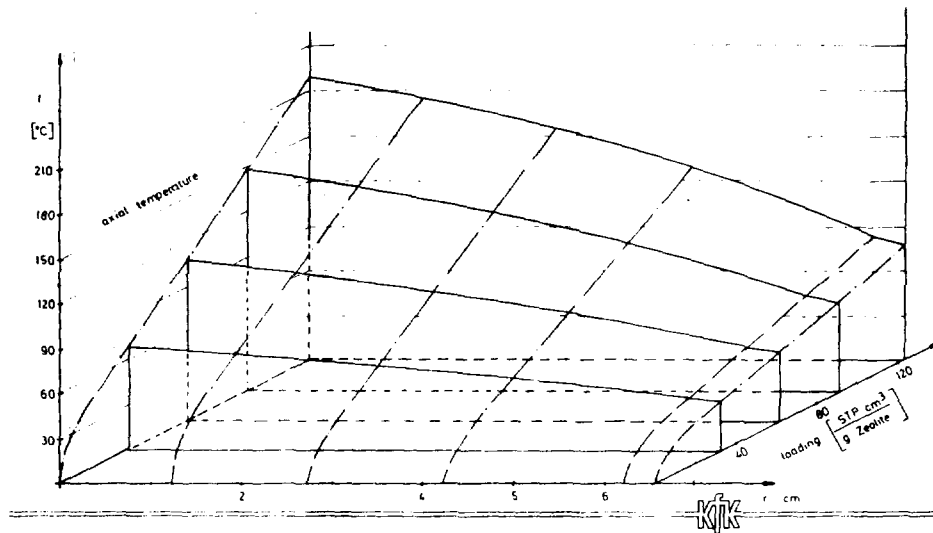


Fig. 2 Tridimensional graph of the axial temperature vs loading and radius of a 134 mm \varnothing vessel containing 2 mm 5A zeolite pellets.

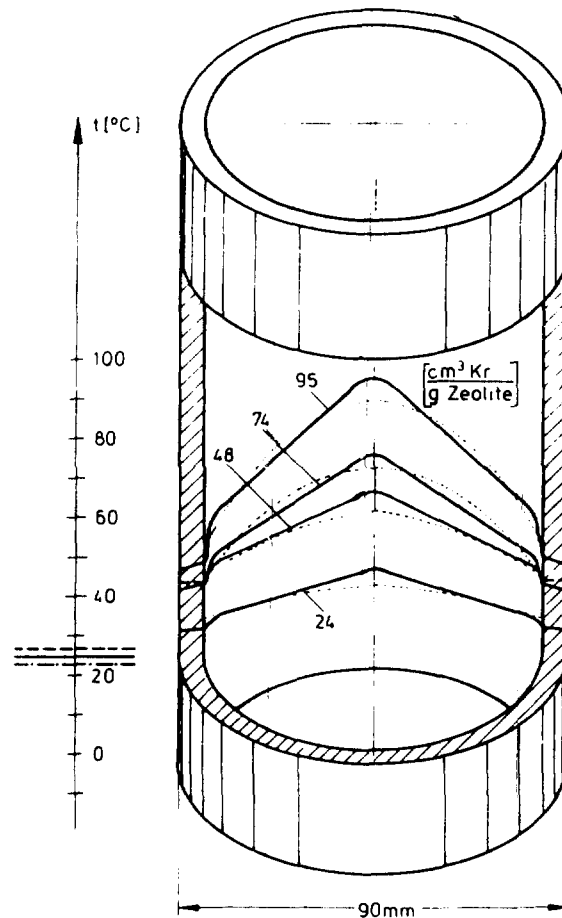


Fig. 3 Temperature profile in a 90 mm \varnothing cylinder as a function of zeolite loading with radioactive krypton. The dotted lines correspond to temperatures calculated with thermal conductivity values obtained in this work.

efficiently than non activated zeolites or zeolites containing trapped noble gas. Furthermore, for commercial krypton disposal, some form of compacted zeolite, having higher thermal conductivity, will probably be employed.

Chemifixation of radioactive krypton

To verify the process and obtain a product for observing the long-term effects of decaying radioactive krypton several hot samples have been prepared. The employed equipment, shown in fig. 4, is very simple. It consists essentially of a one liter storage cylinder, a 4 cm³ pressurization vessel and a 1 cm³ autoclave, containing the zeolite. To carry out a fixation the system is first evacuated. Then the zeolite is activated and radioactive krypton ex-

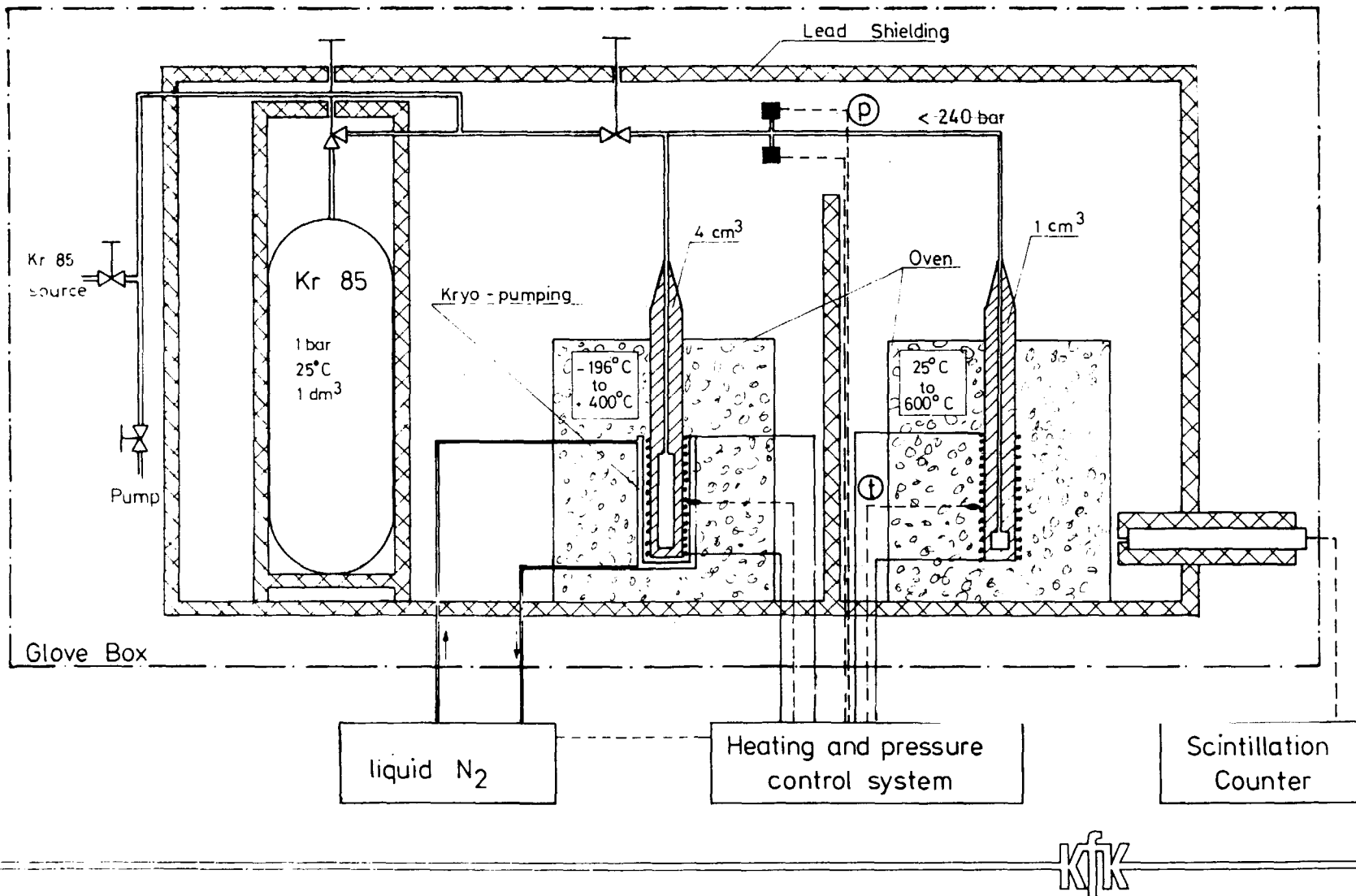


Fig. 4 Fixation of radioactive krypton

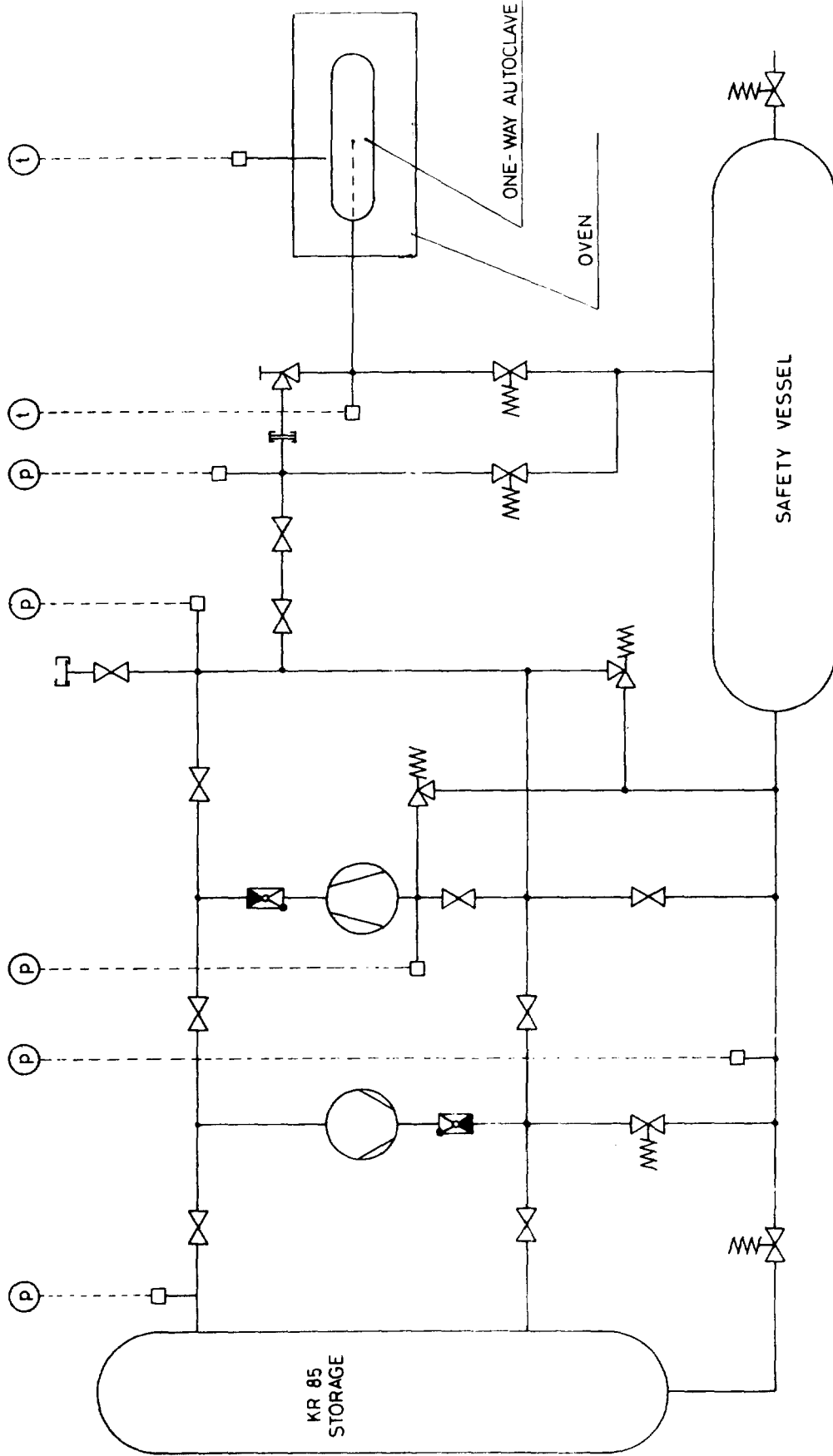


panded into the storage cylinder until a pressure of about 1 bar is reached. Next, Kr is frozen out with liq. N_2 in the pressurization vessel and, after closing the appropriate valve, expanded into the pressurization vessel and the autoclave. When the pressurization vessel is heated up to $400^\circ C$ a pressure of approx. 180 bar builds up. At the same time Kr is sorbed by the zeolite [still at room temperature]. Fixation takes place when, finally, the autoclave is heated up to $520^\circ C$. By the above procedure three active samples have been prepared. Their loading and specific activity were 19.6, 20.6 and 19.4 [cm^3 STP $^{85}Kr/g$] and 3.2, 28.3 and 24.3 [mCi/g] respectively. Qualitative inspection of these samples for a period of approx. three month showed them to be stable. A quantitative evaluation, designed to examine leakage [effect of temperature] and chemical stability is in progress.

Within the next few month's additional samples, having a specific activity of the order of 3 - 10 [Ci/g] will be produced. This specific activity is equal or higher than that expected during final storage.

Facility for the immobilization of krypton

A facility, illustrated schematically in fig. 5, is presently under construction. The major equipment includes an thick-walled externally heated one-way autoclave provided with a quick connector, an oven for the pretreatment of the zeolite also to be employed for the hydrothermal krypton fixation, several pumps, a compressor [up to 7 bar], several storage cylinders manifolded together with stainless steel lines, safety devices, temperature and pressure registration, etc. Gas densification will be achieved by sorption/desorption either at 4.5 bar and room temperature or at 1 bar and $-20^\circ C$ [see fig. 6]. Under these conditions enough gas will be sorbed by the zeolite so that, upon raise of temperature up to $520^\circ C$, a pressure of approx. 300 bar will build up in the autoclave due to desorption, and about 22 [cm^3 STP/g] noble gas will be immobilized by chemifixation. By this procedure the process is considerably simplified, because gas pressurization is achieved without a high pressure compressor or a complicated cryopump. The facility will provide information on large scale pretreatment, heat transport, material behaviour, energy consumption, operation time, loading homogeneity, safety devices, etc.



KJK

Fig. 5

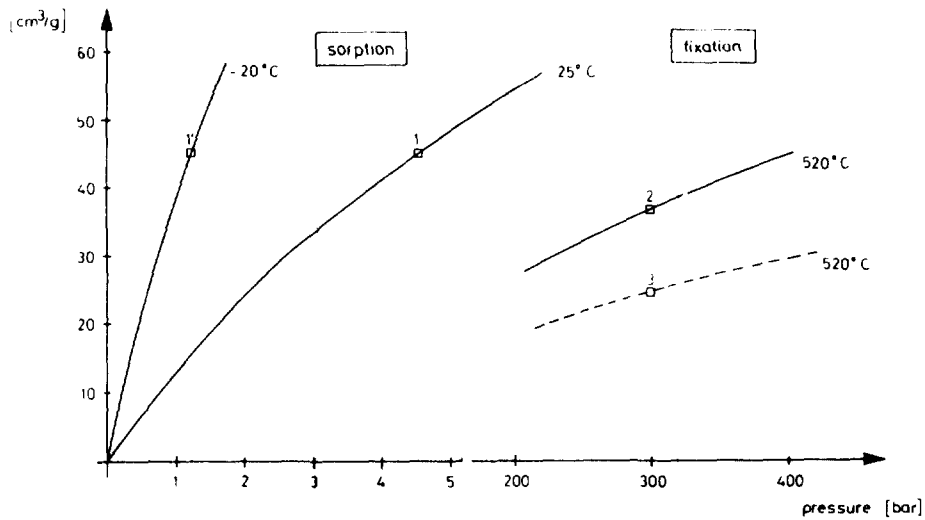


Fig. 6 Sorption and fixation isotherms for krypton in zeolite 5A

The main advantage of the one-way autoclave concept is seen in the simplicity of the process. In addition, the one-way autoclave can be considered a highly safe secondary containment during final disposal because of its inherent resistance towards internal and/or external corrosion, mechanical destruction and temperature excursions.

REFERENCES

- [1] R.-D. Penzhorn, P. Schuster, H.E. Noppel, L.M. Hellwig
Int. Symp. on Management of Gaseous Wastes from Nuclear Facilities, Vienna, Feb. 18-22 [1980]
- [2] R.-D. Penzhorn
16th DOE Nuclear Air Cleaning Conf., San Diego, Calif., Oct. 20-23 [1980]
- [3] R.-D. Penzhorn, P. Schuster, H. Leitzig, H.E. Noppel
to be published in Ber. Bunsen Gesellschaft [1982]
- [4] A.B. Christensen, J.A. DeDebbio, D.A. Knecht, J.E. Tanner, S.C. Cossel
ENICO 1102 [1981]
- [5] A. Kaupa
IMF-Arbeitsbericht Nr 4/65 KfK [1965]
- [6] A.B. Christensen
ICP - 1128 [1977]

DISCUSSION

KNECHT: I would like to comment on the differences in scale of your and our envisioned commercial-scale encapsulation facilities. We are considering a design for a Kr immobilization facility for a 2,000 MTHM per year reprocessing plant while you are considering a design for a 300 MTHM per year reprocessing plant.

PENZHORN: That is correct. We believe that the one-way autoclave concept will be particularly suitable for conditioning the krypton-85 produced in small reprocessing plants (300-350 MTHM per year).

EBY: What do you see as the primary contributing factor for the improvement in loading capacities that you have observed in your recent work as compared to the 1978 studies?

PENZHORN: I like to distinguish between 1) totally reversible sorption, 2) encapsulation, which involves trapping without destruction of the crystal framework and 3) chemifixation, an irreversible process which takes place after the pores to the cavities are closed by a hydrothermal reaction. It was the discovery of the latter form of immobilization that led to improvements of the sorption capacities. By chemifixation, gases can be trapped efficiently in large cavities with large pore openings as opposed to encapsulation where you look for pore openings smaller than the effective kinetic diameter of the gas to be immobilized. Also, in chemifixation, high pressures are no longer required because loading occurs by sorption and not by activated diffusion.

VIKIS: Is the chemical purity of krypton, particularly with respect to the air components, critical to the success of this method?

PENZHORN: No. We think that the composition of the gas to be conditioned is of no consequence to the process. In fact, we have shown that Ne, Ar, Kr and Xe can be trapped in zeolite 5A. Also, 1:1 mixtures of Ar and Xe, as well as Kr and Xe, have been immobilized. In this case, however, we noticed an enrichment of Xe in the zeolite. This is due to the fact that Ar and Kr are sorbed less efficiently by zeolite 5A than Xe.

VOLATILIZATION AND TRAPPING OF RUTHENIUM
IN HIGH TEMPERATURE PROCESSES

M. Klein, C. Weyers, W.R.A. Goossens
SCK/CEN, Nuclear Energy Center
200, Boeretang
B-2400 MOL, Belgium

Work performed within a contract with DWK in Germany in the framework of the HAW technological programme for the vitrification of HLW.

I. Introduction

Solid radioactive aerosols and semi-volatile fission products e.g. Ru, Cs, Sb are generated during high level waste calcination and vitrification processes. The retention of Ruthenium has first been studied because of its strong tendency to form volatile compounds in oxidative media. Since RuO_4 was the suspected form for the high degree of volatilization during high temperature processes, the study has started with testing of capture materials for the trapping of RuO_4 .

II. Materials for the retention of RuO_4

Two types of trapping materials were tested, either adsorbants such as Silica-gel operating above the dew point of the gas, either catalysts such as ferric-oxide/chromium oxide catalyst operating at 300 °C. Detailed results of this laboratory study are reported elsewhere (1) (2).

Three different cases were considered for the carrier gases :

- RuO_4 mixed with dry air ;
- RuO_4 mixed with moist air till a dew point of 85 °C ;
- RuO_4 mixed with NO_x and water vapour produced by high temperature calcination of nitric acid.

For the adsorption on Silica-gel, the bed temperature, which must be higher than the gas dew point, determines the adsorption capacity and the DF. At room temperature, an adsorption capacity of 1 mg/g and a DF of 1000 were obtained for an inlet concentration of 100 mg/m³. At 100 °C, with or without water vapour, the adsorption capacity is lower than 0.2 mg/g and the bed is very rapidly saturated, moreover the presence of high concentrations of water vapour decreases the adsorption capacity of the bed for RuO_4 . For the adsorption of the volatile ruthenium on silica-gel at 100 °C, the presence of NO_x greatly improves the performance of the bed. Indeed, with NO_x , no breakthrough of the bed could be measured and the DF of the bed increased with time (DF from 10 to 100).

In all the cases, the adsorbed species on the bed is slowly reduced into a more stable species, probably ruthenium oxides. Without NO_x , the adsorbed species on the bed can generally be desorbed nearly quantitatively (till 75 %) ; in presence of NO_x , the desorption is limited to 5 % maximum.

For the retention on a ferric oxide/chromium oxide catalyst, in all the cases the capture mechanism is a catalytic decomposition of the volatilized species which is transformed into solid oxides. The deposit of ruthenium oxides enhances the reaction rate so that the DF increases with time. The capacities are higher than 10 mg/g since no bed breakthrough are observed. The initial DF is one order of magnitude lower in presence of NO_x which indicates that the reaction rate is lower. Consequently the RuO_4 very unstable at 300 °C is easily trapped, but in presence of NO_x the species formed is more stable and so has a lower decomposition rate.

A general conclusion of this study is, that in presence of NO_x , the concept of a stable RuO_4 is not any more valid and that the volatile species is probably a nitrosyl ruthenium compound more stable, and more easily adsorbable but more difficulty decomposable than RuO_4 . As a consequence, RuO_4 trapping study was stopped and a study on Ru behaviour during high temperature calcination or vitrification of nitric acid solution of Ru was started.

III. Calcination of nitric acid containing ruthenium

In the CALCILAB laboratory unit described in (2), nitric acid solutions containing $\text{RuNO}(\text{NO}_3)_x(\text{OH})_{3-x}$ complexes are calcined in an inconel calciner with a through-put of about 50 ml/h. The Ru-volatility varies between 50 and 70 % at 600 °C and decreases to 30 % at higher calcination temperatures of 800 to 1000 °C.

The nature of the volatilized species depends also on the calcination temperature ; at 600 °C, the Ru coming out of the calciner is almost completely condensed (DF condensor 360) and only a minute fraction is in aerosol form (0.2 %). If the calcination temperature increases, the % of Ru in aerosol form increases exponentially and reaches respectively 1 and 8 % at 800 °C and 1100 °C. That means that the condensor DF decreases from 80 at 800 °C to 13 at 1100 °C. The condensed form of Ru is soluble in the acidic condensate (pink purple colour) but is slowly reduced to an insoluble oxide. In these conditions, if a specific Ru filter is placed at the exit of the condensor, the efficiency of the bed will be very small since only the aerosol form of Ru is still present in the off-gases.

If the specific Ru filter is placed directly at the exit of the calciner, the volatile species can be trapped. A silica-gel adsorbant bed operating at 100 °C shows an efficiency from 10 to 100 which increases with time. Saturation of this bed is not observed so that the silica-gel capacity is at least higher than 1 mg/g. The adsorption mechanism seems to be similar to the mechanism occurring when RuO_4 and NO_x are mixed together.

A ferric oxide/chromium oxide catalyst can also achieve DF's higher than 10. The mechanism is also similar to these observed when RuO_4 and NO_x were mixed namely :

- increase of the DF with time i.e. with increasing ruthenium oxides deposits ;
- irreversibility of the trapping by catalytic decomposition into stable ruthenium oxides.

IV. Behaviour of Ru in a liquid fed melter

In order to simulate the PAMELA concept for the vitrification of H.L.W., a laboratory unit called VITRILAB with a 2 kg glass capacity and with liquid feed on the molten glass surface has been constructed. The off gas purification line comprises in series a packed bed dust scrubber, a specific Ru filter, an ejector venturi, a condenser and finally a washing bottle and an absolute filter. The liquid feed is a simulated LEWC solution containing traced ruthenium species. The flow sheet of the laboratory VITRILAB unit is given in fig. 1 and the composition of the simulated LEWC solution is given in table I.

Volatilization of Ru from the glass melter

Volatility of Ruthenium with an LEWC liquid feed. The volatility of Ru in a liquid fed melter depends on a number of factors such as liquid flow rate, degree of coverage of the glass pool with a molten salt layer and air sparging flow rate. With a liquid flow rate of 0.14 l/h and an air sparging of 90 l/h, the volatility ranges from 15 to 20 % in the begin of a run but rapidly decreases to values ranging from 10 to 7 % when a molten salt layer covers the glass surface. An increase of the liquid flow rate from 0.14 to 0.17 l/h and a decrease of the sparging air flow from 90 to 60 lN/h result in a decrease of the mean volatility till values of 7 to 3 %.

Table I. Composition of simulated LEWC solution.

NaNO ₃	154	g/l
Fe(NO ₃) ₃ · 9H ₂ O	75	
Al(NO ₃) ₃ · 9H ₂ O	68	
Ni(NO ₃) ₂ · 6H ₂ O	9.5	
Na ₂ MoO ₄ · 2H ₂ O	9	
Ce(NO ₃) ₃ · 6H ₂ O	7.9	
Cr(NO ₃) ₃ · 9H ₂ O	7.4	
Ba(NO ₃) ₂	3.3	
La(NO ₃) ₃	4	
CsNO ₃	3.6	
Y(NO ₃) ₃ · 6H ₂ O	1.9	
Sr(NO ₃) ₂	1.9	
Zn(NO ₃) ₂ · 6H ₂ O	1.2	
RuNO(NO ₃) ₃	6.3	

Specific activity of traced Ru solution

0.1 to 210⁶ Bq/l

Special care is necessary to avoid blockage of the off gas outlet pipe by ruthenium oxides and dust deposition. In order to prevent the formation of a dust layer in the off gas pipe, a small fraction of the circulating liquid of the dust scrubber is fed countercurrent into the outlet pipe, vaporizes in contact with the outlet tube and so washes out the deposit.

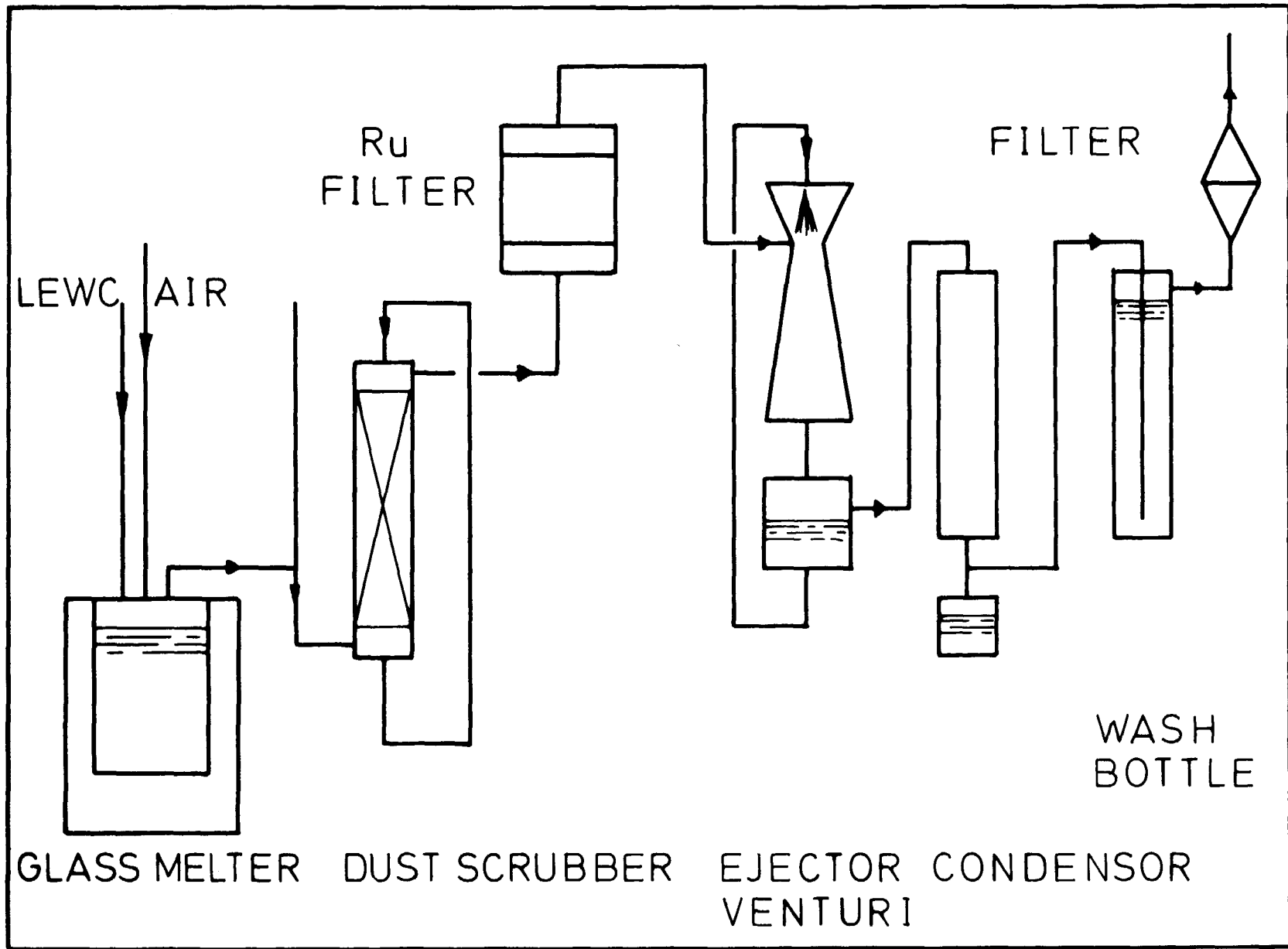


Fig. 1. Flow sheet of VITRILAB laboratory unit

The distribution of Ru present in the off-gases between the aerosol and the volatile form have been determined by sampling with a cascade impactor followed by a condenser, a wash bottle and a final fiber filter. The flow sheet of the sampling unit is given in Fig.2. Very short sampling times (a few minutes) can only be used with the cascade impactor due to clogging of the jet nozzles of the two last stages (ϕ 1 and 0.6 mm) so that the representativity of the sample is not excellent. Moreover, the impactor must be heated up till 150 °C, in order to prevent water condensation, so that volatile Ru present in the off-gases could be partly decomposed on the walls of the impactor. Nevertheless, it seems that the fraction of Ru still volatile is smaller than 10 % (values down to 0.1 % have been obtained). This fraction, passing through the impactor, is trapped in the condenser and no Ru is found in the wash bottle and in the final filter. The activity mass median aerodynamic diameter of the aerosol at the exit of the oven lies between 1 and 7 μ m and the distribution is quite large (geometric standard deviation $S_g = 3$)

Volatility of different Ru species. Experiments have been performed with the aim of comparing the volatilities of different Ru species fed simultaneously with LEWC on a glass pool.

The different tests were :

- RuNO(NO₃)_x(OH)_{3-x} 2 g/l ruthenium in LEWC at a flow rate of 0.14 l/h corresponding to 280 mg Ru/h ;
- RuO₂ 2 g/l as a suspension in LEWC at the same flow corresponding to 280 mg Ru/h ;
- RuO₄ 280 mg Ru/h sparged with air, fed at the top of the glass oven and mixed with the off-gases coming from the LEWC feed ;
- RuNO(NO₃)_x(OH)_{3-x} 2 g/l in LEWC and with the addition of 100 g/l SUGAR (SACCHAROSE) in the LEWC solution.

Clogging problems at the Ru inlet and at the off-gases outlet appeared during the RuO₄ tests. High dust concentration during the sugar test lead also to clogging problems at the outlet of the oven. Due to these experimental difficulties, the interpretation of the results is not simple, nevertheless it seems clear that the DF of the oven varies in function of the Ru species fed. With RuNO(NO₃)_x, the mean DF is 13 ; for RuO₂ the DF is much higher and reaches a value of 40 ; for RuO₄, the error on the DF is great but it seems that before clogging, the DF lies between 3 and 8. For RuNO(NO₃)_x + SUGAR, the DF of the glass oven is 1, for the packed bed scrubber 6 and for the venturi ejector 400. The washing solutions contain a very great amount of insolubles. The addition of sugar seem to induce the formation of a great amount of dust which is not trapped in the molten glass layer.

Volatility of Ru from the glass-oxide melt. When the glass oven containing molten glass and waste oxides is sparged with air a reentrainment of Ru occurs. The fraction of Ru present in the sparging air represents a release of 0.1 to 0.01 % pro hour of the Ru activity in the glass. The release increases with the gas flow rate so that the activity released pro hour increases linearly with the square of the gas flow rate. A decrease of the glass temperature from 1100 °C to 800 °C result in a decrease of the Ru entrainment by a factor of 10 to 100.

17th DOE NUCLEAR AIR CLEANING CONFERENCE

Packed bed dust scrubber for the capture of Ru

The characteristics of the glass packed bed dust scrubber, used as first purification device in the off gas line, are given hereafter - geometric characteristics :

diameter : 5 cm
 height : 25 cm
 packing : Rashig rings
 outside diam. : 0.7 cm
 height : 0.7 cm
 inside diam. : 0.4 cm ;

- liquid flow rate : 100 l/h.

In order to avoid an increase of the volume of the circulating solution, the scrubber operates at a temperature regulated in such a way that the water vapour content of the off gases does not condense out in this scrubber. Therefore, the operating temperature depends on the LEWC liquid feed rate and on the sparging air flow rate. The table II gives the operating temperature for different LEWC and air flow rates.

Table II

LEWC liquid feed l/h	Air gas feed lN/h	Operating temperature °C	Water content % V/V
0.14	90	89	65
0.17	60	93	78

The operation of the dust scrubber is very sensitive to variation in the operating temperature since a 4 degrees variation means an increase of the total gas flow through the scrubber by a factor 1.6. The liquid flow rate is chosen to work below flooding conditions for the highest operating temperature. The representativity of the liquid sampling during a test is doubtful due to the presence of insolubles and to the deposit of ruthenium on the Rashig rings. A mean global DF is determined after each test by measurements of the circulating solution and of two successive rinsing solutions. The distribution between soluble and insoluble fraction is generally 1/1 and the fraction of Ru deposit on the Rashig rings can reach 25 % of the total quantity of Ru trapped in the scrubber. The global DF of the dust scrubber varies between 10 to 50 with a mean value about 20. The activity mass median aerodynamic diameter of the aerosol leaving the dust scrubber lies between 0.3 and 0.6 μm and the distribution is quite narrow ($S_g = 2$).

No significant quantities were found after the cascade impactor which means that the ruthenium at the outlet of the dust scrubber is only in aerosol form.

Specific volatile ruthenium trapping bed

The second barrier for Ru in the off gas line as initially foreseen in the Pamela project, was a silica-gel bed operating at 120 °C in order to avoid condensation problems. Such a filter, which had given favourable results when placed at the exit of a calciner appeared useless in the Vitrilab off gas purification line. The

17th DOE NUCLEAR AIR CLEANING CONFERENCE

ferricoxide-chromiumoxide catalyst gave also very low decontamination factors.

Preheating of the gases between the outlet of the dust scrubber and the inlet of the silica-gel bed resulted in an increase of the DF of the bed with an optimum preheating temperature of 400 - 600 °C. In these conditions, DF higher than 10 could be achieved. In spite of the improvement of the bed efficiency, it has been noted that the activity first decreases with the length of the bed till a minimum and then again increases till the end of the bed. In the last layer, a loose dust deposit containing Ru oxides is accumulated and represents the majority of activity of this layer, whereas in the first layer the Ru is trapped on the silica-gel pellets and reduced to a gray deposit. These observations have led to a modification of the installation in order to determine the distribution of Ru between the aerosol and the volatile form in function of the preheating temperature.

A flow sheet of the modified installation is described in figure 3 and in table III are given for preheating temperatures of 180, 400 and 600 °C :

- the ratio O/I which represents the ratio of the quantity of Ru in the off gases after the preheater to the quantity present at the inlet of the preheater ;
- the distribution of Ru after the preheater between the filter F, the condensor C, the caustic washing bottle B, and the final fiber filter FF.

Table III. Distribution of Ru after the preheater

	Preheating temperature °C		
	180	400	650
O/I	0.8 - 0.9	0.8 - 0.9	0.3 - 0.5
F %	99.7	99.7	93.1
C %	0.2	0.15	6.6
B %	0.1	0.15	0.3
FF	BG*	BG	BG

*BG : measurement not significantly different than the background.

At preheating temperatures from 180 °C to 400 °C, only a small difference was observed between the activity in the off-gases before and after the preheater. But at 650 °C, the activity after the preheater was 30 to 50 % of the activity before ; this means that ruthenium is deposited on the surface of the preheater. Washing of the preheater with water removes only 15 % of the total activity deposited, the rest is only removed from the surface by chemical attack of the stainless steel. At 650 °C the DF of the glass fiber filter is quite lower (15) than for the lower preheating temperatures (DF greater than 300). The ruthenium not trapped by the filter is mainly trapped in the condensor.

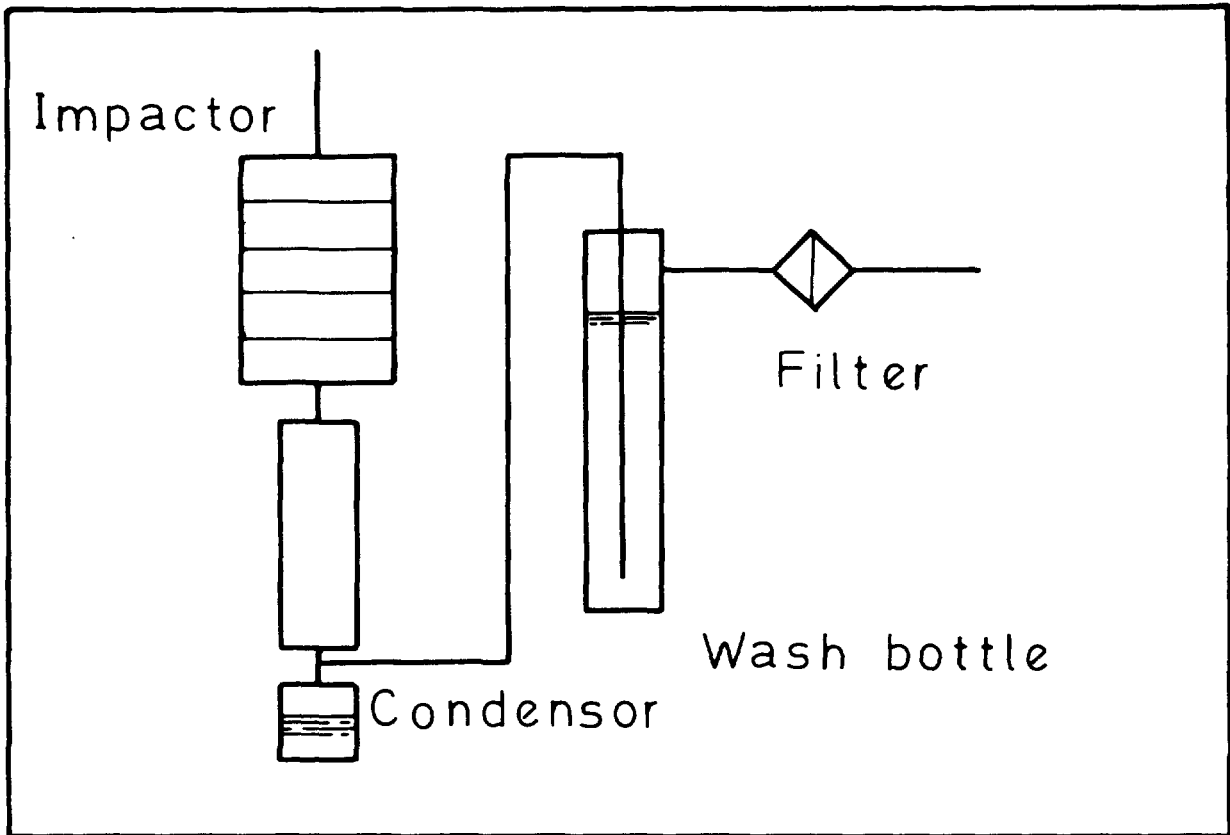


Fig. 2. Flow sheet of the sampling unit

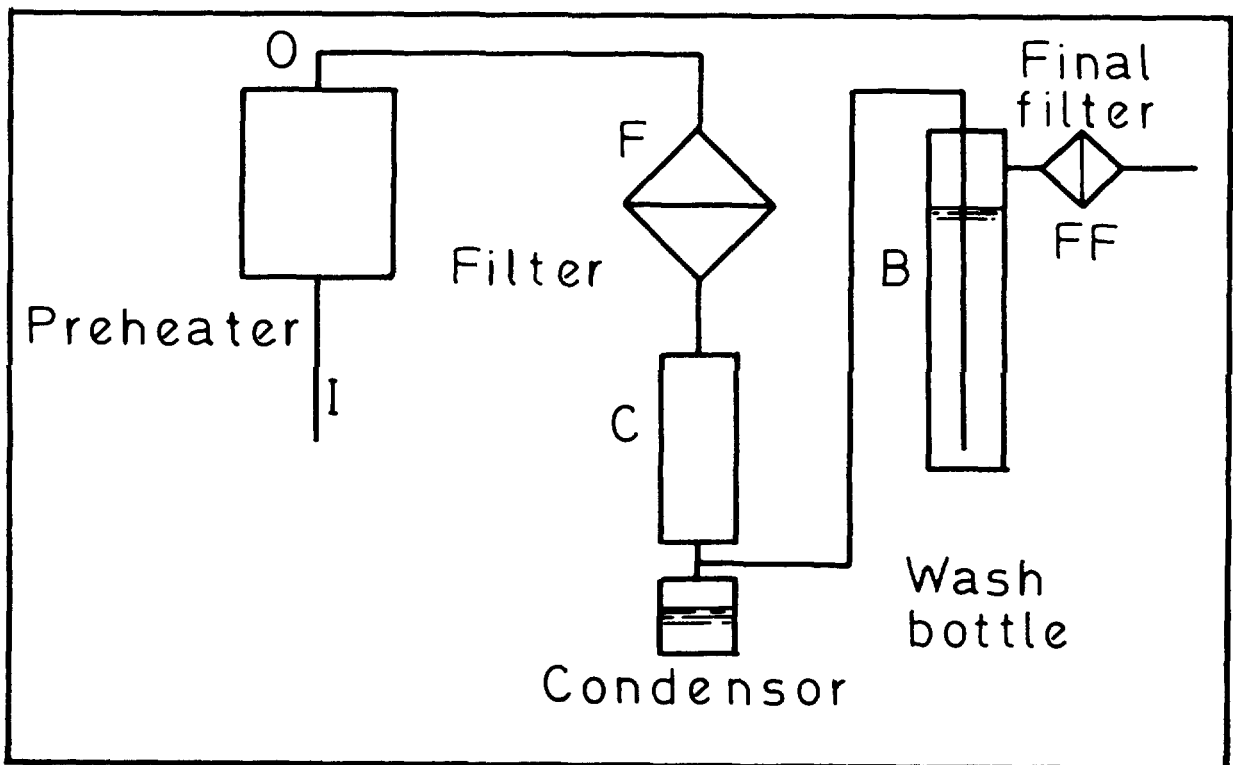


Fig. 3. Modified installation for the study of the influence of the preheating temperature

17th DOE NUCLEAR AIR CLEANING CONFERENCE

Some qualitative observations can be made on the basis of these experimental results :

- at 650 °C, there is a chemical reaction between the Ru and stainless steel (in the literature, the optimum temperature for volatile Ru deposit lies in the range 400-650 °C) ;
- at 650 °C, there could occur a partial volatilization of the aerosols of oxides of ruthenium by the combined action of NO₂ and O₂. This volatile species is not stable at high temperature and reacts with stainless steel, this species at low temperature is condensable and soluble in the acidic condensate.

Ejector venturi

The ejector venturi operates with a nozzle pressure of 3 bars and a liquid flow rate of 300 l/h. The circulating solution is saturated with nitrates to avoid NO degassing problems in the pump. When the ejector venturi is not cooled, the temperature of the circulating solution stabilizes at 84-86 °C so that the volume of the circulating solution is nearly constant. When the circulating solution is cooled, the temperature is stabilized at 50 °C so that the % of water vapour in the off-gases decreases from 55 % to 12 %. The DF of the ejector venturi increases when the DF of the system glass oven-dust scrubber decreases, but decreases in the opposite case so that the over-all DF glass oven-dust scrubber - venturi ejector remains high. During the experimental campaign, over-all DF of $5 \cdot 10^3$ to $2 \cdot 10^4$ were obtained for the three units in series which corresponds to DF's for the ejector ranging from 10 to 50.

V. Conclusion

This experimental study has indicated the importance of moisture and NO_x vapours on the volatility and trapping conditions of ruthenium in high temperature processes. Also the process operating conditions have a great influence on the ruthenium behaviour in the off-gas purification units.

Of particular interests is the observation that the ruthenium release during direct vitrification of simulated high-level liquid waste is a factor of about 5 smaller than the ruthenium release during calcination of this type of waste. Moreover, in the direct vitrification case the ruthenium escapes mostly in the form of an aerosol whereas in the calcination case a volatile ruthenium compound is dominating. Consequently, a specific ruthenium filter is not any more needed in the off-gas line of a direct vitrifier simplifying in this way the number of units in this off-gas line and avoiding the handling and controlling problems of such a ruthenium filter.

In the future, a similar programme will be started on the volatility of cesium and antimony in a liquid fed melter and on the technical reliability of the liquid fed melter and its associated gas purification units on a semi-pilote scale under simulated conditions.

References

- (1) KLEIN, M., "Filtration and capture of semi-volatile nuclides" IAEA-SM-245/51 (1980).
- (2) KLEIN, M., "Volatilization and trapping of ruthenium during calcination of nitric acid solutions". IAEA-SR-72/03 (1982).

DISCUSSION

CHRISTIAN: With regard to the suggested ruthenium nitrosyl vapor species in the presence of NO_x , I obtained spectral evidence for chemical interaction between gaseous ruthenium tetroxide and nitrogen dioxide. When the two gases are placed at measured concentrations in a quartz cell, the uv-visible spectra of both $\text{RuO}_4(\text{g})$ and $\text{NO}_2\text{-N}_2\text{O}_4(\text{g})$ are diminished and a new strong charge transfer band appears. Similarly, the infrared spectrum of the system exhibits no vibrational bands of RuO_4 or nitrogen oxide species and two uncatalogued bands appear. Also, the equilibrium pressure of RuO_4 over RuO_2 in O_2 or NO_2 is insufficient to account for the observed partial pressure of ruthenium in the offgas of a fluidized-bed calciner. This provides additional evidence of the formation of a more volatile, stable species than RuO_4 in the presence of NO_x .

KLEIN: Our observations were quite similar. The following observations, not mentioned in the paper, were made. RuO_4 and NO_x , mixed in the presence of air, react to give a product which deposits in the glass tubing. This deposit is not stable; indeed this deposit is only soluble in nitric acid solution when tube washing is performed immediately. Otherwise, insoluble compounds are formed if the washing is not performed immediately. RuO_4 and NO_x , mixed in the presence of air in a bubbling column containing nitric acid, also react to give various $\text{RuNO}(\text{NO}_3)_x$ compounds soluble in nitric acid.

DEUBER: Did I understand that in your investigations the gaseous Ru specie most difficult to trap was found to be RuO_4 ?

KLEIN: Indeed, the adsorption tendency of RuO_4 on silica-gel is lower than the adsorption tendency of the RuNO complex. However, RuO_4 has a lower stability than the RuNO complex so that, in the case of catalytic beds such as ferric-oxide/chromium oxide catalyst operating at 300°C , RuO_4 is more easily trapped than the RuNO complex.

17th DOE NUCLEAR AIR CLEANING CONFERENCE

PLANT FOR RETENTION OF ^{14}C IN REPROCESSING PLANTS FOR LWR FUEL ELEMENTS

Braun, H.* , Gutowski, H.** , Bonka, H.+ , Gründler, D.**

* Federal Ministry of the Interior, Bonn, F.R.G.

** Linde AG, Höllriegelskreuth, F.R.G.

+ Technical University Aachen, F.R.G.

** Now GRS, Cologne, F.R.G.

ABSTRACT

The ^{14}C produced from nuclear power plants is actually totally emitted from nuclear power plants and reprocessing plants. Using the radiation protection principles proposed in ICRP 26, ^{14}C should be retained at heavy water moderated reactors and reprocessing plants due to a cost-benefit analysis. In the frame of a research work to cost-benefit analysis, which was sponsored by the Federal Minister of the Interior, an industrial plant for ^{14}C retention at reprocessing plants for LWR fuel elements has been planned according to the "double alkali process". The "double alkali process" has been chosen because of the sufficient operation experience in the conventional chemical technique. In order to verify some operational parameters and to gain experiences, a cold test plant was constructed. The experiment results showed that the "double alkali process" is a technically suitable method with high operation security. Solidifying CaCO_3 with cement gives a product fit for final disposal.

I. Introduction

Since about 1972 the radiological significance of ^{14}C emissions from nuclear power plants and reprocessing plants is discussed. It started with the expected emission of reprocessing plants for high temperature nuclear reactor fuel elements /1/. Comparative calculations for other reactors and reprocessing plants showed that their emission rates cannot be neglected while considering radiologically all radioactive emissions /2/.

The retention of ^{14}C has been discussed in Germany in connection with the "Gorleben-Project" /3/, which has been upset in the meantime. At that time a decision was not possible, because no technical solution was available. The Federal Ministry of the Interior in the F.R.G. sponsored within the scope of a cost-benefit analysis, made by the Professorial Chair for Nuclear Reactor Technology of the Technical University Aachen /4/, /5/, the Linde company in Höllriegelskreuth, F.R.G., for designing a plant with data for investment and operation costs. Simultaneously special processing problems should be researched in a nonactive plant /6/.

II. Production and release of ^{14}C from nuclear power plants and reprocessing plants

^{14}C is mainly produced in nuclear power plants due to fission and neutron capture in ^{13}C , ^{14}N and ^{17}O in the fuel elements, in the coolant, in the moderator, and in the air respectively the nitrogen at the outside of the reactor pressure vessel.

This work was sponsored by the Federal Minister of the Interior of the F.R.G. under Contract No. St. Sch. 680a and St. Sch. 680b.

17th DOE NUCLEAR AIR CLEANING CONFERENCE

The ^{14}C production rates and the expected emission rates from the different nuclear power plants have been calculated in various publications, see table I. The total results agree quite well, although greater differences for some reaction rates occur. The calculation results agree extensively with the measured results, see e.g. /27/, /28/, /29/, /30/, /31/, /32/. Table II gives a detailed survey of the production rates according to /16/. The calculations were based on the C-, N- and O-impurities listed in table III.

The expected ^{14}C emission rates from nuclear power plants and reprocessing plants during normal operation are listed in table IV. For water-cooled reactors the ^{14}C that is totally produced in the coolant and moderator is emitted from the nuclear power plant. Measurements showed that in boiling water reactors ^{14}C is emitted to up to more than 95 % /28/, /31/, /32/ as CO_2 and in pressurized water reactors to up to more than 90 % as CH_4 , C_2H_6 and other hydrocarbons /27/, /31/, /32/, due to the hydrogen addition. In reprocessing plants the total ^{14}C in the fuel element is released during the dissolution and emitted to more than 99 % as CO_2 , as measurements at the reprocessing plant Karlsruhe showed /29/, /30/.

III. Radiological significance of the ^{14}C emissions

When regarding the maximum possible individual doses in the vicinity of reprocessing plants, it is obvious, that the radiological impacts of an emission rate of 500 Ci/a via a 200 m stack are small. Fig. 1 shows e.g. the average air concentration at ground level in main wind direction (eastern direction), if 500 Ci/a ^{14}C were emitted via a 100 respectively 200 m stack. The meteorological data of Hannover were used for the calculations. Fig. 2 shows the maximum possible total body annual dose according to the specific activity model /33/ for this case. The natural total body annual dose due to ^{14}C is approx. 1.3 mrem/a for a CO_2 concentration in the atmosphere of 330 vppm. Total body annual doses due to globally distributed ^{14}C in the range of 1 up to 2 mrem/a could be possible in the future, if nuclear energy would be used more intensively /34/, /35/. Fig. 3 shows as an example the change of the total body annual doses due to globally distributed ^{14}C , if the total ^{14}C would be emitted from 1000 nuclear power plants with light water reactors with an electric capacity of 1000 MW each and the corresponding reprocessing plants. The changes due to the combustion of ^{14}C -free fossil fuels and the ^{14}C of the nuclear weapon tests /34/, /35/ has been neglected. 50 % of the annual dose occur due to the emissions of nuclear power plants, see table IV.

A totally different impression occurs, when using the new radiation protection principles in ICRP 26 /36/. According to these principles the aspired retention of radioactive material in nuclear power plants should be determined according to a cost-benefit analysis. On the first path exposure the collective dose due to ^{14}C is 3 man·rem/Ci. The global contribution can be taken from fig. 4; for an integration time of 500 years it is 55 man·rem/Ci. Based on a time of e.g. 500 years, the relation between annual costs, see chapter V, and reduced collective dose (cost effectiveness) results a value of approx. 30 \$/man·rem, taking into account that due to a ^{14}C retention facility in a 1400 t/a reprocessing plant 450 Ci/a are retained and finally disposed. For the retention and the final disposal of ^3H , ^{85}Kr , ^{129}I and the aerosols a cost-effectiveness of approx. 200, 250, 5 respectively 20 \$/man·rem /4/, /37/, /38/ occurs. ^{129}I and the aerosols have to be retained independent from a cost-benefit analysis because of the maximum individual dose. That means, ^{14}C has to be retained before ^3H and ^{85}Kr are retained according to the radiation protection principles in ICRP 26. As a standard value for the costs of detriment it is suitable to base on approx. 100 \$/man·rem according to the costs of fatal road accidents /39/. In the literature values of 10 up to 1000 \$/man·rem are used. Argentine demanded first a ^{14}C -retention facility for a nuclear plant in the heavy water moderated reactor Atucha II /40/.

17th DOE NUCLEAR AIR CLEANING CONFERENCE

TABLE I: Calculated production- and release-rate of ¹⁴C in different nuclear reactor types and reprocessing plants /16/

- a) after measurements at /27/ and /28/
- b) 10 % of production rate at fuel
- c) nitrogen impurity at coolant 5 to 40 ppm
- d) only coolant
- e) with graphite moderator
- f) up to 7 Ci/day calculated, most fixed in structural materials

Reactor-type	Thermal efficiency [%]	Calculated production rate [Ci/(GW(e)·a)]							Calculated release into atmosphere		Reference	
		Coolant and fuel of fuel element					Air around pressure vessel	Structural material	Reactor	Reprocessing plant		
		Coolant		Fuel and graphite moderator at HTR		Total						
		Assumed N ₂ [ppm]	Activity [Ci/(GW(e)·a)]	Assumed N ₂ [ppm]	Activity [Ci/(GW(e)·a)]		[Ci/(GW(e)·a)]	[Ci/(GW(e)·a)]	[Ci/(GW(e)·a)]	[Ci/(GW(e)·a)]		[Ci/(GW(e)·a)]
BWR	33	5	11.2	6	18.9	30.1	5·E-4	3	11.2	18.9	/2/, /7/	
	33	0	11.5	10	32.7	44.2					/8/, /9/	
	33		16 a)	20	13.6	29.7				1.5 b)	/10/	
	33	1	9.2	20	22	31.2					/11/	
	33	0	10.7	0	9	19.7			10.7		/12/	
	34	1	8	1	4.9	12.9		20-30			/13/	
	34	1	8	10	12.2	20.2		20-30			/13/	
	33		4.7	20	14.8	19.5		43.2			/14/	
	33		8	10	16	24					/15/	
	33	5	5.7	10	12.6	18.3	5·E-4	17	6-10 c)	12.6	/16/	
PWR	33	5	11.1	6	16.1	27.2	0.005	3.8	11.1	16.1	/2/, /7/	
	33	0	3.6	10	12.1	15.7					/8/, /9/	
	33		6 a)	20	13.6	19.6				1.5 b)	/10/	
	33	6.4	18			18 d)			18		/17/	
	34	5	5.2			5.2 d)					/18/	
	33	1	3.3	20	22	25.3					/11/	
	33		5	20	15.7	20.7		30.4			/14/	
	33		5	10	12	17			7		/15/	
	33	5	7	10	12.9	19.9	0.005	20		12.9	/16/	
HWR	30		410		50	460					/15/	
	33		557		20	577					/19/, /20/	
	32	5	320	6	23	443					/21/	
	32	5	200	10	40	240		34	200	40	/16/	
MAGNOX	30	200	3	50	87	90		213 e)			/10/	
	30	200	8.5	50	130	140	5·E-4	325 e)	10		/16/	
AGR	40	200	7.5	20	11.7	19.2		255 e)			/10/	
	41	200	8.1	50	16.8	24.9	0.001	126 e)			/16/	
HTR	41				61	61	0.004				61	
				26	160	160						/1/, /2/
				10	250	250						/22/
	41			25	54	54						/23/
	41		0.05	5	142	142					142	/10/
	41			76	76	0.004		0.1			/24/	
	38,5			30	175	175					/7/	
	41		0.02	10	91	91	0.005		1	91	/14/	
	41			91	91	91	0.005				/16/	
FBR [UO ₂ -fuel]	41	1	0.003	6	2.6	2.6	1	14.5	1	2.6	/2/, /7/	
	35			10	2.6	2.6		12.5			/14/	
	35			25	6.3	6.3		12.5			/14/	
	35			75	18.5	18.5		12.5			/14/	
		41			20	4.8	4.8				4.8	/25/
		41	1	0.02	10	5.5	5.5	1	8			/16/
[(U,Pu)N-fuel]	41	1	0.003	(U,Pu)N	1.5E4	1.5E4	1	14.5	1	2.6	/7/	
	41			(U,Pu)N	1.7E4	1.7E4					/25/	
FUSION							2 500 f)				/26/	

17th DOE NUCLEAR AIR CLEANING CONFERENCE

Table II: Calculated production of ^{14}C in the different reactor types in Ci/(GW_e·a) /16/

Specification		^{14}C -Production in Ci/(GW(e)·a)							
		BWR	PWR	HWR	MAGNOX	AGR	HTR	FBR	
Coolant	^{14}N	$5 \cdot 10^{-4}$	0.005	0.005	$5 \cdot 10^{-4}$	0.001	0.005	1	
	^{13}C	$7 \cdot 10^{-7}$	$8 \cdot 10^{-7}$	$3 \cdot 10^{-5}$	0.06	0.06	$4 \cdot 10^{-7}$	$5 \cdot 10^{-7}$	
	^{17}O	0.6	0.8	25	7.3	7.1	0.02	0.02	
Fuel element	Fission	^{14}N	5.1	6.2	175	1.1	1	$5 \cdot 10^{-6}$	$2 \cdot 10^{-6}$
		^{13}C	0.6	0.6	0.6	0.6	0.5	0.5	0.5
		^{17}O	$2 \cdot 10^{-4}$	$2 \cdot 10^{-4}$	$7 \cdot 10^{-4}$	$8 \cdot 10^{-4}$	$2 \cdot 10^{-4}$	$9 \cdot 10^{-5}$	$1 \cdot 10^{-5}$
	Canning	^{14}N	7.6	7.8	26	130	13	3.1	2
		^{17}O	4.4	4.5	13	0.01	3.3	1.6	3
		^{13}C	$3 \cdot 10^{-4}$	$5 \cdot 10^{-4}$	$7 \cdot 10^{-4}$	$4 \cdot 10^{-4}$	$6 \cdot 10^{-4}$	—	$1 \cdot 10^{-5}$
		^{14}N	17	20	34	35	32	—	8
Graphite moderator	^{17}O	0.015	0.02	0.03	0.003	0.003	—	$2 \cdot 10^{-4}$	
	^{13}C	—	—	—	110	35	32	—	
	^{14}N	—	—	—	180	59	54	—	
Total production rate		35	40	27%	500	151	91	15	

Table III: C, N and O impurities used to calculate the rate of ^{14}C production in the different reactor types /16/

Reactor-type	Impurities in ppm or vppm								
	Coolant			Fuel elements					
	C	N	O	Fuel			Canning		
BWR	1	5	H ₂ O	50	10	UO ₂	270	80	1500
PWR	1	5	H ₂ O	50	10	UO ₂	270	80	1500
HWR	1	5	D ₂ O	50	10	UO ₂	270	80	1500
MAGNOX	CO ₂	200	CO ₂	50	50	U	100	50	Oxidation 100
AGR	CO ₂	200	CO ₂	50	20	UO ₂	100	50	100
HTR	CO 3 vppm CO ₂ 1 .. CH ₄ 0.1 ..	1 vppm	CO 3 vppm H ₂ O 12 .. CO ₂ 1 ..	50	10	UO ₂	Graphite *	10	3 *
FBR	20	1	1	50	10	UO ₂	1000	100	30

Table IV: Expected ^{14}C emission rate of nuclear power plants at normal operation and of a reprocessing plant without ^{14}C retention * 10 % as CO₂

Nuclear facility		Emission rate in Ci/a	
		Atmosphere	Surface water
Reactor (1000 MW _e)	BWR	10	0.01
	PWR	7 *	0.01
	HWR	200 - 400	
	MAGNOX	10	
	AGR	10	
	HTR	1	
	FBR	1	
Reprocessing plant (40000 MW _e) full load)	BWR u. PWR	500	
	HTR	3600	
	FBR	220	

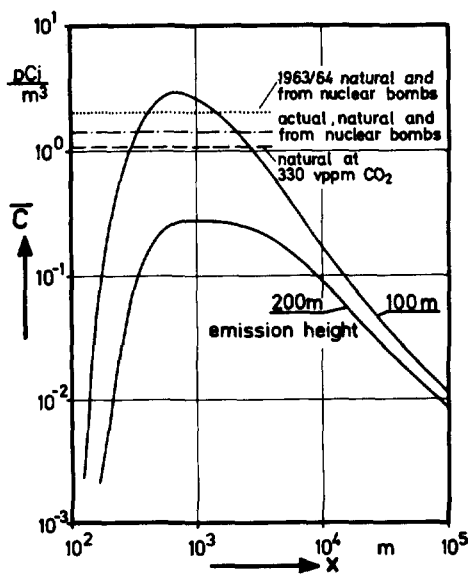


Fig. 1: ^{14}C concentration of the air near ground level in the main wind direction (east), $\dot{E} = 500 \text{ Ci/a}$

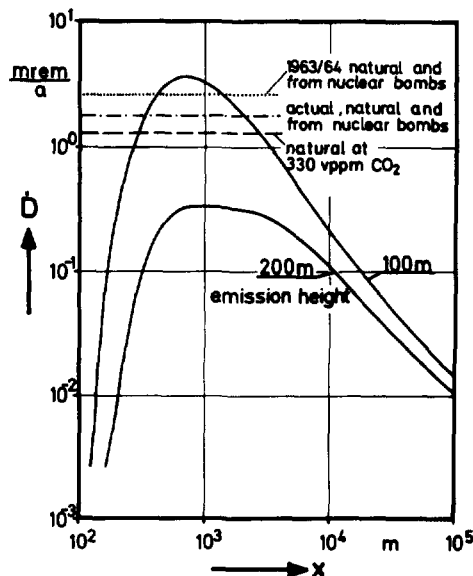


Fig. 2: Maximum radiation exposure due to ^{14}C of an adult in main wind direction (east), $\dot{E} = 500 \text{ Ci/a}$

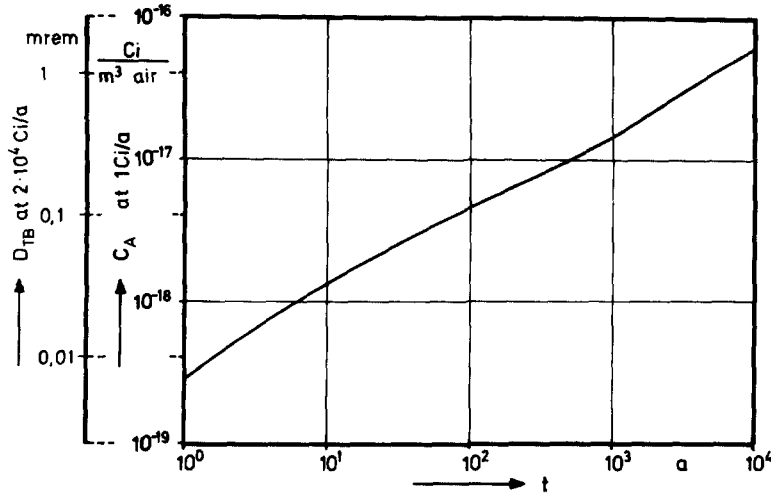


Fig. 3: ¹⁴C activity in the air at ground level after global distribution, if 1 Ci ¹⁴C is emitted per year; total body annual dose for an annual emission of $2 \cdot 10^4$ Ci without ¹⁴C-concentration changes due to nuclear weapon tests; CO₂ concentration in the air 330 vppm = const.

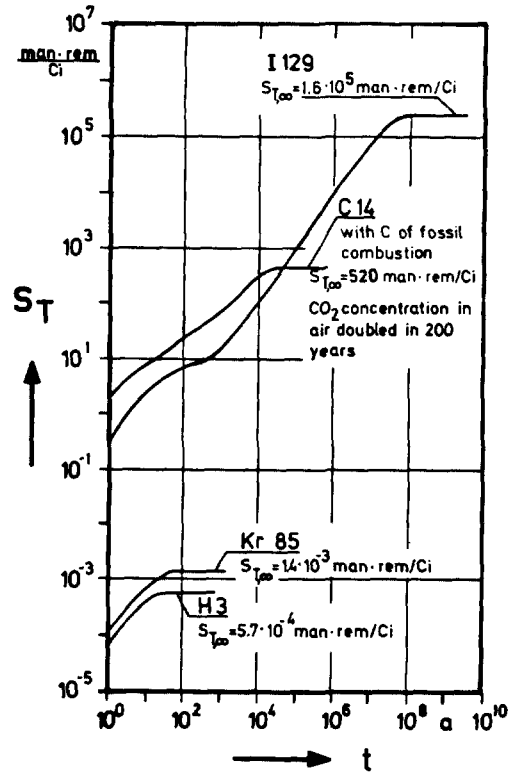


Fig. 4: Total collective effective dose equivalent commitment S_T from globally distributed radionuclides in dependence of integration time (world population $1 \cdot 10^{10}$)

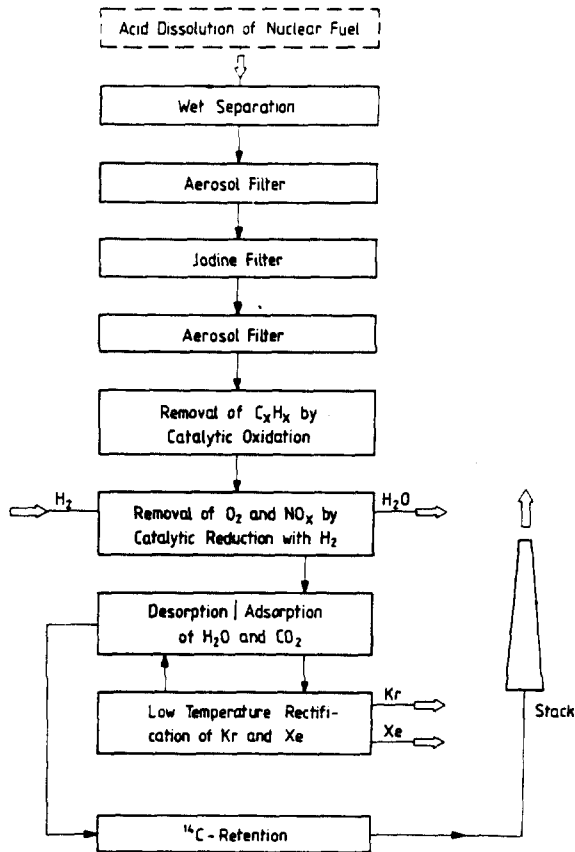
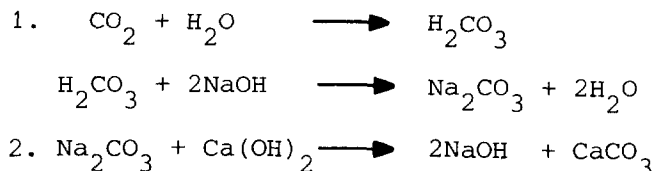


Fig. 5: Scheme for off-gas cleaning for a fuel reprocessing plant for LWR

IV. Methods for ^{14}C separation in reprocessing plants

As carried out in chapter II, in reprocessing plants the ^{14}C is practically released to 100 % as CO_2 into the dissolver-off gas during the dissolution of the fuel. For a reprocessing plant of 1400 t/a the dissolver-off gas amount is approx. 300 m^3/h . CO_2 is adsorbed at the molecular sieve beds installed in front of the low temperature rectification facility for ^{85}Kr separation, if a ^{85}Kr retention is assigned. Fig. 5 shows the conducting of the dissolver-off gas, as it had been designed in the "Entsorgungszentrum" Gorleben /41/. Here, the ^{14}C release occurs with regeneration gas (mainly N_2) of the molecular sieve beds. The CO_2 concentration in the nitrogen varies considerably during the regeneration phase. It mounts up to approx. 3600 vppm at the beginning of the regeneration and then slowly falls down to a few vppm at the end of the regeneration process.

The retention of CO_2 of the regeneration gas can be carried out by absorption in liquids /42/, /43/ or solids /44/, /45/, /46/. Because of the reliability of all operating conditions, the high separation degree, and the high standard of operating experience in the conventional chemical technique, the "double alkali process" has been chosen as reference process, which works according to the following chemical reactions:



The resulting CaCO_3 is chemically stable and after appropriate conditioning it is suitable for final disposal. The use of other alkali or earth alkali metals than Ca, e.g. Ba, is possible. In Argentine Barium is used for the ^{14}C retention of the heavy water moderated reactor Atucha II /40/.

V. Layout for a ^{14}C retention facility for a 1400 t/a reprocessing plant for LWR-fuel elements

The Federal Ministry of the Interior ordered to Linde AG, Werksgruppe TVT, München, a basic engineering of a ^{14}C retention facility according to the "double alkali process" in order to obtain from the industrial point of view technical data and realistic costs. In addition, the results from the Linde-engineering for a ^{85}Kr separation based on the low-temperature rectification /47/ should be taken into consideration and a suitable connection point at the dissolver-off gas system should be determined.

Fig. 5 shows a block diagram with ^{85}Kr separation by low-temperature rectification and ^{14}C retention. After the uranium dissolution the off-gas consists of air as carrier gas, aerosols, iodine, NO_x , Kr, Xe, CO_2 , C_xH_y and H_2O . First, the aerosols and the iodine compounds are separated in the aerosol- and iodine filter train. The hydrocarbons are removed by catalytic oxidation; oxygen and rest parts of NO_x are removed by catalytic reduction. H_2O and CO_2 are retained by the adsorption stretch. The pre-purified off-gas is then fed into the low temperature section which consists of two columns. The Kr-Xe-collecting in the bottom of the first column is separated in the second column, thus removing Kr as the head product from the top. The N_2 that appears at the top of the first column is used to regenerate the H_2O - and CO_2 -loaded adsorbers and is then fed into the ^{14}C retention facility. This connection point was chosen, because the iodine, aerosol as well as Kr-activity has been separated already and carbon 14 appears nearly exclusively as CO_2 . A rest volume of approx. 15 vppm CO results from the catalytic reduction of oxygen and NO_x that is carried out with surplus H_2 . Assuming a reprocessing plant with an annual capacity

17th DOE NUCLEAR AIR CLEANING CONFERENCE

of 1400 t uranium, the gas mixture entering the ^{14}C retention facility has the following compounds (at balance point \diamond of fig. 6):

N_2	0.0937 kg/s
CO_2 max.	(3650 vppm) 0.0006 kg/s
H_2O	$1.4 \cdot 10^{-4}$ kg/s
pressure	1.5 bar
temperature	approx. 573 K up to 283 K

In the heat exchanger, position 1, this gas mixture is cooled down to a temperature of approx. 313 K and is transported to the scrubbing column, position 2, together with the H_2O condensate produced there. In this packed tower the CO_2 is scrubbed with NaOH (6 wt %) up to a residue of approx. 15 vppm (achieved decontamination factor max. 240).

In the head of the column the water is condensed to saturation point at a temperature of approx. 288 K and a pressure of 1.47 bar. The leaving nitrogen is controlled regarding its CO_2 -contents, then heated up in the heat exchanger, position 1, (balance point \diamond), and mixed with other waste air it is emitted via the stack:

N_2	0.0937 kg/s
CO_2 max.	$2.45 \cdot 10^{-6}$ kg/s
H_2O	$0.69 \cdot 10^{-3}$ kg/s
pressure	1.47 bar
temperature	approx. 548 K up to 288 K

The lye circuit is maintained by a caustic solution pump, position 4. 9 m^3/h caustic solution with a total volume of 2.25 m^3 are recycled in the washing circuit.

After about 9 days 62 % of the caustic solution is used. Up to this point it is guaranteed that the CO_2 content in the cleaned gas does not exceed 15 vppm.

The composition of the caustic solution which has been used to 62 % is:

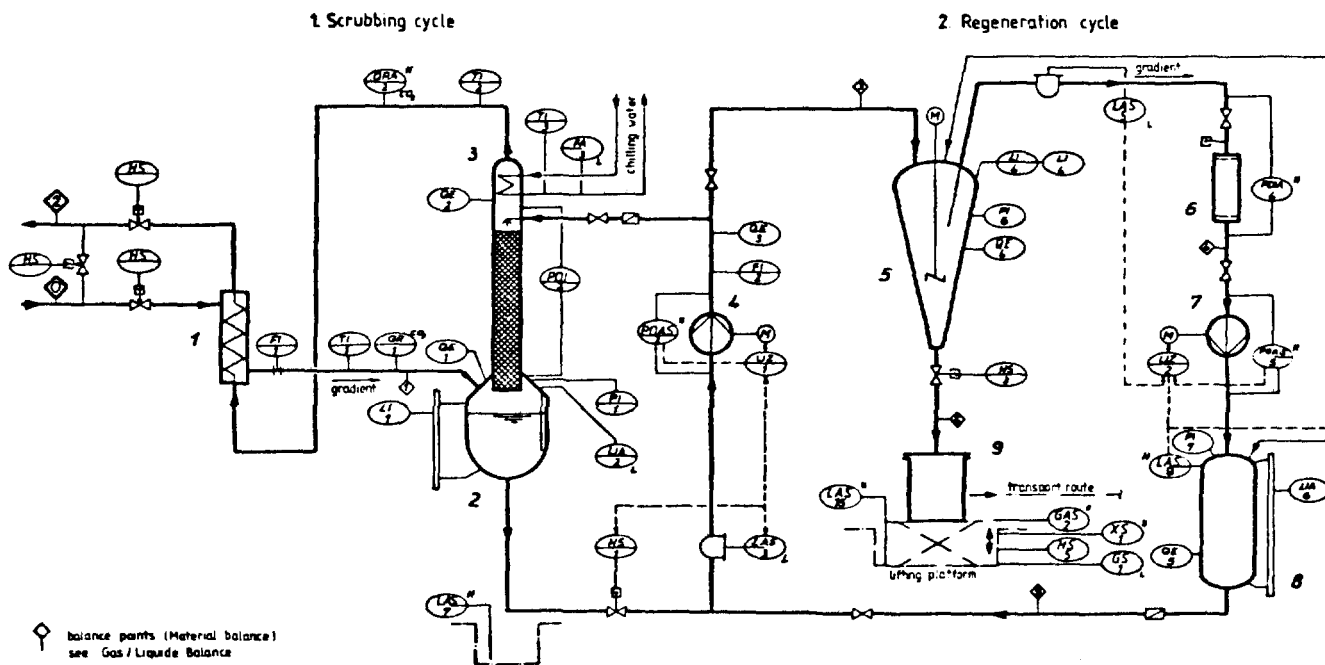
NaOH	54.7 kg
Na_2CO_3	118.4 kg
H_2O	1849.1 kg

This caustic solution is transported into the recovery stirring vessel, position 5, by the caustic solution pump. Then, with the same pump, a second charge of NaOH is drawn from the caustic solution vessel, position 8, in order to substitute the scrubbing solution to be regenerated. The addition of the fresh caustic solution is carried out during CO_2 -free operation. (Only during approx. 3 hours CO_2 is desorbed in an 8-hours cycle).

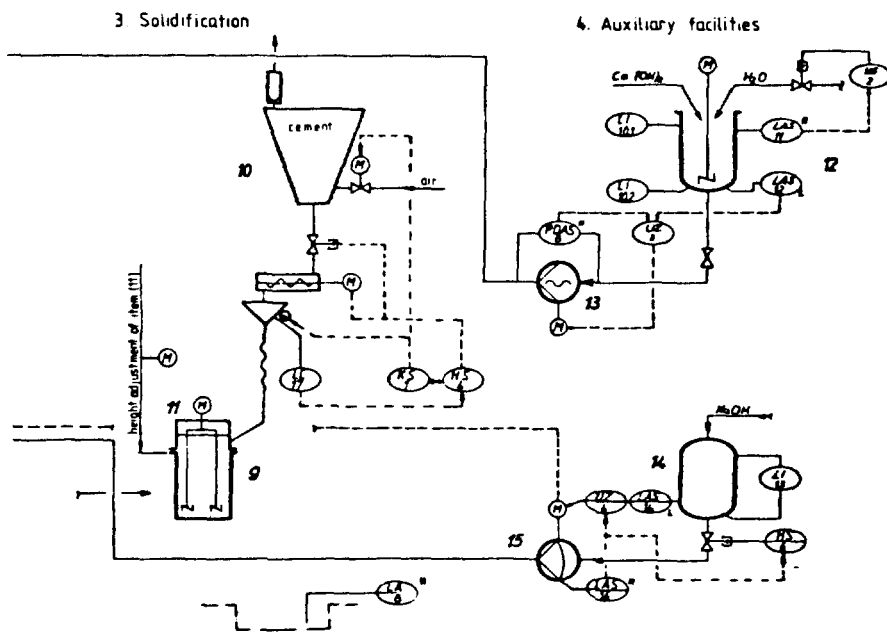
In the suspension stirring vessel, position 12, 74.5 kg of $\text{Ca}(\text{OH})_2$ are suspended in 434 kg H_2O which is then transported into the recovery stirring vessel by a spiral pump, position 13.

To avoid possible clogging of the scrubbing column by non-reacting $\text{Ca}(\text{OH})_2$ that remains in the caustic solution, the addition of $\text{Ca}(\text{OH})_2$ (90 %) is carried out non-stoichiometrically. Accordingly, a residue of Na_2CO_3 can be detected in the regenerated caustic solution.

17th DOE NUCLEAR AIR CLEANING CONFERENCE



1	2	3	4	5	6	7	8
Heat exchanger	Scrubbing column	Condenser	Lye pump	Regenerator	Filter	Lye pump	Lye storage tank



9	10	11	12	13	14	15
Waste tank	Cement feed	Stirring apparatus	Suspension tank	Screw pump	Lye storage tank	Diaphragm metering pump

Fig. 6: Processing scheme of the ¹⁴C retention and solidification

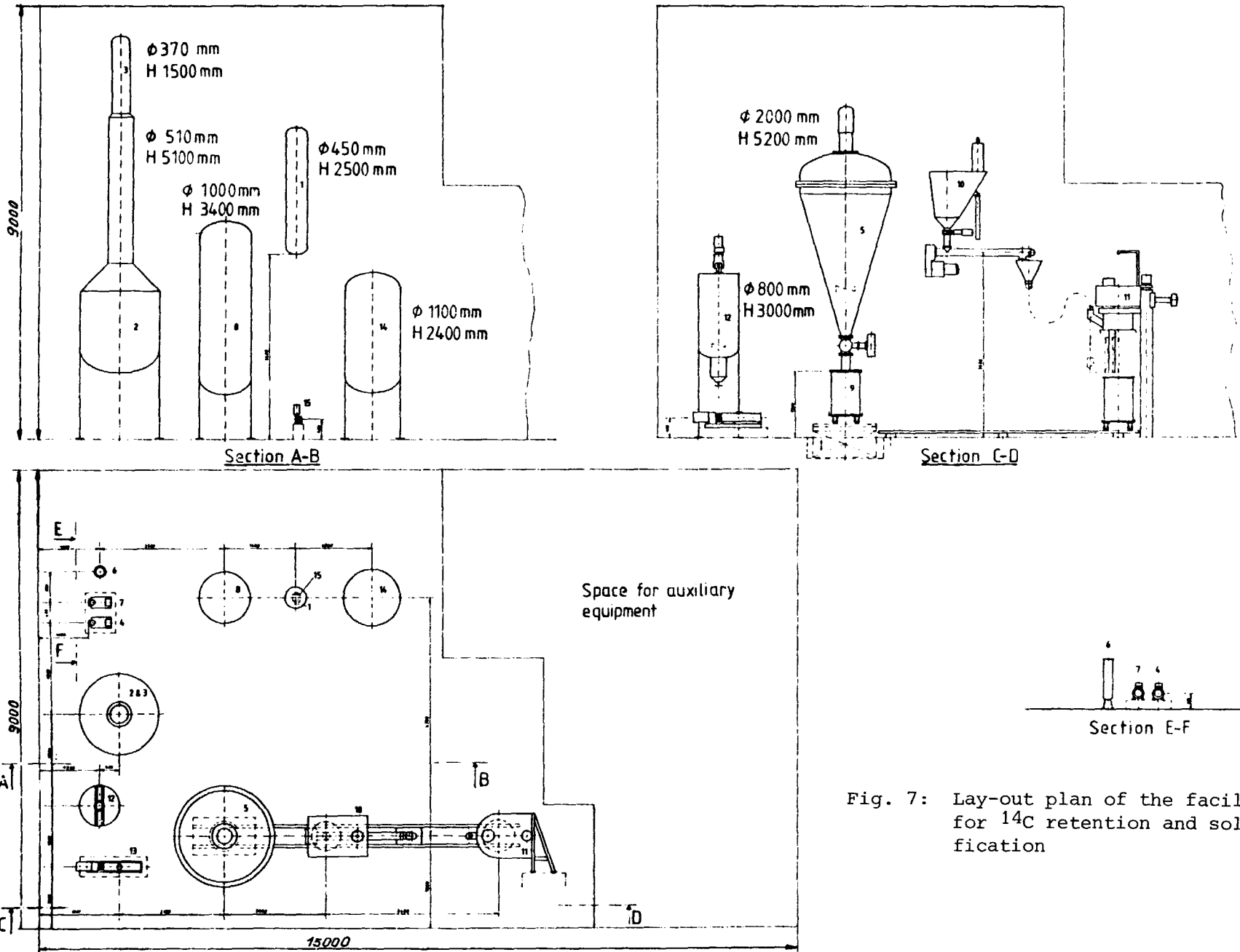


Fig. 7: Lay-out plan of the facility for ^{14}C retention and solidification

17th DOE NUCLEAR AIR CLEANING CONFERENCE

When the stirring of approx. 1 hour is completed, the crystallized CaCO_3 floating in the caustic solution deposits to the bottom of the recovery stirring vessel. This deposition procedure is completed after approx. 2 hours. The regenerated caustic solution is pumped into the NaOH-vessel via a suction tube by the pump, position 7, except for a residue of approx. 70 kg (rest-moisture and caustic solution column). The retention of non-deposited CaCO_3 -particles within the lye is carried-out in the filter, position 6.

As a substitute of the remainder of the lye in the recovery stirring vessel, approx. 42 litres of soda lye (25 wt %) is pumped from the vessel, position 14, into the caustic solution storage with the aid of a metering pump, position 15. Thus, together with the caustic solution removed from the recovery stirring vessel, a 6 wt % fresh caustic solution is obtained.

After the removal described above, the waste to be solidified remains in the recovery stirring vessel with the following compounds:

NaOH	2.2 kg
Na_2CO_3	0.2 kg
H_2O	37.8 kg
CaCO_3	100.6 kg

Once the waste discharge has been completed, the waste container is transported to the mixing station, position 11, with the aid of a transfer car. There, 50 kg cement is metered off and added to the sludge in the waste container. The mixing of the waste material with the cement is carried-out with counter-current, intermeshing mixing elements, thus reaching all parts of the vessel.

After a mixing time of approx. 15 minutes, the mixing elements are turned aside and the vessel with the solidified waste and an activity of approx. 14 Ci are removed from the mixing station.

After the waste has been hardened, the vessel is closed and can be transported to a deposit.

The dimensions of the most important equipments and the space requirements of the complete facility can be taken from the lay-out plan in fig. 7.

The investment costs for this plant including installation and start-up amounts to approx. DM 6.1 million, taking into account the regulations, standards, and guidelines applicable to the construction and operation of nuclear facilities. The annual operation costs are approx. DM 1.1 million (cost index August 1982).

VI. Cold experiments for the "double alkali process"

In order to gain operating experiences, a testing facility according to the "double alkali process" has been built at the professorial chair for nuclear reactor technology of the technical university Aachen.

Experimental setup

Fig. 8 shows the flow scheme and Fig. 9 a photograph of the facility.

The gas which contains CO_2 (generally air with a CO_2 concentration of 330 vppm) flows - after having passed the pre-pressure regulation (1) - in reverse direction to the caustic solution through the caustic solution scrubber (2). If necessary, the CO_2 concentration can be varied via the feed-in (7). The adjustment of the gas mass flow is carried out via throttle (3) and flow meter (4). A part of the off-gas

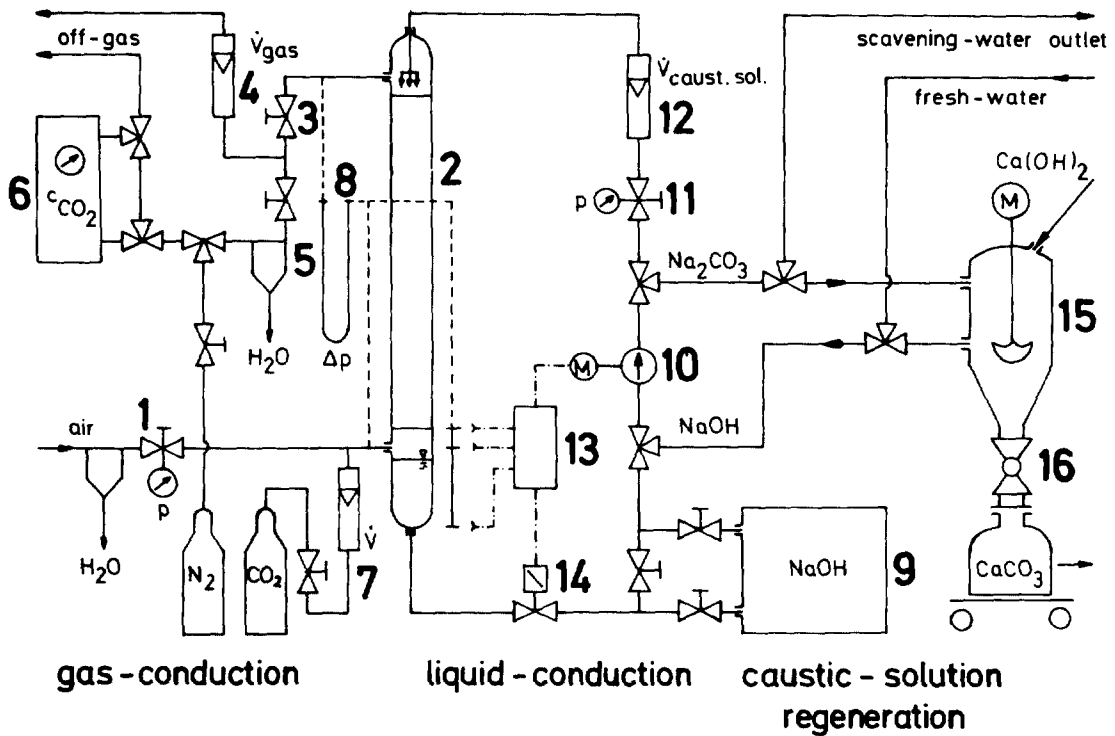
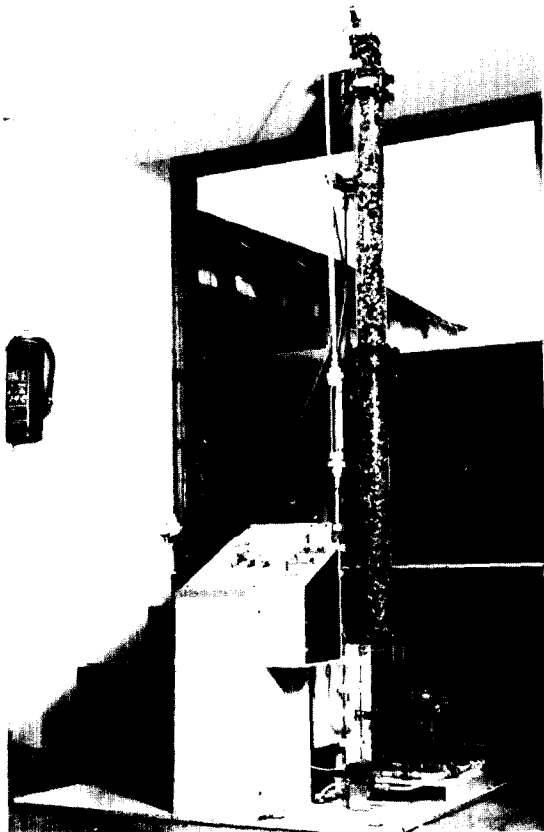


Fig. 8: Flow sheet of the experimental set-up for CO₂-separation



packing volume	: 15,9 l
diameter	: 100 mm
packing height	: 2000 mm
filling bodies	: Pall rings \emptyset 15 mm, stainless steel
caustic solution volume of the facility	: 120 l
caustic solution flow rate	: 0 - 700 l/h
gas flow rate	: 0 - 40 Nm ³ /h at 2.5 bars
CO ₂ -feed	: 0 - 86 Ndm ³ /h at 2.0 bars
design pressure	: 2.5 bars
volume recovery stirring vessel	: 120 l

Fig. 9: Photograph of the test facility with main data

17th DOE NUCLEAR AIR CLEANING CONFERENCE

is analyzed after a water separation (5) with an infrared gas analyzer (6) in order to determine the CO₂-rest concentration. The current resistance at the gas side is determined with the aid of an u-pipe manometer (8).

With the aid of a pump (10) the caustic solution is fed from the storage vessel (9) into the head of the column. The flow rate is regulated with a regulating valve with pressure indication (11) and a flow meter (12). The caustic solution discharge has been adapted to the inlet via an opto-electronical detector (13) and a magnetic valve (14). In danger of flooding, danger-off is initiated by the detector.

The regeneration facility which is made of the settling tank (15) with ball valve (16) for sediment deduction, Ca(OH)₂-feed-in and electric stirrer, is adapted to the caustic solution circuit in that way that a continuous as well as a discontinuous regeneration is possible. The inlet and outlet of further process media - e.g. cleaners - into as well as out of the caustic solution circuit is possible via intersecting points.

Test results

Fig. 10 shows some results for a constant CO₂-inlet concentration of 330 vppm. A better absorption reaction can be stated for higher pressures, higher caustic solution concentration and lower gas flow rate. Fig. 11 shows the mass transfer constant $K_G \cdot a$ of the facility according to the equation /41/:

$$G \cdot dy = K_G \cdot a \cdot p \cdot (y - y_G) \cdot dh \quad (1)$$

- G : gas load (kmol/h m² tower cross section)
K_G : mass transfer value on the gas side (kmol/h m² bar)
a : exchange surface in the scrubbing tower (m²/m³ tower volume)
p : total pressure (bar)
h : height of the exchange layer in the scrubbing tower
y : breaking up of the mole of the gas to be scrubbed out
y_G : breaking up of the mole of the gas to be absorbed at the phase boundary layer in the gas.

The change of the mass transfer constant in dependence of the CO₂-inlet concentration, of the caustic solution flow rate, and the caustic solution concentration is shown in Fig. 12 for a constant pressure of 2 bars. Only a small decrease of the mass transfer constants can be stated for high CO₂-entering concentrations. If the caustic solution flow rate is increased, the mass transfer constant is improved.

Experiments showed that for an operating pressure of 2 bars and gas flow rates of 20 to 30 kg/h for the test facility used here, the optimum caustic solution concentration lies between 1.5n and 1.7n NaOH.

A further analysis was made in order to determine the flow processes in a packed column which is flown through by gas and trickling liquid in counterflow. The processes can be described very well with the aid of the flow pressure loss in dependence of the gas flow rate and the caustic solution flow rate. The caustic solution flow rate has been increased up to the flood point while keeping the gas flow rate constant. Fig. 13 shows the current density curves for 2 operation pressures with the gas speed as a parameter. Up to line AA no fundamental difference of the facility could be stated. After that the liquid volume mounts in the scrubbing tower. In process engineering line BB is called flood limit respectively highest dead load limit.

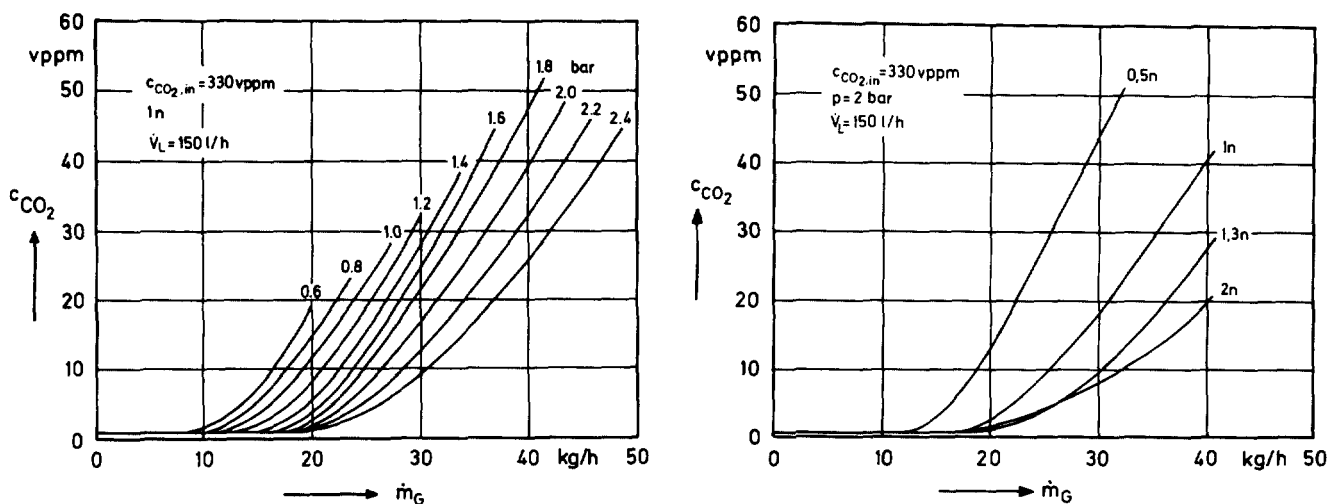


Fig. 10: CO_2 off-gas concentration c_{CO_2} in dependence of the gas flow rate \dot{m}_G , the pressure and the caustic solution concentration at a constant feed concentration of 330 vppm

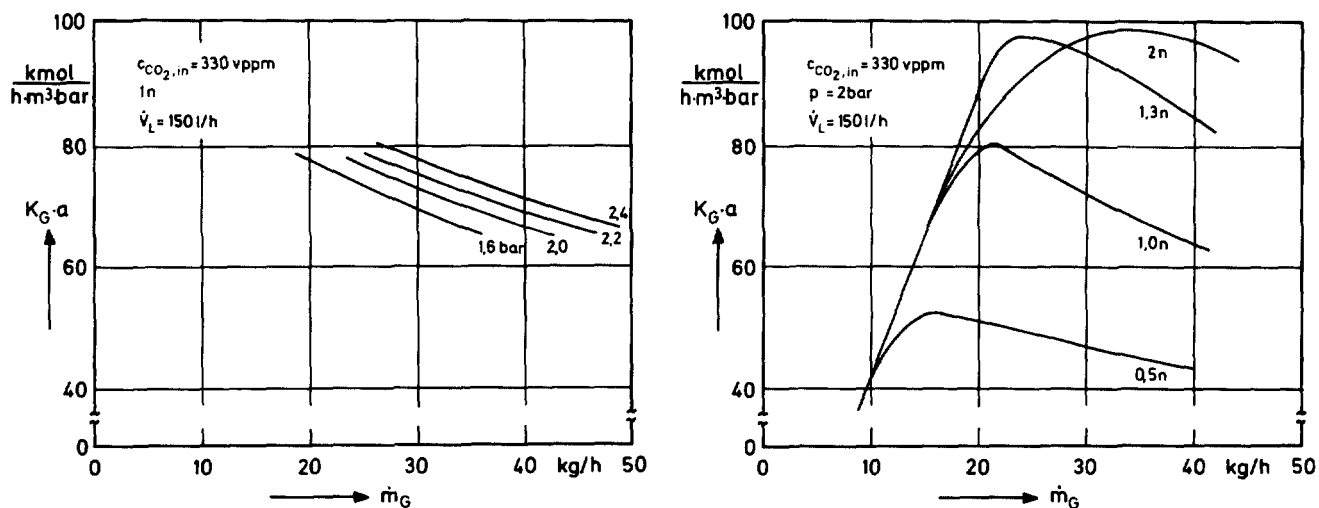


Fig. 11: Mass transfer constant $K_G \cdot a$ in dependence of the gas flow rate \dot{m}_G , the pressure and the caustic solution concentration at a constant feed concentration of 330 vppm

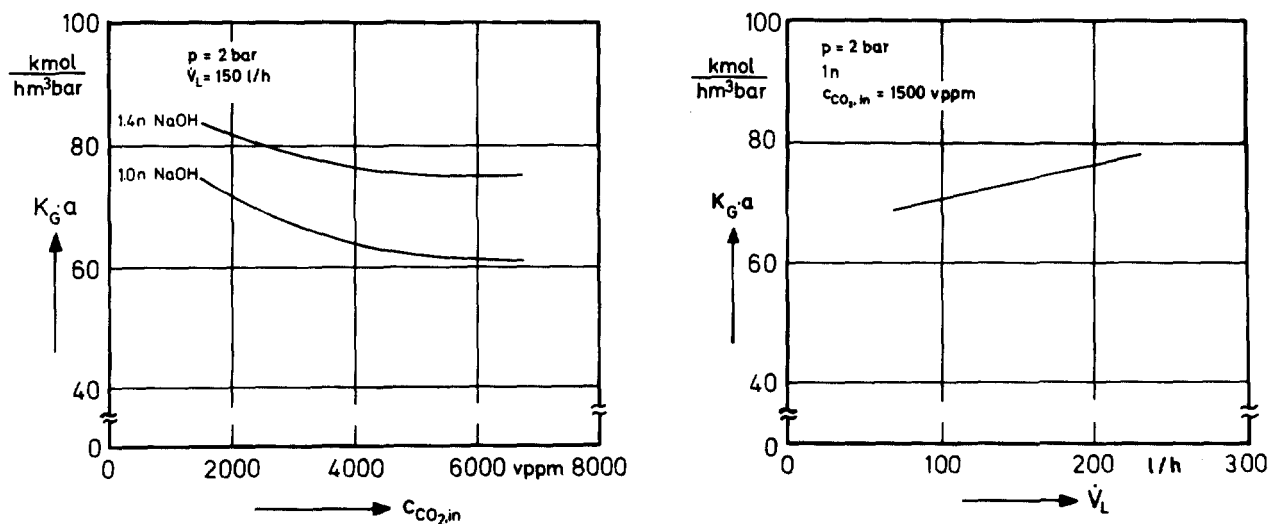


Fig. 12: Mass transfer constant $K_G \cdot a$ in dependence of the feed concentration c_{CO_2} , the caustic solution flow rate \dot{V}_L and the caustic solution concentration

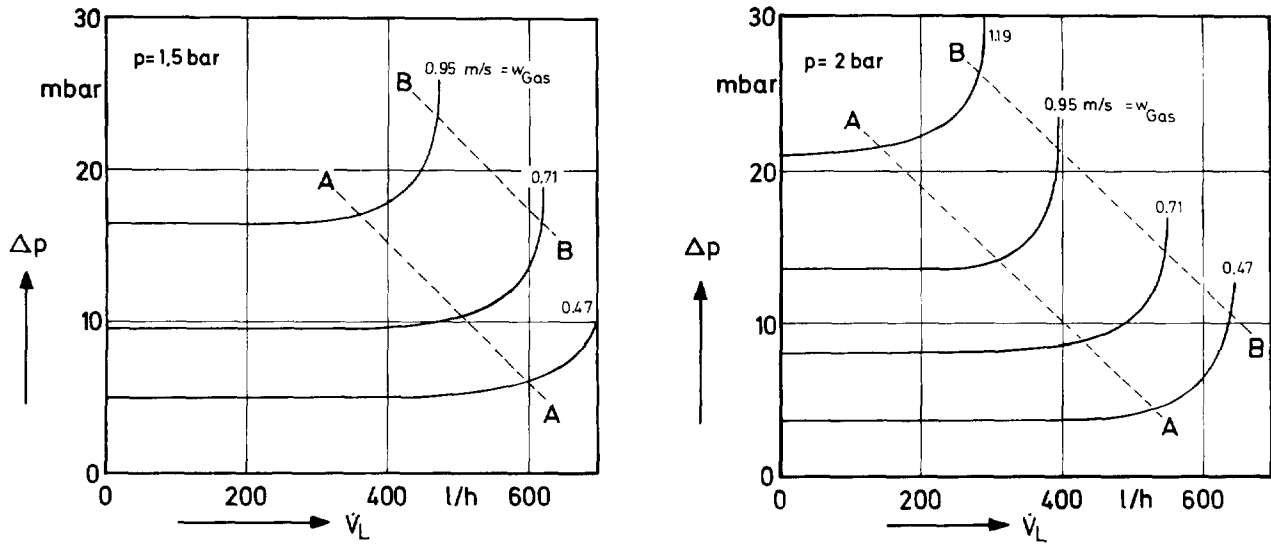


Fig. 13: Pressure drop Δp in dependence of the caustic solution flow rate \dot{V}_L

Operation behaviour

Extensive measurements to test normal behaviour and to determine operation parameters and a stationary long-time test of 200 hours at constant operating conditions (gas flow rate $20 \text{ Nm}^3/\text{h}$, caustic solution flow rate 150 l/h , facility pressure 1.5 bar) were carried out. The test facility is distinguished by the fact that it reacts nearly immediately selfregulating with additional feed, when outer interventions like e.g. change of the gas- and caustic solution flow rate respectively of the CO_2 concentration occur. This flexibility towards given operating conditions allows its use at varying demands. Because of the simple starting and stopping processes, it is also very suitable for discontinual operation. Undesired influences, like variations of pressure, which would have influenced the stationary behaviour, have been compensated with the advanced pressure regulator.

For discontinual operation the regeneration which is necessary in time intervals, allows a regular cleaning of the filling material column. Sedimentations on filling materials and on the bottom of the storage bunker were removed with repeated scrubbing with water. The impurity of the facility, however, remained within certain limits. Even after numerous regeneration periods a CaCO_3 sedimentation could not be noticed. Because of the very good solubility of Na(OH)_2 the danger of obstruction of the filling material column did never occur.

Regeneration of the used caustic solution

In order to determine the optimum process conduction for caustification parameter studies were carried out. The analysis of the sedimentation behaviour of the CaCO_3 were of particular interest. The studies were carried out in a sedimentation vessel - according to Imhoff - with a content of 1000 ml .

After the reaction participants had been mixed with the aid of air stirrers or with electric stirrers, a compression zone was built nearly without transition in about 30 s (no sedimentation zone). The hydrous Na-solution above this zone is clear.

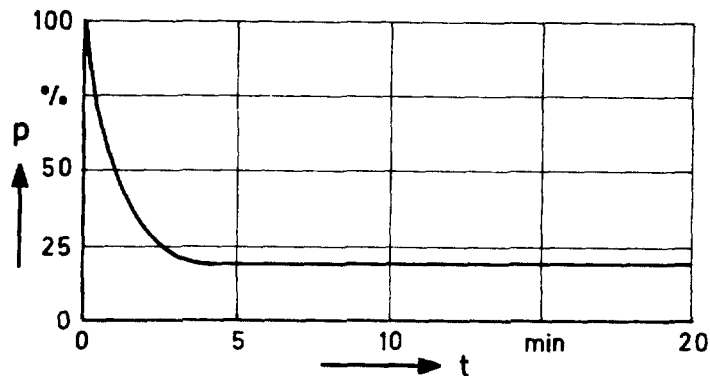


Fig. 14: Conversion in the compression zone, if 1 l poudorous 0.5 mol $\text{Ca}(\text{OH})_2$ is added to 0.5m Na_2OH -solution ans is mixed for 1 minute

Fig. 14 shows e.g. the reaction in the compression zone, if 1 l 0.5m- Na_2CO_3 -solution with 0.5 mol pulverized $\text{Ca}(\text{OH})_2$ is regenerated and mixed for 1 minute with the aid of an air stirrer.

The caustifications carried out in the test time showed that 20 minutes after the stirring period the bottom body is comprimised to 80 % of the final density in the liquid. The final density was achieved after approx. 24 hours. The regenerated caustic solution above the bottom body can already be sucked off 20 minutes after the stirring operation is finished and is so clear that it can again be fed into the caustic solution circuit without further filtering. Experiments showed that even after 200 hours CaCO_3 flowed off without problems as viscous mud.

Conditioning for final disposal

It has to be guaranteed by conditioning and final disposal of the precipitated CaCO_3 that ^{14}C is sealed off biosphere for a period of approx. 50.000 years (that is approx. tenfold half life period). The secure sealing off is mainly detracted from two effects: possible solution of CaCO_3 in water which contains CO_2 constituting $\text{Ca}(\text{HCO}_3)_2$; possible exchange of isotopes with C-compounds in other phases, particularly with atmospheric ^{12}C .

Taking these effects into consideration, the above-ground final disposal and the dumping into the deep sea are not suitable for the final disposal of ^{14}C . The best is the final disposal in salt rock. Actually the salt dome in Gorleben is analyzed to determine its suitability for the final disposal of radioactive material in the Federal Republic of Germany.

For final disposal CaCO_3 is homogenized with cement glue and filled into flange top casks, where the mixture can harden. After that the casks are placed into the underground final depot. The conditioning, packing and final disposal is carried out together with the final treatment of the remaining radioactive waste. Approx. 7 m^3/a of waste containing ^{14}C with a specific activity of approx. 65 Ci ^{14}C per m^3 result from ^{14}C retention.

References

- /1/ Bonka, H., Schwarz, G., Wibbe, H.-B.:
Umweltbelastung durch in Hochtemperaturreaktoren entstandenen Kohlenstoff 14;
Kerntechnik 15 No.7 (1973), S. 297-300

17th DOE NUCLEAR AIR CLEANING CONFERENCE

- /2/ Bonka, H., Brüssermann, K., Schwarz, G.:
Umweltbelastung durch Radiokohlenstoff aus kerntechnischen Anlagen;
Reaktortagung, Berlin (1974), S. 454-457
- /3/ RSK und SSK:
Grundsätzliche sicherheitstechnische Realisierbarkeit des Entsorgungszentrums,
Beurteilung und Empfehlung der Reaktor-Sicherheitskommission (RSK) und der
Strahlenschutzkommission (SSK);
Köln, Gesellschaft für Reaktorsicherheit (1977)
- /4/ Horn, H.-G., Gründler, D., Bonka, H.:
Kosten-Nutzen-Analyse zur Rückhaltung radioaktiver Stoffe in Kernkraftwerken
und Wiederaufarbeitungsanlagen;
Bericht zum Forschungsvorhaben St.Sch. 680a, RWTH Aachen (1982) (Bericht in
Vorbereitung)
- /5/ Horn, H.-G., Bonka, H., Gründler, D.:
Will the Cost-Benefit Analysis Give an Additional Decision-Aid to the Reten-
tion of Radioactive Effluents in Nuclear Facilities?
IAEA-SM-258/3 (1981)
- /6/ Gründler, D., Michaelis, W., Hunsänger, K., Bonka, H.:
Versuchsanlage zur Rückhaltung von C 14 bei Wiederaufarbeitungsanlagen für
LWR-Brennelemente nach dem "Doppelten Alkali-Prozeß";
Bericht zum Forschungsvorhaben St.Sch. 680a, RWTH Aachen (1982) (Bericht in
Vorbereitung)
- /7/ Bonka, H., Brüssermann, K., Schwarz, G., Willrodt, U.:
Production and Emission of Carbon-14 from Nuclear Power Stations and Repro-
cessing Plants and its Radioecological Significance;
IV. IRPA Congress, Paris (1977), Vol. 3, S. 945-947
- /8/ Hayes, D.W., Mac Murdo, K.W.:
Carbon 14 Production by the Nuclear Industry;
Savannah River Laboratory, Aiken, South Carolina, DP-MS-74-33 (1975)
- /9/ Hayes, D.W., Mac Murdo, K.W.:
Carbon-14 Production by the Nuclear Industry;
Health Physics 32 (1977), S. 215-219
- /10/ Kelly, G.N., Jones, J.A., Bryant, P.M., Morley, F.:
The Predicted Radiation Exposure of the Population of the European Community
Resulting from Discharges of Krypton-85, Tritium, Carbon-14 and Iodine-129
from the Nuclear Power Industry to the Year 2000;
Commission of the European Communities, Doc.V/2676/75 (1975)
- /11/ Fowler, T.W., Clark, R.L., Gruhlke, J.M., Russel, J.L.:
Public Health Considerations of Carbon-14 Discharges from the Light-Water-
Cooled Nuclear Power Reactor Industry;
USEPA, ORP/TAD-76-3, Washington, D.C. (1976)
- /12/ Skafi, M.:
Bestimmung der C 14-Aktivität in der Abluft von deutschen und ausländischen
Leichtwasserreaktoren (LWR) und die daraus resultierende Strahlenbelastung;
KWU-Bericht R 315-12-1976 (1976)

17th DOE NUCLEAR AIR CLEANING CONFERENCE

- /13/ Olsson, G.:
C 14-Bildning i Kraftreaktorer, Aktiebolaget Atomenergi;
Studsvik, Nyköping, Schweden, S-541 (1976)
- /14/ Davis, W.Jr.:
Carbon-14 Production in Nuclear Reactors;
ORNL/NUREG/TM-12 (1977)
- /15/ UNSCEAR:
Sources and Effects of Ionizing Radiation;
United Nations (1977)
- /16/ Bonka, H.:
Produktion und Freisetzung von H 3 und C 14 durch Kernwaffenversuche und
kerntechnische Anlagen, einschließlich Wiederaufarbeitungsanlagen;
in: Strahlenschutzprobleme im Zusammenhang mit der Verwendung von Tritium
und Kohlenstoff 14 und ihren Verbindungen;
Institut für Strahlenhygiene des Bundesgesundheitsamtes, STH-Bericht 12/1980
(1980) S. 17-26
- /17/ Martin, H.:
Bildung von C 13 und C 14 in wassergekühlten Reaktoren;
KWU-Bericht R 513 - 198/75 (1975)
- /18/ Apelqvist, G.:
Beräkning av ¹⁴C-Bildningen i Lättvattenreaktorer
Vattenfall PM ER-27/75 (1975-09-17)
Vattenfall PM ER-35/75 (1975-11-19)
- /19/ Kabat, M.J.:
Monitoring and Removal of Gaseous Carbon-14 Species;
15th DOE Nuclear Air Cleaning Conference (1978)
- /20/ Kabat, M.J.:
Ontario Hydro, Canada, private Mitteilung (1979)
- /21/ Bonka, H.:
C 14-Produktionsrate in Schwerwasserreaktoren;
(1978), (unveröffentlicht)
- /22/ Brooks, L.H., Heath, C.A., Kistein, B., Roberts, D.G.:
Carbon-14 in the HTGR Fuel Cycle;
GA-A 13174, UC-77 (1974)
- /23/ Magno, P.J., Nelson, C.B., Ellett, W.H.:
A Consideration of the Significance of Carbon-14 Discharges from the Nuclear
Power Industry;
in: Proceedings of the Thirteenth AEC Air Cleaning Conference, San Francisco,
1974, U.S. Atomic Energy Commission report CONF-740807 (1975) S. 1047-1054
- /24/ Schwarzer, K.:
Abschätzung der C 14-Produktion in einem Hochtemperaturreaktor im Hinblick
auf die Wiederaufarbeitung;
Reaktortagung, Düsseldorf 30. März - 2. April (1976) S. 518-521

17th DOE NUCLEAR AIR CLEANING CONFERENCE

- /25/ Till, J.E., Bomar, E.S., Morse, L.E., Tennery, V.J.:
A Radiological Assessment of Reprocessing Advanced Liquid-Metal Fast Breeder Reactor Fuels;
Nuclear Technology, Vol. 37 (1978) S. 328
- /26/ Young, J.R.:
Fusion Reactor Environmental Effects;
in: Pacific Northwest Laboratory Report on Fusion Energy, July 1976 - September 1976, BNWL - 1939-5
- /27/ Kunz, C.O., Mahoney, W.E., Miller, T.W.:
C 14 Gaseous Effluents from Pressurized Water Reactors;
8. Midyear Topical Symposium, Knoxville, CONF-741018 (1974)
- /28/ Kunz, C.O., Mahoney, W.E., Miller, T.W.:
C 14 Gaseous Effluents from Boiling Water Reactors;
ANS Meeting, New Orleans (1975)
- /29/ Schüttelkopf, H.:
Die Emission von $^{14}\text{CO}_2$ mit der Abluft kerntechnischer Anlagen;
KfK 2421 (1977)
- /30/ Schüttelkopf, H., Herrmann, G.:
 $^{14}\text{CO}_2$ - Emissionen aus der Wiederaufarbeitungsanlage;
Seminar on Radioactive Effluents from Nuclear Fuel Reprocessing Plants,
Commission of the European Communities, Karlsruhe (1977) S. 189-201
- /31/ Riedel, H., Gesewsky, P., Schwibach, J.:
Untersuchungen über die Emission von Kohlenstoff-14 mit der Abluft aus Kernkraftwerken;
Institut für Strahlenhygiene des Bundesgesundheitsamtes, STH-Bericht 13/76 (1976)
- /32/ Riedel, H., Gesewsky, P.:
Zweiter Bericht über Messungen zur Emission von Kohlenstoff 14 mit der Abluft aus Kernkraftwerken mit Leichtwasserreaktor in der Bundesrepublik Deutschland;
Institut für Strahlenhygiene des Bundesgesundheitsamtes, STH-Bericht 13/77 (1977)
- /33/ Bonka, H.:
Berechnung der Dosiswerte nach dem spezifischen Aktivitätsmodell für H 3 und C 14;
Symposium "Strahlenschutzprobleme im Zusammenhang mit der Verwendung von H 3 und C 14 und ihren Verbindungen" (1979), Institut für Strahlenhygiene des Bundesgesundheitsamtes, SHT-Bericht 12/1980 (1980), S. 129-136
- /34/ Bonka, H., Gründler, D., Hesel, D., Münster, M., Schmidlein, P., Sünder, B.:
Radiologische Auswirkungen der Emissionen aus Wiederaufarbeitungsanlagen im bestimmungsgemäßen Betrieb;
Seminar on Radioactive Effluents from Nuclear Fuel Reprocessing Plants,
Commission of the European Communities, Karlsruhe (1977) S. 219-246
- /35/ Bonka, H.:
Strahlenexposition durch radioaktive Emissionen aus kerntechnischen Anlagen im Normalbetrieb;
Verlag TÜV Rheinland (1982)

17th DOE NUCLEAR AIR CLEANING CONFERENCE

- /36/ ICRP:
Recommendations of the International Commission on Radiological Protection;
ICRP Publication 26, Pergamon Press, Oxford (1977)
- /37/ Gründler, D.:
Kosten-Nutzen-Analysen zur Rückhaltung von Tritium, C 14 und Krypton 85 aus
Wiederaufarbeitungsanlagen für LWR-Brennelemente;
Dissertation RWTH Aachen (1981)
- /38/ Horn, H.-G.:
Einfluß verschiedener Dosisbegrenzungskonzepte auf die Rückhaltung von Aero-
solen und Jod bei Wiederaufarbeitungsanlagen;
Dissertation RWTH Aachen (in Vorbereitung)
- /39/ Bonka, H., Gründler, D., Horn, H.-G.:
Use of Optimization Methods in the Field of Radiation Protection for Nuclear
Facilities; Radiation Protection Optimization - Present Experience and Methods;
Proceedings of the European Scientific Seminar held in Luxembourg, Pergamon
Press (1979), S. 112-152
- /40/ Beninson, D.J., González, A.J.:
Application of the Dose Limitation System to the Control of Releases of Car-
bon-14 from Heavy Water Moderated Reactors;
IAEA-SM-258/53 (1981)
- /41/ DWK:
Bericht über das in der Bundesrepublik Deutschland geplante Entsorgungszentrum
für ausgediente Brennelemente aus Kernkraftwerken;
Deutsche Gesellschaft für Wiederaufarbeitung von Kernbrennstoffen mbH,
Hannover (1977)
- /42/ Ullmanns:
Encyklopädie der technischen Chemie - Verfahrenstechnik I;
Verlag Chemie, Weinheim (1977), S. 575-585
- /43/ Schmidt, P.C.:
Alternativen zur Verminderung der C 14-Emissionen bei der Wiederaufarbeitung
von HTR-Brennelementen;
JÜL-1567 (1979)
- /44/ Von der Decken, C.B., Engel, R., Lange, G., Rausch, W.:
Untersuchungen zur Gasreinigung des THTR-Reaktors;
EURATOM 10.5, 1327 (1966)
- /45/ Haag, G.L.:
Carbon-14 Immobilization via the $\text{CO}_2\text{-Ba(OH)}_2$ Hydrate Gas-Solid Reaction;
16th DOE Nuclear Air Cleaning Conference (1981)
- /46/ Cheh, C.H., Glass, R.W., Chew, V.S.:
Removal of Carbon-14 from Gaseous Streams;
IAEA-SM-72/O7 (1982)
- /47/ Gutowski, H., Schröder, E.:
Angewandte Tieftemperatur-Technik zur Kryptonabscheidung in Wiederaufarbei-
tungsanlagen unter kerntechnischen Bedingungen;
Atomenergie, Kerntechnik Bd. 33 (1979), S. 277-280
- /48/ Croff, A.G.:
An Evaluation of Options Relative to the Fixation and Disposal of ^{14}C -Con-
taminated CO_2 as CaCO_3 ;
ORNL/TM-5171 (1976)

MECHANISM OF THE $\text{CO}_2\text{-Ca(OH)}_2$ REACTION

V.S. Chew, C.H. Cheh and R.W. Glass
 Ontario Hydro Research Division
 800 Kipling Avenue
 Toronto, Ontario, Canada M8Z 5S4

Abstract

Recent studies clearly showed the importance of moisture in achieving high Ca(OH)_2 absorbent utilization for removing CO_2 from gas streams at ambient temperatures. However, the role of moisture and the mechanism of the reaction was not well understood. This paper summarizes the results of a study of the mechanism of the $\text{CO}_2\text{-Ca(OH)}_2$ reaction with emphasis on the role of moisture. The reaction between Ca(OH)_2 and CO_2 in moist N_2 was found to be first order with respect to the reactants with a rate constant of about 100 min^{-1} . At high humidities, the rate of reaction was chemically controlled, but at low humidities, the reaction rate was limited by the diffusion through the carbonate layer formed by the reaction. Calculations showed that capillary condensation could have occurred only in about 2% of the pore volume and was unlikely to have affected the reaction rate significantly by allowing the reaction to occur in the liquid phase. It was, therefore, concluded that the main role of moisture was to improve the Ca(OH)_2 utilization by lowering the resistance to diffusion through the carbonate layer.

Nomenclature

C_A	= concentration of gas phase reactant A
k	= rate constant
k_g, k_d, k_s	= rate constants
R	= particle radius
t	= reaction time
T_5	= time at 5% breakthrough
X	= fraction of gas at bed outlet
X_B	= fraction conversion of B
ρ_B	= molar density of B in the solid
τ	= time/(time at $X = 0.5$)
\emptyset	= bed volume/volumetric gas flow

I. Introduction

Recently we presented performance data on an ambient temperature, fixed bed, $\text{Ca}(\text{OH})_2$ absorber developed to remove $^{14}\text{CO}_2$ from the moderator cover gas system of CANDU nuclear reactors. (1) During the development of this process the importance of moisture in achieving high absorbent utilization and, to some extent, removal efficiency, was clear; however the role of moisture in the reaction was not. The present work was conducted to study the mechanism of the reaction, with particular emphasis on the role of moisture.

II. Previous Studies

The reaction of CO_2 with a suspension of $\text{Ca}(\text{OH})_2$ in water has been well studied since early this century (2). The absorption of CO_2 by dry sorbents, in particular soda lime, has been known for many years and this material is widely used today in medical anaesthetic applications and has been extensively studied in divers' re-breather apparatus (3). Nevertheless, the mechanism of the reaction between CO_2 and soda-lime is not well understood. $\text{Ca}(\text{OH})_2$ has been used at elevated temperatures to absorb CO_2 (4)(5) but the mechanism was not well understood. $\text{Ba}(\text{OH})_2$ has been studied by Haag et al (6) where again moisture appears to play an important role in the mechanism of the reaction.

Theory

For the reaction:



a first order reaction in a fixed bed reactor is given by (7):

$$\ln \frac{X}{1-X} = k\phi(\tau - 1) \quad (2)$$

Thus a plot of $\ln(X/(1-X))$ versus $(\tau - 1)$ will give a straight line of slope k , the rate constant.

To identify the rate controlling step in the reaction, the "shrinking unreacted core" model appears to be appropriate (8). In this model, the major controlling resistances are, gas film diffusion, diffusion through product layer and chemical reaction.

Gas film diffusion is given by:

$$t = \frac{\rho_B R}{3b k_g C_A} \cdot X_B \quad (3)$$

Diffusion through product:

$$t = \left(\frac{1}{2} - \frac{1}{3}X_B - \frac{1}{2}(1 - X_B)^{2/3} \right) \frac{\rho_B R}{b k_d C_A} \quad (4)$$

Chemical reaction:

$$t = (1 - (1 - X_B)^{1/3}) \frac{\rho_B R}{b k_s C_A} \quad (5)$$

Although the gas film resistance remains unchanged throughout the reaction, the resistance to chemical reaction increases as the surface of the unreacted core decreases and the resistance to diffusion through the product layer increases as the product layer builds up. The mean rate constant, \bar{k} , defined as the average over the time necessary for the reaction to go to completion, is given by (8)

$$\bar{k} = \frac{1}{1/k_g + 1/k_d + 3/k_s} \quad (6)$$

\bar{k} can be calculated if k_g , k_d and k_s are known. k_g , k_d and k_s can be calculated from Equations (3), (4) and (5). It should be noted that the mean rate constant, \bar{k} , and the rate constant, k , from Equation (2) are related to each other by the total surface area in a unit volume of packed bed⁽⁹⁾.

III. Experimental Studies

The Ca(OH)_2 was prepared using a technique described earlier⁽¹⁾. The physical characteristics of the Ca(OH)_2 are listed in Table I and a typical chemical composition, determined by a thermal gravimetric analyzer (TGA), is shown in Table II. The pore size distribution of the absorbent by volume and by area is plotted in Figures 1 and 2, respectively.

Table I Calcium hydroxide characteristics.

Bulk density	0.56 kg/L
Particle size	-2.38 + 0.50 mm
Apparent (skeletal) density	197 kg/L
BET surface area	28.5 m ² /g
Total intrusion volume	1.29 mL/g
Total pore area	36.1 m ² /g
Median pore diameter (volume)	2.46 μm
Median pore diameter (area)	11.1 nm
Porosity	0.718

17th DOE NUCLEAR AIR CLEANING CONFERENCE

Table II Thermal gravimetric analysis of $\text{Ca}(\text{OH})_2$ samples⁽¹⁾.

	Moisture (g/kg)	$\text{Ca}(\text{OH})_2$ (g/kg)	CaCO_3 (g/kg)	CaO (g/kg)
February, 1981	13	906	57	24
	13	877	86	33
March, 1981	13	898	57	33
July, 1981	21	923	18	38
	16	898	45	50
	13	894	50	43
	12	906	52	30
March, 1982	16	896	51	37

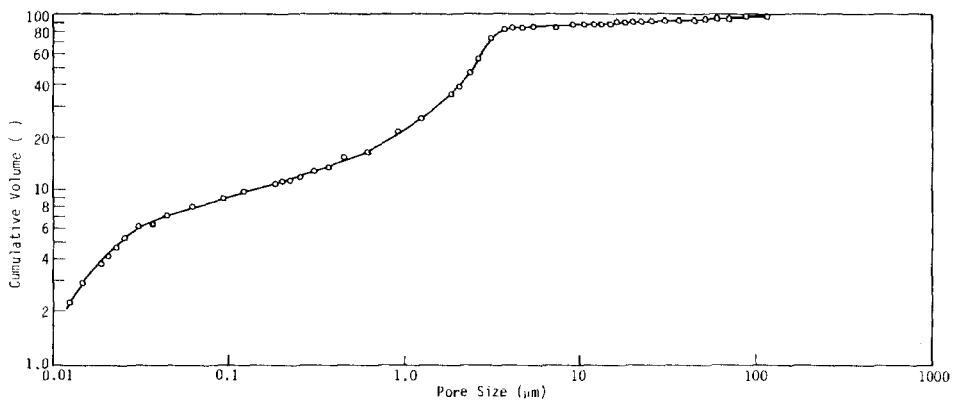


FIGURE 1
PORE SIZE DISTRIBUTION (BY VOLUME) OF $\text{Ca}(\text{OH})_2$ ABSORBENT

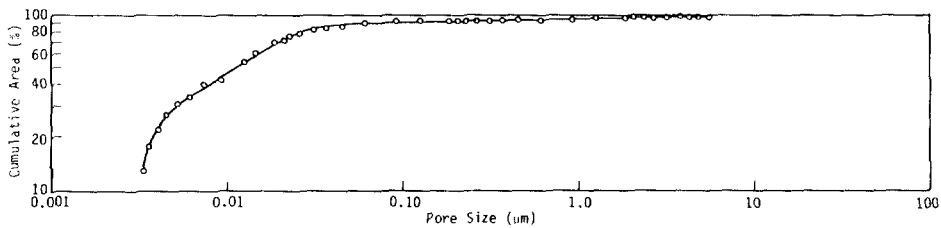


FIGURE 2
PORE SIZE DISTRIBUTION (BY AREA) OF $\text{Ca}(\text{OH})_2$ ABSORBENT

Procedure

A bench scale flow reactor described earlier⁽¹⁾ was used to determine the breakthrough characteristics of the $\text{Ca}(\text{OH})_2$ bed to test the assumption of a first order reaction between CO_2 and the number of moles of $\text{Ca}(\text{OH})_2$ available for reaction per unit bed volume (Equation 2).

The rate constants k_g , k_d and k_s were determined using thermal gravimetric analysis. For these experiments, about 50 mg of $\text{Ca}(\text{OH})_2$ particles (-2.38 + 2.00 mm) were supported on glass wool on the microbalance pan. Moist nitrogen gas was then passed through the system for about one hour to hydrate any remaining CaO present in the $\text{Ca}(\text{OH})_2$ sample and to condition the sample. A N_2/CO_2 mixture was then passed through a water bath and the humidity of the gas stream measured using a dewpoint hygrometer (General Eastern; model 1100AP). This humidified stream entered the microbalance system and the weight change of the $\text{Ca}(\text{OH})_2$ sample was recorded continuously at constant temperature until no further change in weight was observed. The used sample was then transferred to a platinum pan and analyzed for its chemical composition using the TGA.

IV. ResultsOrder of Reaction

The data from bench scale experiment No L-32 (see Table III) were used to construct a plot of $\ln(X/X-1)$ versus $(\tau-1)$ to test the validity of Equation 2 for the reaction. Figure 3 shows that the experimental data fit Equation 2, hence the reaction is first order with respect to the two reactants and the rate constant, k , is 100 min^{-1} .

Table III Summary of bench scale experimental conditions and results.

Experiment No	Gas Flow Rate (ℓ/min)	CO_2 Concentration ($\mu\ell/\ell$)	Bed Height (cm)	Utilization at T_5 (g/kg)	Length of Unused Bed, (LUB) (cm)	Bed Height LUB
L-13	2.0	330	4.5	495	2.0	2.25
L-20	1.6	308	4.0	538	1.6	2.5
L-21	4.0	300	3.8	101	3.4	1.1
L-22	1.0	300	1.9	514	0.81	2.3
L-23	4.0	305	7.6	550	3.0	2.5
L-32	2.0	415	8.0	660	2.0	4.0

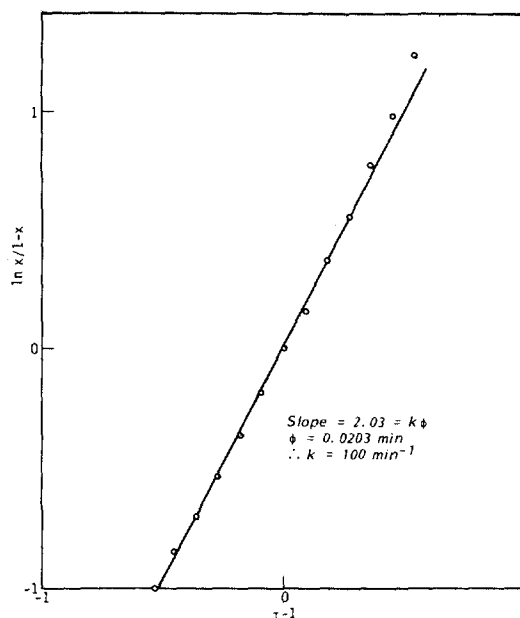


FIGURE 3

DETERMINATION OF REACTION ORDER AND RATE CONSTANT

Rate Controlling Step

Bench scale experiments (Nos L-13, L-22 and L-23) were conducted at a constant gas residence time (0.6 s) but different flow rates (1 to 4 l/min). The results summarized in Table III show that the $\text{Ca}(\text{OH})_2$ utilization remained the same for the gas flow rates studied indicating that gas film resistance does not influence the rate of the reaction.

Typical data obtained from TGA experiments at high humidities and CO_2 concentrations of $400 \mu\text{l/l}$ are shown in Figures 4 to 6. The results show that there is a linear relationship between $1 - (1 - X_B)^{1/3}$ and time; ie, the reaction rate is chemically controlled (Equation 5) depending mainly on the surface area of the unreacted $\text{Ca}(\text{OH})_2$. It is only in the latter stages of the reaction that the $(1/2 - 1/3 X_B - 1/2 (1 - X_B)^{2/3})$ versus t plot becomes linear; ie, the resistance caused by diffusion through the carbonate layer becomes significant. It is primarily because of this resistance that only $\sim 850 \text{ g/kg}$ of $\text{Ca}(\text{OH})_2$ is reacted at the end of typical TGA experiments.

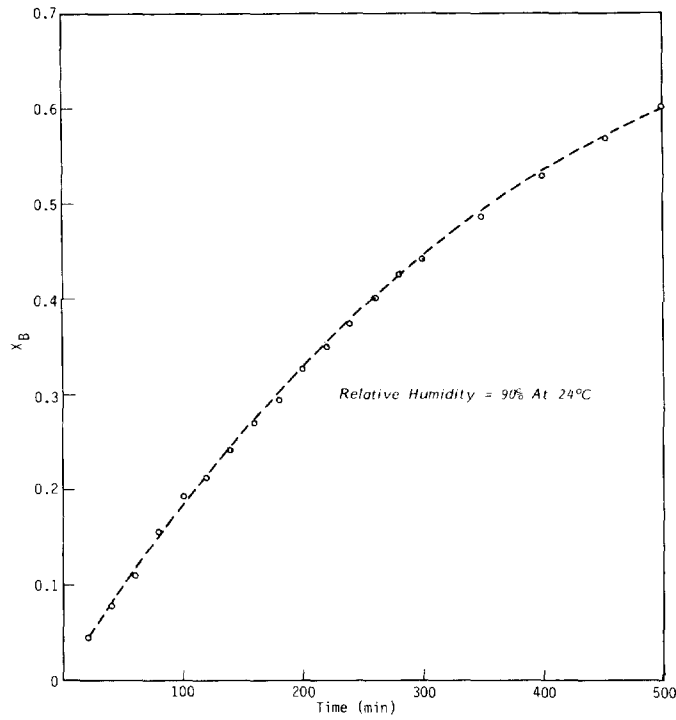


FIGURE 4

DETERMINATION OF RATE CONTROLLING STEP FOR HIGH HUMIDITY EXPERIMENT (G642) (ASSUMING GAS DIFFUSION CONTROLLED)

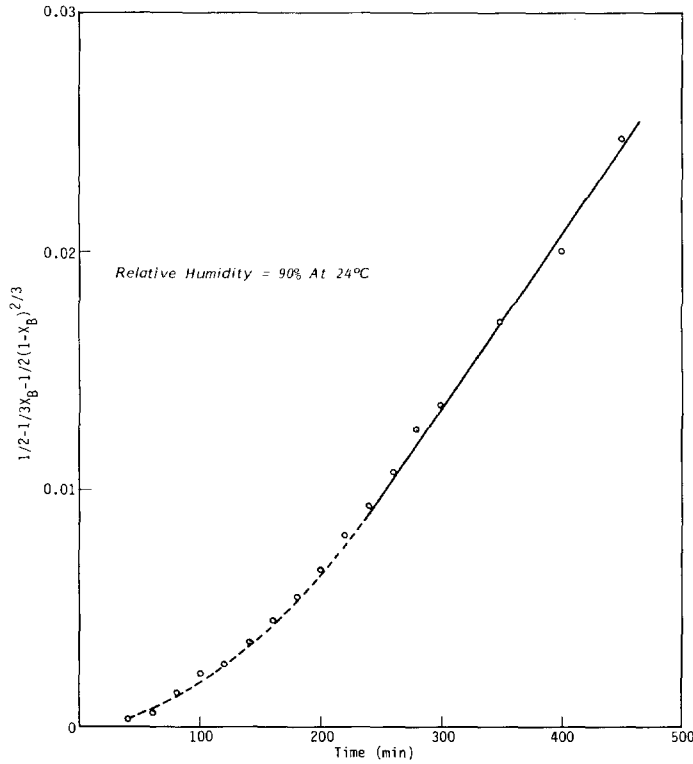


FIGURE 5

DETERMINATION OF RATE CONTROLLING STEP FOR HIGH HUMIDITY EXPERIMENT (G642) (ASSUMING DIFFUSION THROUGH PRODUCT LAYER CONTROLLED)

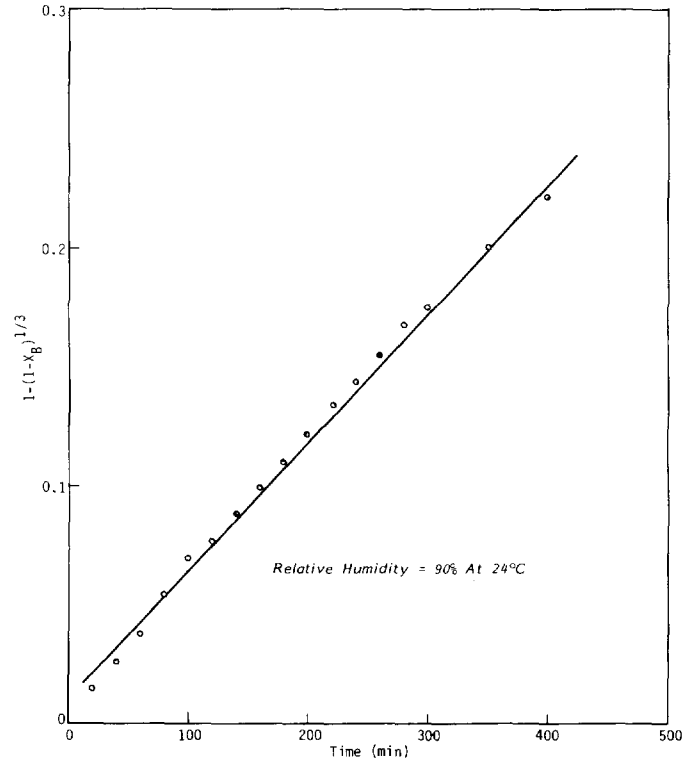


FIGURE 6

DETERMINATION OF RATE CONTROLLING STEP FOR HIGH HUMIDITY EXPERIMENT (G642) (ASSUMING CHEMICAL REACTION CONTROLLED)

17th DOE NUCLEAR AIR CLEANING CONFERENCE

Table IV lists the values obtained for k_s , k_d and k_g under different experimental conditions. These data suggest that k_g is relatively constant in the gas velocity range of 0.8 to 3.3 cm/s and was estimated to be about 28.8 cm/min. It should be noted that the maximum gas velocity that could be used in the TGA system was 3.3 cm/s which is only half of the superficial gas velocity used in the fixed bed bench scale experiments and the actual velocity across the particles in the bed could be much higher. k_d has an average value of 6.24 cm/min for the high relative humidity condition (90% at 24°C). k_s is relatively independent of CO_2 concentrations in the range 400 to 1000 $\mu\ell/\ell$ and has an average value of 23.1 cm/min.

These TGA results indicate that the mean rate constant is 3.0 cm/min (or 77 min^{-1}) for the -2.4 and 2.0 mm $Ca(OH)_2$ particles at 24°C. This is somewhat lower than the mean rate constant obtained from the fixed bed bench scale system (100 min^{-1}) probably due to the lower gas velocity in the TGA apparatus.

Table IV Summary of TGA experimental conditions and results.

Experiment No	G635	G636	G639	G647	G642	G643	G644	G640	G657	G658
Ca(OH) ₂ Size (mm)	2.38+2.00	2.38+2.00	2.38+2.00	2.38+2.00	2.38+2.00	2.38+2.00	2.38+2.00	2.38+2.00	2.38+2.00	2.38+2.00
Temp (°C)	24	24	24	24	24	24	24	24	51	55
RH (%)	90	90	90	90	90	90	90	50	60	24
CO ₂ conc ($\mu\text{L/L}$)	1000	1000	1000	1000	400	400	400	400	400	400
Flowrate (L/min)	1.0	0.6	0.4	0.25	1.0	0.6	0.25	1.0	1.0	1.0
Slope g* (min^{-1})	4.5×10^{-3}	3.3×10^{-3}	3.4×10^{-3}	3.3×10^{-3}	1.7×10^{-3}	1.7×10^{-3}	1.8×10^{-3}	-	2.1×10^{-3}	-
Slope d** (min^{-1})	1.25×10^{-4}	1.32×10^{-4}	1.59×10^{-4}	1.99×10^{-4}	7.2×10^{-5}	8.0×10^{-5}	8.3×10^{-5}	2.7×10^{-6}	2.1×10^{-4}	3.2×10^{-5}
Slope c*** (min^{-1})	1.3×10^{-3}	1.4×10^{-3}	1.6×10^{-3}	1.3×10^{-3}	68×10^{-3}	6.1×10^{-4}	6.1×10^{-4}	-	31.3	-
k_g (cm/min)	27.3	20.0	20.6	20.0	25.8	25.8	27.3	-	18.9	-
k_d (cm/min)	4.55	4.80	5.79	7.24	6.55	7.24	7.50	0.244	43.5	0.288
k_s (cm/min)	24.2	20.7	20.9	21.3	34.4	25.2	24.9	-	-	-

- * Slope g = initial slope of X versus time
 ** Slope d = slope of $1/2 - 1/3 X - 1/2(1 - X)^{1/3}$ versus time
 *** Slope c = slope of $1 - (1 - X)^{1/3}$ versus time

Role of Moisture

The $Ca(OH)_2$ samples (with an initial moisture content of -14 g/kg) were exposed to CO_2 -free nitrogen of different humidities and the moisture absorbed by or desorbed was determined by TGA (see Figure 7). The weight gain of the sample increased sharply as the relative humidity of the gas stream increased beyond 80% at 25°C.

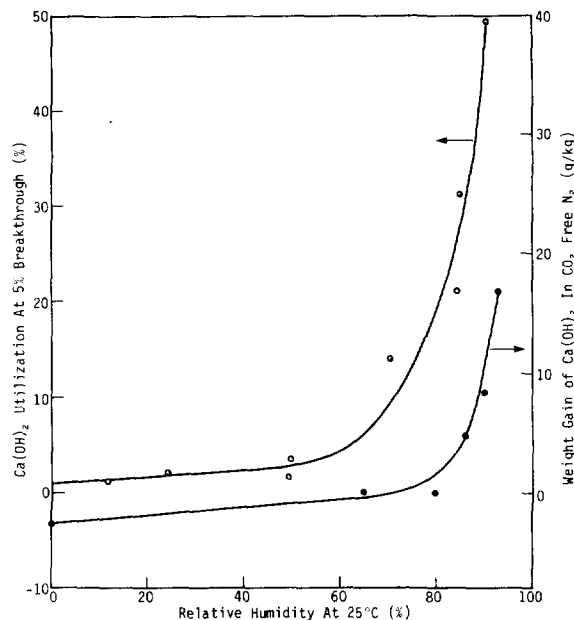


FIGURE 7
THE EFFECT OF HUMIDITY ON THE WEIGHT GAIN
AND UTILIZATION OF Ca(OH)_2

Previous bench scale experiments showed that the Ca(OH)_2 utilization (at 5% breakthrough) also increased sharply as the relative humidity increased beyond 80%⁽¹⁾. This seems to indicate that the increase of utilization is directly related to the increase of moisture content at high relative humidities.

Since the Ca(OH)_2 absorbent used was very porous (porosity ≈ 0.72), it is possible that capillary condensation could have occurred in the small pores and the reaction between CO_2 and Ca(OH)_2 could have proceeded in the liquid phase. However, calculations using a simplified Kelvin equation⁽¹⁰⁾ show that at a relative humidity of 85% at 25°C, capillary condensation can only occur in pores with diameters less than 13 nm, but only 2.5% of the total pore volume of the Ca(OH)_2 samples was found to be less than 13 nm (see Figure 1) as determined by mercury porosimetry. Furthermore, according to the Kelvin equation, the extent of capillary condensation occurring at 45 and 25°C (identical relative humidities) would be approximately the same, but the bench scale experiments showed that the utilization of the Ca(OH)_2 bed was considerably better at 45°C and 65% relative humidity than that at 25°C and at the same relative humidity⁽¹⁾. Again, this suggests that capillary condensation does not play an important role in the present reaction.

It has been suggested that water vapour can increase the porosity of the carbonate layer by modifying its microstructure⁽⁵⁾, thus permitting CO_2 gas to penetrate the carbonate layer. As discussed earlier, the reaction rate for high relative humidity (90%) experiments is chemically controlled. When the relative humidity is lowered from 90% to 50% at 25°C, the reaction is no longer chemically controlled. Instead, the reaction is controlled by diffusion through the product layer (see Figures 8 and 9) and the reaction rate is much

lower. Therefore, the main role of moisture in the reaction is to increase the reaction rate and improve the $\text{Ca}(\text{OH})_2$ utilization by decreasing the resistance to diffusion through the carbonate layer.

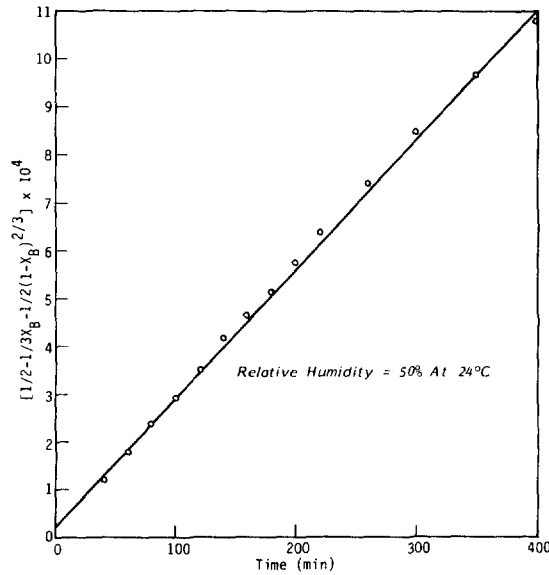


FIGURE 8
 DETERMINATION OF RATE CONTROLLING STEP
 FOR LOW HUMIDITY EXPERIMENT (G640)
 (ASSUMING DIFFUSION THROUGH PRODUCT LAYER CONTROLLED)

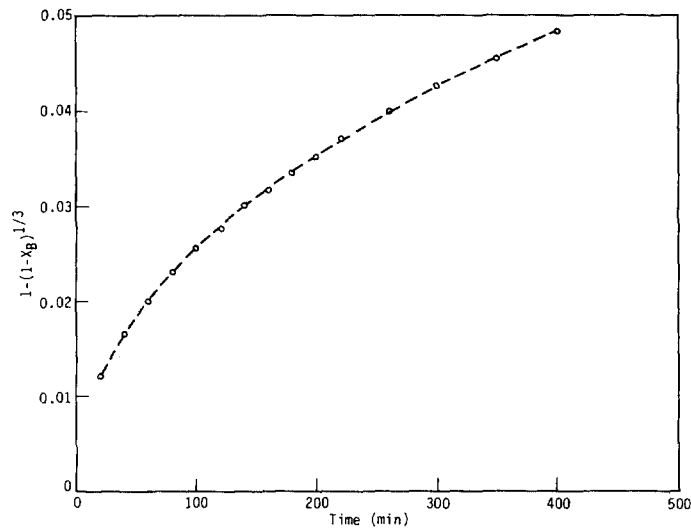


FIGURE 9
 DETERMINATION OF RATE CONTROLLING STEP
 FOR LOW HUMIDITY EXPERIMENT (G640)
 (ASSUMING CHEMICAL REACTION CONTROLLED)

At 50°C, TGA experiments (see Table IV experiment No G658 and G657) show that increasing the relative humidity from 24% to 60% is sufficient to change the reaction rate diffusion control through the product layer to chemical control. This is probably because the vapour pressure of water at a relative humidity of 60% at 50°C is sufficiently high to modify the microstructure of the carbonate layer and improve diffusion through the layer.

Reactor Design Considerations

Results of the bench scale experiments showed that the Length of Unused Bed (LUB) was independent of the bed height and was only a function of the gas velocity - the higher the gas velocity, the longer the LUB⁽¹⁾. As the gas velocity was increased from 3.3 to 13.3 cm/s, the LUB increased from 0.8 to over 3 cm (see Table IV). furthermore, the utilization of the Ca(OH)₂ at 5% breakthrough increased from 100 g/kg to 660 g/kg as the bed height-to-LUB ratio increased from 1 to 4 (see Figure 10). Hence, in order to achieve good utilization (eg, utilization of over 600 g/kg), the bed height-to-LUB ratio should be maintained at above 4 by either increasing the bed height or reducing the gas velocity (to reduce the LUB).

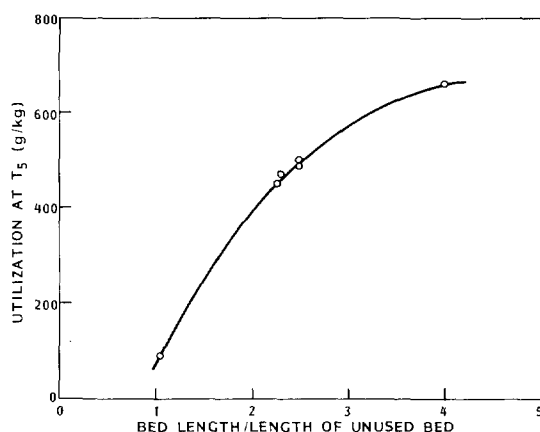


FIGURE 10

THE EFFECT OF (BED HEIGHT/LUB) RATIO ON Ca(OH)₂ UTILIZATION

V. Conclusions

1. The reaction between Ca(OH)₂ and CO₂ in moist N₂ is first order with respect to the two reactants with a rate constant of 100 min⁻¹.
2. The main role of moisture in the reaction is to improve the Ca(OH)₂ utilization by lowering the resistance to diffusion through the carbonate layer formed by the reaction.
3. The Ca(OH)₂ absorbent used was very porous with a porosity of 0.72 and a surface area of 36.1 m²/g.

17th DOE NUCLEAR AIR CLEANING CONFERENCE

4. Capillary condensation could have occurred only in about 2% of the pore volume and was unlikely to affect the reaction rate significantly by allowing the reaction to occur in the liquid phase.
5. At high humidities, the rate of reaction is chemically controlled but at low humidities, the reaction rate is limited by the diffusion through the carbonate layer.
6. The bed height-to-LUB ratio should be kept above 4 in order to achieve good utilization of Ca(OH)_2 .

References

1. Cheh, C.H., Glass, R.W. and Chew, V.S. "Removal of Carbon-14 from Gaseous Streams." Paper presented at the IAEA Seminar on the Testing and operation of Off-Gas Cleaning Systems at Nuclear Facilities, Karlsruhe; FRG. May 3-7, 1982.
2. Statham, N. US Patent 1,178,962. 1916.
3. Veinot, D.E. Defence Research Establishment Atlantic, Canada. Private Communication.
4. Engel, R. and Decken, C.B. "Removing Carbon Dioxide and Water from a Gas Stream." US Patent 3,519,384.
5. Mozes, M.S. Ontario Hydro Research Division Report 80-509-K. 1980.
6. Haag, G.L. "Carbon-14 Immobilization Via the CO_2 - Ba(OH)_2 Hydrate Gas-Solid Reaction." Proc 16th DOE Nuclear Air Cleaning Conference, San Diego, California. October 20-23, 1980.
7. Karlsson, H.T., Klingspor, J. and Bjerle, I. "Adsorption of Hydrochloric Acid on Solid State Lime for Flue Gas Clean Up." J. Air Pollution Control Association 31. pp 1177-1180. 1981.
8. Levenspiel, O. "Chemical Reaction Engineering." p 341. John Wiley and Sons Inc. 1962.
9. Sherwood, T.K. Pigford, R.L. and Wilke, C.R. "Mass Transfer." p 555. McGraw Hill.
10. Gregg, S.J. "The Surface Chemistry of Solids." Chapman & Hall Ltd. 1951.

DISCUSSION

RINGEL: In the process, water is needed for high utilization and reaction. What would it mean if you used Ca(OH)_2 slurry instead of Ca(OH)_2 particles?

CHEH: The dry Ca(OH)_2 process developed by Ontario Hydro has the advantages of a Ca(OH)_2 slurry process, such as high absorbent utilization and high DFs, but avoids the many disadvantages of a wet process which involves more complicated operations such as filtration and handling of contaminated liquid and slurry streams.

HAAG: What is the assumed particle geometry in your studies? What is the maximum reactant utilization and required relative humidity? Is caking a problem at 100% relative humidity?

CHEH: The particles are assumed to be spherical in this study. Utilization of the Ca(OH)_2 absorbent can be as high as 85% and the relative humidity should be in the range of 85-100% at 25°C for the same bed temperature. Our pilot plant results showed that caking is not a problem at 100% relative humidity if the bed temperature is 20-25°C. This result is reported in another paper presented at the IAEA Seminar on the Testing and Operation of Off-gas Cleaning Systems at Nuclear Facilities, 3-7 May, 1982.

HAAG: Just a point of observation. In our studies on the barium hydroxide system, we noticed that our surface area is a definite function of relative humidity. Dr. Paul Edment of Oregon State University has observed in his systems that when he obtained two or three monolayers of water on the surface, it acted as if it were a liquid solution with respect to transport properties. In our own studies, what we feel to be happening is that solution is resulting in transport of the barium ions and hydroxide ions, and our surface does decrease as our humidity increases. So, it is almost as if there is a liquid solution sitting there on the surface. Also, we have noticed that our surface area tends to decrease as the rate of reaction decreases. It appears that the slower the rate of reaction the more defined the crystal structure is within the material. In essence, if the reaction takes place in a more orderly environment, our crystalites are much bigger. I think what you are seeing, and what we are seeing, are very closely parallel.

CHEH: It makes sense that the CO_2 and the calcium hydroxide react in the liquid phase, but we don't seem to get evidence of it in our studies. Perhaps a study similar to yours could tell us a bit more on this point.

BONKA: The highest ^{14}C emission rates from nuclear power plants are from heavy water reactors. Argentina decided after a cost-benefit analysis to retain ^{14}C at the reactor Atuche II. Has there been a similar decision or discussion in Canada?

CHEH: Although the ^{14}C emissions from Ontario Hydro's nuclear generating stations are below 1% derived emission limit, an

17th DOE NUCLEAR AIR CLEANING CONFERENCE

effort has been devoted by Ontario Hydro to further reduce ^{14}C emissions. The development of the dry air ambient temperature $\text{Ca}(\text{OH})_2$ system for the moderator cover-gas and nitrogen annulus gas of the Candu reactor is part of this effort. An engineering design of this procedure is being prepared and testing of this system in our nuclear stations is under consideration.

KABAT: I have a comment to this point, too. Carbon-14 removal in Canada is not officially required by regulation. It is a voluntary action of Ontario Hydro to reduce the carbon-14 stack emissions in order to remove ^{14}C from the systems. The moderator system is the major contribution to the stack. In Pickering, where we have a nitrogen annulus gas in two units, a carbon-14 recovery system will be installed on the annulus gas systems, eventually. The point is that, since the process we developed is so simple and reliable (we tested it for a long period of time) with very little maintenance required, if we put it in the moderator cover gas system it would probably last well over two years before it will need to be changed. This is one of the main reasons we are thinking that perhaps we should put it in anyway.

17th DOE NUCLEAR AIR CLEANING CONFERENCE

^{14}C RELEASE AT LIGHT WATER REACTORS

C. Kunz

Center for Laboratories and Research
New York State Department of Health
Albany, New York 12201

Abstract

The quantity, discharge pathway, and chemical form were determined for the ^{14}C released from two pressurized water reactors (PWR) and one boiling water reactor (BWR) in northeastern U.S. Continuous stack samplers were used to measure either total ^{14}C or $^{14}\text{CO}_2$ in the gaseous effluent. In addition, grab samples were taken of stack gas, containment air, and gas in decay tanks and analyzed for ^{14}C in specific chemical species such as CO_2 , CH_4 , C_2H_6 , C_3H_8 , and C_4H_{10} . Samples of primary coolant taken before and after passage through the clean-up demineralizers were also analyzed to determine the ^{14}C in the coolant and the decontamination factors for the demineralizers.

The ^{14}C gaseous discharge rate for a 490 MW(e) PWR was 11.6 Ci/GW(e)-yr. Venting of gas decay tanks accounted for 42% of the total ^{14}C released; 35% was discharged through auxiliary building ventilation and 23% through containment venting. The average chemical composition was 69% as $^{14}\text{CH}_4$, 16% as $^{14}\text{C}_2\text{H}_6$, 5% as $^{14}\text{C}_3\text{H}_8$ and $^{14}\text{C}_4\text{H}_{10}$, and 10% as $^{14}\text{CO}_2$.

The ^{14}C gaseous discharge rate for a 1000 MW(e) PWR was 8.0 Ci/GW(e)-yr. Venting of gas decay tanks accounted for about 7% of the total ^{14}C released. The predominant pathway for ^{14}C gaseous discharge at this PWR was pressure relief venting and purging of the containment air. $^{14}\text{CO}_2$ made up 19% of the total ^{14}C , with the balance as $^{14}\text{CH}_4$ and other hydrocarbon gases.

The ^{14}C gaseous discharge rate for an 850 MW(e) BWR was 12.3 Ci/GW(e)-yr. Approximately 97% of the gaseous ^{14}C release was as off-gas discharge, and the chemical composition of the discharge was about 98% $^{14}\text{CO}_2$.

There was no measurable removal of ^{14}C by the coolant demineralizers for the PWRs. A decontamination factor of 7 was observed for the clean-up demineralizer at the BWR, resulting in a ^{14}C removal rate of approximately 0.5 Ci/GW(e)-yr.

Introduction

In light water reactors ^{14}C is produced as an activation product in the coolant, fuel, and structural material. The most important production reactions and their thermal neutron cross-sections for ^{14}C formation in light water reactors are:



The isotopic abundance of ^{17}O is 0.04% of oxygen, which is a major constituent of the coolant water and oxide fuel. Production of ^{14}C from ^{17}O is therefore unavoidable. The isotopic abundance of ^{14}N is 99.62% of the nitrogen, which is present as an impurity in both the coolant and fuel. Production of ^{14}C through the activation of ^{14}N is difficult to estimate, since the nitrogen concentrations in the coolant water and the fuel are not well known. If approximately 50 ppm of atomic nitrogen is present in the coolant, the amount of ^{14}C produced from

dissolved ^{14}N is about equal to that from the activation of the ^{17}O in the H_2O .

In 1974 Bonka et al.⁽¹⁾ estimated the rate of formation of ^{14}C in nuclear reactors; Magno et al.⁽²⁾ discussed the radiological significance of ^{14}C discharges; and Kunz et al.⁽³⁾ reported on measurements of ^{14}C at pressurized water reactors (PWRs). Since 1974 there have been a number of publications on the calculated and measured production and discharge of ^{14}C at light water reactors. The most extensive measurements have been made in the Federal Republic of Germany.⁽⁴⁾

Bonka⁽⁵⁾ has summarized eight studies, including his own work, to calculate estimates of the production of ^{14}C in light water reactors. The average calculated production rates in the primary coolant were 6.7 and 8.2 Ci/GW(e)-yr for PWRs and boiling water reactors (BWRs) respectively. Although ^{14}C is also formed in the fuel and the structural material of the core, only the ^{14}C formed in the coolant is subject to release during normal plant operation.

Two-year studies of the ^{14}C discharge have been conducted at each of three light water reactors; a 490 MW(e) PWR, a 1000 MW(e) PWR, and an 850 MW(e) BWR. The studies at the 490 MW(e) PWR have been completed, and the results are discussed here in detail. Samples and data are still being analyzed for the 1000 MW(e) PWR and the 850 MW(e) BWR, so only the results obtained as of this writing will be summarized here.

Experimental

Stack samplers were operated continuously to obtain integrated samples for measurement of total ^{14}C or $^{14}\text{CO}_2$ in the gaseous effluent. In addition, grab samples of stack gas, containment air, off-gas, and gas in decay tanks were analyzed for ^{14}C content as specific chemical species: CO_2 , CH_4 , C_2H_6 , C_3H_8 , and C_4H_{10} . The several chemical species were separated by gas chromatography,⁽⁶⁾ and the ^{14}C was measured by internal gas proportional counting.⁽⁷⁾

A schematic of the continuous sampler is shown in Fig. 1. A sample flow of 100 cc/min is maintained in the sampler by using a diaphragm pump. The sampled gas is drawn through a tube furnace at 600°C containing palladium-on-alumina and platinum-on-alumina pellets. All carbon species, such as CH_4 , C_2H_6 , and CO , are oxidized to CO_2 . From the furnace the gas flows through a solid absorbent, such as Drierite, to remove the water vapor and then through a cartridge containing a solid absorbent of 8- to 20-mesh Ascarite, which contains NaOH on a solid support material to trap CO_2 . Water vapor must be removed, prior to the Ascarite step, in order to avoid dissolving the NaOH and clogging the tube. The CO_2 absorbent cartridges contain 25 g of Ascarite and are changed at biweekly intervals.

To prepare the sample for measurement of ^{14}C content, CO_2 must first be evolved by acidifying the Ascarite. The 25 g of Ascarite are added to 50 ml of water in a flask attached to the gas flow apparatus, and helium is bubbled through the mixture. Approximately 50 ml of concentrated HCl is added to the Ascarite-water mixture, and the helium flow is maintained for 30 min. The helium containing the evolved CO_2 is passed through a cold water condenser and a cold trap at approximately -60°C to remove water vapor and finally through a liquid nitrogen cold trap to collect the CO_2 . The volume of collected CO_2 is measured (~ 650 cc for a 2-week sampling period), and about 50 cc is chromatographically purified and loaded into an internal gas proportional tube for counting.

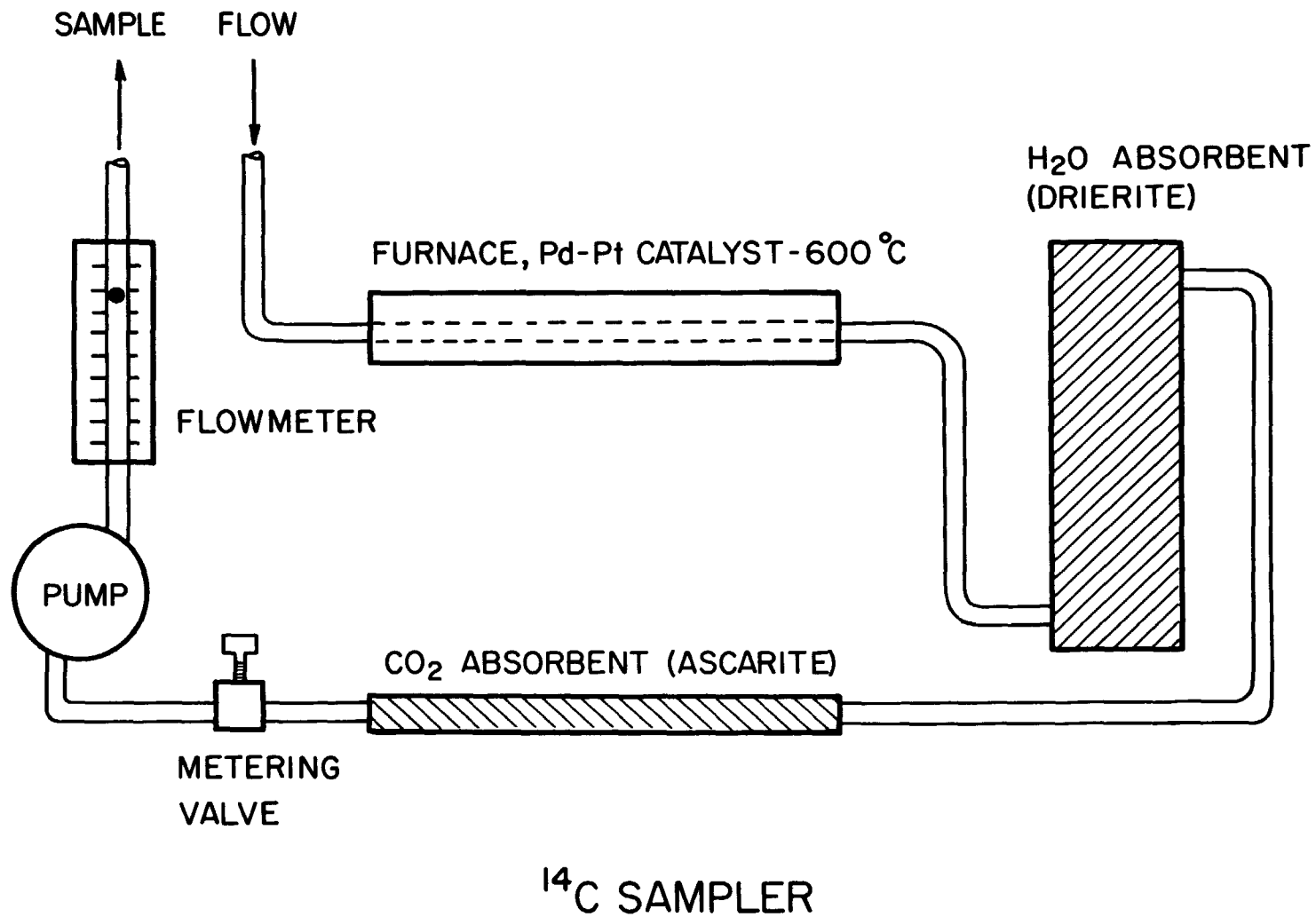


Figure 1 ^{14}C sampler used to continuously sample vented gases. All carbon species are oxidized to CO_2 and trapped on a solid absorbent.

17th DOE NUCLEAR AIR CLEANING CONFERENCE

The specific activity ($^{14}\text{C}/\text{cc}$ of CO_2) is measured, and the ^{14}C concentration per cubic centimeter of vent gas is calculated. The volume of air sampled is determined from the sampler flow rate and also from the total amount of CO_2 trapped, assuming that the sampled gas contains the ambient concentration of CO_2 in air (325 ppm).

The analytical uncertainty associated with the measurement of the concentration of ^{14}C in each 2-week sample is less than $\pm 10\%$. In determining the quantity of ^{14}C discharged, additional uncertainties are associated with determining the volume of gas sampled and the flow rate of the plant vent. Considering these three factors, the uncertainty in determining the quantity of ^{14}C released is estimated at $\pm 25\%$.

Results and Discussion

490 MW(e) PWR

Plant Ventilating System. The two main vents at this plant - the plant vent and the containment vent - are both rooftop vents discharging gas at a height of about 45 m. Four gas decay tanks are used to hold cover gas from the primary system to allow time for short-lived gaseous radionuclides to decay prior to discharge. The gas decay tanks and all building ventilation air except for containment are exhausted through the plant vent at a flow rate of 2.97×10^7 cc/s. The building air is exhausted continuously. The gas decay tanks are vented approximately 20 times each year, and about 10 h are required to vent each tank. The containment building is vented at 1.18×10^7 cc/s during refueling outages and some repair outages. When the plant is operating, containment is not vented. All releases through the plant vent and containment vent pass through charcoal and HEPA filters to remove radioactive iodine and particulates.

Gaseous Grab Samples. Grab samples of decay tank gas, containment air, and stack gas have been collected at various times since 1973 and analyzed for the concentration of ^{14}C as CH_4 , C_2H_6 , C_3H_8 , C_4H_{10} , and CO_2 . For some of the samples aliquots were passed through a combustion furnace to oxidize all carbon compounds to CO_2 which was measured for ^{14}C . These results were compared to the total ^{14}C obtained by summing the specific chemical species measured separately. The results agreed within 10%, indicating that all major species of ^{14}C were accounted for.

The average chemical composition of the ^{14}C in the gas decay tanks was 74% as $^{14}\text{CH}_4$, 16% as $^{14}\text{C}_2\text{H}_6$, 6% as $^{14}\text{C}_3\text{H}_8$ and $^{14}\text{C}_4\text{H}_{10}$, and 4% as $^{14}\text{CO}_2$.

The cover gas for the primary coolant was predominantly hydrogen. In this hydrogen atmosphere and under the intense radiation of the reactor core any carbon present tends to be reduced to form hydrocarbons. Our results indicate that the more hydrogen-saturated volatile species, CH_4 and C_2H_6 , were preferentially formed.

The average concentration of total ^{14}C in the gas decay tanks was 1×10^{-3} $\mu\text{Ci}/\text{cc}$. During an 88-week period when the discharge of ^{14}C was measured with continuous stack samplers, gas decay tanks were vented 31 times. The volume of each tank is 13.3m^3 and they are normally filled to a pressure of 6.3×10^5 Pa (92 psi). The average concentration of ^{14}C and the total volume of gas released corresponds to a release rate of 1.5 Ci/yr from the gas decay tanks.

In the containment air the total ^{14}C concentration ranged from 8×10^{-7} to 6×10^{-6} $\mu\text{Ci}/\text{cc}$. The chemical composition of the ^{14}C in containment averaged

17th DOE NUCLEAR AIR CLEANING CONFERENCE

74% as $^{14}\text{CH}_4$, 21% as $^{14}\text{C}_2\text{H}_6$, 3% as $^{14}\text{C}_3\text{H}_8$ and $^{14}\text{C}_4\text{H}_{10}$, and 2% as $^{14}\text{CO}_2$. This is similar to the chemical composition of the ^{14}C in the gas decay tanks, with only a small percentage as $^{14}\text{CO}_2$. Apparently the ^{14}C found in the containment air is formed in the reactor vessel and leaks into the containment building. If the ^{14}C were formed in containment by interaction of neutrons with containment air, the predominant gaseous chemical species should be $^{14}\text{CO}_2$ and ^{14}CO , due to the oxidizing conditions of the containment air.

Containment is purged during shutdowns and isolated when the reactor is operating. The rate of accumulation of ^{14}C in containment can be estimated from the length of time containment is isolated before grab samples are taken, assuming that containment was well purged of radioactive gas during venting. The average rate of accumulation determined from three containment samples was 0.4 Ci/yr. This corresponds to the amount of ^{14}C leaking into the containment building when the reactor is operating. It does not include ^{14}C leaking into containment during an outage.

Two samples of building ventilation air from the main plant vent were taken when the gas decay tanks were not being vented. The chemical composition of the ^{14}C in one sample was similar to that found in the decay tank and containment samples. However, in the other sample the $^{14}\text{CO}_2$ comprised 49% of the total ^{14}C . The origin of the higher fraction of $^{14}\text{CO}_2$ in the main plant vent is not known.

Continuous Gas Sampling. To more accurately measure the rate of discharge of gaseous ^{14}C , samplers were used to draw off continuously a small flow of gas from the main plant vent and the containment vent. The main plant vent is the discharge point for the gas decay tanks and for all building ventilation except in the containment building, which is vented through the containment vent. The containment vent is normally operated only during refueling operations and other outages. At such times containment is continuously vented; it is then isolated when the reactor is started up.

When containment was not being vented, the containment sampler was used to sample the main plant vent for $^{14}\text{CO}_2$ only. This was accomplished by not using the oxidizing furnace. In those periods the main plant vent was thus sampled simultaneously for total ^{14}C and for $^{14}\text{CO}_2$.

The continuous ^{14}C samplers were placed on the vents on 14 March 1980. The results for the next 88 weeks of continuous sampling of the main plant vent are shown in Fig. 2.

During and just before outages the ^{14}C releases were the greatest, most probably for the following reasons: During outages the gases covering and dissolved in the primary coolant system are purged into the gas decay tanks. The tanks are vented to make room for the cover gas, and after a hold-up period the cover is discharged. During an outage, therefore, when radioactive gases that have accumulated in the primary coolant are removed and released from the gas decay tanks, the discharge of ^{14}C is the greatest. After an outage the concentration of radioactive gases in the primary system is reduced, and less ^{14}C is discharged.

The release of ^{14}C is greater during periods when gas decay tanks are vented. However, even when decay tanks are not being vented, a substantial quantity of ^{14}C is discharged. The release of ^{14}C during such periods indicates that ^{14}C is leaking from various reactor components in auxiliary buildings outside the containment building. For example, there may be some leakage of radioactive gases from

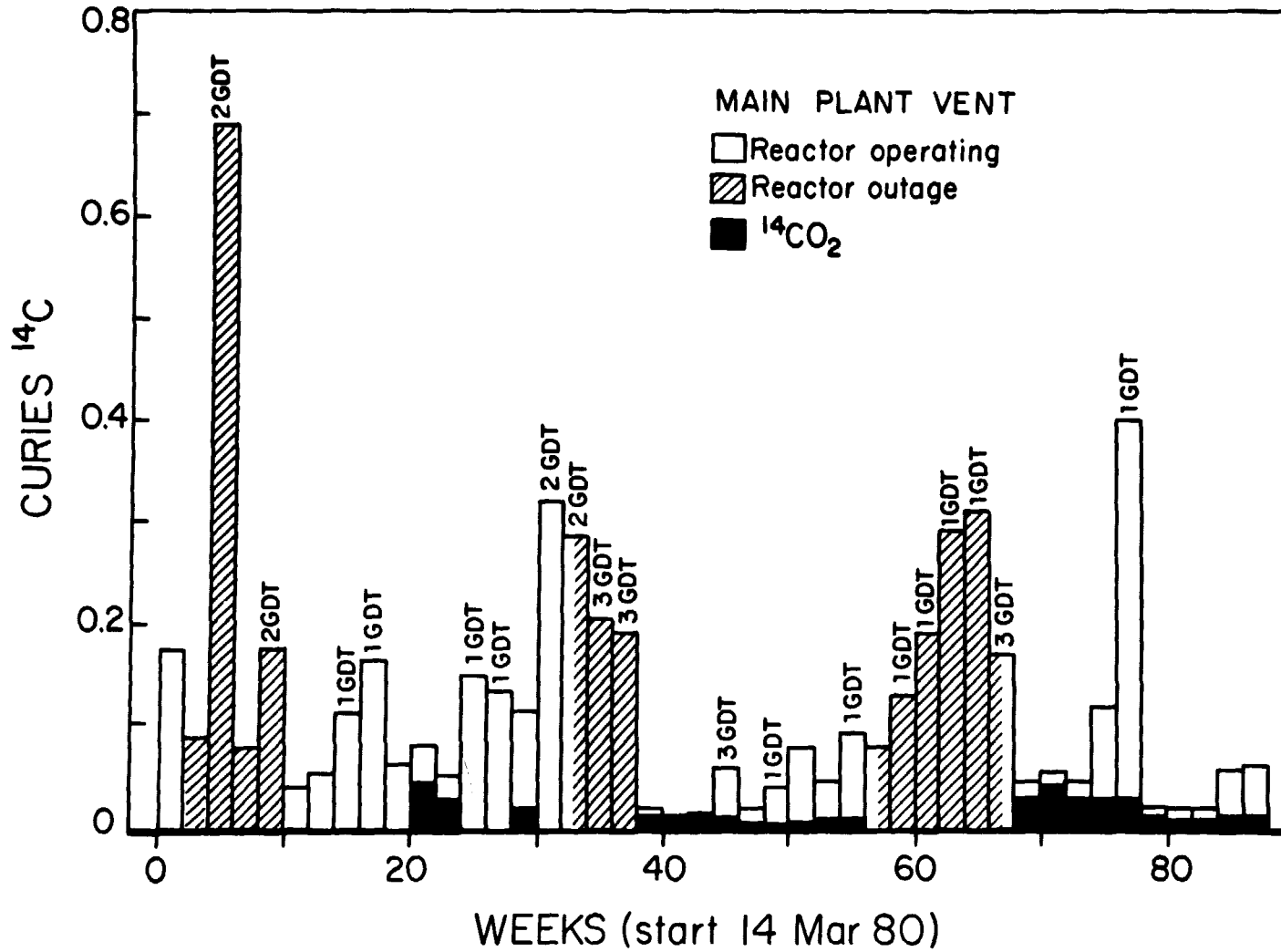


Figure 2 Biweekly measurements of ^{14}C discharge from main plant vent of a 490 MW(e) PWR. Gas decay tank (GDT) releases are indicated for each 2-week period.

17th DOE NUCLEAR AIR CLEANING CONFERENCE

the primary to the secondary coolant, and these gases could be released in buildings outside the containment building. Gases released in auxiliary buildings are discharged through the main plant vent.

During 50 weeks of the 88-week test period there were no releases from the gas decay tanks through the main plant vent. During these 50 weeks a total of 1.48 Ci of ^{14}C were discharged from the main plant vent, for a discharge rate of 1.5 Ci of $^{14}\text{C}/\text{yr}$ from auxiliary building ventilation.

The $^{14}\text{CO}_2$ fraction of the total ^{14}C in the main plant vent was measured during 44 weeks of the test period. A total of 0.37 Ci of $^{14}\text{CO}_2$ was released, which corresponds to a discharge rate of 0.4 Ci of $^{14}\text{CO}_2/\text{yr}$. The concentration of $^{14}\text{CO}_2$ in the main plant vent does not appear to be affected by the release of gas from the decay tanks. This is not surprising in view of the very low concentration of $^{14}\text{CO}_2$ in the grab samples from gas decay tanks. The $^{14}\text{CO}_2$ appears to be associated primarily with the continuous auxiliary building discharge from the main plant vent. The source of the $^{14}\text{CO}_2$ is not known. Analyses of grab samples from gas decay tanks and of containment air indicate that very little $^{14}\text{CO}_2$ is formed in the pressure vessel, decay tanks, or containment building.

The results for continuous sampling of the containment vent are shown in Fig. 3. During the first outage a total of 0.91 Ci was released from this vent. During the second and third outages 0.31 and 0.43 respectively were released. The total amount of ^{14}C released from the containment vent during the 88-week test period was 1.65 Ci, for a rate of 1.0 Ci/yr.

The grab samples indicated that ^{14}C was accumulating in the containment building at a rate of 0.4 Ci/yr during periods when the plant was operating. It appears that over half of the ^{14}C discharged from containment was released from reactor components during the outages. Apparently ^{14}C in the pressure vessel, steam generators, and other reactor components is released during refueling and repairs and is discharged with the containment venting.

Considering the discharge from both the main plant vent and the containment vent (Fig. 4), the total amount of ^{14}C discharged during the 88-week test period was 7.2 Ci. This corresponds to a discharge rate of 4.3 Ci/yr.

The sources or location of the ^{14}C discharges can be roughly apportioned. The ^{14}C release rate from the containment vent was 1.0 Ci/yr. The ^{14}C discharged continuously through the main plant vent from the venting of auxiliary building air was estimated at 1.5 Ci/yr. This leaves a balance of 1.8 Ci/yr for the ^{14}C discharged from the gas decay tanks, a value which agrees within analytical error with the rate of 1.5 Ci/yr estimated from the grab sample data.

Therefore about 58% of the total ^{14}C is discharged by ventilating the containment and auxiliary buildings and about 42% in the gas decay tank releases. The stack flow rates for the containment and auxiliary building vents are 1.18×10^7 and 2.97×10^7 cc/s respectively. These flow rates seem too great to make practical any processing of the gas for ^{14}C removal. However, the discharge from the gas decay tanks could be processed to remove ^{14}C .

The release rate for total ^{14}C , determined by continuous sampling for 88 weeks, was 4.3 Ci/yr. During this test period the reactor operated for about 75% of the time at close to its design power level of 490 MW(e) gross. Therefore the ^{14}C release rate of 4.3 Ci/yr corresponds to a release rate of 11.6

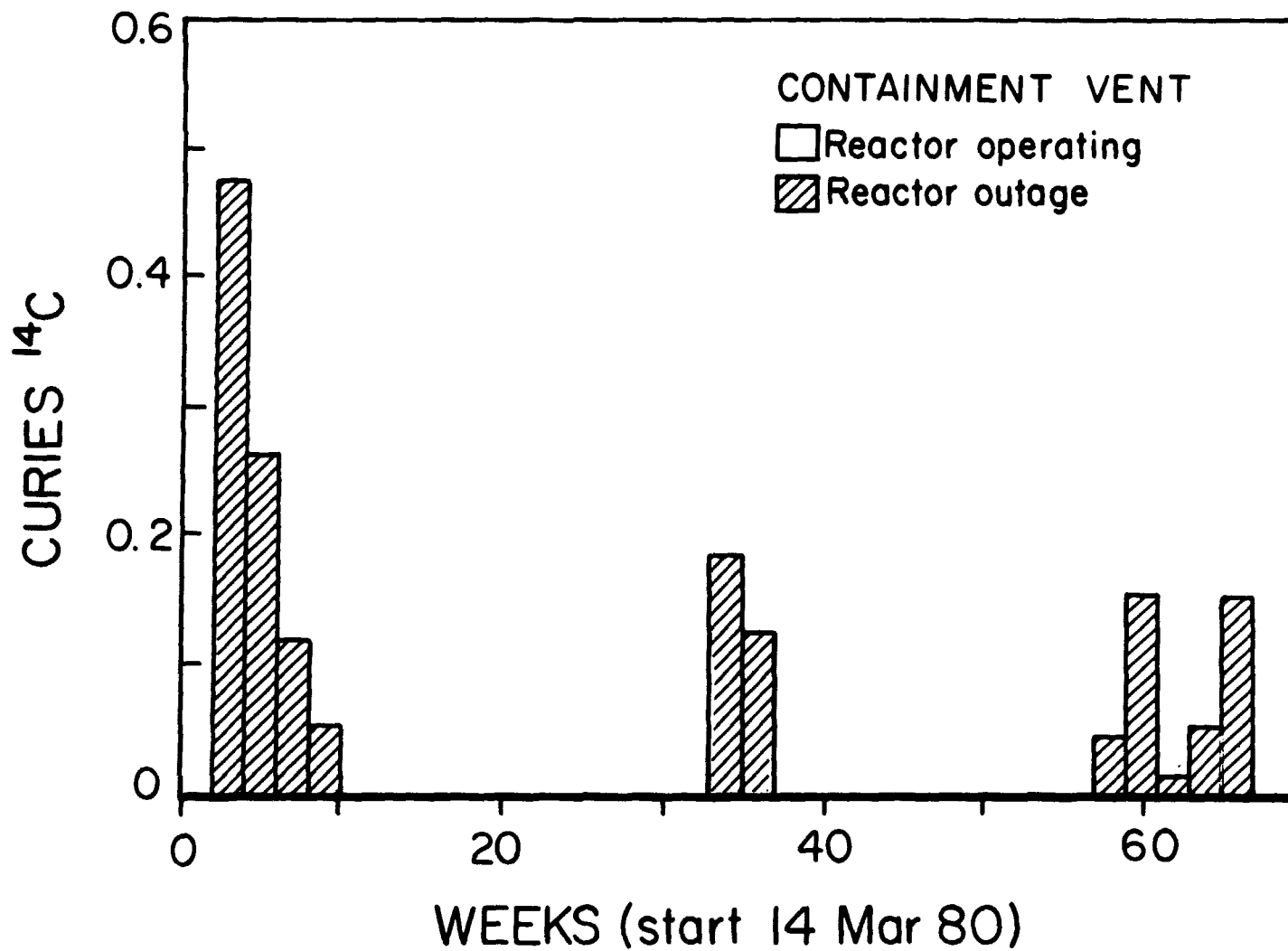


Figure 3 Biweekly measurements of ^{14}C discharge from containment vent of a 490 MW(e) PWR.

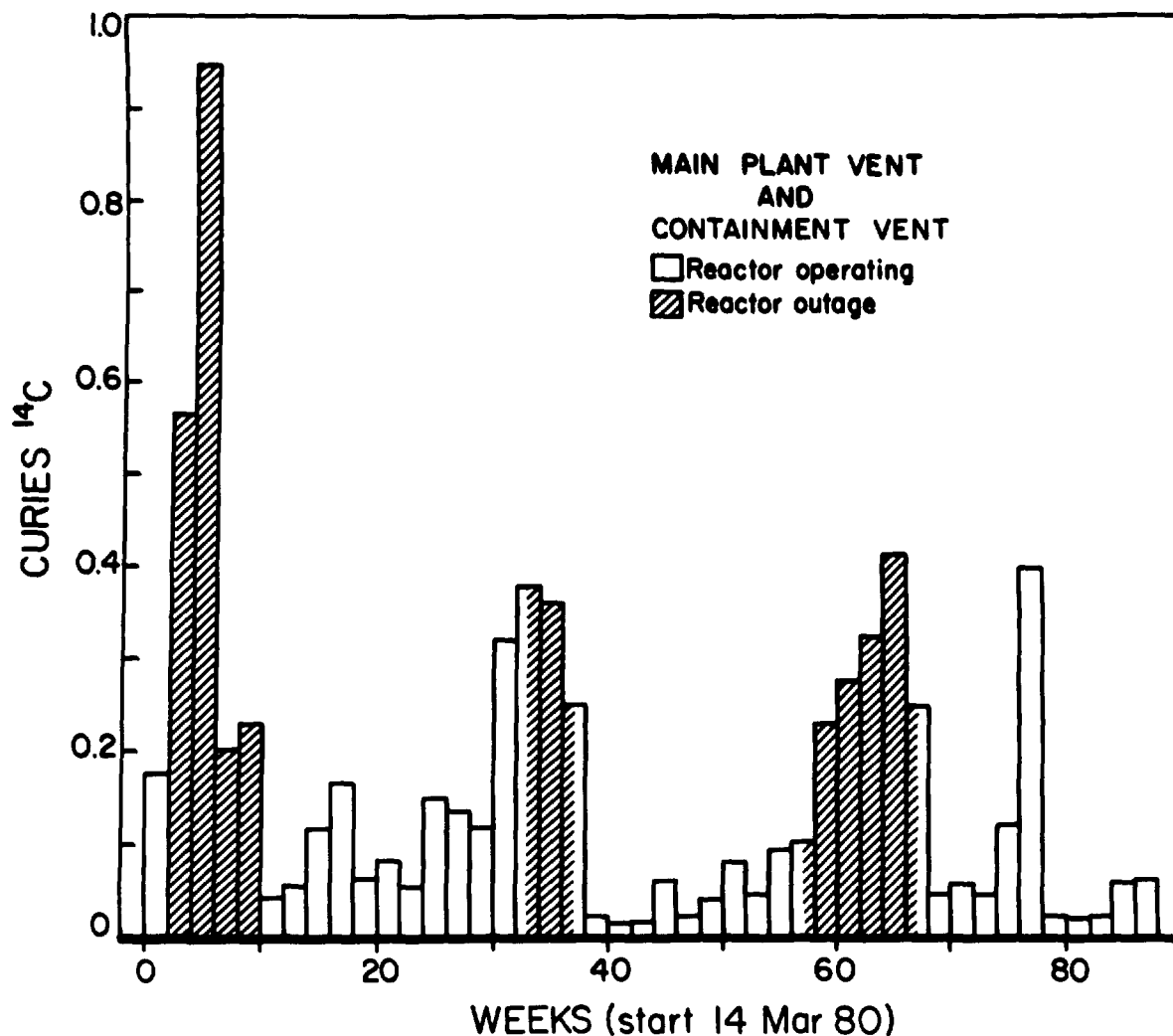


Figure 4 Combined ^{14}C discharge from main plant vent and containment vent of a 490 MW(e) PWR.

Ci/GW(e)-yr.

The average value calculated for production of ^{14}C in the coolant of generic PWRs is 6.7 Ci/GW(e)-yr.⁽⁵⁾ The 490 MW(e) reactor is one of the older reactors and has about one-half the generating capacity of newer PWRs. The unique design of this reactor may result in higher production rates of ^{14}C in the coolant than has been calculated for generic designs.

Liquid Grab Samples. Primary coolant samples were analyzed for inorganic and organic ^{14}C . Samples were taken before and after passage through the primary coolant clean-up demineralizers to determine the decontamination factor for ^{14}C . The total ^{14}C concentration, obtained by adding the inorganic and organic concentrations, indicates that there is no measurable removal of ^{14}C by the ion-exchange resins.

If, however, only 10% of the ^{14}C in the primary coolant were removed in

17th DOE NUCLEAR AIR CLEANING CONFERENCE

passing through the clean-up demineralizers, a quantity not recognizable by differential analysis of the primary coolant, the removal rate would be 1.7 Ci/GW(e)-yr , or about 15% of the gaseous discharge rate. Measurements of the ^{14}C concentrations in the demineralizer resins and filter sludge should be made in addition to the coolant measurements to determine the amount of ^{14}C discharged as low-level solid wastes.

The average concentration of total ^{14}C in the primary coolant was $1.1 \times 10^{-4} \text{ } \mu\text{Ci/ml}$ and varied by less than a factor of 2 from sample to sample. By measuring the leak rate of primary coolant, the discharge of ^{14}C via this pathway could be estimated. Assuming a primary coolant leak rate of 130 cc/min and an average concentration for total ^{14}C of $1 \times 10^{-4} \text{ } \mu\text{Ci/ml}$, the liquid discharge rate was 0.007 Ci/yr .

A wastewater composite sample was also analyzed for inorganic and organic ^{14}C . The composite included contaminated water from sources such as controlled area equipment and floor drains, radiochemistry laboratory drains, and laundry and shower drains, which is collected in a wastewater hold-up tank. Evaporators are used to concentrate the radioactive material as evaporator bottoms or sludge and to recover the distilled water. The evaporator sludge is packaged in drums for disposal in low-level burial sites. Based on the measured ^{14}C concentration of $5.1 \times 10^{-7} \text{ } \mu\text{Ci/ml}$ in the wastewater and assuming that a maximum of 8000 cc of wastewater/min is processed and that all the ^{14}C is collected in the evaporator bottoms, a total of 0.002 Ci/yr would be shipped to burial.

1000 MW(e) PWR

Plant Ventilating System. All building air, containment air, and gas decay tanks at this reactor are vented through the main plant vent at a flow rate of $2\text{-}4 \times 10^7 \text{ cc/s}$. Building air is continuously vented; containment air and gas in decay tanks are released periodically.

Gaseous Grab Samples. Samples of decay tank gas collected in 1976 and 1978 contained 3% to 4% of the total ^{14}C as $^{14}\text{CO}_2$, whereas a sample taken in 1981 contained 25% of the total ^{14}C as $^{14}\text{CO}_2$. The balance of the ^{14}C was in the form of $^{14}\text{CH}_4$ and other hydrocarbon gases. During the recent test period (August 1980-April 1982), gas decay tanks were vented at a rate of 48 tanks/yr. The volume of each tank is 14.9 m^3 , and they are normally filled to a pressure of $6.9 \times 10^5 \text{ Pa}$ (100 psi). The average concentration of total ^{14}C in the gas decay tanks was $5.3 \times 10^{-5} \text{ } \mu\text{Ci/cc}$, which results in a release rate of 0.26 Ci/yr .

The $^{14}\text{CO}_2$ concentration in a sample of containment air collected in 1978 was 7% of the total ^{14}C concentration. In a 1981 sample $^{14}\text{CO}_2$ was 15% of the total, with the balance as $^{14}\text{CH}_4$ and other hydrocarbon gases. The containment air is vented at a rate of $7.1 \times 10^5 \text{ cc/s}$ for about 3 h every 3 days to relieve excess pressure. This corresponds to exchanging the containment air every 23 days, or about 16 times each year. In addition the containment is purged two or three times each year. The average concentration of ^{14}C in the containment air was $3.4 \times 10^{-6} \text{ } \mu\text{Ci/cc}$, which indicates a ^{14}C discharge rate of 3.5 Ci/yr through pressure relief and purging of containment air.

Continuous Gas Sampling. Continuous samplers were used to measure both total ^{14}C and $^{14}\text{CO}_2$ releases from the main plant during an 84-week period beginning in August 1980. Measurements of total ^{14}C (Fig. 5) show that the rate of discharge of ^{14}C tended to increase with time after an outage. The amount

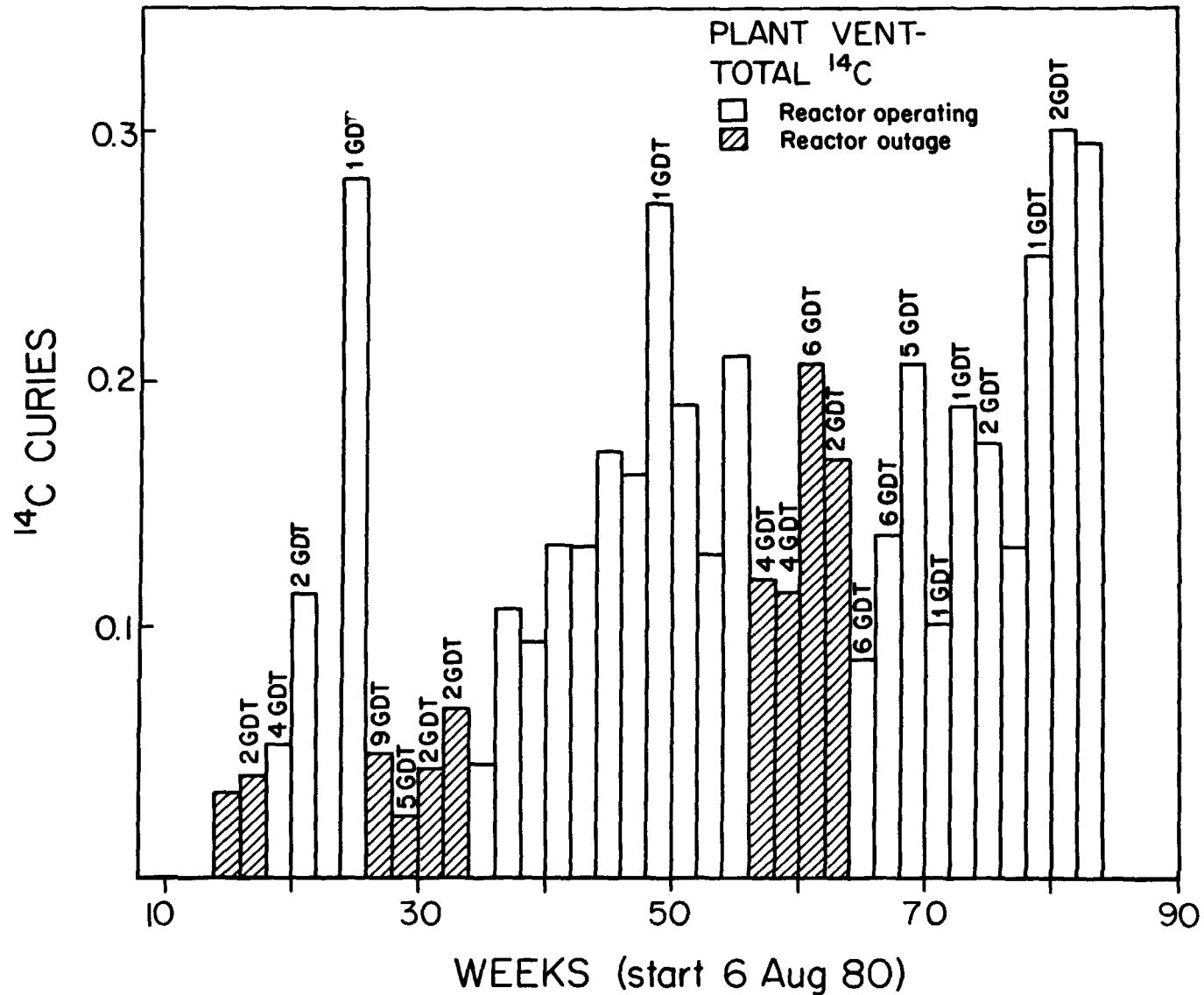


Figure 5 Biweekly measurements of total ^{14}C discharge from plant vent of a 1000 MW(e) PWR. Gas decay tank (GDT) releases are indicated for each 2-week period.

17th DOE NUCLEAR AIR CLEANING CONFERENCE

of ^{14}C released varied considerably from week to week, with no apparent correlation between the quantity discharged and the gas decay tank releases.

During the 68-week period when total ^{14}C was measured, 4.9 Ci was discharged, a rate of 3.7 Ci/yr. Since the reactor was operating at 48% of full power, this rate corresponds to 8.0 Ci/GW(e)-yr.

During 26 weeks when no gas decay tanks were vented, a total of 1.8 Ci of ^{14}C was released, - a rate of 3.7 Ci/yr - the same rate as for the entire 68-week sampling period. Thus indicating that the amount of ^{14}C discharged via gas decay tank releases was only a small fraction of the total. The grab sample data further indicated that 0.26 Ci/yr, or about 7% of the total ^{14}C , was discharged through gas decay tank releases. The grab sample estimates of ^{14}C released through pressure relief venting and purging of containment indicate that containment releases were the major pathway for ^{14}C discharge.

The amount of ^{14}C discharged as $^{14}\text{CO}_2$ is shown in Fig. 6. The $^{14}\text{CO}_2$ discharge was greatest during outages. For the last 54 weeks of the test period both total ^{14}C and $^{14}\text{CO}_2$ were measured. During this period 0.81 Ci of $^{14}\text{CO}_2$ was discharged, and the total ^{14}C discharged was 4.25 Ci. Therefore $^{14}\text{CO}_2$ represented 19% of the total ^{14}C released.

Liquid Grab Samples. Samples of primary coolant were taken before and after passage through the clean-up demineralizers and were analyzed for inorganic and organic ^{14}C . There was essentially no change in ^{14}C concentration, indicating that the decontamination factor for ^{14}C is small. A decontamination factor of only 10% would be unmeasurable by this method but would result in about 1 Ci of ^{14}C /yr being removed by the clean-up demineralizers. The average concentration of ^{14}C in the primary coolant was 7×10^{-5} $\mu\text{Ci/ml}$, about half organic and half inorganic carbon. Assuming a primary coolant leak rate of 2000 cc/min, a liquid discharge rate of 0.07 Ci/yr is estimated for this possible pathway.

850 MW(e) BWR

Plant Ventilating System. The off-gas stripped from the primary steam at the BWR is released through a 117-m stack. The unprocessed off-gas has a flow rate of about 7×10^4 cc/s, which is reduced to about 2×10^4 cc/s when the advanced off-gas system is used. The off-gas is diluted with outside air, resulting in a stack flow rate of 3×10^6 cc/s. The reactor building, turbine building, refuel floor, and radwaste building each have a separate building vent.

Gaseous Grab Samples. Three samples from the off-gas stack were analyzed for ^{14}C . $^{14}\text{CO}_2$ comprised between 97% and 99% of the total ^{14}C , with the balance as $^{14}\text{CH}_4$ and other hydrocarbon gases. Under the oxidizing conditions in the coolant of a BWR, carbon appears to be predominantly oxidized to CO_2 . The average concentration of total ^{14}C in the off-gas stack was 9×10^{-8} $\mu\text{Ci/cc}$. Since the stack flow rate was 3×10^6 cc/s, the estimated ^{14}C discharge rate was 9 Ci/yr based on grab sample measurements.

Continuous Gas Sampling. The stack gas was sampled for total ^{14}C for 98 consecutive weeks, beginning in July 1980 (Fig. 7). During outages the ^{14}C release dropped rapidly to essentially zero. When the plant was operating, the quantity of ^{14}C released tended to be directly related to the reactor power level. During the 98-week test period a total of 11.9 Ci of ^{14}C was discharged from the off-gas stack, a discharge rate of 6.3 Ci/yr. Since the reactor operated at 61% of full

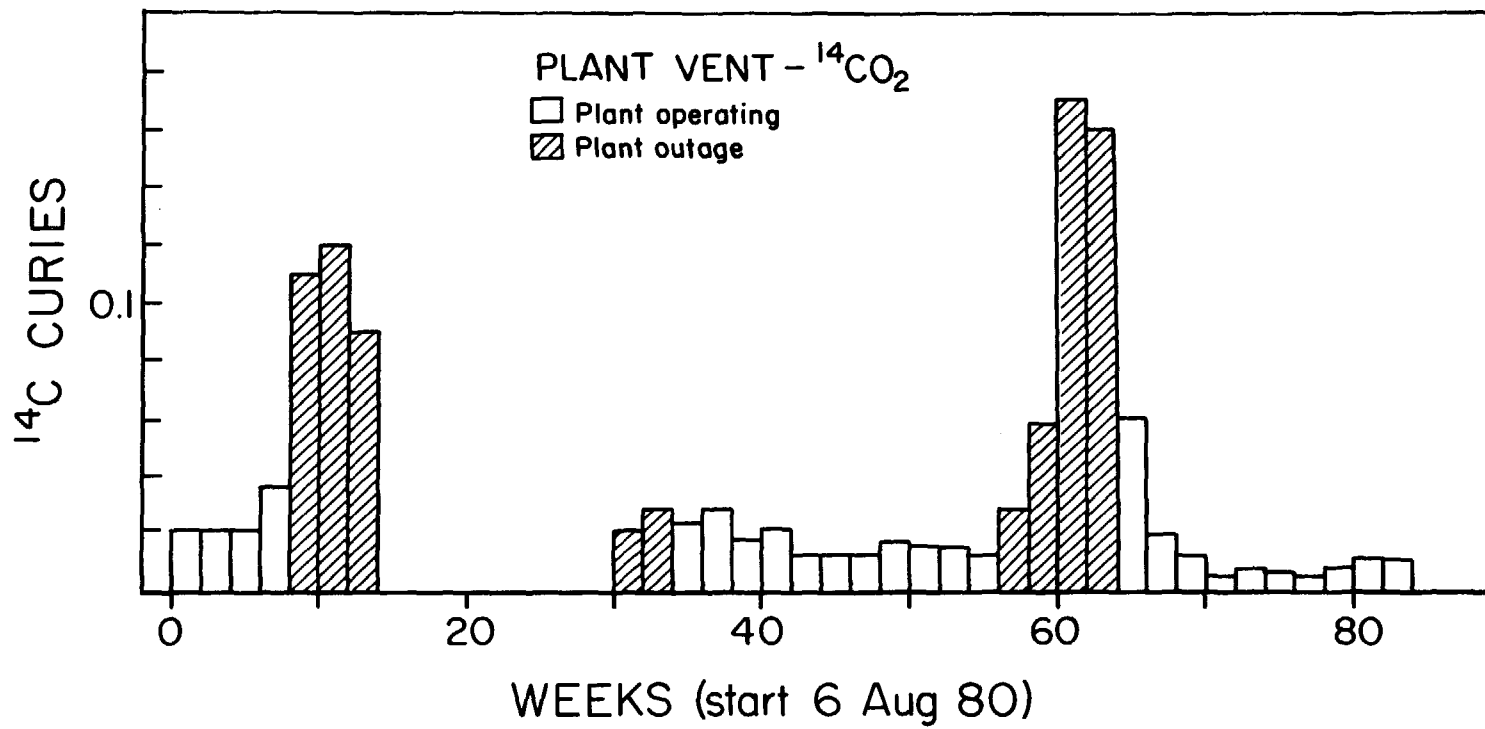


Figure 6 Biweekly measurements of $^{14}\text{C}\text{O}_2$ discharge from plant vent of a 1000 MW(e) PWR.

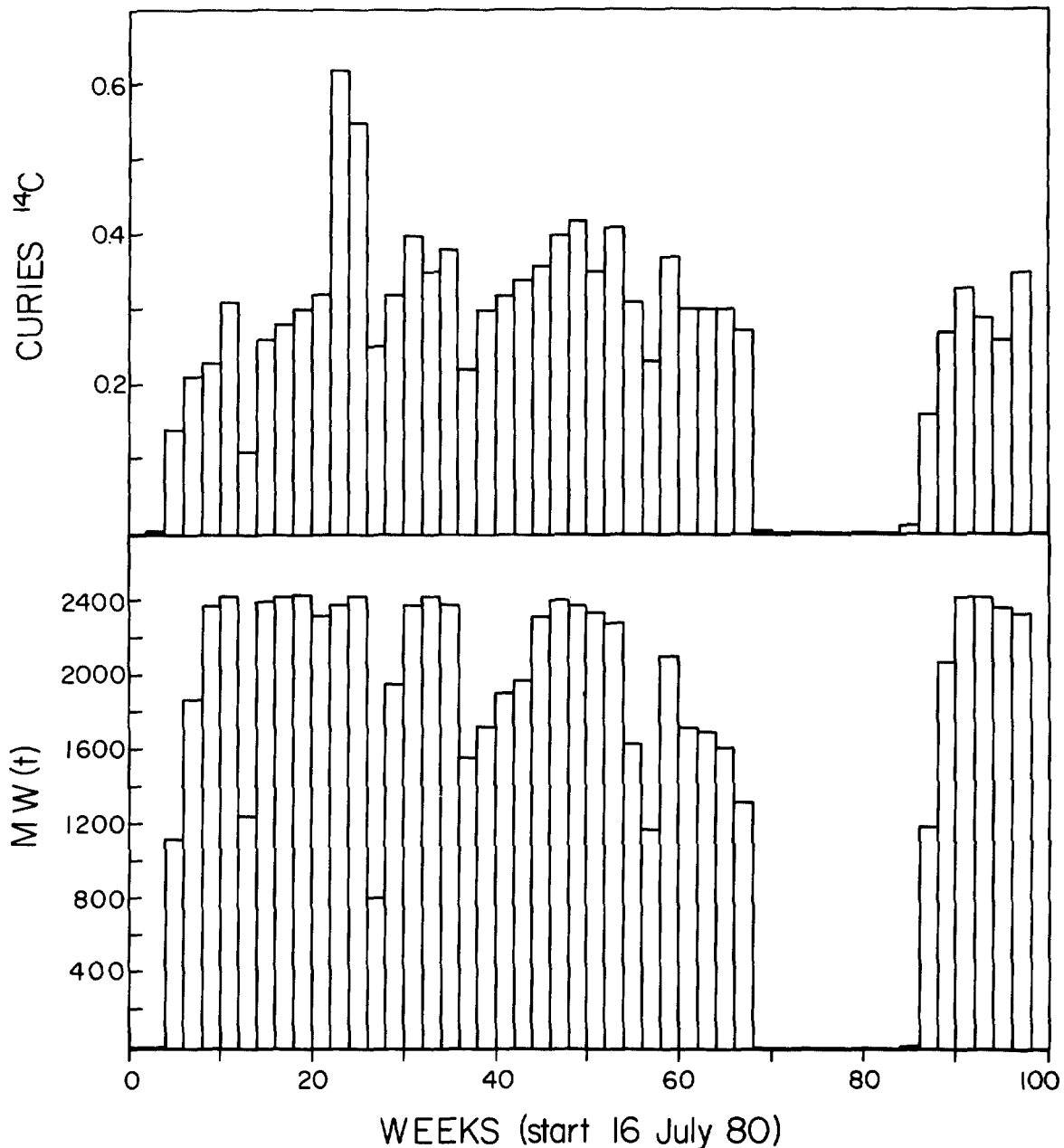


Figure 7 Biweekly measurements of ^{14}C discharge from off-gas stack and average power levels of an 850 MW(e) BWR.

power, the discharge rate is equivalent to 12.3 Ci/GW(e)-yr.

A continuous sampler was used to sample the total ^{14}C discharge from each of the building vents for a period of about 3 months on each vent. The reactor building, turbine building, and radwaste building vents were sampled when the reactor was operating; the refuel floor vent was sampled during an outage. The rates of ^{14}C discharge were 0.018 Ci/yr for the reactor building, 0.035 Ci/yr for the turbine building, 0.048 Ci/yr for the radwaste building, and 0.12 Ci/yr for

17th DOE NUCLEAR AIR CLEANING CONFERENCE

the refuel floor. Thus gaseous ^{14}C appears to be discharged almost entirely via the off-gas stack.

Liquid Grab Samples. One set of coolant samples taken before and after passage through both the clean-up and condensate demineralizers was analyzed for inorganic and organic ^{14}C . A decontamination factor of 7 was found for the clean-up demineralizer, whereas the condensate demineralizer showed no removal of ^{14}C . The concentration of ^{14}C in the coolant before the clean-up demineralizer was 2×10^{-6} $\mu\text{Ci/ml}$, which, when combined with a decontamination factor of 7, results in a ^{14}C removal rate of 0.5 Ci/yr. Additional coolant samples, as well as resins and filter sludge, could be analyzed for ^{14}C to determine more accurately the amount of ^{14}C removed by the demineralizers.

The primary coolant leak rate was about 3×10^4 cc/min. This water is recycled after demineralizer cleanup. Assuming that all the ^{14}C is removed during cleanup, 0.03 Ci/yr would be retained in the recycled water cleanup systems.

Conclusions

Continuous stack samplers with a solid absorbent to trap CO_2 were used to monitor the gaseous ^{14}C released from two PWRs and one BWR. The samplers were run continuously for 84 to 98 weeks at each reactor; sample cartridges were exchanged biweekly.

The ^{14}C discharge rates measured for a 490 MW(e) PWR and a 1000 MW(e) PWR were 11.6 and 8.0 Ci/GW(e)-yr respectively. In other studies the average calculated estimate for the production of ^{14}C in the coolant of a PWR was 6.7 Ci/GW(e)-yr,⁽⁵⁾ and the average measured value for five PWRs in the Federal Republic of Germany was 6 Ci/GW(e)-yr.⁽⁴⁾ The somewhat higher rate of 11.6 Ci/GW(e)-yr determined for the 490 MW(e) PWR may be due to the unique design of this older reactor. Otherwise there is fairly good agreement between the calculated and measured values for PWRs.

The chemical form of the ^{14}C gaseous discharge at the PWRs was over 80% as $^{14}\text{CH}_4$ and other hydrocarbon gases, with the balance as $^{14}\text{CO}_2$. The ^{14}C release was quite variable from week to week, with substantial quantities released during outages. Most of the ^{14}C was released through containment and auxiliary building ventilation, where the large volume flow rates would appear to make ^{14}C removal impractical.

The ^{14}C discharge rate measured for an 850 MW(e) BWR was 12.3 Ci/GW(e)-yr. The average calculated estimate for production of ^{14}C in the coolant of a BWR was 8.2 Ci/GW(e)-yr,⁽⁵⁾ and the average measured value at four BWRs in the Federal Republic of Germany was 14 Ci/GW(e)-yr.⁽⁴⁾ These initial results indicate that the actual production rate for a BWR is over 50% higher than the average calculated estimate. The chemical form was almost entirely $^{14}\text{CO}_2$, and the discharge pathway was almost entirely via the off-gas stack. The off-gas flow rate of $2-7 \times 10^4$ cc/s would appear to be amenable to ^{14}C removal. The release of ^{14}C showed a correlation to reactor power, dropping to essentially zero during outages.

From initial measurements of the ^{14}C decontamination factors for the primary coolant clean-up systems it appears that the discharge of ^{14}C in solid wastes is small compared to the gaseous discharge.

17th DOE NUCLEAR AIR CLEANING CONFERENCE

Acknowledgment

Partial funding of this study was provided by the Rochester Gas and Electric Company and the Power Authority of the State of New York. Staff members at the three nuclear plants were extremely helpful in providing guidance and assistance throughout this study.

References

1. Bonka, H., Brussermann, K., Schwarz, G., "Umweltbelastung durch Radiokohlenstoff aus kerntechnischen Anlagen", Reaktortagung, Berlin (April 1974).
2. Magno, P. J., Nelson, O. B., Ellett, N. H., "A consideration of the Significance of carbon-14 discharges from the nuclear power industry", 13th AEC Air Cleaning Conf., San Francisco (1974).
3. Kunz, C., Mahoney, W. E., and Miller, T. W., "C-14 gaseous effluent from pressurized water reactors", Health Physics Soc. Symposium on Population Exposures, Knoxville, TN, 21-24 October 1974.
4. Schwibach, J., Riedel, H., and Bretschneider, J., "Investigations into the emission of carbon-14 compounds from nuclear facilities", Report No. V-3062/78-EN, Commission of the European Communities, Luxembourg, November 1978.
5. Bonka, H., "Produktion und freisetzung von ^3H and ^{14}C durch kernwaffenversuche, testexplosionen und kerntechnische anlagen", Einschliesslich Wiederaufarbeitungsanlagen, Wissenschaftliches Symposium des Instituts für Strahlenhygiene, Berlin, 14-16 November 1979.
6. Kunz, C., "Separation techniques for reactor-produced noble gases", Proc. Noble Gases Symposium, Las Vegas, NV, pp. 209-217 (1973).
7. Paperiello, C. J., "Internal gas-proportional beta-spectrometry for measurement of radioactive noble gases in reactor effluents", Proc. Noble Gases Symposium, Las Vegas, NV, pp. 239-248 (1973).

DISCUSSION

BONKA: You mentioned that the measured ^{14}C emission rate of boiling water reactors is nearly 50% higher than the calculated rate. The reason should be a higher nitrogen impurity in the water of the primary circuit. In the literature I found one value for the nitrogen impurity in the water. That is a nitrogen measurement in a water sample of the boiling water reactor Muhleberg/Swiss at a laboratory in New York. The nitrogen impurity was nearly 50ppm.

KUNZ: I am not aware of the Swiss measurement or any other measurement of the nitrogen impurity in the coolant of boiling water reactors. It may be possible to estimate the nitrogen in the coolant from the nitrogen content of the off-gas. Assuming that the source of the nitrogen in the off-gas is the coolant and is not due to air in-leakage to the off-gas stream, I believe the coolant concentration could be as high as 20ppm atomic nitrogen.

17th DOE NUCLEAR AIR CLEANING CONFERENCE

SIEGLER: Commenting on the last question, I believe that the speaker's estimate of 20 ppm N_2 in BWR reactor water is high by a factor of 50 to 100 based on measurements made at operating BWRs. Also, N_2 in off-gas is due to air in-leakage.

HAYES: Can you explain the reason why the 490 MW(e) PWR shows 45% (about 5 Ci/GW(e)-yr) of $C-14$ released from the waste gas decay tanks while the larger (1,000 MW(e)) PWR shows only 7% or 0.56 Ci/GW(e)-yr released from the waste gas decay tanks?

KUNZ: Our results indicate that at the 1,000 MW(e) PWR most of the $C-14$ is leaking from reactor components into the containment air during plant operation. At the 490 ME(e) PWR the radioactive gases are better contained in the primary system during plant operation and a higher fraction of the total $14C$ is transferred to the GDTs.

BANGART: As a further comment on the last question, I would like to add that the amount of $C-14$ released from WG-DT will be dependent upon the type of gas stripping of the let-down flow, i.e., full or partial stripping. Similarly, $C-14$ releases to building ventilation may depend upon the amounts of mainenance being conducted.

17th DOE NUCLEAR AIR CLEANING CONFERENCE

CARBON-14 IMMOBILIZATION VIA THE $\text{Ba}(\text{OH})_2 \cdot 8\text{H}_2\text{O}$ PROCESS*

G. L. Haag, J. W. Nehls, Jr., and G. C. Young
Chemical Technology Division
Oak Ridge National Laboratory
Oak Ridge, Tennessee

Abstract

The airborne release of ^{14}C from various nuclear facilities has been identified as a potential biohazard due to the long half-life of ^{14}C (5730 years) and the ease with which it may be assimilated into the biosphere. At Oak Ridge National Laboratory (ORNL), technology is under development, as part of the Airborne Waste Management Program, for the removal and immobilization of this radionuclide. Prior studies have indicated that ^{14}C will likely exist in the oxidized form as CO_2 and will contribute slightly to the bulk CO_2 concentration of the gas stream, which is airlike in nature (~ 330 ppmv CO_2). The technology under development utilizes the CO_2 - $\text{Ba}(\text{OH})_2 \cdot 8\text{H}_2\text{O}$ gas-solid reaction with the mode of gas-solid contacting being a fixed bed. The product, BaCO_3 , possesses excellent thermal and chemical stability, prerequisites for the long-term disposal of nuclear wastes. For optimal process operation, studies have indicated that an operating window of adequate size does exist. When operating within the window, high CO_2 removal efficiency (effluent concentrations < 100 ppbv), high reactant utilization ($> 99\%$), and an acceptable pressure drop across the bed (3 kPa/m at a superficial velocity of 13 cm/s) are possible. This paper will address three areas of experimental investigation: (1) microscale studies on 150-mg samples to provide information concerning surface properties, kinetics, and equilibrium vapor pressures; (2) macroscale studies on large fixed beds (4.2 kg of reactant) to determine the effects of humidity, temperature, and gas flow rate upon bed pressure drop and CO_2 breakthrough; and (3) design, construction, and initial operation of a pilot unit capable of continuously processing a $34\text{-m}^3/\text{h}$ ($20\text{-ft}^3/\text{min}$) air-based gas stream.

I. Introduction

The release of ^{14}C from the nuclear fuel cycle has been identified as a potential biohazard because of its long half-life (5730 years) and the ease with which it may be assimilated into the biosphere.¹⁻²⁰ In nuclear reactors, ^{14}C is produced primarily by neutron interactions with ^{13}C , ^{14}N , and ^{17}O , which are present in the fuel, the cladding, and the coolant. The bulk of the ^{14}C is released in gaseous form either at the reactor or when the spent fuel is reprocessed. Presented in Table I are representative release rates at various nuclear facilities.

*Research sponsored by the Division of Waste Products, Office of Nuclear Waste Management, U.S. Department of Energy under contract W-7405-eng-26 with the Union Carbide Corporation.

17th DOE NUCLEAR AIR CLEANING CONFERENCE

Table I. Approximate production and release rates of several types of facilities

Facility	Rate [Ci/Gw(e)yr]
Nuclear reactors	
LWR	8-10
CANDU	500
Reprocessing plants	
LMFBR	6
LWR	18
HTGR	200

Source: ref. 2.

Carbon-14, like ^3H , ^{85}Kr , and ^{129}I , is a global radionuclide. That is, upon release to the environment, its dosage impact is not limited to the region of release, a release which may be legislated by local government, but rather the net dosage is distributed globally in a nearly uniform manner. Furthermore, because of its long half-life, ^{14}C release poses a health hazard to both present and future generations. Modeling studies have been conducted for predicting the dosage effects from ^{14}C release. However, these studies require major assumptions concerning the effects of low-level radiation, future population growth, and time span of dosage integration. Depending upon the assumptions, total dosage estimates typically vary from 400 to 590 man-rem/Ci. In a modeling study by Killough and Rohwer at ORNL, a total dosage estimate of 540 man-rem/Ci was obtained. This study also predicted dosage estimates for time periods of 30 and 100 years of 18 and 23 man-rem/Ci, respectively.¹⁷ More recent modeling studies by Killough et al. have indicated that for ^{14}C release from a 30.5-m (100-ft) stack at the Morris, Illinois, or Barnwell, South Carolina, reprocessing plants, 0.02 and 0.002% of the total dosage would occur within 100 km of the respective points of release.¹⁸ A study by the Nuclear Energy Agency (NEA) on the release of global radionuclides ^3H , ^{14}C , ^{85}Kr , and ^{129}I restricted the time period of interest to 10,000 years. Hence a partial dosage for ^{14}C of 290 man-rem/Ci was used.¹⁶ With knowledge of the worldwide release of ^{14}C , the resulting dosage per curie released, and assuming 146 fatal effects, 105 nonfatal cancers, and 76 serious genetic effects per million man-rem of dosage as estimated by Fowler and Nelson,²⁰ an estimate of the health effects resulting from ^{14}C release may be made. However, these health effects must be placed in proper perspective; that is, they may occur any place and any time within the time limits of dosage integration. For global radionuclides with long half-lives, the often cited cost-effective values for controlling radionuclide release, \$100 to \$1000 per man-rem, may not be justified, as certain questions of a philosophical and technical nature must first be answered. However, if a technology with suitable cost-effectiveness is shown to exist, the control of ^{14}C

release will then be warranted. Therefore, the primary goal of this research effort is to develop such a cost-effective technology.

II. Technology Development

In the development of technology for controlling the release of ^{14}C from the nuclear fuel cycle, we have established the following criteria for candidate processes:

1. acceptable process efficiency, with a nominal decontamination factor of 10;
2. acceptable final product form for long-term waste disposal;
3. excellent on-line process characteristics;
4. process operation at near-ambient conditions; and
5. acceptable process costs (<\$10/man-rem).

Based upon these criteria, an operationally simple process that utilizes fixed-bed canisters of $\text{Ba}(\text{OH})_2 \cdot 8\text{H}_2\text{O}$ has been developed at ORNL. At ambient temperatures and pressures, this process is capable of removing CO_2 (330 ppmv) in air to concentrations <100 ppbv. Thermodynamic calculations indicate equilibrium concentrations to be at the part-per-trillion level.²¹ The product, BaCO_3 , possesses excellent thermal and chemical stability as it decomposes at 1450°C and is sparingly soluble in water, 0.124 mg-mol/L at 25°C .^{22,23} Furthermore, the soluble reactant undergoes 100% conversion, thus ensuring an extremely stable material for final disposal. Gas throughputs are such that reactor size remains practical for the treatment of anticipated process streams. For a design superficial velocity of 13 cm/s, a reactor with a diameter of 0.70 m (27 in.) would be required for the treatment of a $170\text{-m}^3/\text{h}$ ($100\text{-ft}^3/\text{min}$) off-gas stream. Although extensive cost studies have not been completed, initial comparative studies with alternative technologies have indicated the process to be extremely cost competitive.^{16,20,24-31} The estimated process cost is <\$10/man-rem.

This paper highlights the contents of two major technical reports that are in preparation.^{32,33} For additional information, these reports should be consulted. Studies concerning the development of the $\text{Ba}(\text{OH})_2 \cdot 8\text{H}_2\text{O}$ process for $^{14}\text{CO}_2$ removal will be broken into three areas: (1) microscale studies, (2) fixed-bed macroscale studies, and (3) design and operation of a pilot plant.

Experimental studies have concentrated upon the use of flakes of $\text{Ba}(\text{OH})_2 \cdot 8\text{H}_2\text{O}$. As shown in Fig. 1, the material is a free-flowing solid and when reacted with CO_2 under proper conditions, the flake form remains intact upon conversion to BaCO_3 . Vendor specifications indicate that the material is substoichiometric in water and possesses an overall hydration of 7.0 to 7.9 H_2O . Discussions with the vendor indicated that the water deficiency is intentional so as to ensure a free-flowing, nonsticking product.

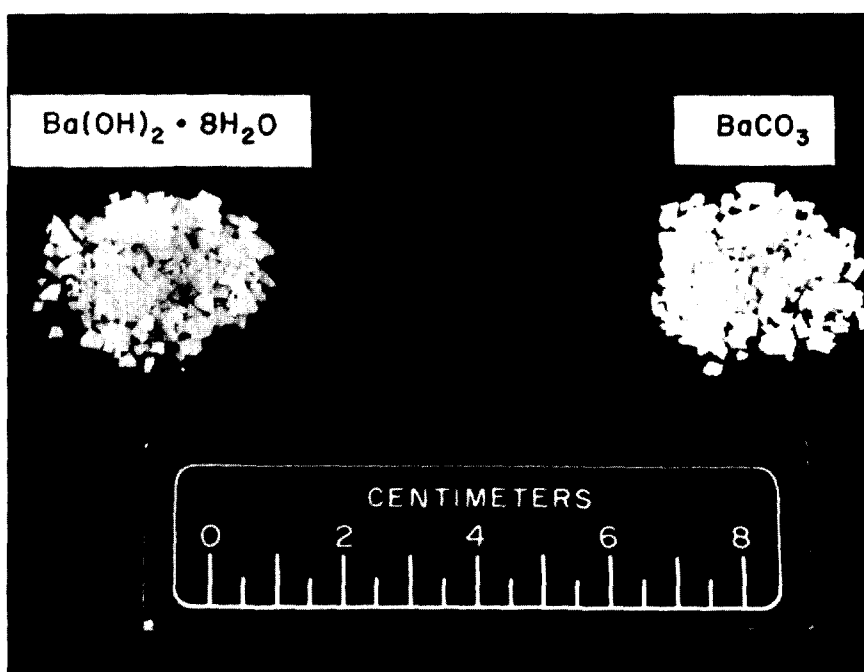


Fig. 1. Commercial $\text{Ba(OH)}_2 \cdot 8\text{H}_2\text{O}$ flaked reactant and BaCO_3 flaked product. The product was obtained at a process relative humidity <60%.

The flakes are prepared by distributing a Ba(OH)_2 hydrate magma ($\sim 78^\circ\text{C}$) on a stainless steel conveyor belt, which is cooled on the underside with cooling water.³⁴ The resulting flakes have variable thicknesses [an average thickness 0.10 cm (1/16 in.)]. The results of a particle-size analysis on material originating from two batches are presented in Table II. Analysis of samples obtained from these batches indicated stoichiometries of approximately 7.5 and 7.0 H_2O

Table II. Particle-size analysis of commercial $\text{Ba(OH)}_2 \cdot 8\text{H}_2\text{O}$ flakes obtained from two different batches

Particle size		Weight percent	
Mesh	mm	Batch 1	Batch 2
4 +	4.75	18.5	5.8
8 + 4	2.36 + 4.75	46.9	33.0
20 + 8	0.850 + 236	31.6	54.5
50 + 20	0.300 + 0.850	2.0	4.9
120 +	0.125 + 0.300	0.4	1.2
+ 120	+ 0.125	0.6	0.6

respectively. For a given batch, little variation was observed in the extent of hydration. X-ray analysis of the two samples failed to confirm the presence of $\text{Ba}(\text{OH})_2 \cdot 3\text{H}_2\text{O}$, the next stable hydrate of lower stoichiometry. However, the existence of a $\text{Ba}(\text{OH})_2 \cdot 3\text{H}_2\text{O}$ - $\text{Ba}(\text{OH})_2 \cdot 8\text{H}_2\text{O}$ eutectic with an overall water stoichiometry of 7.19 has been reported.^{35,36} We speculated that the trihydrate species was not detected because of its extremely small crystallite size. Sorption isotherm studies indicated that the reactant displayed negligible micro-porosity ($d < 2$ nm) or restrictive mesoporosity (2 nm $< d < 150$ nm). Mercury porosimetry studies indicated that the pore size distribution was bimodal with maximas of 0.17 and 1.0 μm and that the flake porosity was 12%. When a flake was exposed to a water vapor pressure less than or greater than the vapor pressure of $\text{Ba}(\text{OH})_2 \cdot 8\text{H}_2\text{O}$, the material either dehydrated to the trihydrate or hydrated to the octahydrate. Rehydration was observed to proceed in one of two regimes and was dependent upon the relative humidity. This factor will be addressed in subsequent sections. The best correlation for predicting the vapor pressure of $\text{Ba}(\text{OH})_2 \cdot 8\text{H}_2\text{O}$ appears to be that presented by Kondakov et al.:³⁷

$$\log P = - \frac{58230}{19.155T} + 13.238 ,$$

where

P = pressure, Pa or nt/m²,

T = temperature, K.

With respect to published vapor pressure data on $\text{Ba}(\text{OH})_2 \cdot 8\text{H}_2\text{O}$, a comprehensive, chronological review of the published vapor pressures is presented in ref. 32.

As shown in Fig. 1, operating conditions exist for which the integrity of the flake form is retained upon conversion to BaCO_3 . Because of the low molar volume of the product as compared to that of the reactant, a ratio of 0.31, and an initial particle voidage of 12%, one would predict a final product porosity of 73%. Mercury porosimetry studies have indicated product porosities of 66 to 72%.^{21,32} Visual evidence of this porosity may be observed by comparing scanning electron micrographs of the reactant and product (Fig. 2).

The following $\text{Ba}(\text{OH})_2$ hydrate nomenclature, will be used in the remainder of this paper: The substoichiometric flakes will be referred to as commercial $\text{Ba}(\text{OH})_2 \cdot 8\text{H}_2\text{O}$ (7.5). Where it is of significance, the term in parenthesis will refer to the initial hydration stoichiometry. The term $\text{Ba}(\text{OH})_2 \cdot 8\text{H}_2\text{O}$ will refer to the stable crystalline species with 8 waters of hydration.

III. Microscale Studies

Realizing that an understanding or at least an awareness of phenomena which occur on the microscale is often required to develop an understanding of macroscale phenomena, basic studies were conducted



Fig. 2. Scanning electron micrographs of a flake of commercial $\text{Ba(OH)}_2 \cdot 8\text{H}_2\text{O}$ (top) and the BaCO_3 product. The product was obtained at a process humidity $<60\%$ (original photo, 8.9×11.4 cm; magnification, $5000\times$).

on the hydrates of $\text{Ba}(\text{OH})_2$ and the BaCO_3 product. Analytical techniques consisted of scanning electron microscopy; mercury intrusion for porosimetry determination; acid-base titrations and overall mass balances to determine the extent of conversion and hydration; x-ray diffraction analysis; single-point BET analysis; and operation of a microbalance system whereby studies of a kinetic, thermodynamic, and surface morphological nature could be performed on 150-mg samples (Fig. 3). Results from these studies were useful in the characterizing the $\text{Ba}(\text{OH})_2 \cdot 8\text{H}_2\text{O}$ reactant, which was reported in the preceding section. The intent of this section is to highlight experimental results from the microscale studies, which are as follows.

1. Methods to prepare $\text{Ba}(\text{OH})_2 \cdot \text{H}_2\text{O}$, $\text{Ba}(\text{OH})_2 \cdot 3\text{H}_2\text{O}$ and $\text{Ba}(\text{OH})_2 \cdot 8\text{H}_2\text{O}$ were developed, and the presence of these species was confirmed.

2. Commercial $\text{Ba}(\text{OH})_2 \cdot 8\text{H}_2\text{O}$ flakes were found to display negligible surface area. Hydration to $\text{Ba}(\text{OH})_2 \cdot 8\text{H}_2\text{O}$ was observed to proceed in one of two regimes. For relative humidities $<60\%$, the increase in surface area was small and the flake form remained intact. For relative humidities $>60\%$, the flake recrystallized in a manner which resulted in greater surface area, but the increase in activity also resulted in a more fragile product.

3. Dehydration of commercial $\text{Ba}(\text{OH})_2 \cdot 8\text{H}_2\text{O}$ to $\text{Ba}(\text{OH})_2 \cdot 3\text{H}_2\text{O}$ and subsequent rehydration to $\text{Ba}(\text{OH})_2 \cdot 8\text{H}_2\text{O}$ at relative humidities $<60\%$ was modeled by a shrinking core model. The relative rate was found to be dependent upon the difference between the water sorbed on the surface for a given P/P_0 value (i.e., relative humidity) and that required on the surface for $\text{Ba}(\text{OH})_2 \cdot 8\text{H}_2\text{O}$ to exist in a stable form.

4. There was evidence of considerable hydrogen bonding within the $\text{Ba}(\text{OH})_2 \cdot 8\text{H}_2\text{O}$ crystal. These results paralleled the crystallography studies of Monohar and Ramaseshan in which they cited difficulty in differentiating the location of the hydroxyl ions from the waters of hydration.³⁸

5. The vapor pressure correlation for $\text{Ba}(\text{OH})_2 \cdot 8\text{H}_2\text{O}$ cited in the previous section was indirectly verified at two temperatures.

6. At low CO_2 vapor pressures, $\text{Ba}(\text{OH})_2 \cdot 8\text{H}_2\text{O}$ was observed to be 3 orders of magnitude more reactive toward CO_2 than either $\text{Ba}(\text{OH})_2 \cdot 3\text{H}_2\text{O}$ or $\text{Ba}(\text{OH})_2 \cdot \text{H}_2\text{O}$.

7. For relative humidities $<60\%$, the increase in surface area with product conversion was found to be a very strong function of the specific rate of reaction and was not a linear function of conversion.

8. The surface area of BaCO_3 product was determined to be a function of relative humidity. In a manner analogous to the dehydration of commercial $\text{Ba}(\text{OH})_2 \cdot 8\text{H}_2\text{O}$ and the rehydration of $\text{Ba}(\text{OH})_2 \cdot 3\text{H}_2\text{O}$, surface water appeared to aid in the transport of the reactant and product species, thus resulting in lower surface areas at higher values of P/P_0 . However, the authors feel that the increase in

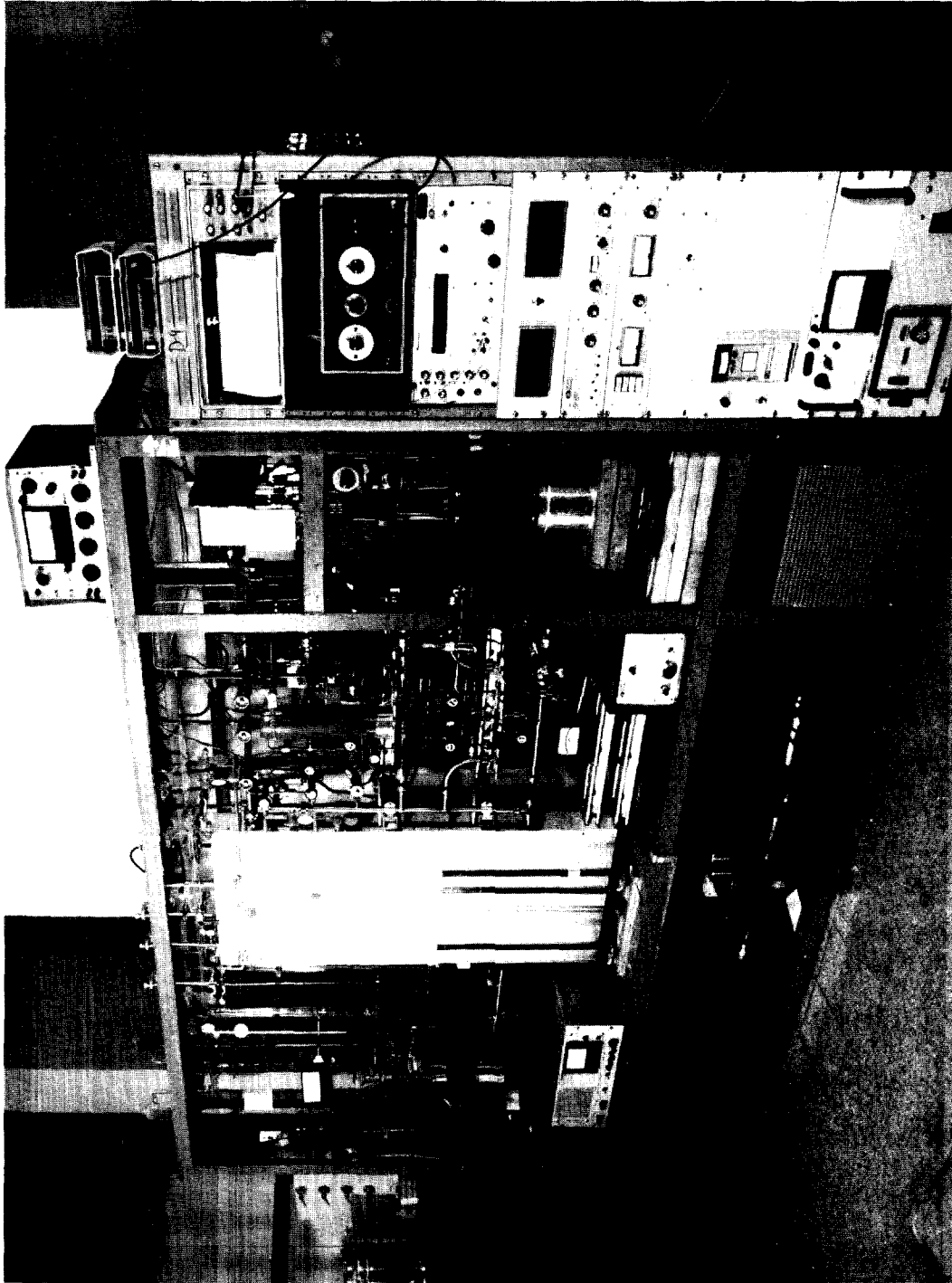


Fig. 3. The microbalance system.

surface water could not account for the drastic difference in CO_2 reactivity observed for the various hydrate species. The difference in reactivity appears to result from the additional water in the crystal structure and the greater mobility of the hydroxyl ions.

9. Based upon the analysis of nitrogen sorption isotherm data, there were no indications of hysteresis. Therefore if capillary condensation should occur, one would speculate it to result from the wall effects of noncircular pores (e.g., V-shaped points of intersurface contact).

Detailed information appears in ref. 32, which is as yet unpublished.

IV. Fixed-bed macroscale studies

Over 18,000 hours of experimental operating time have been completed on fixed beds of $\text{Ba}(\text{OH})_2 \cdot 8\text{H}_2\text{O}$. These beds typically contained from 2.9 to 4.3 kg of reactant. A schematic of the experimental system, which has been described in detail in a previous paper,²¹ is presented in Fig. 4. The intent of this aspect of the study was to determine the effects of air flow rate (superficial gas velocities of 7-21 cm/s), operating temperature (22-42°C), and water vapor pressure or relative humidity (0-80%) on the operational characteristics of the fixed bed, most notably the shape of the breakthrough curve and the pressure drop across the fixed bed. Since the reaction is endothermic, the reactor was jacketed and the temperatures of the influent and effluent streams were held constant. Presented in Fig. 5 is a typical breakthrough curve and pressure drop plot. For this particular run, the pressure drop increase was noticeable and was not solely a function of bed conversion.

In the course of these fixed-bed studies, it was observed that for a given mass throughput, certain process conditions resulted in a greater pressure drop than others. In several instances, the increase in pressure drop during a run behaved in an autocatalytic manner and necessitated discontinuation of the run. The increase in pressure drop appeared to result from two phenomena: a slow gradual increase that was a function of bed conversion and a rapid increase that was a function of relative humidity. The magnitude of the latter often overshadowed the former. The observed pressure drop, plotted as a function of relative humidity at two temperatures (295 and 305 K) and a superficial velocity of ~13 cm/s, is presented in Fig. 6. It is significant that the data are consistent at the two temperatures as the saturation vapor pressures differed by a factor of 1.8. Furthermore, the dependency upon relative humidity indicates the presence of a surface adsorption phenomenon. For physical adsorption on surfaces, the extent of adsorption is dependent upon the extent of saturation, P/P_0 , or in the case of water, the relative humidity. The fact that the pressure drop became more severe at ~60% relative humidity indicates that capillary condensation is likely present. Since no hysteresis was observed during nitrogen adsorption studies, we speculate that the condensation occurs at V-shaped contact points or pores. The presence of the condensed water then provides sites of rapid recrystallization. Because the flaked reactant

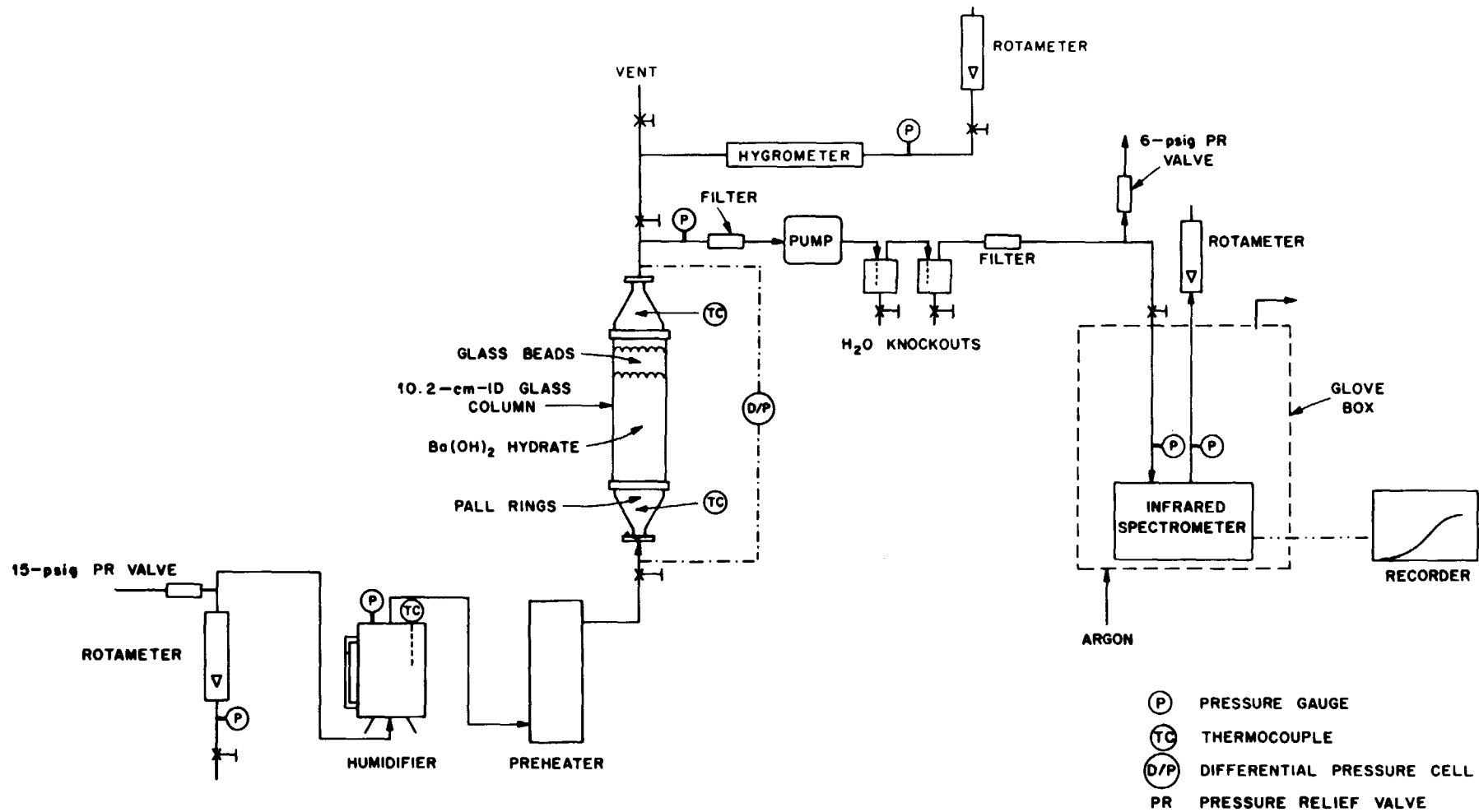


Fig. 4. The fixed-bed experimental equipment.

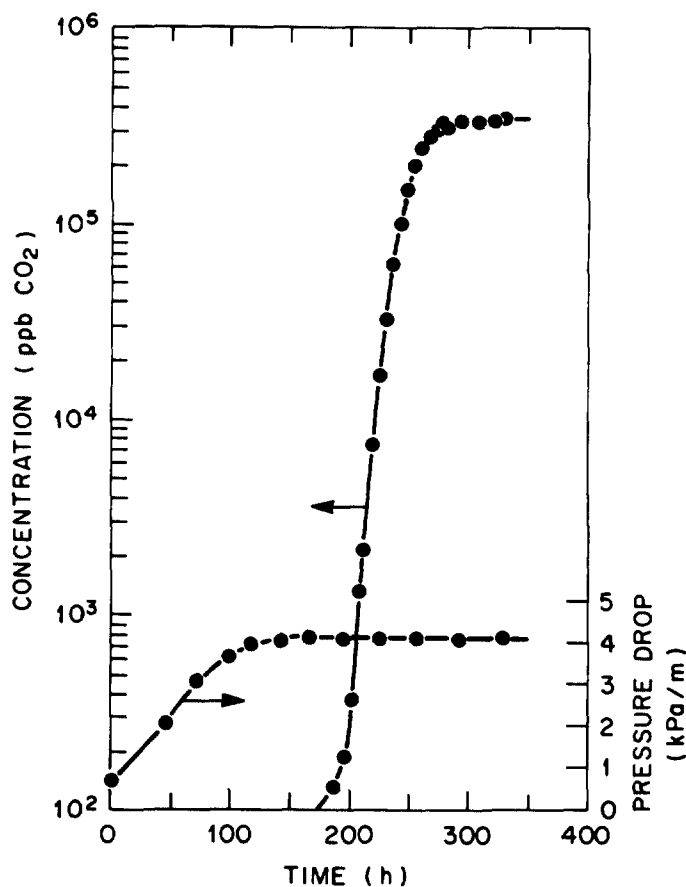


Fig. 5. Logarithm of the experimental breakthrough profile and the change in pressure drop across the bed presented as function of time (superficial gas velocity, ~ 13 cm/s).

was prepared by the rapid cooling of a magma that was substoichiometric in octahydrate (7.0 to 7.9 waters of hydration), the rate of recrystallization is likely enhanced by a need to reduce internal energy locked within the flake. This energy may be present as defects within the crystallites or surface energy resulting from the small size of the crystallites and the presence of the $\text{Ba}(\text{OH})_2 \cdot 3\text{H}_2\text{O}$ – $\text{Ba}(\text{OH})_2 \cdot 8\text{H}_2\text{O}$ eutectic. Photographs of commercial $\text{Ba}(\text{OH})_2 \cdot 8\text{H}_2\text{O}$ flakes after recrystallization at a relative humidity $>60\%$ are presented in Fig. 7. For rehydration at lower humidities, external changes of the flake were small.

The functional dependency of pressure drop upon relative humidity is helpful in understanding the autocatalytic pressure drop behavior observed at high relative humidities. For a fixed influent water vapor concentration, any increase in system pressure at constant temperature will result in an increase in the water vapor pressure and likewise the relative humidity, P/P_0 . Therefore as the pressure drop across the bed increases, so does the relative humidity within the bed and each continues to increase until the run must be terminated. At lower relative humidities, the rate of increase in pressure drop as a function of relative humidity is not sufficient to autocatalyze the process.

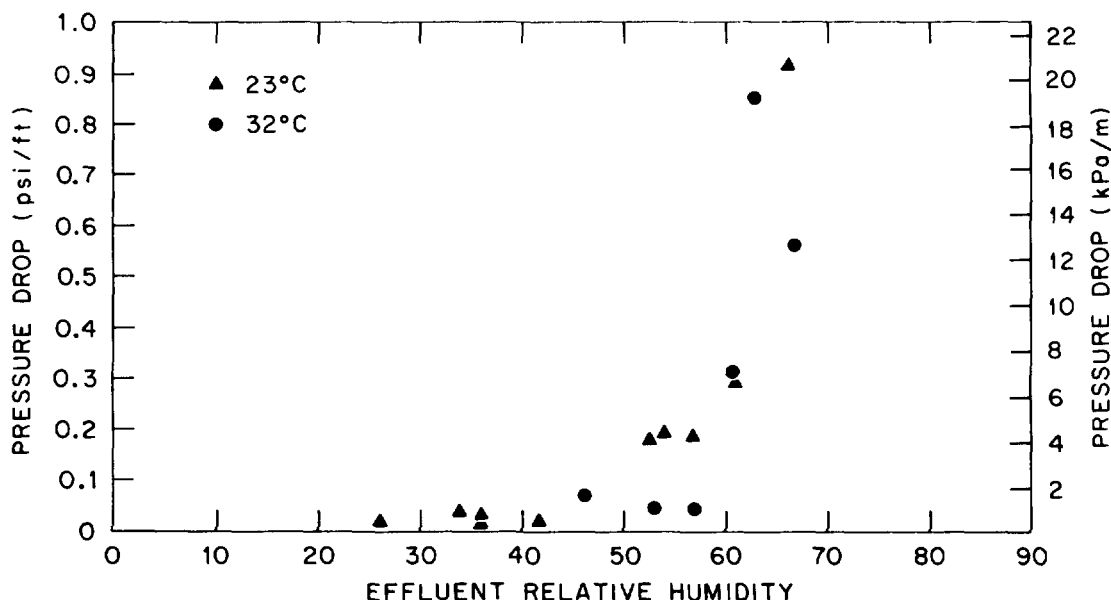


Fig. 6. Pressure drop as a function of relative humidity during fixed-bed studies on commercial $\text{Ba}(\text{OH})_2 \cdot 8\text{H}_2\text{O}$ flakes (superficial gas velocity, ~ 13 cm/s).

The pressure drop dependency upon relative humidity also restricts the upper flow rate that the process may treat. Increased gas flows result in greater pressure drops across the bed (i.e., a greater pressure at the entrance to the bed). Therefore, the relative humidity at the entrance of the bed must be $< 60\%$, but the influent water vapor pressure must be greater than the dissociation vapor pressure of $\text{Ba}(\text{OH})_2 \cdot 8\text{H}_2\text{O}$.

Extensive modeling studies were performed on the breakthrough curves from the fixed-bed studies. Because of the nature of the governing partial differential equations and their respective boundary conditions, solutions were of a numerical nature. An in-depth review of the method of analysis and of the associated assumptions is presented elsewhere.³² The analysis indicated that the rate expression could be modeled by an equation of the form:

$$R = K_F A_0 (1 - X) C,$$

where

K_F = gas film mass transfer coefficient,

A_0 = initial surface area available for mass transfer,

X = fractional conversion of reactant,

C = bulk CO_2 concentration.

Data analysis indicated $K_F A_0$ to be a weak function of temperature and a strong function of velocity, indicative of gas-film

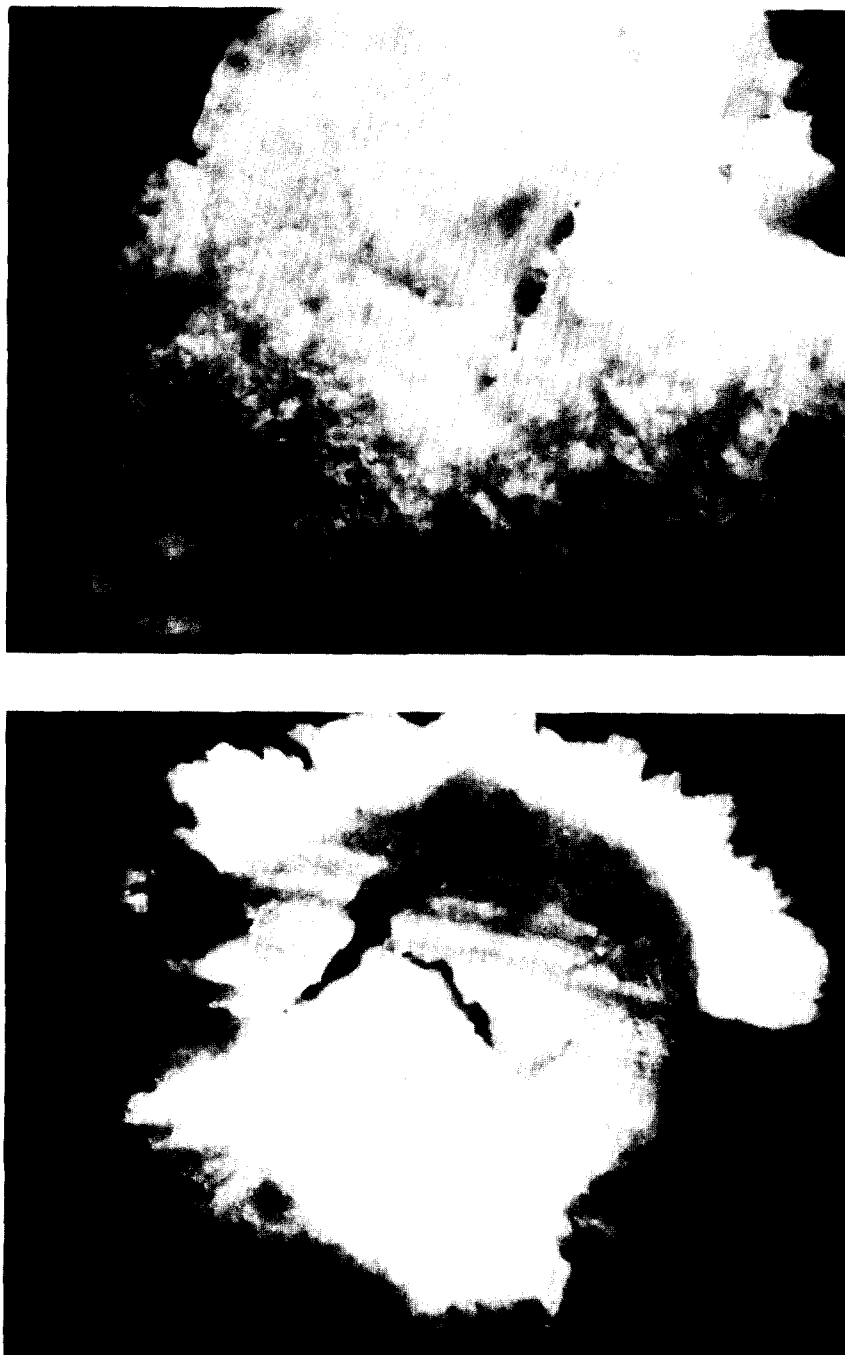


Fig. 7. Top and bottom views of a commercial $\text{Ba}(\text{OH})_2 \cdot 8\text{H}_2\text{O}$ flake subjected to relative humidity $>60\%$.

control. Considerable dispersion in the value of the $K_F A_0$ coefficients was observed for a given mass throughput. There were indications that the dispersion resulted from differences in the actual area available for mass transfer and the possible presence of localized channeling. Based upon published correlations for the K_F coefficient, the correlation for the $K_F A_0$ coefficient possessed a greater functional dependency upon velocity than expected. Because the studies were conducted on flaked material with considerable interparticle contact, we speculate that the amount of surface area available for mass transfer increased as a function of gas velocity, thus resulting in the greater than anticipated functional dependency of $K_F A_0$ upon velocity. This factor may also account for the greater than anticipated dispersion in $K_F A_0$ as some localized packing arrangements would be more conducive to restructuring. Representative breakthrough curves and the model-predicted curves are presented in Fig. 8.

V. Pilot Unit Development

In the development of this fixed-bed technology, a pilot unit capable of processing $34 \text{ m}^3/\text{h}$ ($20 \text{ ft}^3/\text{min}$) was designed, constructed, and is currently in operation. Specific goals of this aspect of process development are to provide

1. the basis for the design of a ^{14}C immobilization module for future testing under hot conditions;
2. data at operating conditions not achievable with present bench-scale equipment, in particular operation at near-adiabatic conditions;
3. necessary scale-up data; and
4. operating data on key hardware items and instrumentation.

Presented in Fig. 9 is a flow schematic of the ^{14}C immobilization pilot unit; a photograph of the system is presented in Fig. 10. The designed gas throughput at a superficial velocity of 13 cm/s in the reactor is $34 \text{ m}^3/\text{h}$ ($20 \text{ ft}^3/\text{min}$). The system consists of two reactors which contain canisters loaded with 32 kg (70 lb) of commercial $\text{Ba}(\text{OH})_2 \cdot 8\text{H}_2\text{O}$ reactant. Due to the size of the canisters and the relatively long loading times prior to breakthrough, continuous operation with only two reactors is possible. The steam, air, and CO_2 flow stations are unique to our pilot unit and will not be discussed in detail.

The overall pilot unit is controlled by a 5TI logic controller manufactured by Texas Instruments. The unit is currently capable of monitoring 8 DC and 16 AC input signals and providing 24 DC and 16 AC output signals. The logic controller monitors alarm signals from the CO_2 analyzer, hygrometer, flowmeters, timers, and pressure and temperature sensors. Upon sensing an alarm condition such as a CO_2 concentration of 1 ppmv in the effluent gas stream, valves are actuated

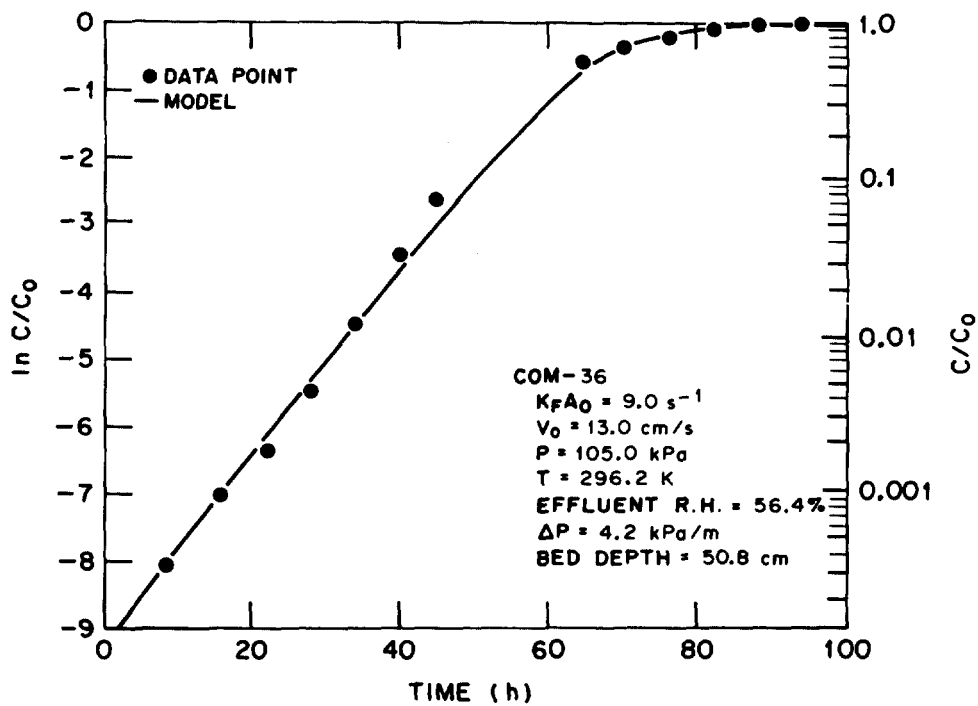
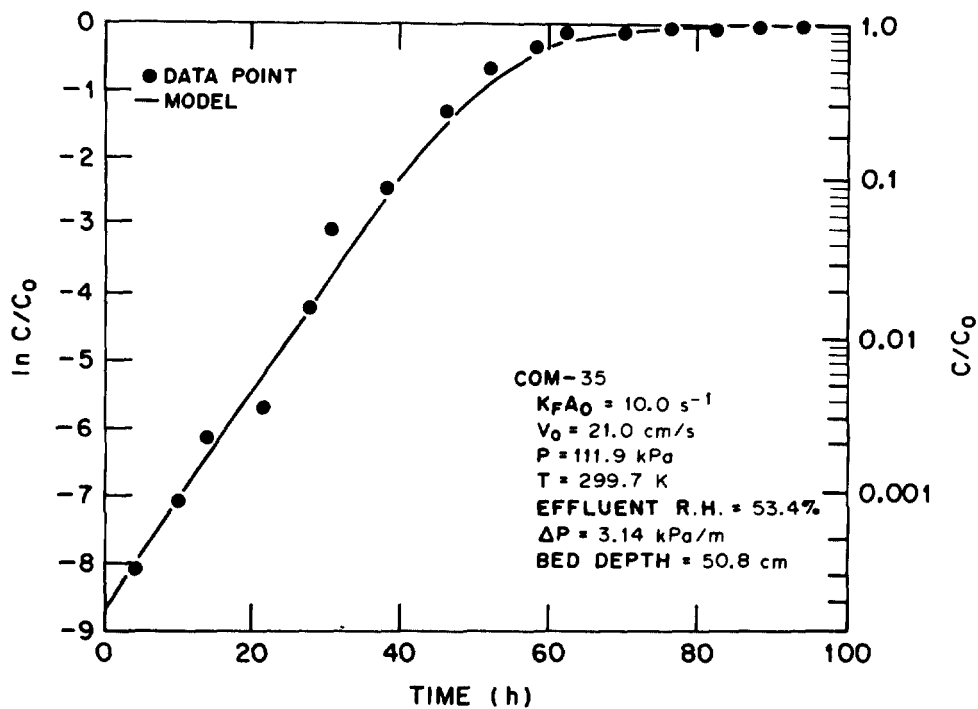


Fig. 8. Breakthrough curves and model-predicted breakthrough curves for typical fixed-bed runs.

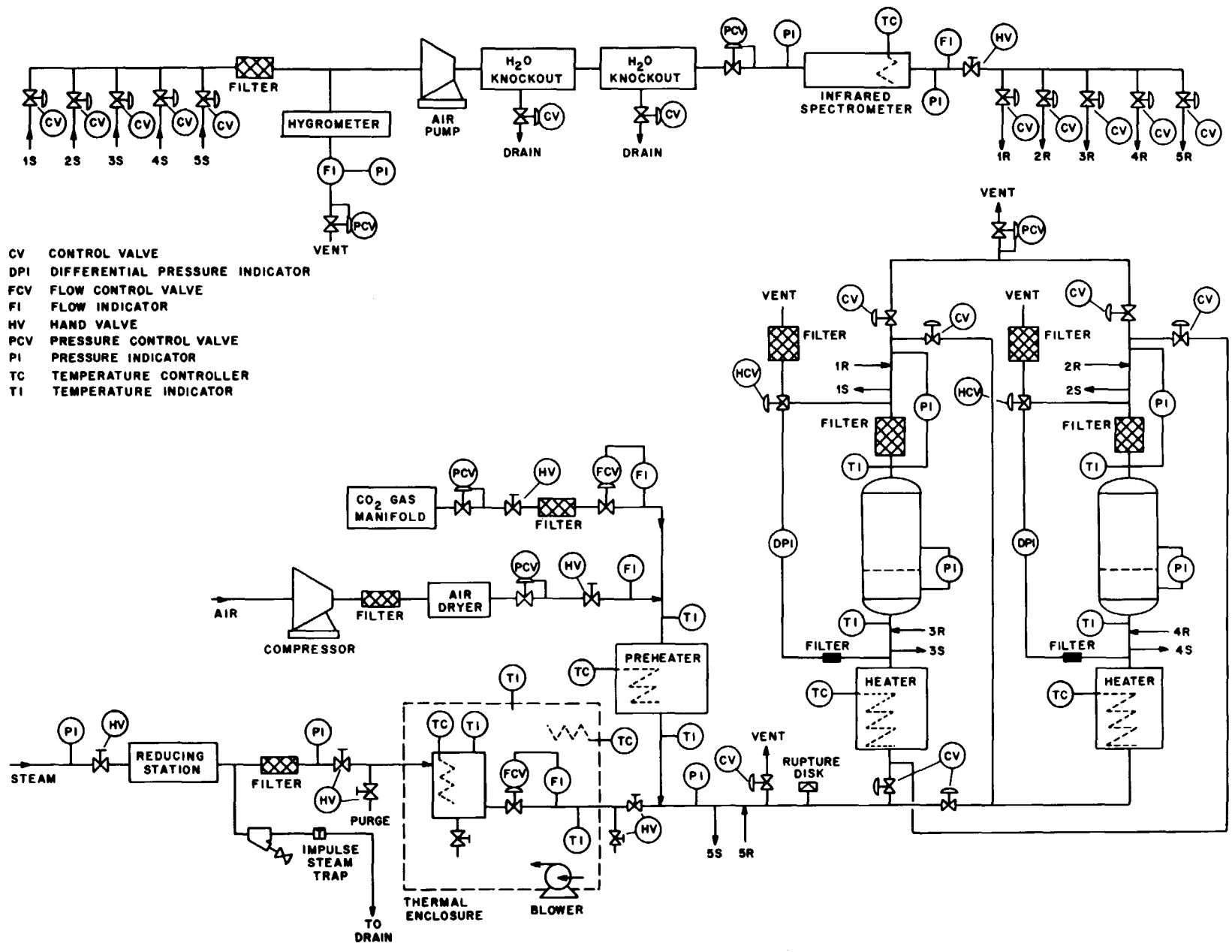


Fig. 9. The ¹⁴C immobilization pilot unit.

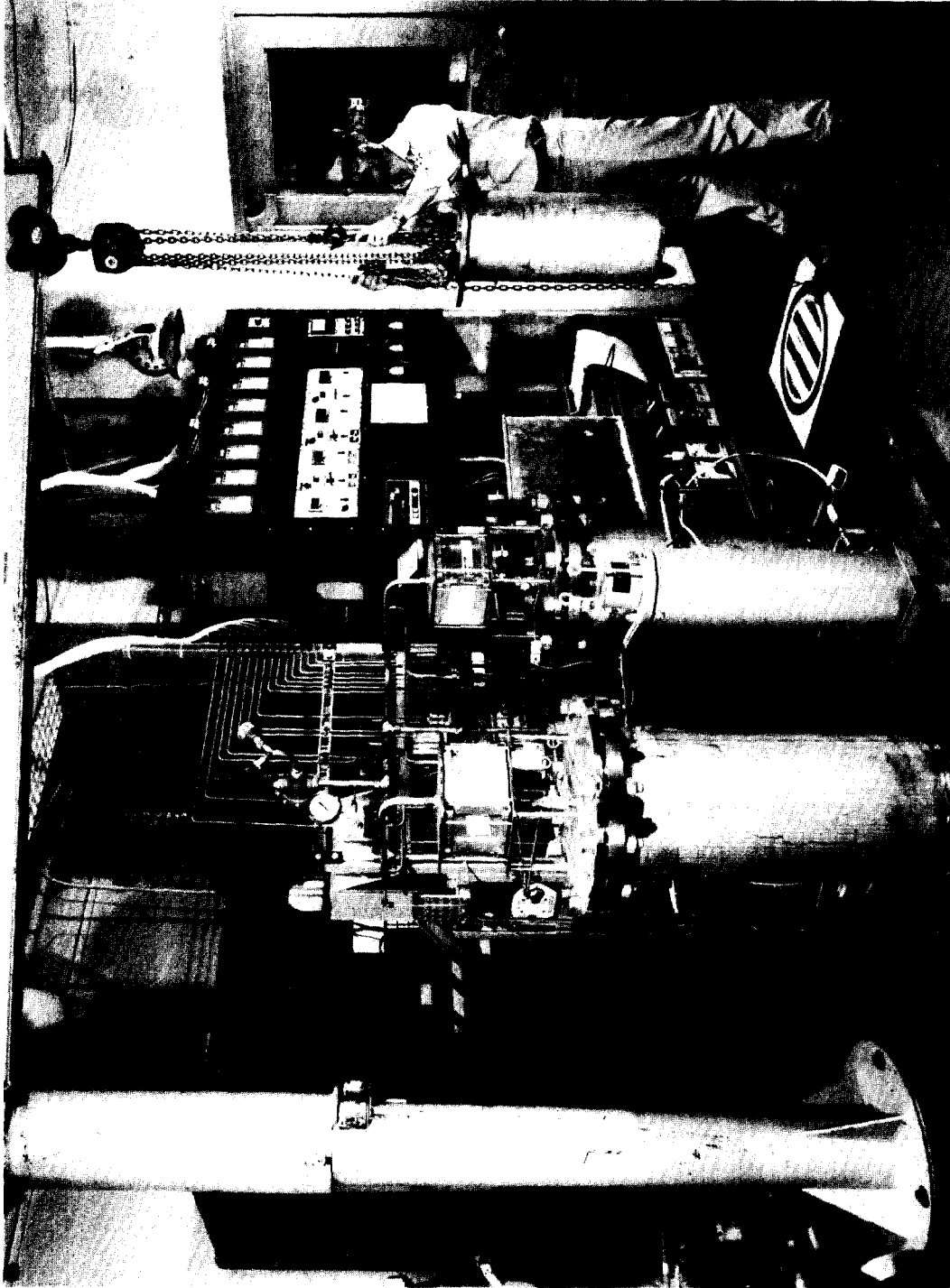


Fig. 10. The ^{14}C immobilization pilot unit.

in the proper sequence at prescribed time intervals thus diverting flow to the second column. Numerous 3/4- and 1/4-in. Whitey ball valves are located within the system for bulk flow control and for gas sampling. For valve actuation, electronic DC signals from the logic controller are converted to pneumatic signals using modular Humphrey TAC³ electric air valves. The Whitey ball valves are then actuated pneumatically via Whitey actuators. Gas samples may be routinely taken and returned from any one of five points within the system. Sampling from these locations may be controlled by the logic controller. The sample gas is filtered and a portion of it fed to a General Eastern model 1200 APS hygrometer sensor. The unit utilizes the "vapor condensation on a mirror" principle, thus providing a true dewpoint determination. Because of the small sensor volume and the resulting small gas throughput (0.5 L/min), this portion of the gas sample is vented to the atmosphere. The remainder of the sample gas is pressurized via a metal bellows pump, fed to two knockout vessels for H₂O removal, and then moves to a Wilks-Foxboro Miran 1A infrared spectrometer. This unit, described elsewhere,^{21,32} is capable of analyzing CO₂ over the continuous 100 ppbv to 330 ppmv CO₂ range. Because of the 5.6-L sensor volume and to ensure an adequate instrument response time, the gas throughput is appreciable and the sample stream is recycled to the pilot unit.

Gas preheaters connected to Barber-Coleman series 520 temperature controllers are located before each reactor to provide the desired influent temperature. The pressure drop across each column and the gauge pressure at the base of the column are monitored via Foxboro model E13DH differential pressure cells. Dwyer Photohelix pressure gauges/switches monitor the pressure drop across the gas distributors and HEPA filters. Thermocouples are located throughout the system for temperature control and sensing. Original plans were to enclose the pilot unit in a thermal-regulated structure so that studies could be conducted at 30 and 40°C under highly controlled conditions. These studies are currently in jeopardy because of funding uncertainties.

Whereas prior studies on the 10.2-cm-I.D. fixed beds were conducted at near-isothermal conditions, the pilot unit studies are being done under near-adiabatic conditions. For the treatment of an air-based (330-ppmv-CO₂) gas stream, one would predict a temperature drop of ~4°C in the gas stream due to the endothermic nature of the reaction (364 kJ/mol). Such a temperature drop has been verified experimentally. Because of the sensitivity of the operational characteristics of the bed (i.e. pressure drop) upon relative humidity and the dependency of relative humidity upon system temperature, the results from these studies are extremely valuable in determining conditions for optimal process operation. Experiments will also be conducted to determine if preconditioning the bed prior to contact with CO₂ is beneficial in reducing pressure drop problems. During the preconditioning step, the substoichiometric commercial Ba(OH)₂·8H₂O will be hydrated to Ba(OH)₂·8H₂O at conditions which ensure the retention of flake integrity (relative humidity <60%). We speculate that pressure drop problems during subsequent CO₂ removal at relative humidities >60% will be reduced.

VI. Conclusions

Extensive studies have been conducted on $\text{Ba}(\text{OH})_2$ hydrates, their reaction with CO_2 , and the operation of a fixed-bed process for CO_2 removal. Microscale studies indicated that (1) the published vapor pressure data for $\text{Ba}(\text{OH})_2 \cdot 8\text{H}_2\text{O}$ is valid, (2) the rate of dehydration or rehydration is proportional to the amount of free water on the surface (i.e. a function of relative humidity), and (3) the reactivity of $\text{Ba}(\text{OH})_2 \cdot 8\text{H}_2\text{O}$ for CO_2 is 3 orders of magnitude greater than that of either $\text{Ba}(\text{OH})_2 \cdot 3\text{H}_2\text{O}$ or $\text{Ba}(\text{OH})_2 \cdot \text{H}_2\text{O}$. Macroscale studies under near-isothermal conditions on 10.2-cm-ID fixed beds of commercial $\text{Ba}(\text{OH})_2 \cdot 8\text{H}_2\text{O}$ flakes indicated that the pressure drop across the bed increased dramatically as 60% relative humidity in the effluent gas was approached. It is speculated that this phenomenon results from the capillary condensation of water at V-shaped contact points or pores and that this facilitates the subsequent rehydration and recrystallization of the flake. Although the resulting flakes have greater external surface area, they are more fragile and degrade more readily upon conversion to BaCO_3 , thus resulting in increased pressure drop across the fixed beds.

Experimental studies indicated that the transfer of the reactant gas through the gas film is the major resistance to mass transfer. A model, assuming gas film control, was developed, and exact numerical solutions were obtained. An excellent correlation between the model-predicted breakthrough curves and the experimental breakthrough curve was obtained when the area available for mass transfer was modeled as a linear function of conversion [i.e. $A = A_0(1 - X)$]. The magnitude of the mass transfer coefficient was characteristic of literature values. There were indications that the magnitude of the initial surface area available for reaction, A_0 , may be a weak function of velocity due to a realignment of the flakes. This realignment results from fluid shear forces and an accompanying reduction in the number of planar contact points between neighboring flakes, thus increasing the area available for mass transfer.

Based upon the experimental data obtained during this study and its subsequent analyses, a window or regime of optimal process operation under near-isothermal conditions was determined to exist for the fixed-bed process. The window is bounded on the lower side by the dissociation vapor pressure of $\text{Ba}(\text{OH})_2 \cdot 8\text{H}_2\text{O}$ and on the upper side by the onset of appreciable capillary condensation and subsequent pressure drop problems (~60% relative humidity). An operating envelope is presented in Fig. 11 for the treatment of a 330-ppmv- CO_2 gas stream at a system pressure of 104.8 kPa (0.5 psig). The relative humidity of the influent gas must fall within the envelope for optimal gas throughput. If changes are made either in the CO_2 concentration, thus affecting the amount of water vapor produced, or in the system pressure, which will affect the partial pressure of the water vapor and subsequently the relative humidity (P/P_0), the operating envelope will change. The operating envelope also demonstrates why operational problems at 22 and 32°C were not severe and why considerable difficulty was encountered when trying to operate the process at 42°C.

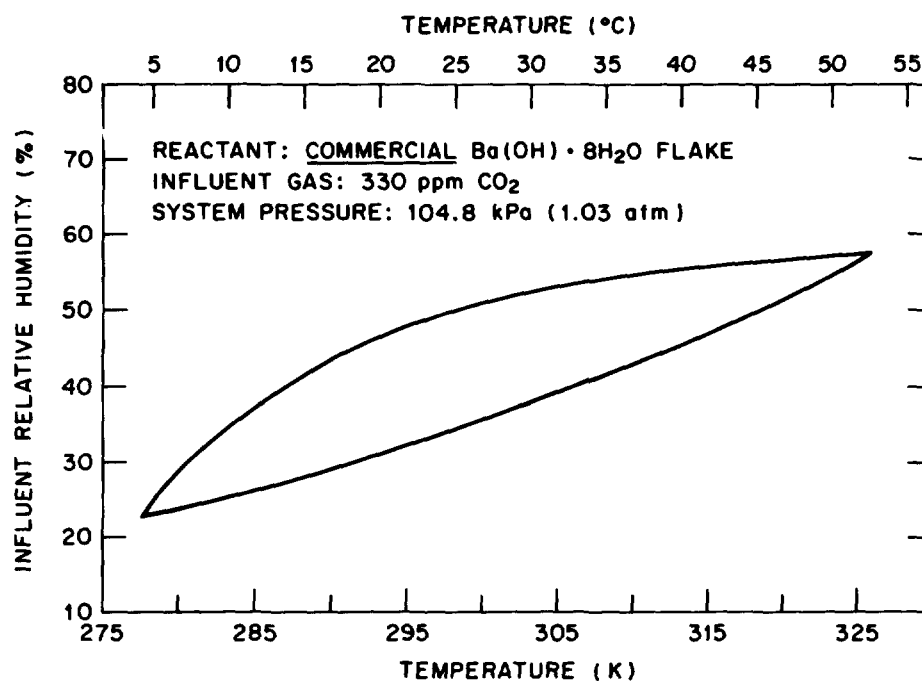


Fig. 11. Operating window for contacting a 330-ppmv CO₂ gas stream with fixed beds of commercial Ba(OH)₂·8H₂O flakes under isothermal conditions.

Successful isothermal operation of the process at higher effluent relative humidities (>60%) is possible by significantly reducing the gas throughput. The effect of operating the bed at conditions of water vapor saturation, whereby the water product would remain in the bed and the reaction would become exothermic, was not examined in detail. However, the reaction does proceed readily at these conditions and the BaCO₃ product is extremely insoluble.

Studies are under way on a pilot unit to determine the effects of operation at near-adiabatic conditions, whereupon the endothermic reaction results in a 4°C drop in the gas temperature upon passing through the bed. We speculate that complete reactant utilization and an acceptable pressure is possible when the relative humidity, based upon the effluent water vapor pressure and the effluent saturation vapor pressure, falls within the operating window. This speculation is based upon a relative comparison of the rate of axial movement of the reaction zone through the bed and the rate of dehydration and accompanying deactivation of commercial Ba(OH)₂·8H₂O flakes. Furthermore, studies are under way to determine if prior hydration of the water-deficient commercial Ba(OH)₂·8H₂O to Ba(OH)₂·8H₂O at conditions which retain the integrity of the flake (a relative humidity <60% and a water vapor pressure greater than the dissociation vapor pressure of Ba(OH)₂·8H₂O), will enable subsequent CO₂ removal at much higher relative humidities in the absence of significant pressure drop problems.

17th DOE NUCLEAR AIR CLEANING CONFERENCE

References

1. H. Bonka et al., "Contamination of the environment by carbon-14 produced in high-temperature reactors," *Kernetechnik* 15(7), 297 (1973).
2. W. Davis, Jr., *Carbon-14 production in nuclear reactors*, ORNL/NUREG/TM-12 (February 1977).
3. C. D. Kunz, "Continuous stack sampling for ^{14}C at the R. E. Ginna pressurized water reactor," *Trans. Am. Nucl. Soc.* 38, 100 (1981).
4. C. O. Kunz, W. E. Mahoney, and T. W. Miller, "Carbon-14 gaseous effluents from boiling water reactors," *Trans. Am. Nucl. Soc.* 21, 91 (1975).
5. C. O. Kunz, W. E. Mahoney, and T. W. Miller, "C-14 gaseous effluent from pressurized water reactors," pp. 229-34 in *Proceedings of the health physics society 8th midyear symposium*, CONF 741018 (1974).
6. M. J. Kabat, "Monitoring and removal of gaseous carbon-14 species," *Proceedings of the 15th DOE nuclear air cleaning conference*, CONF 780819 (1979).
7. H. Schuttelkopf, *Releases of $^{14}\text{CO}_2$ from nuclear facilities with gaseous effluents*, Kernforschungszentrum Karlsruhe KFK 2421, June 1977 (translated from German) ORNL-tr-4527 (1978).
8. *Program strategy document for the management of radioactive airborne wastes - draft*, Exxon Nuclear Idaho Company, Inc., prepared for Department of Energy, Idaho Operations Office (1981).
9. P. J. Magno, C. B. Nelson, and W. H. Ellett, "A consideration of the significance of carbon-14 discharges from the nuclear power industry," p. 1047 in *Proceedings of the thirteenth AEC air cleaning conference*, CONF-740807 (1975).
10. G. G. Killough, *A diffusion-type model of the global carbon cycle for the estimation of dose to the world population from releases of carbon-14 to the atmosphere*, ORNL/TM-5269 (1977).
11. G. G. Killough et al., *Progress report on evaluation of potential impact of ^{14}C releases from an HTGR reprocessing facility*, ORNL/TM-5284 (July 1976).
12. L. Machta, "Prediction of CO_2 in the atmosphere," *Carbon and the biosphere*, G. M. Woodwell and E. V. Pecan, eds., Technical Information Center, Office of Information Services, U.S. Atomic Energy Commission (August 1973).
13. J. W. Snider and S. V. Kaye, "Process behavior and environmental assessment of ^{14}C releases from an HTGR fuel reprocessing facility." Paper presented at and published in the proceedings of the ANS-AIChE topical meeting, Sun Valley, Idaho, Aug. 5-6, 1976.

17th DOE NUCLEAR AIR CLEANING CONFERENCE

14. L. Pauling, "Genetic and somatic effects of carbon-14," *Science* 128, 1183 (1958).
15. J. Schwibach, H. Riedel, and J. Bretschneider, *Studies on the emission of carbon-14 from nuclear facilities (nuclear power plants and reprocessing plants): Its measurement and the radiation exposure resulting from emissions*, Series of the Institute for Radiation Hygiene of the Federal Health Office, No. 20 (translated from German), OLS-80-233 (1979).
16. *Radiological significance and management of tritium, carbon-14, krypton-85, iodine-129 arising from the nuclear fuel cycle*, Nuclear Energy Agency, Organization for Economic Cooperation and Development, Paris, France (1980).
17. G. C. Killough and P. S. Rohwer, "A new look at the dosimetry of ^{14}C released to the atmosphere as carbon dioxide," *Health Phys.* 4, 141 (1978).
18. G. C. Killough, J. E. Till, E. L. Etnier, B. D. Murphy, and R. J. Roridon, "Chapter 11, dose equivalent due to atmospheric releases of carbon," taken from *Models and parameters for environmental radiological assessment*, C. W. Miller, ed., DOE/TIC-11368 (in press).
19. G. C. Killough and J. E. Till, "Scenarios of ^{14}C releases from the world nuclear industry from 1975 to 2020 and the estimated radiological impact," *Nucl. Saf.* 19(5), 602 (1978).
20. T. W. Fowler and C. B. Nelson, *Health impact assessment of Carbon-14 emissions from normal operations of uranium fuel cycle facilities*, EPA 520/5-80-004 (1981).
21. G. L. Haag, "Carbon-14 immobilization via the $\text{CO}_2\text{-Ba(OH)}_2$ hydrate gas-solid reaction," *Proceedings of the 16th DOE nuclear air cleaning conference*, CONF 801038 (1981).
22. *Handbook of chemistry and physics*, 52nd ed., The Chemical Rubber Co., Cleveland, Ohio (1972) pp. 13-70.
23. W. F. Linke and A. Seidell, *Solubilities of inorganic and metal organic compounds*, 4th ed., American Chemical Society, Washington, D.C. (1958).
24. A. G. Croff, *An evaluation of options relative to the fixation and disposal of ^{14}C -contaminated CO_2 as CaCO_3* , ORNL/TM-5171 (April 1976).
25. A. G. Evans, W. E. Prout, J. T. Buckner, and M. R. Buchner, *Management of radioactive waste gases from the nuclear fuel cycle - Volume 1, Comparison of alternatives*, NUREG/CR-1546, DPST-NUREG-80-5, vol. 1 (1980).
26. D. W. Holladay, *Experiments with a lime slurry in a stirred tank for the fixation of carbon-14 contaminated CO_2 from simulated HTGR fuel reprocessing off-gas*, ORNL/TM-5757 (1978).

17th DOE NUCLEAR AIR CLEANING CONFERENCE

27. D. W. Holladay, *An experimental investigation of the distribution of krypton from simulated HTGR fuel reprocessing off-gas during the removal and fixation of CO₂ by the CO₂-Ca(OH)₂ slurry reaction*, ORNL/TM-6539 (in preparation).
28. D. W. Holladay and G. L. Haag, "Removal of ¹⁴C-contaminated CO₂ from simulated LWR fuel reprocessing off-gas by utilizing the reaction between CO₂ and alkaline hydroxides in either slurry or solid form," pp. 548-69 in *Proceedings of the 15th DOE nuclear air cleaning conference*, CONF 780819 (1979).
29. K. J. Notz, D. W. Holladay, C. W. Forsberg, and G. L. Haag, "Processes for the control of ¹⁴CO₂ during reprocessing," paper presented at the International Symposium on Management of Gaseous Wastes from Nuclear Facilities, Vienna, Austria, Feb. 18-22, 1980.
30. G. R. Bray, C. L. Miller, T. D. Nguyen, and J. W. Rieke, *Assessment of carbon-14 control technology and costs for the LWR fuel cycle*, EPA 520/4-77-013 (1977).
31. J. L. Kovach, *Review of carbon-14 control technology and cost*, NUCON 8EP555/01 (1979).
32. G. L. Haag, *Application of the CO₂-Ba(OH)₂·8H₂O gas-solid reaction for the treatment of dilute CO₂-bearing gas streams*, Ph.D. Dissertation, University of Tennessee, Knoxville; and ORNL-5887 (both in preparation).
33. G. L. Haag, G. C. Young, J. W. Nehls, Jr., *Pilot unit development of the Ba(OH)₂·8H₂O-CO₂ gas-solid reaction for ¹⁴C immobilization*, (to be published as ORNL/TM-8433).
34. Jim Nillis, Sherwin Williams Company, Coffeerville, Kansas, personal communication, 1981.
35. M. Michaud, "Contribution to the study of the hydroxides of potassium and barium," *Revue de Chimie Minerale*, t.5, 89 (1968).
36. M. Michaud, "Inorganic Chemistry - Study of the binary water-barium hydroxide system," *C. R. Acad. Sci. Paris* 262.CV, 1143 (1966).
37. B. A. Kondakov, P. V. Kovtunencko, and A. A. Bundel, "Equilibria between gaseous and condensed phases in the barium oxide-water system," *Russ. J. Phys. Chem.* 38(1), 99-102 (1964).

DISCUSSION

CHRISTIAN: With the present concept, most of your water product will result from inactive atmospheric CO₂. Since you obtain less than 100 ppb CO₂ in the exit gas from the Ba(OH)₂·8H₂O bed, the goal DF of 100 could still be obtained if the inlet purge air to a dissolver were treated with molecular sieves to remove atmospheric CO₂ to about 10 ppm and the waste volume might be reduced by a factor of 30. Have you tested the bed at reduced inlet concentrations to verify that this would, indeed, work?

HAAG: This is an excellent point. With present analytical techniques, we are capable of analyzing CO₂ to a lower concentration limit of 100 ppb. Thermodynamic calculations indicate an equilibrium concentration of the order of parts per trillion. Therefore, I see no difficulty in obtaining a DF of 100 or a 1,000 for the treatment of a 10 ppm CO₂ gas stream. Our process model has indicated the rate-controlling steps to be mass transfer across the gas film. Therefore, the major effect may be a slight increase in the length of the mass transfer zone. However, the pretreatment of the dissolver off-gas for a 100 ft³/min off-gas stream would decrease the waste volume from .7 ft³/d to .02 ft³/d, the mass of waste from 26 lb/d to .81 lb/d, and the reactant cost from \$15/d to \$0.45/d.

EBY: As I understand it, your tests were evaluated at 330 ppm. Could you speculate what effects you might expect as far as loading and breakthrough for CO₂ concentrations in the neighborhood of 50%. For instance, if we were to remove CO₂ in a fluorocarbon process and concentrate it prior to final fixation?

HAAG: The bulk of our studies have been conducted with 330 ppm CO₂. However, during initial studies, concentrations as great as 88% were used with excellent removal efficiencies. The difficulty that arises under such conditions results from the fact that 9 molecules of water are released per molecule of CO₂ reacted thus causing water condensation within the bed for higher CO₂ concentrations. The condensation of water causes the reaction to become slightly exothermic rather than endothermic. Because of the low solubilities of Ba(OH)₂ and BaCO₃ in water, and the low gas flow rates required of the system, water condensation was not extremely detrimental to bed operation. However, column cooling capabilities would be required for a 50% CO₂ gas stream. Additional studies are required using a 50% CO₂ gas stream as a reference point. Such a system would be required to handle only 0.03 to 0.33 ft³/min for a typical 1,500 MTHM/y reprocessing plant with a 100-500 ft³/min, 330 ppm CO₂ off-gas stream being fed to the fluorocarbon process.

CLOSING REMARKS OF SESSION CHAIRMAN:

In this session, results were presented from an off-gas study of liquid-fed joule-heated ceramic melters, which established the off-gas and effluent characteristics from which optimal effluent control systems can be designed. The experimental study on the volatilization and trapping of ruthenium resulted in the optimization of airborne ruthenium species removal from high temperature processes.

The major part of this session was related to carbon-14 removal. We were told about three removal systems presently being developed in USA, Germany, and Canada: the double alkali process, which was tested and previously applied on a relatively large scale, and two dry systems, which apparently have very good potential for this application. These dry systems are: the barium hydroxide system which is in the stage of pilot testing at ORNL, and the calcium hydroxide system, which was developed in Canada, initially for the selective sampling of ^{14}C airborne species. This sampler, which requires elevated temperature for the catalytic conversion of hydrocarbons to CO_2 , was developed in 1978 and was described at the 15th Air Cleaning Conference. It was used in 1979-1981 in Candu nuclear power stations for the analysis of ^{14}C species in gaseous effluents. An alternative application is being developed for the removal of $^{14}\text{CO}_2$ from Candu systems at ambient temperature. The results, presented at this session, are also promising for this purpose.

It is apparent from the presentations that all three systems are cost effective, can efficiently remove CO_2 from large streams, and transfer it to solid, insoluble forms which are suitable for long term disposal.

The analysis of ^{14}C sources, its chemical forms and releases from light water reactors, provides data for the evaluation of environmental hazards from ^{14}C and the need for its removal from light water reactor systems.

From two papers, presented at this session, it is also apparent that ^{85}Kr solidification and its long term disposal will be feasible at a reasonable cost in the near future.